Characterizing the localization and role of *lin-5* and *era-1* mRNAs in early *C. elegans* embryos

THÈSE N^{O} 6355 (2014)

PRÉSENTÉE LE 26 SEPTEMBRE 2014
À LA FACULTÉ DES SCIENCES DE LA VIE
UNITÉ DU PROF. GÖNCZY
PROGRAMME DOCTORAL EN APPROCHES MOLÉCULAIRES DU VIVANT

ÉCOLE POLYTECHNIQUE FÉDÉRALE DE LAUSANNE

POUR L'OBTENTION DU GRADE DE DOCTEUR ÈS SCIENCES

PAR

Zoltán Péter SPIRÓ

acceptée sur proposition du jury:

Prof. J. Lingner, président du jury
Prof. P. Gönczy, directeur de thèse
Prof. D. Constam, rapporteur
Dr A. Ephrussi, rapporteuse
Dr H. Grosshans, rapporteur

ÉCOLE POLYTECHNIQUE
FÉDÉRALE DE LAUSANNE

Suisse
2014

Nagymamának

Summary

Asymmetric cell division is essential for the generation of diversity during development and the function of stem cell lineages. The *Caenorhabditis elegans* zygote is an attractive model to investigate the mechanisms of spindle positioning during asymmetric cell division. In this polarized cell, the asymmetric distribution of cortical force generators along the antero-posterior axis and pulling on astral microtubules leads to the unequal cleavage of the one-cell embryo. The mechanisms underlying such cortical force generation are thought to act strictly at the protein level.

In this thesis work we report that the mRNA encoding the cortical force generator component LIN-5 is enriched around centrosomes in early embryos, in a manner that depends on microtubules and dynein. We found a likewise enrichment in *C. briggsae*, indicating evolutionary conservation of such localization. We established that the *lin-5* coding sequence is necessary and sufficient for mRNA enrichment around centrosomes in *C. elegans.* In addition, we found that *lin-5* mRNA is mislocalized in *lin-5*(*ev571*) mutant embryos, which harbor a 9 nucleotide insertion in the coding sequence. Moreover, an intragenic revertant of *lin-5*(*ev571*), *lin-5*(*ev571he63*), also exhibits mislocalized *lin-5* mRNA distribution. We demonstrated that this is accompanied by diminished pulling forces on the posterior spindle pole, suggesting that centrosomal localization of *lin-5* mRNA is important for robust pulling forces. We found also that *lin-5* mRNA centrosomal enrichment is slightly asymmetric during anaphase, with more transcripts present on the anterior side. We developed a novel FRAP-based assay, which revealed that *lin-5* is translated/folded preferentially in the cytoplasm compared to centrosomes. Furthermore, we found that morpholino-mediated inhibition of *lin-5* translation diminishes pulling forces on the posterior side during anaphase. Together, these findings lead us to propose that preferential translation/folding of *lin-5* in the posterior cytoplasm following release of the mRNA from the posterior centrosome contributes to asymmetric cortical distribution of force generators, and thus to proper spindle positioning.

Moreover, we found that the mRNA of an uncharacterized gene, *era-1* is enriched on the anterior side of the zygote and is inherited by the anterior blastomeres. Similar to *era-1* mRNA, a YFP fusion of ERA-1 protein is also asymmetrically distributed. *era-1* mRNA and protein asymmetry is disturbed when the polarity of the cell is compromised. Moreover, asymmetric distribution of both *era-1* mRNA and YFP-ERA-1 protein requires the *era-1* 3' UTR. Furthermore, the RNA-binding protein MEX-5 is needed for both asymmetric *era-1* mRNA localization and for its translational activation.

Furthermore, we report that the clathrin heavy chain CHC-1 negatively regulates pulling forces acting on centrosomes during interphase and on spindle poles during mitosis in one-cell *C. elegans* embryos. We establish a similar role for the cytokinesis/apoptosis/RNA-binding protein CAR-1 and uncover that CAR-1 is needed to maintain normal levels of CHC-1. We demonstrate that CHC-1 is necessary for proper organization of the cortical acto-myosin network and for full cortical tension. Furthermore, we establish that the centrosome positioning phenotype of embryos depleted of CHC-1 is alleviated by stabilizing the acto-myosin network. Conversely, we demonstrate that slight perturbations of the acto-myosin network in otherwise wild type embryos results in excess centrosome movements resembling those in *chc-1*(*RNAi*) embryos. Overall, our findings lead us to propose that clathrin plays a critical role in centrosome positioning by promoting acto-myosin cortical tension.

Keywords: *C. elegans* embryos, asymmetric cell division, pulling forces, *lin-5* mRNA, *era-1* mRNA, clathrin heavy chain

Résumé

La division cellulaire asymétrique est essentielle pour assurer la diversité au cours du développement et le fonctionnement de lignées de cellules souches. Le zygote de *Caenorhabditis elegans* est un modèle intéressant pour étudier les mécanismes de positionnement du fuseau mitotique lors de la division cellulaire asymétrique. Dans cette cellule polarisée, la répartition asymétrique des générateurs de force corticaux le long de l'axe antéro-postérieur et tirant sur les microtubules astraux conduit à un clivage inégal du zygote. Les mécanismes à l'origine de la génération d'une telle force corticale sont censés agir strictement au niveau des protéines.

Dans ce travail de thèse, nous rapportons que l'ARNm qui code le composant générateur de force corticale LIN-5 est enrichi autour des centrosomes dans les embryons précoces, d'une manière qui dépend des microtubules et de la dynéine. Nous avons également observé un enrichissement chez *C. briggsae* qui indique une conservation de cette localization au cours de l'évolution. Nous avons établi que la séquence codante de *lin-5* est nécessaire et suffisante pour l'enrichissement d'ARNm autour des centrosomes chez *C. elegans*. En outre, nous avons constaté que le *lin-5* ARNm est localisé de manière uniforme chez des *lin-5(ev571)* embryons mutants qui ont une insertion des neuf nucléotides dans la séquence codante. Un révertant intragénique de *lin-5(ev571)*, *lin-5(ev571he63)*, manifeste également une distribution de *lin-5* ARNm uniforme. Nous avons démontré que ceci s'accompagne d'une diminution des forces de traction sur le pôle postérieur du fuseau mitotique, ce qui suggère que la localisation centrosomale de *lin-5* ARNm est importante pour obtenir des forces de traction robustes. Nous avons également constaté que l'enrichissement centrosomal des *lin-5* ARNm est légèrement asymétrique lors de l'anaphase, avec plus de transcripts présents sur du côté antérieur. Nous avons développé un nouveau test sur la base du FRAP, qui a révélé que le *lin-5* ARNm est traduit / plié de manière préférentielle dans le cytoplasme par rapport à centrosomes. En outre, nous avons trouvé que l'inhibition induite par morpholino de la traduction de *lin-5* diminue les forces de traction du côté postérieur lors de l'anaphase. Ensemble, ces résultats nous permettent de proposer que la traduction / pliage préférentiels de *lin-5* dans le cytoplasme postérieur après la libération de l'ARNm du centrosome postérieur contribuent à la distribution corticale asymétrique de générateurs de force, et donc au positionnement approprié du fuseau mitotique.

En outre, nous avons constaté que l'ARNm d'un gène non caractérisé, *era-1*, est enrichi du côté antérieur du zygote et est hérité par les blastomères antérieures. D'une facon similaire au *era-1* ARNm, une fusion YFP de la protéine ERA-1 est également distribuée de manière asymétrique. L'asymétrie de l’ARNm de *era-1* ainsi que de YFP-ERA-1 sont perturbées quand la polarité de la cellule est compromise. La distribution asymétrique de *era-1* ARNm et YFP-ERA-1 nécessite l'*era-1* 3 'UTR. En outre, la protéine de liaison à l'ARN MEX-5 est nécessaire à la fois pour la localisation et l'activation traductionelle de l'*era-1* asymétrique.

Finalement, nous rapportons que la chaîne lourde de la clathrine CHC-1 régule négativement les forces de traction agissant sur les centrosomes pendant l'interphase et sur les poles du fuseau lors de la mitose dans le zygote de *C. elegans*. Nous établissons un rôle similaire pour la cytokinèse/apoptose/protéine de liaison à l'ARN CAR-1 et observons que la CAR-1 est necessaire pour maintenir des niveaux normaux de CHC-1. Nous démontrons que CHC-1 est nécessaire pour la bonne organisation du réseau acto-myosine cortical et pour une tension corticale complète. En outre, nous établissons que le phénotype de positionnement du centrosome des embryons déplétés de CHC-1 par RNAi est atténué par la stabilisation du réseau acto-myosine. Inversément, nous démontrons que de légères perturbations du réseau acto-myosine dans des embryons de type sauvage provoquent un excès de mouvements des centrosomes qui ressemble à ceux des embryons *chc-1(RNAi)*. Dans l'ensemble, nos résultats nous amènent à proposer que la clathrine joue un rôle essentiel dans le positionnement du centrosome par la promotion de la tension corticale du réseau acto-myosine.

Mots-clés: embryons de *C. elegans*, division cellulaire asymétrique, forces de traction, *lin-5* ARNm, *era-1* ARNm, chaîne lourde de la clathrine

Table of contents

1. INTRODUCTION 10

  1A. Asymmetric cell division 10

    Axis formation during *C. elegans* development 12

    Model systems to study asymmetric cell division 13

      The *C. elegans* zygote 13

        Processes in the one-cell stage embryo 14

        Molecular mechanisms 15

          Symmetry breaking 16

          Polarity establishment and maintenance 17

          Segregation of cell fate determinants 18

          Spindle positioning 20

      Asymmetric cell division and spindle positioning in other systems 33

        The *Drosophila* neuroblast 34

        Mammalian systems 38

    The *Drosophila* oocyte 41

    The *Xenopus* oocyte 44

    ash1 mRNA localization in budding yeast 46

    Translational control during early *C. elegans* development 48

    Polarized mRNAs in early *C. elegans* embryos 51

2. AIMS OF THE STUDY 54

3. CHARACTERIZATION OF THE MECHANISMS AND FUNCTION OF *LIN-5* MRNA LOCALIZATION 55

3A. RESULTS 55

  lin-5 mRNA is enriched around centrosomes in early *C. elegans* embryos 55

  Microtubules and dynein are necessary for *lin-5* mRNA enrichment around centrosomes 58

  The 3' UTR is dispensable for *lin-5* mRNA localization 60

  The coding region is necessary for *lin-5* mRNA localization 61

  A 9-nucleotide insertion in the coding region interferes with *lin-5* mRNA localization 62

  lin-5 mRNA mislocalization correlates with decreased posterior pulling forces and with misdistribution of the force generator complex 67

  lin-5 mRNA centrosomal enrichment is asymmetric in anaphase 70

  de novo lin-5 translation/folding occurs preferentially in the cytoplasm during mitosis 72

  Morpholino-mediated inhibition of *lin-5* mRNA translation leads to decreased posterior pulling forces 76

3B. DISCUSSION 79

  mRNA enrichment around centrosomes: beyond *lin*-5 80

  Localization as a means to control translation of *lin-5* mRNA 82

  lin-5 mRNA localization, preferential translation and asymmetric pulling forces 83

4. CHARACTERIZATION OF THE MECHANISMS DRIVING *ERA-1* MRNA DISTRIBUTION 86

4A RESULTS 86

  The mRNA of the W02F12.3 gene is enriched on the anterior side of P_0 and is inherited by the anterior lineage 86

  era-1 mRNA localization is driven by MEX-5 and its 3'UTR 87

  YFP-ERA-1 protein is enriched in anterior blastomeres and is negatively regulated by the *era-1* 3'UTR 90

  MEX-5/6 positively regulates *era-1* translation via the *era-1* 3'UTR 94

Bioinformatic analysis of *era-1* 97
Attempts to analyze the phenotypic consequences of *era-1* depletion 99
Phenotypic consequences of ERA-1 mislocalization 102

4B. DISCUSSION 103
era-1 mRNA and ERA-1 protein distribution 103
Regulation by MEX-5 103
era-1 mRNA distribution by other mechanisms 105
Potential function of ERA-1 105

5. CHARACTERIZATION OF THE EFFECT OF THE CLATHRIN HEAVY CHAIN ON FORCE GENERATION 107

5A. RESULTS 107
The clathrin heavy chain CHC-1 negatively regulates pulling forces in *C. elegans* embryos 107
CAR-1 depletion also leads to MTOC positioning defects and results in lower CHC-1 levels 112
Higher forces in *chc-1(RNAi)* do not arise from increased levels of cortical force generators 115
Clathrin is needed for proper organization and tension of the cortical acto-myosin network 119
Alterations in the acto-myosin network likely cause the centrosome positioning phenotype of *chc-1(RNAi)* embryos 124

5B. DISCUSSION 129
Clathrin, as a regulator of the acto-myosin network 129
Slight perturbation in the actin network and force generation 130

6. MATERIALS AND METHODS 133
Worm strains and RNAi 133
Microscopy, spindle severing, drug treatment and image analysis 134
Digoxigenin *in situ* hybridization and single molecular FISH 135
RT-qPCR 137
Antibodies, western blotting and indirect immunofluorescence 138
Fluorescence Recovery After Complete Photobleaching (FRAcP) and Fluorescence Loss in Photobleaching (FLIP) 139
Morpholino treatment 139
Statistical analysis 140

7. ACKNOWLEDGMENTS 142

8. REFERENCES 145

9. CURRICULUM VITAE 163

1. INTRODUCTION

1A. Asymmetric cell division

The generation of various cell types is a prerequisite for the establishment of a multicellular organism. A fundamental mechanism by which such diversity of cell types is achieved during development is asymmetric cell division (reviewed in Gönczy, 2008). The resulting two daughter cells following an asymmetric division acquire different fates and give rise to distinct tissues in the adult organism. Asymmetric cell division is present in unicellular organisms as well as in plants and animals, and is also crucial for the maintenance of stem cell lineages (Figure 1 and reviewed in Knoblich, 2008).

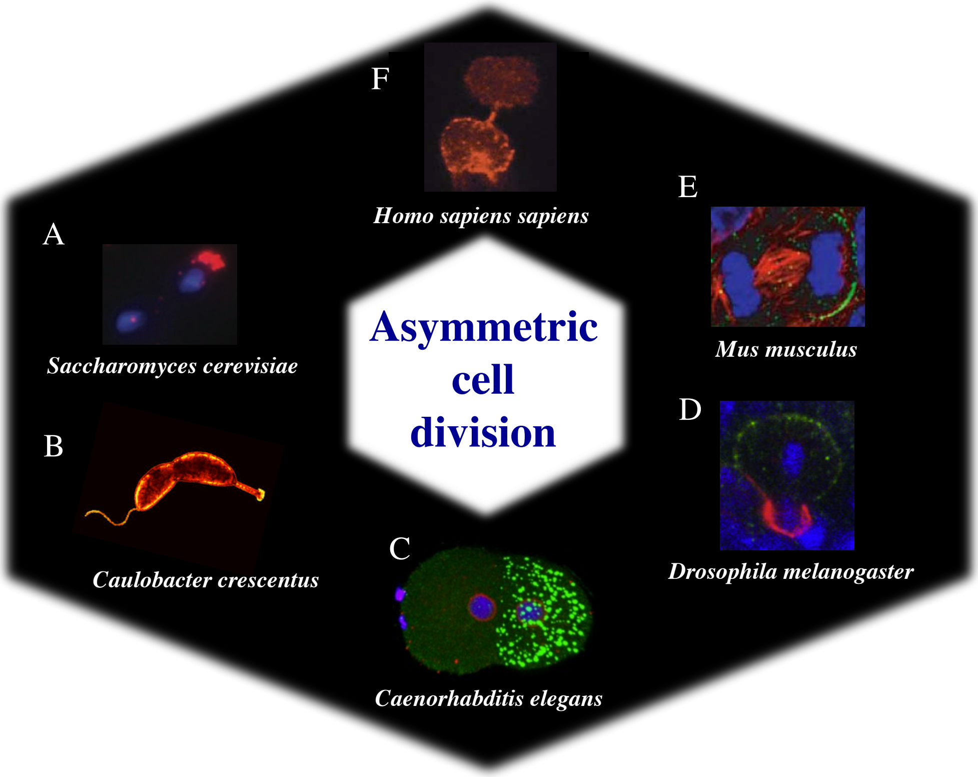
F
Homo sapiens sapiens
E
Mus musculus
A
Saccharomyces cerevisiae
Asymmetric cell division
B
Caulobacter crescentus
D
Drosophila melanogaster
C
Caenorhabditis elegans

Figure 1. Asymmetric cell division in various organisms.
A *ash1* mRNA distribution (red) in a dividing budding yeast (Trcek et al., 2012). **B** Dividing *Caulobacter crescentus* (source: microbewiki.kenyon.edu/index.php/Caulobacter) **C** P-granule distribution (green) in a 2-cell stage *C. elegans* embryo (source: bio.research.ucsc.edu/people/strome/Site/Research.html). **D** Mira (red) and Par6 (green) distribution during *Drosophila* neuroblast division (Yoshiura et al., 2012). **E** LGN distribution in a dividing keratinocyte (Lechler and Fuchs, 2005). **F** Numb distribution during hematopoetic stem cell division (Zimdahl et al., 2014).

The position of the mitotic spindle determines the division plane in animal cells. Therefore spindle positioning is important in determining if a given cell division is symmetric or asymmetric (compare Figure 2A with C). There are several types of asymmetric cell division. In the case of extrinsic asymmetric cell divisions, the two daughter cells are identical at the time of birth and subsequent signaling stemming from the neighbors drives the distinction between them. By contrast, a cell undergoing intrinsic asymmetric cell division possesses polarized domains prior to division, leading to the differential segregation of various cell fate determinants (proteins and/or RNAs) and organelles in the newborn cells. Moreover, depending on the relative sizes of the two daughter cells, an intrinsically determined asymmetric cell division can be equal or unequal, a feature depending on the position of the mitotic spindle (compare Figure 2C with D).

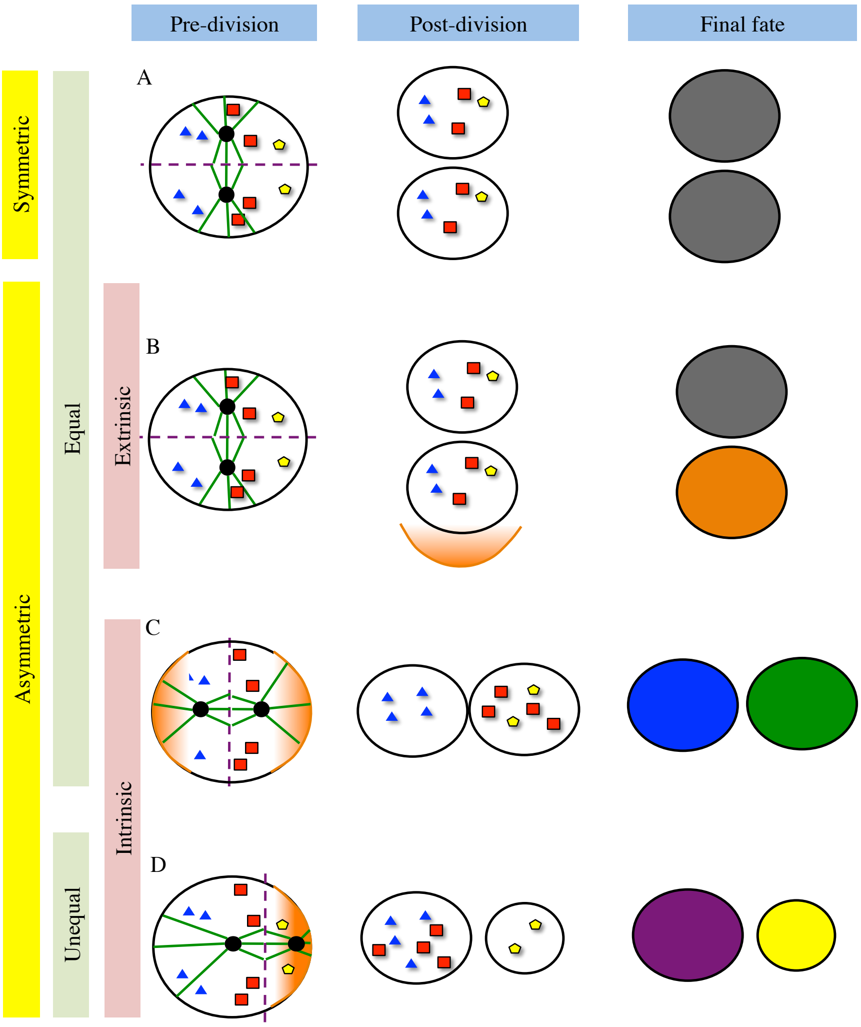

Figure 2. Types of cell divisions **A-D** Depending on the plane of division, cell fate determinants (blue triangle, red square and yellow octagon) are segregated differently in the daughter cells, leading to various cell fates (colored cells in the third row). Equal symmetric (**A**), equal extrinsic asymmetric (**B**), equal intrinsic asymmetric (**C**) and unequal intrinsic asymmetric (**D**) cell divisions are depicted. The plane of division is shown as a purple dotted line in the first column.

Axis formation during *C. elegans* development

The early development of *C. elegans* provides an excellent example of how asymmetric segregation of cell fate determinants executed by asymmetric cell divisions is capable of setting up the three main body axes within 4 rounds of division (Figure 3). Through these divisions, six founder cells (AB, MS, E, C, D and P_4) are generated that are responsible for building up the various tissues of the embryo (Sulston et al., 1983). The antero-posterior (A-P) axis is defined shortly after fertilization in the zygote (see below for details). This cell, called P_0 divides asymmetrically along the A-P axis, giving rise to a larger anterior cell, named AB, and a smaller posterior cell, P_1 (Figure 3A and B). Thereafter, AB divides symmetrically generating an anteriorly and a posteriorly positioned cell, ABa and ABp, respectively, whereas P_1 divides asymmetrically, leading to the formation of the larger EMS and the smaller P_2 cells (Figure 3C). The dorso-ventral axis is set up at this stage, as the position of the midbody remnant arising from the previous cell division drive the position of EMS, thus establishing the ventral side of the embryo (Singh and Pohl, 2014). The left-right axis is created by the symmetric divisions of ABa and ABp that generate ABa1 and ABpl, which define the left side of the embryo. On the opposite side, ABar and ABpr mark the presumptive right side. In this third round of division, EMS and P_2 divide again asymmetrically, generating MS and E, as well as C and P_3 respectively (Figure 3D). Thereafter the asymmetric division of P_3 gives rise to D and P_4 (Figure 3E). The descendants of each founder cell differentiate into specific cell types later on as follows: AB - hypodermis, neurons, pharynx; MS – muscle, pharynx, neurons, somatic gonad; C- muscle, hypodermis, neurons; D – muscle; E – intestine, - P_4 - germ line (Figure 3F). Of note, the nomenclature of some of the genes reflects defects in cell specification when mutated or upon RNAi-mediated depletion. Some examples for such genes will be given in the later sections.

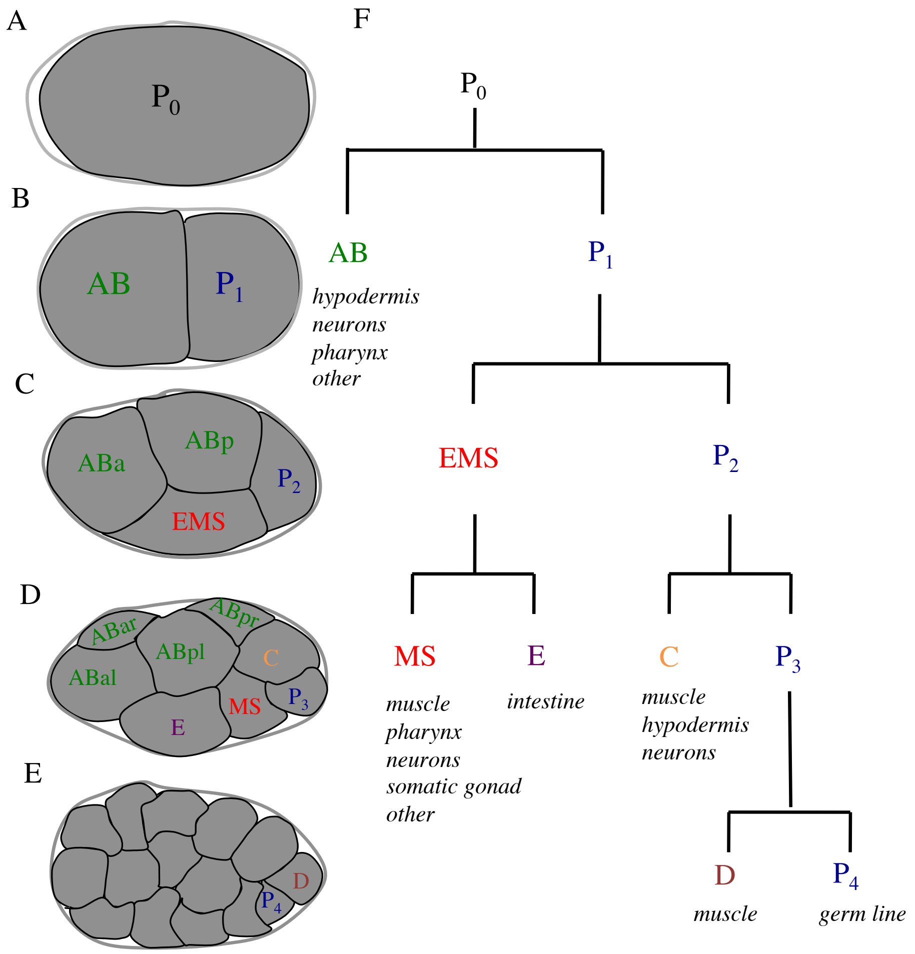
A
F
P_0
B
AB
P_1
AB
P_1
hypodermis
neurons
pharynx
other
C
ABa
ABp
P_2
EMS
EMS
P_2
D
ABar
ABpr
ABpl
ABal
C
MS
P_3
E
MS
E
C
P_3
muscle
pharynx
neurons
somatic gonad
other
intestine
muscle
hypodermis
neurons
E
P_4
D
D
P_4
muscle
germ line

Figure 3. Early embryonic development of *C. elegans*
A-E The first four rounds of cell division give rise to the major three embryonic axes and to the generation of six founder cells. 1-cell stage (**A**), 2-cell stage (**B**), 4-cell stage (**C**), 16-cell stage (**D**), 64-cell stage (**E**). The name of the cells is indicated; in panels **D** and **E,** only the first layer of cells is seen. **F** Generation of the six founder cells (AB, MS, E, C, D, P_4) through the first four cell divisons. The tissues generated from each founder cell are listed below the cell.

Model systems to study asymmetric cell division

The C. elegans zygote

Given its large size (50x30µm), its relative ease of handling and the available genetic and genomic tools, the first cell division of the *C. elegans* zygote became an attractive model system to study asymmetric cell division. The phenotypic events occurring in this cell are easily detectable using Differential Interference Contrast (DIC) microscopy (Figure 4A; Albertson, 1984; Nigon et al., 1960; Gönczy et al., 1999). Furthermore, an increasing number of fluorescently-tagged transgenic lines allow researchers to detect proteins and analyze their dynamics with high spatial and temporal resolution, as is exemplified in embryos shown in Figure 4B-E. Moreover, *in situ* hybridization and immunofluorescence methods have been optimized to reveal localization of mRNAs and proteins in fixed specimens. In the following sections, the events occurring in the one-cell stage embryo as well as the molecular mechanisms leading to its asymmetric division are introduced.

Processes in the one-cell stage embryo

The sperm, containing the paternal DNA and a pair of centrioles, fertilizes the oocoyte. Fertilization triggers the completion of female meiosis I and, shortly thereafter, the two pronuclei appear on the two sides of the zygote (pronuclear formation, Figure 4A). The female pronucleus is located at the presumptive anterior, the male at the presumptive posterior side of the embryo. While the two pronuclei increase in size, the plasma membrane ingresses at the embryo center from both sides, mimicking cytokinesis. This ingression is the pseudocleavage furrow. Then, both the female and the male pronuclei migrate towards the center of the cell with the female pronucleus moving faster; therefore pronuclear meeting occurs at the posterior side. The two pronuclei are now associated with the centrosomes that are aligned orthogonal to the A-P axis. This nucleo-centrosomal complex moves toward the center of the embryo while undergoing a 90° rotation (this process is named centration/rotation). At the end of this process, the two pronuclei and the associated centrosomes are located in the middle of the cell, aligned parallel to the A-P axis. Following nuclear envelope breakdown (NEBD), the mitotic spindle is formed in the cell center. During metaphase, the spindle is displaced towards the posterior side of the cell and this displacement becomes even more pronounced in anaphase. During anaphase, the posterior spindle pole undergoes oscillations perpendicular to the A-P axis, which dampen at the onset of cytokinesis. The cytokinetic furrow ingresses and bisects the mitotic spindle. As a result, the zygote is split into two daughter cells with different sizes, a larger anterior AB blastomere and a smaller posterior P_1 blastomere. Still images of a zygote recorded by time-lapse DIC microscopy are shown in Figure 4A.

Molecular mechanisms

An intrinsic asymmetric cell division can be thought of as occuring through four steps (Figure 4). First, the initial symmetry of the cell must be broken. Second, polarization leads to distinct domains within the cell. Third, cell fate determinants segregate in response to this polarization. Fourth, the mitotic spindle is oriented in a way that ensures the proper segregation of cell fate determinants.

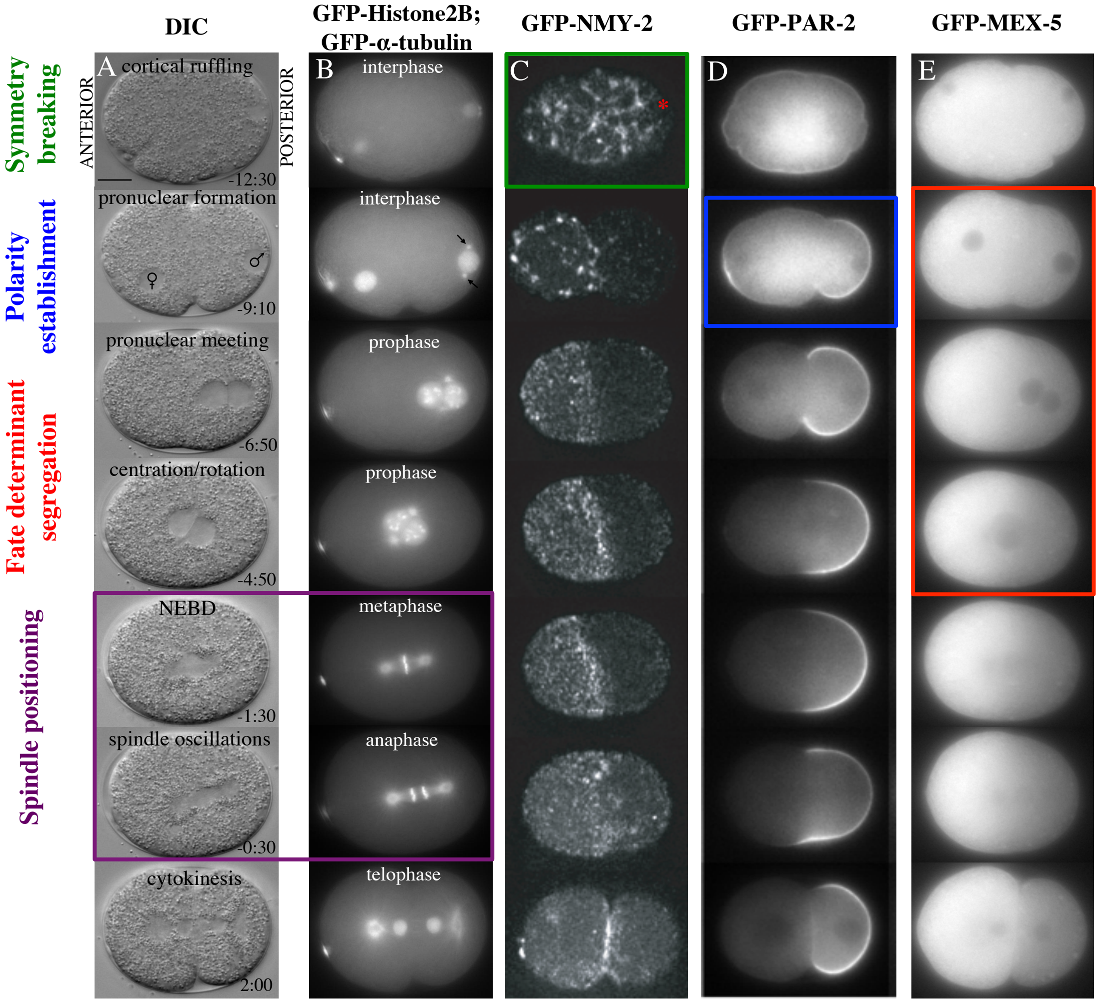
DIC
GFP-Histone2B; GFP-α-tubulin
GFP-NMY-2
GFP-PAR-2
GFP-MEX-5
Symmetry breaking
Polarity establishment
Fate determinant segregation
Spindle positioning
ANTERIOR
POSTERIOR
A
cortical ruffling
-12:30
pronuclear formation
♀
♂
-9:10
pronuclear meeting
-6:50
centration/rotation
-4:50
NEBD
-1:30
spindle oscillations
-0:30
cytokinesis
2:00
B
interphase
interphase
prophase
prophase
metaphase
anaphase
telophase
C
*
D
E

Figure 4. The first cell division of the *C. elegans* embryo
Four steps of an asymmetric division (Symmetry breaking, Polarity establishment, Fate determinant segregation and Spindle positioning) are shown in embryos expressing different fusion proteins. The embryo and stage where one of the four steps of asymmetric cell division discussed in the text is visible is marked with a colored rectangle. **A** Snapshots from Differential Interference Contrast (DIC) recording visualizing the first cell division of a GFP-Histone2B;GFP-α-tubulin expressing embryo. The stages are indicated on top of the images. The male and the female pronuclei are indicated in the second frame. In all the embryos shown in this thesis, anterior is to the left, posterior to the right. Here and elsewhere, unless otherwise stated, scale bar represents 10µm. t=0 corresponds to cytokinesis onset. **B** The GFP channel visualizes the DNA and the microtubules in the embryo shown in A. Cell cycle stages are indicated above each frame. Two arrows mark the centrosomes in the second frame. **C** Embryo expressing a GFP fusion of the non-muscle myosin II (NMY-2) (Image source: Munro et al., 2004). The stages of the embryo here and in panel D and E roughly correspond

to the embryo in panels A and B. Red star marks the site of symmetry breaking. **D** Embryo expressing a GFP fusion of PAR-2. (Image source: Cuenca et al., 2003). **E** Embryo expressing a GFP fusion of MEX-5. (Image source: Cuenca et al., 2003).

Symmetry breaking

Following fertilization, the acto-myosin rich meshwork located just below the oocyte cell membrane (hereafter referred to as the cell cortex) undergoes contractions throughout the whole cell. These contractions are based on the activity of the non-muscle myosin II, NMY-2 and involve also the Rho family GTPase RHO-1, as well as the Rho binding kinase LET-502 (Kumfer et al., 2010; Motegi and Sugimoto, 2006; Munro et al., 2004; Schonegg and Hyman, 2006; Shelton et al., 1999). Upon fertilization, these cortical contractions cease locally in the vicinity of the male pronucleus (Bienkowska and Cowan, 2012; Cheeks et al., 2004; Cowan and Hyman, 2004a; Cuenca et al., 2003; Hamill et al., 2002; Munro et al., 2004). Why are these contractions locally inactivated? The answer lies in the fact that the centrosome brought in by the sperm triggers symmetry breaking. Indeed, laser ablation of centrosomes (Cowan and Hyman, 2004b; Hamill et al., 2002) or interfering with centrosomal proteins, like SPD-2, SPD-5 or CYE-1 (Cowan and Hyman, 2006; Hamill et al., 2002; O'Connell et al., 2000) leads to the absence of symmetry breaking. At the molecular level, the RHO-1 G-protein exchange factor (GEF) ECT-2, previously present all over the cell periphery, is locally removed from the cortex near the centrosomes (Motegi and Sugimoto, 2006; Schonegg and Hyman, 2006). On the other hand, CYK-4, a RHO-1 GAP introduced by the sperm is thought to be also important in this process, as removal of CYK-4 from sperm cells compromises symmetry breaking (Jenkins et al., 2006). The involvement of microtubules in this process is somewhat controversial, given that polarity was reported to be unaffected in the absence of α-tubulin *tba-2* and γ-tubulin *tbg-1* (Cowan and Hyman, 2004b; Sonneville and Gönczy, 2004), but a significant delay in polarity establishment has been observed in zygotes expressing GFP-tagged PAR-6 lacking both α-, and β-tubulin (Tsai and Ahringer, 2007). This controversy has recently been solved by Motegi and coworkers (Motegi et al., 2011), who showed that the microtubule-mediated loading of the posterior polarity protein PAR-2 is compromised in the absence of microtubules, leading to delay in polarization that becomes corrected afterwards.

Polarity establishment and maintenance

After symmetry breaking, the smooth, non-contractile cortical region retracts towards the presumptive anterior and reaches ~50% egg-length (Figure 4C; Cuenca et al., 2003; Hird and White, 1993). This process is concomitant with an anteriorly-directed cortical flow initiating from the future posterior side. This contraction of the acto-myosin towards the anterior results in a sequence of events that establishes the anterior and the posterior domains of the cell. Six *par*tioning defective (*par*) are key in building these two domains: the anterior domain comprise the PDZ proteins PAR-3 and PAR-6 and the atypical protein kinase PKC-3, while the posterior domain consists of the Ser/Thr kinase PAR-1 and the RING-finger protein PAR-2. Moreover, the Ser/Thr kinase PAR-4 and the 14-3-3 protein PAR-5 are also crucial for proper polarity. The anterior PAR-complex, initially enriched all over at the cell cortex (Etemad-Moghadam et al., 1995; Hung and Kemphues, 1999; Tabuse et al., 1998) becomes cleared from the posterior and retracts together with the acto-myosin cortex as judged by the concomitant movements of GFP-NMY-2 and GFP-PAR-6 (Cuenca et al., 2003). In turn, PAR-2 and PAR-1 are recruited to these cleared posterior cortical regions (Figure 4D; Boyd et al., 1996; Guo and Kemphues, 1995). Although the exact mechanisms of this recruitment is unclear, it has been shown that PAR-2 is a microtubule- and lipid-binding protein that can localize to the cortex and lead to proper polarization even in the absence of cortical flows (Motegi et al., 2011; Zonies et al., 2010). The acto-myosin network and the PAR proteins are interdependent for polarization, as actin is needed for polarization (Guo and Kemphues, 1996; Hill and Strome, 1988; Shelton et al., 1999) and polarization of NMY-2 is abolished upon depletion of *par-3*, *par-4*, *par-5* or *par-6* (Cheeks et al., 2004; Cuenca et al., 2003; Morton et al., 1992; Munro et al., 2004). What is the mechanical driving force for the anterior-directed cortical movements of the acto-myosin network? Anisotropies in cortical tension is the answer (Mayer et al., 2010). Cortical tension, measured by outward velocities of GFP-NMY-2 foci following a cortical laser cut (cortical laser ablation, COLA) parallel to the A-P axis is uniform throughout the embryo. By contrast, the tension orthogonal to the A-P axis is twice as high in the anterior cortex as compared to the posterior one. This difference results in anisotropies that can serve as mechanical basis for cortical flows (Mayer et al., 2010). As a result of this dynamic polarization process, the *C. elegans* zygote has two distinct anterior and posterior cortical domains at the stage of pseudocleavage (Figure 4D). The maintenance of these two domains is executed through mutual inhibition between the anterior and posterior domain. First, PKC-3 phosphorylates PAR-2, thereby preventing PAR-2 from localizing to the anterior cortex (Hao et al., 2006). In turn, PAR-2, in concert with PAR-1 and PAR-5, inhibits the posterior localization of the anterior PAR complex (Hao et al., 2006). The small GTPase CDC-42 contributes to polarity maintenance by remodeling the actin cytoskeleton. Moreover, CDC-42*GTP has been shown to interact and colocalize with PAR-6 (Aceto et al., 2006; Gotta et al., 2001; Schonegg and Hyman, 2006). Furthermore, CDC-37, a member of the Hsp90 family stabilizes PKC-3 thereby helping maintaining polarity (Beers and Kemphues, 2006). Apart from these proteins, there are other associated components involved in polarity establishment and maintenance that are not discussed here (reviewed in Gönczy and Rose, 2005).

Segregation of cell fate determinants

The newly established cortical asymmetry must result in cytoplasmic asymmetries of cell fate determinants along the antero-posterior (A-P) axis in order to achieve proper developmental patterning. A few asymmetries are already present at the end of the first cell cycle, such as the distribution of MEX-5/6, PIE-1 and P-granules. Other polarity mediators and cell fate regulators become enriched in distinct cells later on during development; some of these proteins will be mentioned in the following sections.

MEX-5 and MEX-6 (from *m*uscle *ex*cess, hereafter referred to collectively as MEX-5/6) are two highly identical and partially redundant CCCH zinc finger proteins (Schubert et al., 2000). MEX-5/6 distribution show a polarity-dependent antero-posterior gradient at the time of pronuclear meeting, with higher levels in the anterior (Figure 4E; Cuenca et al., 2003; Schubert et al., 2000). Interestingly, higher mobility of MEX-5 in the posterior has been suggested to drive this gradient (Daniels et al., 2010; Tenlen et al., 2008). PAR-1 contributes to the establishment of differential

MEX-5 mobility by phosphorylating it (Griffin et al., 2011). This leads to the release of MEX-5 from RNA-binding complexes, thereby increasing its mobility specifically in the posterior side. In the anterior, reduced level of PAR-1 is overcome by dephosphorylation executed by PP2A phosphatase, leading to lower MEX-5 mobility at the anterior (Griffin et al., 2011). Furthermore, a positive feedback loop ensures proper polarity establishment. MEX-5/6 themselves promote the posterior expansion of PAR-2 and PAR-1, presumably by clearing the anterior PARs from the posterior (Cuenca et al., 2003), but the exact molecular mechanism remains elusive. MEX-5/6 are crucial for setting up soma-germline asymmetries by regulating the distribution of numerous proteins. In embryos depleted of *mex-5* and *mex-6*, the posterior enrichment of various cell fate determinants, like PIE-1, SKN-1, MEX-1, POS-1 and PAL-1 becomes symmetric (Schubert et al., 2000). Moreover, in the 4-cell stage embryo, MEX-5/6 contributes to the anterior enrichment of the Notch receptor GLP-1 (Schubert et al., 2000).

PIE-1 (*p*harynx and *i*ntestine in *e*xcess) is another CCCH zinc finger containing protein whose distribution in P_0 is the converse of MEX-5/6 (Cuenca et al., 2003; Mello et al., 1996; Reese et al., 2000): PIE-1-GFP shows posterior enrichment at the time of pronuclear meeting and is inherited in the posterior blastomeres in a polarity-dependent manner (Reese et al., 2000). Interestingly, like in the case of MEX-5/6, differential diffusion coefficients between the anterior and posterior sides are responsible for setting up the PIE-1 gradient (Daniels et al., 2010). The initial asymmetry in PIE-1 levels is further reinforced by MEX-5/6-regulated proteasomal degradation of residual PIE-1 in somatic cells (DeRenzo et al., 2003). PIE-1 is crucial for germ line development by inhibiting transcription of soma-related genes in the P-lineage and by promoting translation of maternally provided genes such as *nos-2* and *apx-1* (Mickey et al., 1996; Seydoux and Dunn, 1997; Seydoux et al., 1996; Tenenhaus et al., 2001).

P-granules are protein-RNA complexes that are important for germline specification and are analogous to the perinuclear nuage in mouse and human germ cells (reviewed in Updike and Strome, 2010). P-granule assembly in the germline is disrupted in *deps-1*, *glh-1*, *pgl-1*, and *ife-1* mutants (Amiri et al., 2001; Kawasaki et al., 1998; Spike et al., 2008a; Spike et al., 2008b) and simultaneous mutations in these four genes results in germ line underproliferation and failure in oocyte and sperm production (Amiri et al., 2001; Kawasaki et al., 2004; Spike et al., 2008a; Spike et al., 2008b). In the early embryos, P-granules dynamically localize to the posterior part of P_0 during centration/rotation and thus they are inherited by P_1 (Figure 1C and Figure 62A; Strome and Wood, 1983). Subsequently, P-granules are inherited again strictly by the P-lineage during later development. The asymmetric distribution of P-granules is under the control of A-P polarity cues (Guo and Kemphues, 1995; Tabuse et al., 1998) and immunostaining with antibodies directed against the P-granule component PGL-1 has been widely used as marker of proper polarity in the one-cell stage. Surprisingly, asymmetric distribution of P-granules is dispensible for germline development, as embryos depleted of the PP2A phosphatase regulatory subunit *pptr-1* exhibit homogenous P-granule distribution whilst the majority of the resulting worms undergo apparently normal germline development (Gallo et al., 2010). This suggests that asymmetric P-granule distribution is rather a consequence of, and not the driving force for, germline specification.

Spindle positioning

An asymmetrically dividing cell must position its spindle in a way that cell fate determinants are inherited properly by the daughter cells after cell division. As mentioned before, the first cell division of the *C. elegans* zygote is unequal, giving rise to a larger anterior and a smaller posterior cell. Spindle positioning in this zygote includes two steps: spindle orientation and spindle displacement. Centration/rotation ensures that the two centrosomes are located in the center of the embryo and aligned parallel to the A-P axis. Thus, the newly formed spindle is set up in the center with a proper orientation. Afterwards, the spindle is displaced towards the posterior part of the cell, giving rise to the characteristic excentric spindle position and unequal cleavage plane (Figure 4A).

ACTIN AND MICROTUBULES

Cytoskeletal components, namely the actin network as well as microtubules are involved in the mechanisms driving centrosome and spindle positioning.

The actin network is one of the three main types of biopolymers building up the cytoskeleton. Actin filaments (F-actin) are polarized flexible structures with a diameter of 5-9 nm composed of two parallel protofilaments twisting around each other (reviewed in Alberts et al., 2002, chapter 16). Actin filaments are most abundant in the cell periphery, thereby forming a structure called the cell cortex. Actin filaments are very dynamic and this dynamicity is regulated by several actin-associated proteins (reviewed in Allard and Mogilner, 2013; Blanchoin et al., 2014). Non-muscle myosin II is a molecular motor that binds to actin filaments and is able to move towards the plus end of the actin filament utilizing ATP hydrolysis. Major functions of F-actin include cell shape maintenance, contraction, motility and cytokinesis.

Microtubules are composed of parallel protofilaments joined laterally, thereby building up a hollow cylinder with a diameter of 25 nm (reviewed in Alberts et al., 2002, chapter 16). The protofilaments comprise globular subunits of α-tubulin and β-tubulin heterodimers. Microtubules are polarized structures possessing a more dynamic plus-end, where the heterodimers can be incorporated in the structure upon GTP-hydrolysis of β-tubulin. Microtubule nucleation occurs at the microtubule organizing centers (MTOCs) that contains the γ-tubulin ring complex (reviewed in Kollman et al., 2011). In animal cells, the main MTOC is the centrosome. Microtubules constantly undergo growth and shrinkage, leading to their dynamic instability. Plus (kinesins) and minus (dynein) end directed motor protein complexes are able to move along microtubules by hydrolyzing ATP, thereby contributing to a variety of cellular processes, such as organelle transport, nuclear migration and spindle positioning (reviewed in Roberts et al., 2013).

Forces driving centrosome and spindle positioning can be actin and/or microtubule-dependent. Thus, interfering with actin dynamics blocks meiotic spindle positioning in mouse oocytes (Li et al., 2008; Schuh and Ellenberg, 2008). By contrast, actin depolymerization does not prevent spindle positioning in *C. elegans* zygotes (Hill and Strome, 1988). However, dynamic microtubules are crucial, as treating mitotic embryos with the microtubule depolymerizing agent nocodazole leads to exaggerated spindle displacement (Gönczy et al., 2001). Conversely, stabilizing microtubules with taxol or using a temperature sensitive allele of the β-tubulin gene *tbb-1* result in more stable microtubules interferes with unequal cell division (Nguyen-Ngoc et al., 2007).

FORCES DRIVING CENTRATION/ROTATION

Nuclear positioning to the center in animal cells can be exerted in several ways (Figure 5). This includes pushing force arising from microtubule polymerization, whereby newly incorporated tubulin dimers exert force on the microtubule (Figure 5A). Minus-end directed motor proteins such as dynein are also able to move nuclei in several ways, depending on the place of anchoring. These motors can be anchored in the cytoplasm (Figure 5B), on the cortex (Figure 5C) or on the nucleus (Figure 5D) resulting in force generation and nuclear movements (reviewed in Reinsch and Gönczy, 1998). Motor proteins anchored in the cytoplasm give rise to length-dependent force, as the longer the microtubule is, the more motor proteins can bind and the more force can be generated.

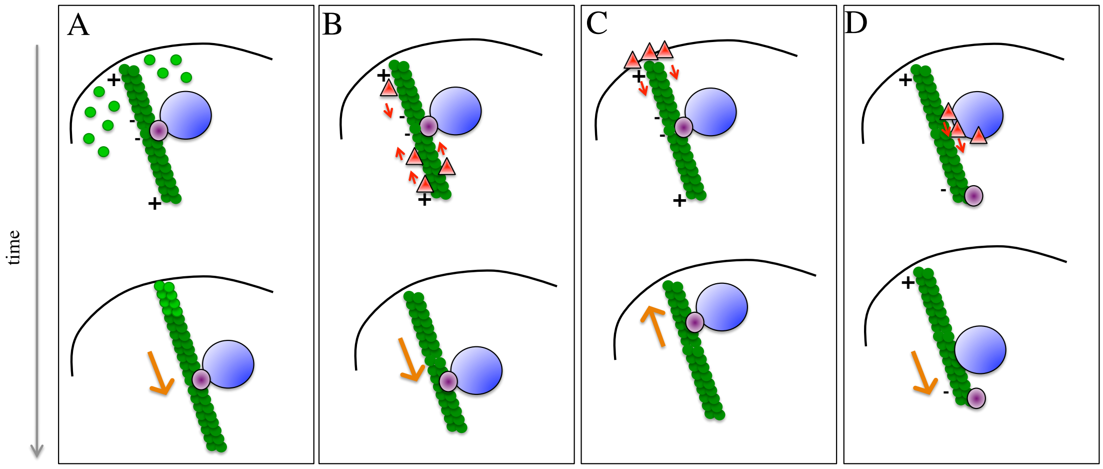

Figure 5. Different mechanisms of nuclear positioning.

Nuclear positioning can be executed by pushing force arising from microtubule polymerization (A), by minus-end directed motor proteins anchored in the cytoplasm (B) or else on the cortex (C), or by motor proteins bound to the nucleus (D). The nucleus (blue circle), the MTOC (purple circle), tubulin dimers (green circles) forming a microtubule and minus-end directed motors (red triangle) are shown. The lower image displays the resulting movement of the nucleus. The polarity of microtubules is indicated with – and + symbols. Individual motors exert force (red arrows) that result in a net force (orange arrow). Newly incorporated tubulin dimers in A are shown in bright green.

In *C. elegans*, after pronuclear meeting, the two pronuclei and the centrosomes move to the cell center. What is the nature of the forces driving this movement? At an earlier stage, computer simulation revealed that, during female pronuclear migration, forces act in a length dependent manner (Kimura and Onami, 2005). It has been postulated that similar mechanisms act during centration/rotation and that force generator entities are bound to endomembranes distributed throughout the cell (Kimura and Kimura, 2011). In this model, endomembrane movements towards the minus-end of microtubules generate an overall pulling force on the centrosome acting in the opposite direction. Depletion of DYRB-1, a light chain subunit of cytoplasmic dynein, blocks centration as well as the movements of early and late endosomes. Interfering with the early and late endosomal proteins RAB-5 or RAB-7 slows down the pace of centration without blocking it completely (Kimura and Kimura, 2011), indicating that this regulation is likely only part of the whole picture.

FORCES DRIVING SPINDLE DISPLACEMENT

Where are the forces driving spindle displacement generated? Microtubule-dependent pushing force intrinsic to the spindle (Leslie and Pickett-Heaps, 1983) or forces external to the spindle and pulling on astral microtubules (Aist and Berns, 1981; Aist et al., 1993; Berns et al., 1981) have been implicated in spindle pole separation in other systems. In the case of the *C. elegans* zygote, the latter seems to be the major source of force generation. This conclusion was drawn from experiments in which the anaphase spindle was severed by a UV laser; as a consequence, the liberated spindle poles exhibited outward movements (Figure 6; Grill et al., 2001). Moreover, centrosomal fragments following optically induced centrosomal disintegration (OICD) travelled all the way until they reached the cell periphery, indicative of cortically based force generation (Grill et al., 2003). Thus, as opposed to pronuclear migration and centration/rotation, where length-dependent forces participate in driving centrosome movements, cortically driven forces drive metaphase/anaphase spindle positioning.

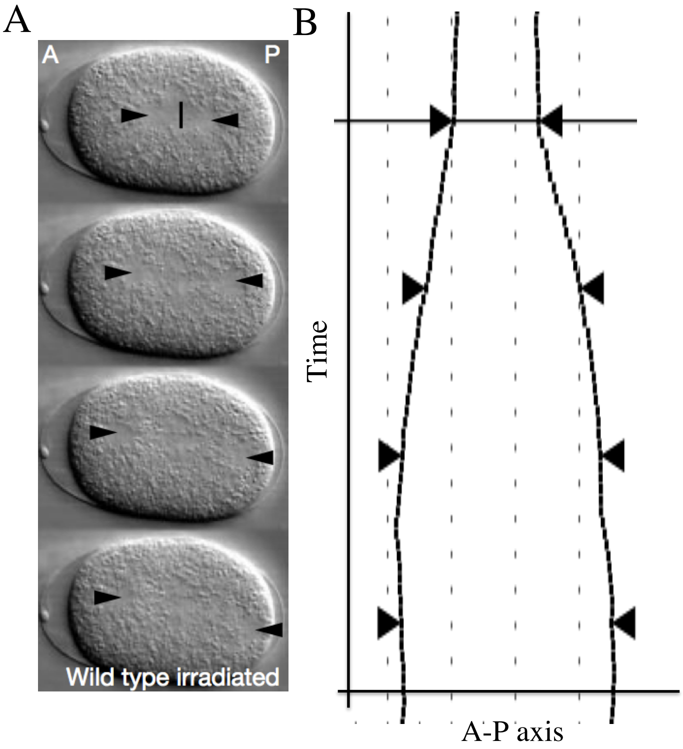

Figure 6. Spindle severing experiment to estimate the extent of pulling forces acting on spindle poles during anaphase
A Spindle pole movements after spindle severing (black line). The triangles indicate the position of the two spindle poles.
B Kymograph of spindle pole tracking, the y-axis corresponds to time, the x-axis represents the A-P axis. Tracking the movements of the spindle poles reveals difference in velocity on the anterior and posterior sides. Modified from Grill 2001).

Interestingly, the spindle severing experiments also revealed that the posterior spindle pole moves towards the cortex with a higher velocity as compared to the anterior one and that this difference is under A-P polarity control (Figure 6; Grill et al., 2001). This indicated that net cortical pulling forces acting on the posterior spindle pole are higher than those on the anterior one, explaining the root of posterior spindle displacement. Further experiments demonstrated that a higher number of active force generating units functioning at the posterior cortex is responsible for such an imbalance in pulling forces (Grill et al., 2003). Interestingly, the sites of active force generation can be visualized as membrane invaginations upon partial disruption of the acto-myosin network (Redemann et al., 2010). Such invaginations are dependent on microtubules and occur more frequently at the posterior side in a polarity dependent manner.

CORTICAL FORCE GENERATOR COMPLEX

During the last decade or so, mutational analyses and RNAi-based screens lead to the identification of components involved in the generation of pulling force during mitosis. These studies revealed the existence of a conserved force generator protein ensemble located at the cell cortex (Figure 7). The α-subunits of two heterotrimeric G proteins have been identified as members of these complexes (Afshar et al., 2004; Colombo et al., 2003; Gotta and Ahringer, 2001; Grill et al., 2003). This is illustrated by the fact that simultaneous depletion of the two partially redundant Gα subunits GOA-1 and GPA-16 impairs pulling forces and leads to equal first cell division (Colombo et al., 2003; Gotta and Ahringer, 2001). These Gα proteins form a so called ternary complex together with the two nearly identical GoLoco containing proteins GPR-1 and GPR-2 (hereafter referred to collectively as GPR-1/2) and the coiled-coil protein LIN-5 (Colombo et al., 2003; Couwenbergs et al., 2007; Gönczy et al., 2000; Gotta and Ahringer, 2001; Gotta et al., 2003; Nguyen-Ngoc et al., 2007; Park and Rose, 2008; Srinivasan et al., 2003; Tsou et al., 2003). Similarly to double Gα depletion, inactivation of GPR-1/2 or LIN-5 function results in diminished pulling forces and equal cell division (Colombo et al., 2003; Couwenbergs et al., 2007; Gotta et al., 2003; Nguyen-Ngoc et al., 2007; Srinivasan et al., 2003). Biochemical studies established that the GDP-bound Gα proteins associate with GPR-1/2, which in turn binds to LIN-5 (Couwenbergs et al., 2007; Nguyen-Ngoc et al., 2007; Park and Rose, 2008). Apart from providing the basis of force generation during mitosis, the ternary complex also contributes to centration/rotation (Goulding et al., 2007; Park and Rose, 2008).

The analysis of immunostained embryos revealed that some components of the ternary complex exhibit a non-uniform cortical localization during mitosis. While the cortical levels of GOA-1 and GPA-16 seem to be similar throughout the cell cortex (Afshar et al., 2004; Afshar et al., 2005; Gotta and Ahringer, 2001; Miller and Rand, 2000; Park and Rose, 2008), GPR-1/2 displays a slight asymmetry in anaphase, showing higher enrichement at the posterior (Colombo et al., 2003; Gotta et al., 2003; Tsou et al., 2003 and Figure 29). As far as LIN-5 is concerned, ~50% of the embryos exhibit higher relative posterior cortical enrichment, as compared to the anterior cortex, while the rest show high levels on both cortices of the cell (bipolar pattern) (Park and Rose, 2008). Why LIN-5 does not mirror the localization of GPR-1/2 is so far unresolved. During centration/rotation, both LIN-5 and GPR-1/2 are more enriched on the anterior cortex, correlating with the direction of force at that stage (Park and Rose 2008). Extra copies of GPR-1 in a transgenic lines expressing YFP-

GPR-1 result in exaggerated centrosomal movements during centration/rotation and to increased net pulling forces at anaphase (Redemann et al., 2011). This suggests that tight regulation of GPR-1/2 levels is crucial for the establishment of proper pulling forces.

How can the ternary complex generate cortically based force along astral microtubules? Dynein activity is crucial for this to occur. Embryos with diminished dynein activity or depleted of the associated proteins LIS-1 and DYRB-1 exhibit diminished pulling forces during mitosis (Couwenbergs et al., 2007; Nguyen-Ngoc et al., 2007). Importantly, the cortical localization of the dynein heavy chain DHC-1 and that of LIS-1 depend on the ternary complex (Nguyen-Ngoc et al., 2007). Furthermore, LIN-5 and GPR-1/2 co-immunoprecipitates with the dynein complex, with GPR-1/2 being dispensible for LIN-5-dynein association, whereas LIN-5 is needed for forming the GPR-1/2-dynein complex (Nguyen-Ngoc et al., 2007). The current model posits that mirystoylated Gα anchors GPR-1/2 associated with LIN-5 to the plasma membrane, thus creating a bridge between the dynein complex and the plasma membrane (Figure 7).

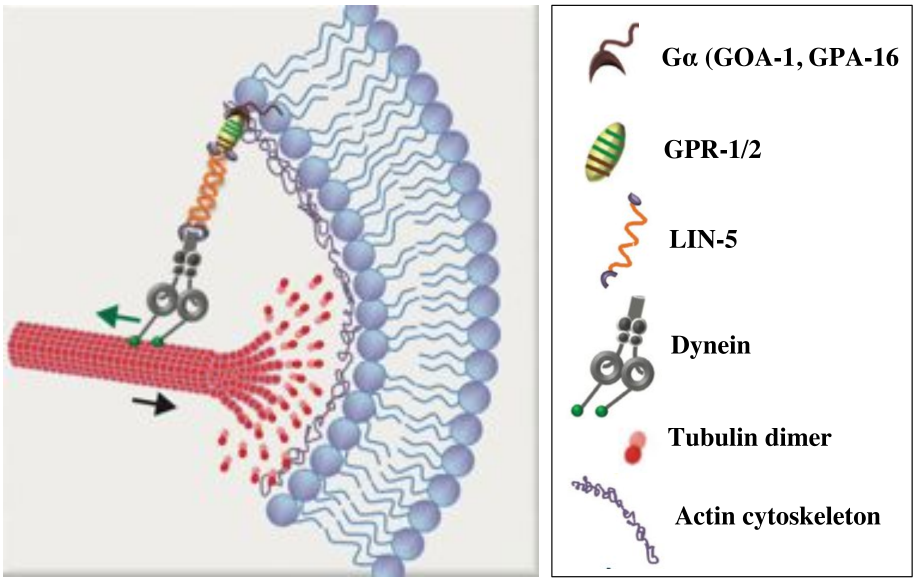

Figure 7. Model of cortical force generation. See text for details. Adapted from Kotak and Gönczy, 2013.

A convenient phenotypic readout of asymmetric force generation during anaphase is the vigorous oscillation of the posterior spindle pole that takes place as posterior spindle displacement is occuring (Figure 20A). Embryos lacking one copy of the Gα proteins fail to undergo vigorous posterior oscillation, whereas spindle displacement is not affected and the cell division remains unequal as in the wild type (Afshar et al., 2005). Similarly, gradual decrease of the levels of the dynein light intermediate chain DLI-1 or of GPR-1/2 prevents posterior spindle pole oscillation, whilst the division is unequal (Pecreaux et al., 2006). This suggests that different thresholds in the levels of cortical force generator components operate for spindle displacement and for posterior oscillation, with the latter requiring more than the former.

How could dynein exert pulling force on astral microtubules? Two scenarios can be envisaged. First, dynein could function as a molecular motor by attempting to move towards the minus end of microtubules; however, dynein being anchored to the cortex, this attempt generates a pulling force on the astral microtubule instead. Alternatively, dynein could serve as coupling device that holds onto the microtubule plus ends and the pulling force generated by virtue of microtubule depolymerization. Modeling experiments of spindle displacement revealed that each force generator can exert a force of ~50 pN, which is in the range of that generated by a single depolymerizing microtubule, but almost a magnitude higher than the force deployed by a single dynein motor (Kozlowski et al., 2007). This suggests that dynein rather may rather serve as a coupling device and that the driving force for spindle displacement is generated by microtubule depolymerization. This is in accordance with the finding that preventing microtubule dynamics leads to the diminution of pulling forces (Nguyen-Ngoc et al., 2007). Supporting this model, purified dynein from yeast bound to the edge of micro-fabricated chambers captures microtubules and promotes microtubule catastrophe, thereby resulting in microtubule depolymerization (Laan et al., 2012).

REGULATION OF FORCE GENERATION

Regulation exerted by individual proteins

Several proteins have been identified that influence the force generation machinery (Figure 8). As expected, the asymmetric enrichment of GPR-1/2 is under the control of A-P polarity (Colombo et al., 2003; Gotta et al., 2003; Park and Rose, 2008; Tsou et al., 2003). Regulation at the level of the heterotrimeric G-proteins is also important. Single depletion of GPA-16 or of GOA-1 results in reduced GPR-1/2 cortical signal (Afshar et al., 2005), whereas double depletion of these proteins leads to the absence of GPR-1/2 at the cortex (Colombo et al., 2003) and to equal cell division. In the absence of RIC-8, a protein acting as a Guanine nucleotide exchange factor (GEF) for GOA-1 and that is needed for cortical GPA-16 enrichment, cortical GPR-1/2 recruitment is reduced (Afshar et al., 2004). A G-protein activator factor (GAP) has also been shown to modulate force generation at the level of GOA-1. Indeed, loss of the GAP protein RGS-7 leads to lower net pulling forces on the anterior side (Hess et al., 2004). In other systems, Gα proteins associate with β and γ subunits to form an inactive complex. In *C. elegans*, the β subunit GPB-1 and the γ subunit GPC-2 negatively regulate spindle positioning, as depletion of either of these two components results in excess centrosome movements during centration/rotation and in higher net pulling forces during anaphase (Afshar et al., 2004; Afshar et al., 2005; Tsou et al., 2003). This increase in pulling forces correlates with increased cortical GPR-1/2 levels at the anterior in *gpb-1(RNAi)* embryos during centration/rotation (Thyagarajan et al., 2011; Tsou et al., 2003). Importantly, depletion of the Gα components rescues the excess movements observed in *gpb-1(RNAi)* (Tsou et al., 2003), indicating that GPB-1 acts via negative regulation of the Gα proteins, and not through an independent mechanism.

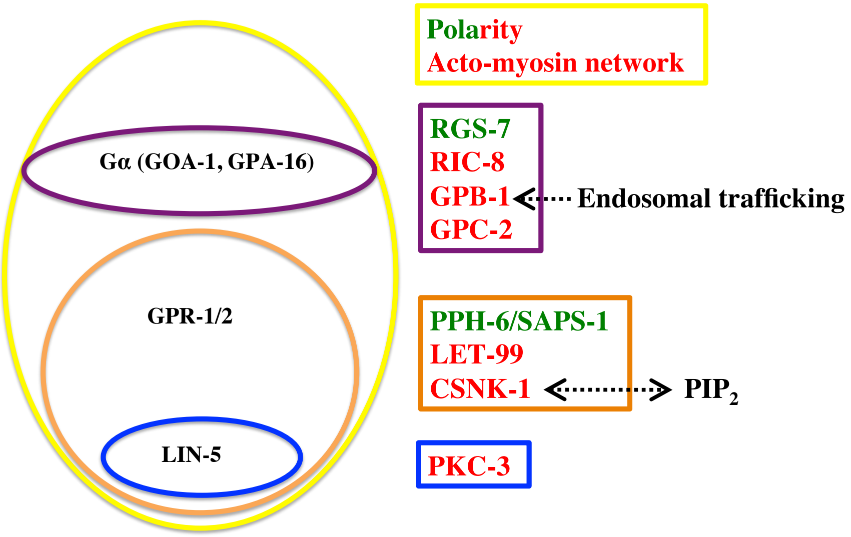

Figure 8. Regulators of force generation in *C.elegans* one-cell stage embryos.
Regulation occurs at the level of the entire ternary complex (yellow), at the level of the Gα proteins (purple), influencing GPR-1/2 and LIN-5 (orange) or impinging on LIN-5 *per se* (blue). Positive regulators are shown in green, negative regulators in red. Disruption of

polarity can lead to increase or decrease in pulling forces, depending on which complex is compromised. See text for details.

Regulation occurs also at level of LIN-5 and GPR-1/2 distribution (Figure 8). The DEP-domain protein LET-99 is enriched in a posterio-lateral band and negatively regulates pulling forces during centration/rotation and anaphase (Krueger et al., 2010; Tsou et al., 2002; Tsou et al., 2003). In wild type embryos, GPR-1/2 and LIN-5 signals are lowest in the region where LET-99 is highest and, suggestively, *let-99(RNAi)* leads to higher than normal anterior GPR-1/2 and LIN-5 levels during centration/rotation and to uniform distribution at anaphase (Krueger et al., 2010; Park and Rose, 2008; Tsou et al., 2003). How the absence of two lateral bands of LET-99 at the posterior can have an impact on the anterior cortex is an intriguing and so far unresolved question.

Two kinases and one phosphatase are also part of the list of proteins that impinge on the force generation complex. Thus, PKC-3-mediated phosphorylation of four LIN-5 Ser residues has been shown to have an impact on force generation (Galli et al., 2011). In accordance with the anterior localization of PKC-3, immunostaining with phospho-specific antibody recognizing one of the four Ser residues revealed that P-LIN-5 decorates the anterior cortex of the cell. Moreover, LIN-5 phosphorylation by PKC-3 is dependent on the mitotic master regulator CDK-1. The phosphorylation status of these residues appear to be functionally relevant, as expression of non-phosphorylatable LIN-5 4A in the absence of endogenous LIN-5 leads to exaggerated oscillatory movement during centration/rotation and to an increase in anterior pulling forces. Conversely, introducing phosphomimetic mutations causes decreased oscillation during mitosis, although this experiment was performed at 16°C, where forces have been demonstrated to be lower (Johnston et al., 2008). Of note, this phenotype differs from *lin-5(RNAi)*, as the division remains unequal, indicating that PKC-3-mediated phosphorylation is not the sole mechanism ensuring proper LIN-5 distribution and activity (Galli et al., 2011).

The casein kinase Iγ CSNK-1 functions as another regulator of LIN-5 and GPR-1/2 levels, as well as of GPR-1/2 asymmetry (Panbianco et al., 2008). *csnk-1(RNAi)* leads to excess centrosome movements during centration/rotation and to higher pulling forces at anaphase. GPR-1/2 and LIN-5 levels are increased in embryos depleted of CSNK-1. CSNK-1 is enriched in the anterior cell membrane, and it is necessary for the posterior enrichment of its potential substrate, the PI(4)P5 kinase PPK-1. PPK-1 generates PtIns(4,5)P_2 and it is plausible that PPK-1 influences spindle positioning by regulating the distribution of PIP_2 in an asymmetric manner. However, such asymmetry has not been reported using the PIP_2 biomarker GFP-PH(PLC1d1) (Audhya et al., 2005). It is speculated that creating homogenous PPK-1 distribution in *csnk-1(RNAi)* changes the lipid composition in the anterior, thus influencing GPR-1/2 levels, but how such regulation may occur at the molecular level remains to be investigated. The identification of the potential molecular link between phospholipid composition and the distribution of the force generator complex will definitely be an exciting discovery.

The phosphatase PPH-6 and its associated partner SAPS-1 positively regulate force generation (Afshar et al., 2010). Depletion of *pph-6* or *saps-1* results in decreased GPR-1/2 and LIN-5 cortical levels, reduced posterior pulling forces, as well as in the lack of posterior spindle pole oscillations. How the action of this phosphatase is executed mechanistically is not yet known, but, interestingly, the PPH-6/SAPS-1 complex seems to act downstream of CSNK-1, as simultaneous depletion of *saps-1* and *csnk-1* results in phenotypes analogous to that of *saps-1(RNAi)* (Afshar et al., 2010).

Regulation by more general mechanisms

Regulation by intracellular trafficking

Intracellular trafficking enables exchange between different endomembrane compartments within a eukaryotic cell. Intracellular trafficking involves the secretory, the endocytic and the recycling pathways (reviewed in Doherty and McMahon, 2009; Glick and Nakano, 2009; Mayor and Pagano, 2007; Stolz and Wolf, 2010). The main components of the secretory pathway are the endoplasmic reticulum (ER) and the Golgi network, which are responsible for the delivery of proteins to the plasma membrane. The endocytic pathway is involved in the uptake of molecules from the extracellular space or from the plasma membrane. The recycling pathway is responsible for the replenishment of molecules onto the plasma membrane. There are several endocytic pathways, including the clathrin mediated endocytosis pathway. In this case, clusters of cargos molecules are surrounded with clathrin and its adaptor proteins. Clathrin heavy chain, by its remarkable triskelion structure, is able to self-assemble into a structure that allows the invagination and finally the budding of these clathrin-coated pits from the plasma membrane (reviewed in Brodsky et al., 2001; Kirchhausen, 2000). The clathrin coated vesicles then fuse with the early endosomes where the decision is made concerning the next step; the vesicles can undergo lysosome-mediated degradation, be transported to the Golgi network or be recycled to the plasma membrane (reviewed in Bonifacino and Rojas, 2006; Grant and Donaldson, 2009; Hsu and Prekeris, 2010; Johannes and Popoff, 2008).

Several instances are known at present where intracellular trafficking is important for various processes in the *C. elegans* zygote. Polarity, for instance, is influenced by some of the component of the endosomal network. Thus, dynamin, a protein taking part in an early step of endocytic vesicle formation and in membrane fission, is needed for proper polarity maintenance (Nakayama et al., 2009). Upon *dyn-1* depletion, embryos display decreased level of PAR-6 in the anterior, concomitant with an expansion of the PAR-2 domain. On the other hand, depletion of RAB-11, a protein that functions in recycling endosomes, cause the opposite effect, with an expansion of the PAR-6 domain and a smaller PAR-2 domain (Zhang et al., 2008). Early endosomes are also implicated in regulating polarity. Interfering with the early endosomal protein RAB-5 results in a subtle change in cortical dynamics of GFP-PAR-6, but without alteration in PAR-2 localization (Hyenne et al., 2012). Interestingly, both early and recycling endosomes, as well as the ER are enriched at the anterior side of the zygote (Andrews and Ahringer, 2007; Balklava et al., 2007; Poteryaev et al., 2005). The asymmetric enrichment of these components is A-P polarity dependent. Moreover, the anterior PAR complex and CDC-42 regulate endocytosis (Balklava et al., 2007). Together, these observations suggest that multidirectional regulation operates between the PAR proteins, the endosomal network and components influenced by intracellular trafficking.

What components are influenced by intracellular trafficking? An example is offered by the intracellular trafficking of the Gβ subunit GPB-1. As mentioned before, embryos depleted of GPB-1 show elevated GPR-1/2 levels on the anterior side of the cell (Tsou et al., 2003). Importantly, the levels of GPB-1 on the cell membrane is tighly regulated by intracellular trafficking ensuring low cortical GPB-1 levels during mitosis (Thyagarajan et al., 2011). GPB-1 associates both with early and recycling endosomes, raising the possibility that GPB-1 cortical level is regulated by dynamic trafficking. In support of this hypothesis, inactivation of RAB-5 or of dynamin leads to polarity-dependent asymmetric GPB-1 accumulation in the cytoplasm, with more accumulation in the anterior side. It has been proposed that this asymmetric nature of GPB-1 trafficking influences GPR-1/2 cortical level, likely through modulating the availabilty of the active GDP-bound form of Gα proteins for interaction with GPR-1/2 (Thyagarajan et al., 2011).

Regulation by the acto-myosin network

The acto-myosin network influences several processes in the one-cell stage *C. elegans* embryo. As mentioned before, the acto-myosin network is responsible for setting up polarity in the zygote, thereby contributing to proper pulling forces and asymmetric cell division (Guo and Kemphues, 1996; Hill and Strome, 1988; Shelton et al., 1999). Experiments using time resolved drug treatments targeting the actin network were developed to address the involvement of the actin network in force generation after polarity establishment. Depolymerizing the actin network with Latrunculin A or Cytochalasin D leads to elevated pulling forces and increased spindle pole oscillations at the anterior (Afshar et al., 2010; Berends et al., 2013). In these conditions, however, the cortical levels of LIN-5 are not altered (Berends et al., 2013). It is thus clear that the actin network is a negative regulator of forces in the anterior during mitosis, but how this regulation occurs is not yet known. Interestingly, computer simulation experiments investigating the nature of spindle displacement predicted that lowering cortical rigidity, i.e. the strength of the acto-myosin network initially increases spindle pole oscillation, whereas further decrease in the rigidity dampens oscillation (Kozlowski et al., 2007). However, the involvement of the acto-myosin network in regulating centration/rotation might differ from its role during anaphase. Intriguingly, cortical GFP-NMY-2 foci display short-range anterior-directed movements during centration/rotation that were implicated in force generation (Goulding et al., 2007). In accordance with this hypothesis, partial depletion of *nmy-2* lowers the pace of centration/rotation. Furthermore, apart from the effect on mitotic pulling forces, NMY-2 organization at the time of female pronuclear migration is defective in embryos depleted of PPH-6 and SAPS-1 (Afshar et al., 2010), possibly explaining the lack of pseudocleavage in these embryos. Whether this function of the PPH-6/SAPS-1 complex is linked to its role during spindle positioning or distinct from it remains to be investigated.

In summary, these regulatory mechanisms illustrate that the molecular events driving spindle positioning in *C. elegans* are thought to act strictly at the protein level and mRNA-based mechanisms have not been implicated in this process. This is surprising given that spatially restricted mRNA localization coupled with regulated translation have been shown to influence polarity-related processes in other systems (see next chapter). During the course of this thesis work, we provided evidences that the 'protein-hegemony' dogma does not entirely hold for one-cell stage *C. elegans* embryos, as localization of *lin-5* mRNA may be an important positive regulator of spindle positioning (see pages 55-84).

Asymmetric cell division and spindle positioning in other systems

Functional homologues of the ternary complex components are crucial for cortical dynein anchoring and thereby are involved in spindle positioning in other systems as well. Thus, the GPR-1/2 homologue Pins and the LIN-5 homologue Mud are implicated in asymmetric cell division of *Drosophila* neuroblasts (reviewed in Sousa-Nunes and Somers, 2013). Likewise, LGN (GPR-1/2 homologue) and NuMA (a LIN-5 homologue) function to position the mitotic spindle in human cells (reviewed in Kotak and Gönczy, 2013). A thorough understanding of the mechanisms governing spindle positioning will likely arise from comparing and contrasting findings from different systems. The mechanisms involved in asymmetric cell division and spindle positioning in *Drosophila* larval neuroblasts and in mammalian systems are introduced below (Figure 9).

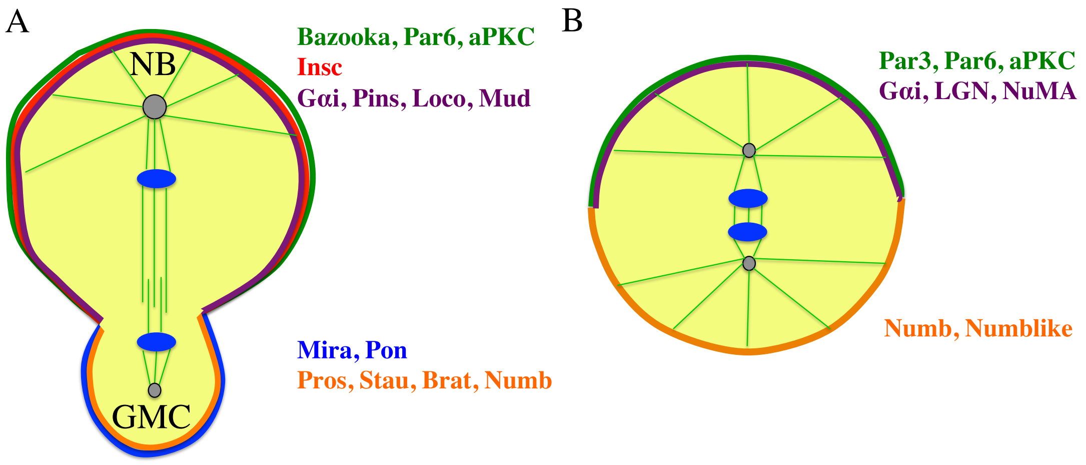

Figure 9. Division of a *Drosophila* neuroblast and of a polarized mammalian cell
The components important for cleavage plane specification and cell fate determinant segregation in *Drosophila* neuroblast (A) and in a polarized mammalian cell (B). Details are in the text.

The *Drosophila* neuroblast

The diversity of the *Drosophila* central nervous system stems in part from several rounds of asymmetric cell divisions of neuroblasts in the developing brain. Type I neuroblasts undergo 12 cycles of asymmetric cell divisions before entering into quiescence in the embryo (Bossing et al., 1996) Hartenstein et al., 1987). Afterwards, in the larva, these cells divide again asymmetrically to give rise to neurons in the adult fly (Ito and Hotta, 1992). The embryonic neuroblasts delaminate from ectodermal epithelium, retaining their A-P polarity, while larval neuroblast gain apico-basal polarity in an unclear manner (reviewed in Campos-Ortega, 1993; Homem and Knoblich, 2012). A neuroblast divides asymmetrically and unequally: the larger apical cell, called neuroblast (NB) retains stem cell fate and gives rise to an other round of asymmetric cell division, while the smaller basally located cell (named ganglion mother cell, GMC) differentiates into glial cell or neuron after subsequent divisions (Figure 9A).

The establishment of these fates is due to the asymmetric segregation of cell fate determinants along the apico-basal axis, driven by two apical complexes. The first complex comprises Par3 (Bazooka in *Drosophila*), Par6 and the atypical protein kinase C (aPKC) (Petronczki and Knoblich, 2001; Wodarz et al., 2000; Wodarz et al., 1999). This complex is linked to the second complex by the adaptor protein Inscutable (Insc) that interacts with both PAR-3 and Pins, a member of the second apical complex (Kraut and Campos-Ortega, 1996; Kraut et al., 1996; Parmentier et al., 2000; Schaefer et al., 2001; Schober et al., 1999; Wodarz et al., 2000; Yu et al., 2000). Intriguingly, *insc* mRNA localizes as well to the apical complex, but this localization is dispensable for protein localization (Knoblich et al., 1999; Li et al., 1997). Thus the role of *insc* mRNA localization, if any, is unclear. The second apical complex comprises the heterotrimeric G-protein subunit Gαi, Partner of Inscutable (Pins), Locomotive defects (Loco) and the coiled coil domain protein Mud (Bowman et al., 2006; Izumi et al., 2006; Siller et al., 2006). Pins and Loco function as GDI for Gαi and thus stabilize the GDP-bound form of Gαi (Parmentier et al., 2000; Schaefer et al., 2001; Schaefer et al., 2000; Yu et al., 2000; Yu et al., 2005), thereby promoting its activity. The Pins-Gαi complex is needed for proper spindle orientation (Schaefer et al., 2000; Yu et al., 2002). Furthermore, depleting the Gβ protein, Gβ13F or the Gγ subunit Gγ1 also results in severe defects in asymmetric cell division (Fuse et al., 2003; Schaefer et al., 2001; Yu et al., 2003). This implicates that, similarly to *C. elegans,* Gβ proteins influence spindle positioning in *Drosophila*, but whether the mechanisms are the same remains unclear. Interestingly, unlike in *C. elegans*, the Gαi-Pins complex is necessary for proper polarity in neuroblasts (Parmentier et al., 2000; Schaefer et al., 2000; Yu et al., 2000; Yu et al., 2005).

What are the downstream effectors whose asymmetric distribution is regulated by the PAR-Gαi complex? These include the proteins Prospero (Pros), Brain tumor (Brat), Staufen, Numb and Partner of Numb (Pon), which all segregate in the GMC during division and play crucial roles in defining the GMC fate. The homeobox transcription factor Pros serves as a binary switch in the GMC, where it represses genes responsible for proliferation and self-renewal (such as cyclin E, cdc25/String) and switches on genes required for differentiation (Choksi et al., 2006; Doe et al., 1991; Hirata et al., 1995; Knoblich et al., 1995; Li and Vaessin, 2000; Southall and Brand, 2009; Spana and Doe, 1995). Interestingly, apart from Pros protein, *pros* mRNA is also enriched in the GMC after cell division, driven by the asymmetric segregation of the mRNA-binding protein Staufen that binds to the 3' UTR of *pros* mRNA (Broadus et al., 1998; Schuldt et al., 1998). Brat likewise shows enrichment in the GMC where it downregulates Myc expression (Bello et al., 2006; Betschinger et al., 2006; Lee et al., 2006b). The phosphotyrosine binding protein Numb together with its adaptor protein Pon inhibit Notch signaling in the GMC, thereby contributing to its fate (Lu et al., 1998; Rhyu et al., 1994; Uemura et al., 1989).

What are the mechanisms ensuring the asymmetric segregation of these components? Two pathways have been identified. First, the basal distribution of Pros, Brat and Staufen is regulated by their interaction with the basally enriched adaptor protein Mira (Figure 1D, (Betschinger et al., 2006; Ikeshima-Kataoka et al., 1997; Lee et al., 2006b; Matsuzaki et al., 1998; Schuldt et al., 1998; Shen et al., 1997). The N-terminal of Mira interacts with Insc, while Pros, Brat and Staufen bindings sites were mapped in the Mira C-terminal region (Fuerstenberg et al., 1998; Shen et al., 1998). Interestingly, *mira* mRNA is also asymmetrically localized in neuroblast, but, surprisingly, it is enriched in the apical side of the cell (Schuldt et al., 1998). Given the opposite distribution pattern of Mira mRNA and protein, it is postulated that Mira translation occurs on the apical side and that newly synthesized Mira protein rapidly relocalizes to the basal cortex (Erben et al., 2008). Mira is enriched in the basal cortex from prometaphase onwards in a manner that depends on actin, myosin II (Zipper) and myosin VI (Jaguar) (Barros et al., 2003; Petritsch et al., 2003; Shen et al., 1997), thereby promoting the asymmetric distribution of its cargos, Pros, Brat and Staufen. After mitosis, the release of the cargo proteins is achieved through the degradation of Mira (Matsuzaki et al., 1998; Schuldt et al., 1998; Shen et al., 1998). The second pathway ensures correct distribution of Numb by asymmetrically segregating the adaptor protein Pon (Lu et al., 1998). In the beginning of mitosis, Pon is distributed throughout the whole cell cortex, and becomes gradually enriched in the basal cortex (Lu et al., 1999). The apical clearance of Pon is mediated by phosphorylation exerted by Polo kinase (Wang et al., 2007). Although *insc* mutations result in aberrant Mira and Pon distribution at metaphase, this defect is corrected at telophase by a mechanism known as telophase rescue (Peng et al., 2000; Schober et al., 1999; Wodarz et al., 1999).

How is polarity linked to the segregation of Mira and its downstream effectors? Neuroblasts harboring mutation in the gene lethal giant larvae (Lgl) exhibit normal polarity but disturbed segregation of Mira and Pon (Ohshiro et al., 2000; Peng et al., 2000), suggesting that Lgl is an important component. aPKC-mediated phosphorylation plays a crucial in regulating Lgl localization. Prior to mitosis, Lgl is associated with Par6 and aPKC in the apical cortex. Upon aPKC activation by the mitotic Ser/Thr kinase Aurora A, aPKC phosphorylates Lgl, which results in its removal from the apical cortex (Betschinger et al., 2005; Wirtz-Peitz et al., 2008). In the absence of Lgl, Par3 associates with the complex that recruits and phosphorylates Numb. Phospho-Numb relocates to the cytoplasm and then with the help of Zipper finally becomes enriched in the basal cortex (Lee et al., 2006a; Smith et al., 2007; Strand et al., 1994; Wang et al., 2006; Wirtz-Peitz et al., 2008).

To ensure the proper segregation of the above-mentioned cell fate determinants, the mitotic spindle must be aligned along the apico-basal axis. Following delamintaion from the epithelium, the spindle in the neuroblast becomes oriented along the A-P axis by undergoing a 90° rotation (Kaltschmidt et al., 2000). As the position of the centrosomes remains aligned along the apico-basal axis following the first cell division, subsequent NB divisions do not require spindle rotation (Rebollo et al., 2009). Reduced levels of Gαi, Pins, Mud or of the lissencephaly related protein Lis1 cause spindle orientation defects, while polarity is unaffected in these cases, indicating that these components act more specifically to regulate spindle positioning (Bowman et al., 2006; Cabernard and Doe, 2009; Izumi et al., 2006; Parmentier et al., 2000; Schaefer et al., 2001; Schaefer et al., 2000; Siller et al., 2006; Siller and Doe, 2008; Yu et al., 2000). The centrosomal protein Ana2 contributes to Pins-independent Mud localization through an interaction with the dynein light chain protein Cut up (Wang et al., 2011). Moreover, the Pins-interacting PDZ domain protein Canoe is also important for cortical Mud recruitment by interacting with RanGTPase through its Ras association domain (Speicher et al., 2008; Wee et al., 2011). A model operating with cortically anchored dynein/dynactin exerting a pulling force on astral microtubules emanating from the apical centrosome has been put forth, reminiscent of the spindle positioning mechanisms acting in the *C. elegans* zygote (reviewed in Siller and Doe, 2009).

The missegregation of the cell fate determinants described above lead to deleterious effects, such as overproliferation and tumor formation (Betschinger et al., 2006; Lee et al., 2006b). Based on this and related findings, it is believed that correct cell fate determination executed by asymmetric cell division functions as a tumor suppressor mechanism.

Mammalian systems

Although less well documented as compared to invertebrate model organisms, asymmetric cell division and spindle positioning have been investigated during mammalian development and in cell culture (Figure 9B).

Asymmetric cell divisions occur extensively in the developing vertebrate cerebral cortex. The progenitor cells in the ventricular zone of the brain can divide symmetrically, giving rise to two progenitors, or asymmetrically leading to the birth of one progenitor cell and of one cell that differentiates into a neuron. The symmetric divisions are present mostly during early embryogenesis, while the asymmetric cell divisions occur thereafter. Spindle orientation with respect to the plane of the neuroepithelium does not always correlate with the division being symmetric or asymmetric (reviewed in Huttner and Brand, 1997). In some instances, divisions perpendicular to the neuroepithelium lead to asymmetric cell divison (Chenn and McConnell, 1995; Haydar et al., 2003; Noctor et al., 2004), but divisions parallel to the neuroepithelium have also been observed in both cases (Konno et al., 2008). The players involved in spindle positioning in invertebrate systems seem to be conserved in mammals. Thus, the progenitors are polarized through a Par3/Par6/aPKC-rich apical domain (Manabe et al., 2002). Par3 interacts with Numb and drives its apical enrichment (Bultje et al., 2009). In the absence of Numb or of its interacting protein Numblike, overproduction of neurons in the forebrain or reduction in the number of differentiated motoneurons is observed (Petersen et al., 2004; Zhong et al., 1996; Zilian et al., 2001). Inscutable is important for establishing the plane of division in the retina, where the spindle is normally oriented perpendicular to the neuroepithelium, as interfering with Insc causes the plane of division to be parallel to the neuroepithelium and disrupts cell fate (Zigman et al., 2005). Interfering with the $\beta\gamma$ subunits of the heterotrimeric G proteins alters the division plane and leads to overproduction of differentiated neurons (Sanada and Tsai, 2005). Here, AGS3, a homologue of GPR-1/2 and Pins promotes dissociation of $G\beta\gamma$ from $G\alpha$, and reduction of AGS3 levels phenocopies the depletion of $G\beta\gamma$ (Sanada and Tsai, 2005). Similarly, depletion of LGN, a protein related to GPR-1/2, and Pins, also leads to spindle misorientation (Konno et al., 2008; Shitamukai et al., 2011). Moreover, centrosomal proteins also influence spindle positioning. Thus, loss of the human ortholog of the abnormal spindle gene Aspm or of the Lis-1interacting protein mNde1 lead to defects in cleavage plane orientation, to a progressive decrease in the number of progenitor cells and finally to a smaller cerebral cortex, resulting in a condition termed microcephaly (Bond et al., 2002; Feng and Walsh, 2004).

An attractive system to study asymmetric spindle positioning in mammals is the developing mouse skin (Figure 1E; reviewed in Fuchs and Raghavan, 2002). During early development, cell divisions parallel to the underlying membrane produce a large number of progenitor cells that divide later in a perpendicular manner to produce basal and suprabasal cells. The former retains proliferative potential, while the latter differentiates into a specific cell type. Perpendicular divisions thus drive morphogenesis (stratification) of the skin. Mouse inscutable (mInsc) interacts at the apical membrane with Par3 and LGN, and they all form an apical crescent in mitotic cells (Lechler and Fuchs, 2005). The choice of a given cell to undergo symmetric or asymmetric cell division is determined by the apical localization of mInsc and NuMA (Poulson and Lechler, 2010). Furthermore, depleting LGN, NuMA or dynactin leads to aberrant spindle orientation and to defects in cell fate determination via the loss of the stratification-promoting Notch signaling (Williams et al., 2011).

Cell biological studies allied with the power of biochemical techniques in cultured cells largely contributed to understanding the mechanisms ensuring spindle positioning. As mentioned before, the ternary complex related to the Gα-GPR-1/2-LIN-5 and the Gαi/Pins/Mud complex is composed of Gαi-LGN-NuMA in human cells. This complex is important in regulating spindle positioning in polarized vertebrate cells (Du and Macara, 2004; Peyre et al., 2011; Williams et al., 2011; Zheng et al., 2010) and in non-polarized HeLa cells relative to a fibronectin substratum (Kiyomitsu and Cheeseman, 2012; Kotak et al., 2012; Woodard et al., 2010). The cortical enrichment of NuMA is prevented by phosphorylation by the mitotic kinase CDK1. The proportion of phosphorylated NuMA decreases as CDK1 activity drops at the metaphase to anaphase transition, leading to elevated non-phosphorylated NuMA in anaphase. This provides a temporal switch for establishing proper cortical dynein levels and robust spindle positioning (Kotak et al., 2013). Moreover, the polo-like kinase Plk1 negatively regulates dynein by inhibiting its interaction with the ternary complex during metaphase (Kiyomitsu and Cheeseman, 2012). Like in *C. elegans*, the downstream effector dynein is linked to the ternary complex through interaction with NuMA (Kiyomitsu and Cheeseman, 2012; Kotak et al., 2012; Merdes et al., 1996), and it is believed that the sole function of the ternary complex is to anchor dynein to the cortex (Kotak et al., 2012).

1B. Polarized mRNA localization and translational control

Zygotic transcription is usually not active during the early steps of embryogenesis, and localization of maternal mRNAs and the regulation of their translation are widespread mechanisms utilized to drive early embryonic processes in many systems. The importance of mRNA localization can be appreciated for instance by the fact that ~70% of the 3370 mRNAs analyzed in a large scale *in situ* hybridization experiment in *Drosophila* embryos exhibit non-uniform intracellular localization (Lecuyer et al., 2007).

Below, the mechanisms driving such mRNA-related processes will be discussed, focusing on the *Drosophila* and the *Xenopus* oocytes, as well as on *ash1* mRNA localization in budding yeast. Finally, regulation of mRNA translation and a few instances of asymmetrically localized mRNAs in early *C. elegans* embryos will be introduced.

The *Drosophila* oocyte

Probably the best studied system where the role of mRNA localization and translational control has been investigated is the *Drosophila* oocyte. The *Drosophila* oocyte develops within an egg chamber, where an oocyte is surrounded by 15 nurse cells (Figure 10, reviewed in King, 1970). The transcriptionally active nurse cells endow the oocyte with proteins and mRNAs through intercellular cytoplasmic bridges called ring canals. At the end of oogenesis the nurse cells undergo apoptosis. The localization of four mRNAs, *oskar* (*osk*), *bicoid* (*bcd*), *nanos* (*nos*) and *gurken* (*grk*) has been extensively studied, as these mRNAs are localized to different part of the oocyte and are responsible for establishing the main axes of the future embryo (reviewed in Bastock and St Johnston, 2008; Becalska and Gavis, 2009; Lasko, 2012). The localization of *bcd* and *grk* mRNA is essential to specify the antero-posterior and dorso ventral axes, respectively (Berleth et al., 1988; Driever and Nusslein-Volhard, 1988; Frohnhofer et al., 1986; Neuman-Silberberg and Schupbach, 1993). *osk* is a germline determinant (Ephrussi et al., 1991; Ephrussi and Lehmann, 1992; Lehmann and Nusslein-Volhard, 1986), whereas *nos* is involved in germline an abdominal development (Gavis and Lehmann, 1992; Lehmann and Nusslein-Volhard, 1991;

Wang et al., 1994; Wang and Lehmann, 1991). A common theme for an initial step in loading these mRNAs is the dynein-dependent transport of *grk*, *bcd* and *osk* mRNAs from the nurse cells to the oocyte (Cha et al., 2001; Clark et al., 2007; Mische et al., 2007; Schnorrer et al., 2000).

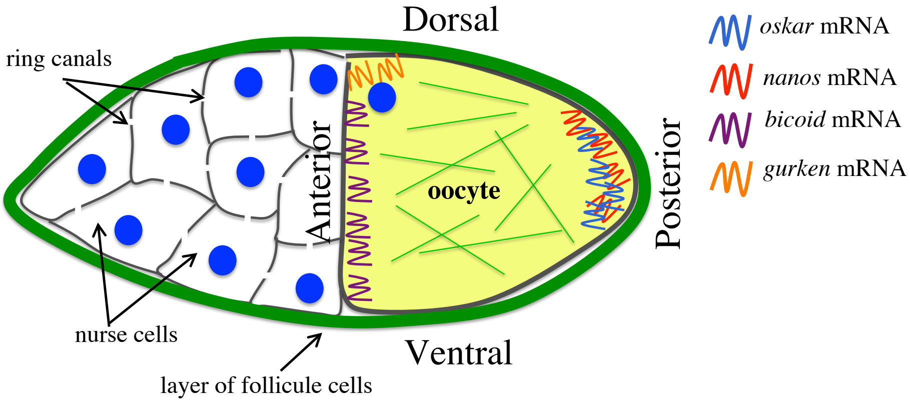

Figure 10. mRNA localization in the *Drosophil*a oocyte
Nuclei (blue) and microtubules (green) are depicted. mRNA distribution of *oskar*, *nanos*, *bicoid* and *gurken* are shown.

Once in the oocyte, *bcd* mRNA becomes enriched in the anterior part through several steps, including initial loading and anchoring (St Johnston et al., 1989). The initial anterior enrichment is driven by the RNA-binding protein Exuperantia (Exu), whose activity is under the control of the kinase Par1 (Berleth et al., 1988; Cha et al., 2001; Mische et al., 2007; Riechmann and Ephrussi, 2004). Staufen is likewise necessary for anterior enrichment of *bcd* mRNA by binding to its 3' UTR (Ferrandon et al., 1994; St Johnston et al., 1989) and Swallow is important in a subsequent anchoring step of the pathway by regulating the actin cytoskeleton (Weil et al., 2010). The endosomal sorting complex ESCRT-II is necessary for proper *bcd* mRNA enrichment, with the ESCRT-II complex subunit VPS36 binding directly to the *bcd* 3' UTR (Irion and St Johnston, 2007). This regulation, however, might not be linked to endosomal sorting, as the ESCRT-I and III complexes that likewise function in endosomal sorting do not regulate *bcd* mRNA localization (Irion and St Johnston, 2007). *bcd* mRNA is under translational repression until fertilization, and the Bicoid protein gradient is established thereafter solely as a result from the mRNA localization and local translation. In the embryo, Pumilio negatively controls *bcd* translation by binding to its 3' UTR and a similar mechanisms might take place in the oocyte to ensure temporal regulation of *bcd* translation (Gamberi et al., 2002). In turn, Bcd protein is important to regulate the P-A protein gradient of the transcription factor Caudal (Cad) by repressing the translation of *cad* mRNA (Dubnau and Struhl, 1996; Rivera-Pomar et al., 1996). Bcd binds to the *cad* 3' UTR and recruits the 4E homology protein 4EHP, leading to the formation a translationally-inactive circularized *cad* mRNA (Cho et al., 2005; Hernandez et al., 2005).

osk mRNA accumulates at the posterior pole of the oocyte, where Osk protein translation starts at mid-oogenesis. Oskar nucleates the formation of a specialized region of the cytoplasm, termed the pole plasm, where large ribonucleoprotein complexes form and include posterior and germ cell determinants, such as Nos. In the case of *osk* mRNA, localized mRNA is coupled with spatially restricted translational regulation. Localization requires the 3' UTR and also signals stemming from the activity of the exon-junction complex that drive splicing (Hachet and Ephrussi, 2001, 2004; Kim-Ha et al., 1993; Newmark and Boswell, 1994). *osk* mRNA lacking introns can localize solely in the presence of the endogenous *osk* transcript via RNA-RNA interactions through the 3' UTRs (Jambor et al., 2011). After its initial dynein-mediated enrichment has been established, the plus end motor kinesin, the actin cytoskeleton, the endosomal network and one of the Oskar isoforms itself together contribute to the posterior anchoring of *osk* mRNA (Rongo et al., 1995; Tanaka and Nakamura, 2011; Vanzo et al., 2007; Zimyanin et al., 2008). The RNA-binding protein Staufen is needed for *osk* mRNA localization and for translational activation by interacting with the *osk* 3' UTR (Braat et al., 2004; Kim-Ha et al., 1995; Micklem et al., 2000). Translational repression during early oogenesis requires genes implicated in the RNAi pathway (*armitage*, *zucchini*, *quash*) and the polypirimidine tract binding protein PTB that binds to the *osk* 3' UTR (Besse et al., 2009; Cook et al., 2004; Pane et al., 2007; Tomari et al., 2004). Later on, translational repression is executed by Bruno, a protein that binds to the *osk* 3' UTR (Kim-Ha et al., 1995; Snee et al., 2008). Bruno recruits the eIF4E binding protein Cup, leading to the accumulation of the CCR4 deadenylase complex, resulting in the shortening of the *osk* poly-A tail (Igreja and Izaurralde, 2011; Nakamura et al., 2004). It has been postulated that through this mechanism Cup protects *osk* mRNA from further degradation.

The posterior enrichment of *nos* mRNA is driven by the proteins Rumpelstilskin and Aubergine, which are associated with the *nos* 3' UTR (Becalska et al., 2011; Jain and Gavis, 2008). Since the posterior enrichment of *nanos* mRNA is not efficient (only 4% of all *nos* mRNA is localized (Bergsten and Gavis, 1999), translational regulation takes place to prevent Nos protein from localizing to the anterior. These regulatory mechanisms involve a 90 nt long element in the *nos* 3' UTR termed the translational control element, or TCE (Crucs et al., 2000; Forrest et al., 2004). The secondary structure of the TCE is recognized by several translational repressors, including Glorund and Smaug (Kalifa et al., 2006; Nelson et al., 2004). Smaug interacts both with Cup and with Pop2, a subunit of the CCR4 deadenylase complex, thereby leading to translational repression of *nos* (Semotok et al., 2005; Zaessinger et al., 2006). Oskar counteracts the Smaug-mediated repression in the germ pole, leading to enrichment of Nos protein in the very posterior (Zaessinger et al., 2006).

gurken mRNA is associated with the oocyte nucleus that is initially located at the posterior side and relocates thereafter to the antero-dorsal part of the oocyte. *grk* mRNA localization is dynein-dependent and involves squid/hnRNP (Delanoue et al., 2007; Jaramillo et al., 2008). The localization signal lies in the coding region, which is necessary but not sufficient for anterodorsal enrichment (Lan et al., 2010; Van De Bor et al., 2005). *grk* mRNA is also under translation control. The eIF5B interacting protein Vasa is a translational activator, as oocytes mutant for *vasa* or expressing Vasa protein incapable of interacting with eIF5B, result in decreased Gurken protein level (Johnstone and Lasko, 2004; Styhler et al., 1998; Tomancak et al., 1998).

The *Xenopus* oocyte

The *Xenopu*s oocyte is a polarized cell, possessing an animal and a vegetal pole (Figure 11). Oocyte maturation goes through six stages, referred to as Stage I-VI (reviewed in Dumont, 1972). Whereas mechanisms driving mRNA localization to the animal pole are not known, the enrichment of mRNAs in the vegetal pole is executed by two pathways: the early message transport organizer (METRO) pathway and the late pathway (Forristall et al., 1995; Kloc and Etkin, 1995).

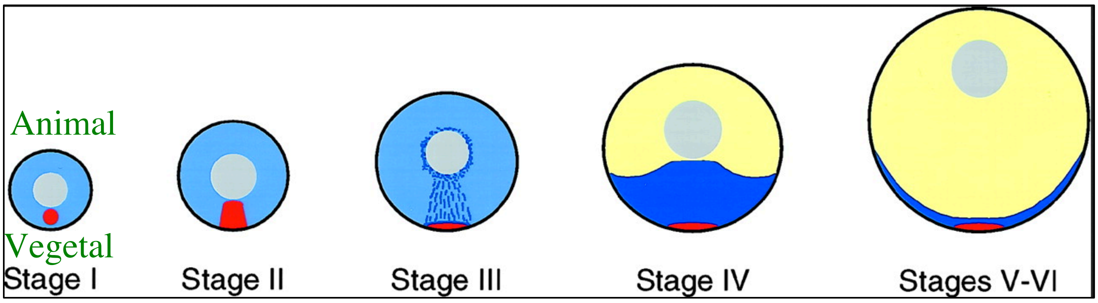

Figure 11. mRNA localization pathways in the *Xenopus* oocyte
The early pathway acts through stages I-III (red), while the late pathway starts driving mRNAs distribution between stage III and VI (blue). Adapted from Mowry and Cote, 1999.

The METRO pathway localizes several mRNAs encoding RNA-binding proteins important for germline specification, such as the *nanos*-related *Xcat2* and *XdazI* (Forristall et al., 1995; Houston et al., 1998; Kloc and Etkin, 1995; Mosquera et al., 1993). Interestingly, the translation of these mRNAs can be repressed for several months (MacArthur et al., 1999). These mRNAs are associated with the mitochondrial cloud, or Balbiani body, a structure formed around the centrioles that is enriched with ER, Golgi and mitochondrial membranes (Heasman et al., 1984; Kloc et al., 1996). Dynein-mediated transport has been implicated in building up the Balbiani body (Heasman et al., 1984; Kloc et al., 2004; Kloc et al., 2002; Pepling et al., 1999), while the mRNAs are thought to be delivered there by diffusion and by entrapment mechanisms that can occur in the absence of microtubules and actin (Kloc et al., 1996). Some *cis*-elements have also been identified as being important for mRNA distribution, such as a 164-nt long region in the *Xcat2* 3'UTR that is necessary and sufficient for localization to the Balbiani body (Kloc et al., 2000).

The T-box transcription factor VegT and the TGF-β growth factor Vg1 are the best-studied examples of mRNAs localized by the late pathway (Stennard et al., 1996; Weeks and Melton, 1987; Zhang and King, 1996). VegT and Vg1 take part in mesoderm and endoderm formation (Dale et al., 1993; Horb and Thomsen, 1997; Thomsen and Melton, 1993). Unlike the METRO pathway, the late pathway utilizes microtubules to localize mRNAs (Yisraeli et al., 1990) and the final enrichment at the vegetal cortex is exerted through several steps. The initially homogenously distributed Vg1 mRNA becomes enriched on the smooth ER in the vegetal pole in a microtubule dependent manner (Deshler et al., 1997; Kloc and Etkin, 1998). Afterwards, Vg1 mRNA is transported to the cortex by the motor proteins kinesin I and II (Betley et al., 2004; Messitt et al., 2008; Yoon and Mowry, 2004). The connection between the motor complex and the mRNA is thought to be mediated by Staufen that binds both Vg1 3' UTR and kinesin I (Yoon and Mowry, 2004). When arrived to its final destination, actin-based anchoring through the protein Prrp ensures Vg1 mRNA localization at the vegetal cortex (Zhao et al., 2001).

ash1 mRNA localization in budding yeast

Among the ~30 mRNAs (Aronov et al., 2007; Shepard et al., 2003) that are actively transported to the bud, the mechanisms driving *ash1* mRNA localization and translation are the best studied (Figure 12). The protein ASH1 (Asymmetric synthesis of HO) is enriched in the daughter cell after division and functions as a repressor of the HO endonuclease, thereby inhibiting mating type switching in this cell (Chartrand et al., 1999; Takizawa et al., 1997). Such asymmetric enrichment of ASH1 in the daughter cell is the end result of active mRNA transport to the bud during late anaphase coupled with translational repression (Figure 1A). Four *cis*-elements have been identified that are all sufficient for localization (Chartrand et al., 1999; Gonzalez et al., 1999): three of them are in the coding region, while the fourth overlaps with the coding and the 3' UTR. All four elements fold in a stem-loop that is recognized by the RNA-binding protein She2p (Bohl et al., 2000; Long et al., 2000). She2p, via its binding partner She3p, is associated with the type V myosin Myo4p, forming the so-called locasome (Bohl et al., 2000; Long et al., 2000; Takizawa et al., 1997). As its name indicates, this complex is responsible for transporting cargos (in this case mRNAs) along the actin cytoskeleton (Takizawa et al., 1997; Zhao et al., 2001). Interestingly, the cortical transport of the endoplasmic reticulum is likewise mediated by She3p-Myo4p complex, and it may be linked with bud-directed mRNA trafficking (Estrada et al., 2003; Schmid et al., 2006). Furthermore, ASH1 protein is also crucial for *ash1* mRNA localization, but whether this is the result of a direct or indirect interaction is not known (Gonzalez et al., 1999).

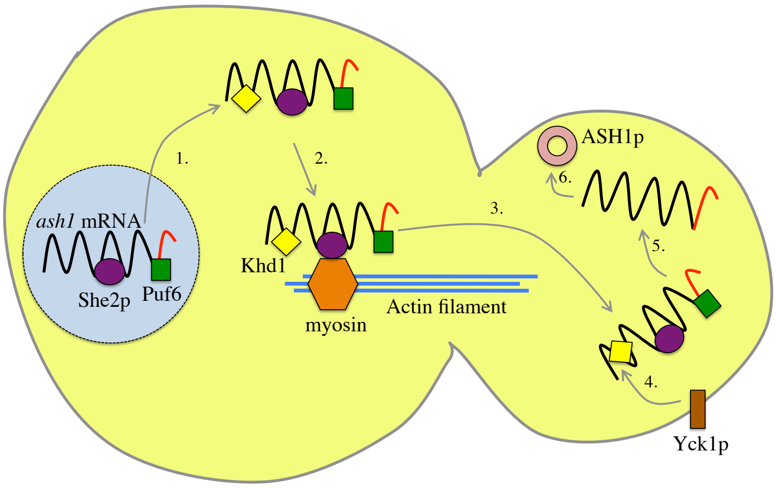

Figure 12. ***ash1*** **mRNA localization and translational control in yeast**
Localization and translational control of ash1 mRNA goes through several steps. 1. Translocation to cytoplasm. 2. Binding to Myo4p. 3. Transport to the bud tip. 4. Yck1p-mediated phosphorylation. 5. Release from translational repression 6. Translation. Image adapted from Besse and Ephrussi, 2008.

Translational repression of *ash1* mRNA is exerted by two proteins, Puf6p and Khd1p. Puf6p belongs to the Pumilio family of RNA-binding proteins and interacts with the fourth localization element in the *ash1* mRNA (Gu et al., 2004). *puf6* deletion results in reduced asymmetry of both the mRNA and the protein, indicating that translational repression is somehow linked to mRNA localization. The regulation by Khd1p acts via the first localization element and involves competition with eIF4G1 (Paquin et al., 2007). Khd1p overexpression results in mislocalized *ash1* mRNA and decreased Ash1p levels (Irie et al., 2002). An elegant regulatory circuit mediated by the casein casein kinase CK2 and the Yck1p kinase anchored at the bud tip releases *ash1* mRNA from translational repression in a localized manner by phosphorylating Khd1p (Deng et al., 2008; Paquin et al., 2007).

Translational control during early *C. elegans* development

Although not as widespread as in other systems such as the *Drosophila* oocyte, translational control has been shown in some cases to be important for early developmental processes in *C. elegans* (Figure 13, reviewed in Hwang and Rose, 2010).

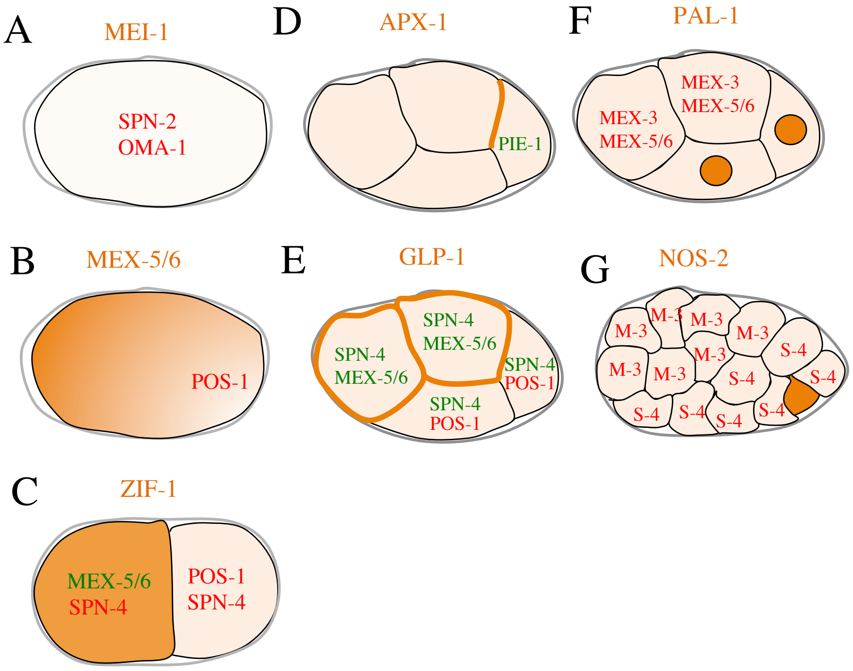
A
MEI-1
SPN-2
OMA-1
B
MEX-5/6
POS-1
C
ZIF-1
MEX-5/6
SPN-4
POS-1
SPN-4
D
APX-1
PIE-1
E
GLP-1
SPN-4
MEX-5/6
SPN-4
MEX-5/6
SPN-4
POS-1
SPN-4
POS-1
F
PAL-1
MEX-3
MEX-5/6
MEX-3
MEX-5/6
G
NOS-2
M-3
M-3
M-3
M-3
M-3
M-3
M-3
M-3
S-4
S-4
S-4
S-4
S-4
S-4
S-4
S-4

Figure 13. Instances where translational regulation has been shown to be important in early *C. elegans* embryos
Positive regulators (translational activators) of the mRNAs encoding the indicated proteins are shown in green, negative regulators (translational repressors) are in red. Note that in all cases, the mRNA is distributed uniformly in the embryo. See text for more details. **A** MEI-1 protein level regulated by SPN-2 and OMA-1. **B** MEX-5/6 regulation by POS-1. **C** Regulation of ZIF-1 by MEX-5/6, SPN-4 and POS-1. **D** APX-1 regulation by PIE-1. **E** GLP-1 regulation by SPN-4, MEX-5/6 and POS-1. **F** Regulation of PAL-1 exerted by MEX-3 and MEX-5/6. **G** NOS-2 regulation by MEX-3 and SPN-4 (M-3, S-4).

Interfering with the function of genes encoding the Nanos homologue *nos-3*, the Pumilio-related genes *fbf-1/2* and the Brat homologues *ncl-1*, *nhl-1*, *nhl-2* and *nhl-3* (collectively referred to as ‘Cebrats’) each suppress lethality of the *par-2(it5)* temperature sensitive mutants (Hyenne et al., 2008; Labbe et al., 2006). In *Drosophila*, homologues of these proteins act as translational repressors in the oocyte. It has been indicated that the regulation observed in *C. elegans* occurs through altering the levels of PAR-6, as *nos-3* mutants exhibit lower PAR-6 levels in the embryos (Pacquelet et al., 2008). How could a potential translational repressor lead to decreased level of a given protein? NOS-3 represses translation of the E3-ligase subunit FEM-3, by binding to the 3' UTR of *fem-3* mRNA in the gonad (Kraemer et al., 1999). The FEM-3 based E3 ligase CBC-FEM-3 binds PAR-6 *in vitro* (Pacquelet et al., 2008). Thus, in the absence of NOS-3, increased levels of FEM-1 can direct more PAR-6 for proteasomal-mediated degradation presumably in the oocyte, thereby balancing out the effect caused by reduced PAR-2 function.

One example of translational regulation happening probably also in the oocyte that bears consequences in the early embryo is offered by the action exerted by SPN-2 on MEI-1 protein levels (Figure 13A). SPN-2 is an eIF4E binding protein whose depletion leads to defects in spindle orientation (Li et al., 2009). In *spn-2* mutant embryos, the mitotic spindle in the zygote fails to align properly along the A-P axis, leading to problems in cleavage plane orientation. Interestingly, ectopic expression of MEI-1, a subunit of the katanin complex responsible for severing microtubules, was observed in *spn-2* mutants. MEI-1 is needed for proper meiotic spindle assembly, but is normally eliminated from the zygote before mitotic spindle formation, thus ensuring proper spindle positioning (Clark-Maguire and Mains, 1994a, b; Srayko et al., 2000). Suggestively, reducing *mei-1* levels suppressed the spindle orientation defects in *spn-2* embryos, indicating that ectopic MEI-1 expression is causative of the phenotype. eIF4E binding proteins inhibit the assembly of the translational initiation complex, such that the regulation of MEI-1 levels is thought to act through translational repression. In support of this hypothesis, SPN-2, in complex with an RNA-binding protein, OMA-1 binds to the *mei-1* 3' UTR (Li et al., 2009).

A bidirectional regulation takes place between MEX-5/6 and POS-1 (Figure 13B). As mentioned before, upon depletion of MEX-5/6, POS-1 is no longer restricted to the posterior lineage (Schubert et al., 2000). Mechanistically, this is thought to happen both at the level of *pos-1* mRNA and POS-1 protein. As opposed to the wild type situation where *pos-1* mRNA is enriched in P_1 as compared to AB, this is no longer observed in single *mex-5* mutant embryos, while POS-1 protein is still enriched in the posterior cell (Tenlen et al., 2006). However, *mex-5* and *mex-6* double mutant embryos exhibit homogenous POS-1 protein distribution (Schubert et al., 2000). These observations argue that POS-1 protein level is also regulated by MEX-5/6 either at the level of translation or at the level of protein degradation. Hinting towards the latter possibility, POS-1 undergoes E3-ligase mediated degradation in the somatic lineages by the CUL-2-ZIF-1 complex in a MEX-5/6 dependent manner (DeRenzo et al., 2003; Reese et al., 2000). One possibility that has been suggested is that MEX-5/6 functions as a translational activator of *zif-1* mRNA, although this idea needs to be tested experimentally (Figure 13C). Regulation also exists from POS-1 to the MEX-5/6 complex. Thus, reduction of *pos-1* function rescues phenotypic defects normally present in *mex-5* mutant embryos (Tenlen et al., 2006). This argues that POS-1 is a negative regulator of MEX-5 (and potentially MEX-6), maybe through translational regulation, as it has been shown for POS-1 in the case of *glp-1* mRNA (Ogura et al., 2003). Supporting this model, POS-1 interacts with the *mex-6* 3' UTR (Tenlen et al., 2006).

At the end of the second cell division, ABa and ABp are born with identical developmental potential (Figure 3C) and signaling arising from P_2 is responsible for the specification of the ABp fate (Bowerman et al., 1992). It turned out that the Notch signaling from P_2 to ABp plays a key role in this process (reviewed in Evans and Hunter, 2005; Priess, 2005). How does this work at the molecular level? The spatial regulation of both the ligand and the receptor is the answer (Figure 13D and E). GLP-1, the Notch receptor, is solely present on the plasma membranes of ABa and ABp, while it is only at the P_2 - ABp boundary that the Notch receptor APX-1 is present (Evans et al., 1994; Mickey et al., 1996). Both *glp-1* and *apx-1* mRNAs are homogenously distributed in the 4 blastomeres; therefore translational regulation must take place to achieve the observed non-uniform protein distribution. APX-1 protein is not detectable in *pie-1* mutant embryos, indicating a role for PIE-1 in *apx-1* mRNA translational activation (Mickey et al., 1996). Extensive regulation of the *glp-1* mRNA has also been found, leading to its observed protein distribution. POS-1 and an other RNA binding protein GLD-1, bind to *glp-1* 3'UTR elements, leading to its translational repression (Marin and Evans, 2003; Ogura et al., 2003). Thus, loss of *pos-1* leads to GLP-1 enrichment in the posterior cells (Ogura et al., 2003). Furthermore, SPN-4 activates the translation of *glp-1* mRNA by binding to an other region of the 3' UTR of *glp-1* mRNA, with the loss of *spn-4* activity resulting in the absence of GLP-1 protein (Ogura et al., 2003). Furthermore, GLP-1 protein levels are diminished in *mex-5/6* double mutant embryos (Schubert et al., 2000). Given the abovementioned degradation of POS-1 in the somatic blastomeres, SPN-4-MEX-5/6 mediated translational activation wins in the anterior cells, giving rise to the presence of GLP-1 protein only in those cells.

The homeobox protein PAL-1 is the *C. elegans* Caudal homologue. PAL-1 is required for the specification of the C and D fates and thus for proper hypodermal development (Waring and Kenyon, 1990, 1991). *pal-1* mRNA is present only in the posterior nuclei at the 4-cell stage, while its mRNA is evenly distributed (Figure 13F; (Edgar et al., 2001; Lei et al., 2009), raising the possibility of another instance of translational regulation. PAL-1 protein is misdistributed in embryos lacking MEX-5/6 or MEX-3 (Huang et al., 2002; Schubert et al., 2000). Does PAL-1 distribution involve the 3' UTR? Indeed, as a LacZ reporter construct harboring the *pal-1* 3'UTR recapitulates the posterior expression pattern in a *mex-3*-dependent manner (Hunter and Kenyon, 1996). Moreover, MEX-3 interacts with the *pal-1* 3' UTR (Pagano et al., 2009). A model emerges where MEX-3, together with MEX-5/6, acts as translational repressor of *pal-1* mRNA in the anterior blastomeres. Whether MEX-5/6 interact directly with *pal-1* mRNA or act through MEX-3 remains an open question.

MEX-3 likewise regulates the restricted translation of NOS-2, a transcription factor important for the acquisition of P-cell fate (Figure 13G; Jadhav et al., 2008; Pagano et al., 2009; Subramaniam and Seydoux, 1999). MEX-3 binds to the *nos-2* 3' UTR and represses its translation until the 28-cell stage, where NOS-2 appears in P_4. Similarly to the case of *pal-1*, a repressor (MEX-3) and an activator (PIE-1) function in concert here to establish spatially restricted protein distribution. Apart from these proteins, SPN-4 also seems to play a role in regulating NOS-2 distribution, as ectopic NOS-2 is observed in *spn-4* mutant embryos (Jadhav et al., 2008).

Polarized mRNAs in early *C. elegans* embryos

Polarized distribution of mRNAs is not frequent in *C. elegans* early embryos and the majority of mRNAs exhibits homogenous localization and thus falls into the group of so-called class I mRNAs (Figure 14A; Seydoux and Fire, 1994). However, several mRNAs have been identified as being polarized in embryos from the 2 to 28-cell stage. One group of such maternally provided mRNAs are the class II mRNAs that go from being homogenously distributed in the zygote to being enriched in the P-lineage later during development (Figure 14B; Seydoux and Fire, 1994). This process potentially involves degradation mechanisms acting in the somatic cells. Examples of such mRNAs are *cey-2*, *skn-1* and the already mentioned *pos-1* (Seydoux and Fire, 1994; Tabara et al., 1999). Interestingly, *glp-1* mRNA also shows enrichment in the P-lineage in 8-cell stage embryos, suggesting that robust degradation takes place to remove *glp-1* mRNA after the action of Notch-Delta signaling between ABp and P_2. Apart from these transcripts, P-granules seem to enrich mRNAs, as visualized by poly-A-tail probes (Class III, Figure 13C), but the nature of these mRNAs remains to be addressed. Recently, single cell mRNA deep sequencing revealed that 13 mRNAs are enriched in AB, while 4 transcripts are more abundant in P_1 (Class IV, Figure 14 D and Table 1 on page 97; Hashimshony et al., 2012). Potentially interesting mRNAs are enriched in the AB cell, such as the mRNA of the anterior polarity gene *par-3*. It would be very interesting to probe if such anterior of *par-3* mRNA is important in regulating polarity. It is unknown whether the asymmetric distribution of these mRNAs is executed by asymmetric mRNA transport in the zygote and/or relying on differential degradation mechanisms acting in the two cell stage.

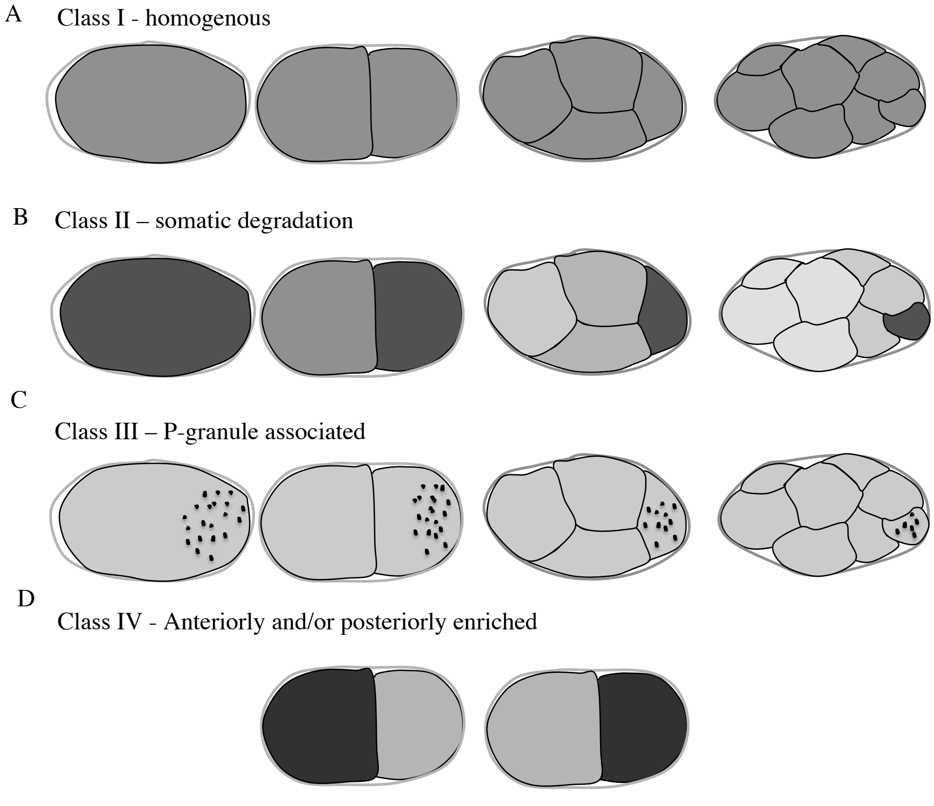
A
Class I - homogenous
B
Class II – somatic degradation
C
Class III – P-granule associated
D
Class IV - Anteriorly and/or posteriorly enriched

Figure 14. Polarized mRNAs in early *C. elegans* embryos
A Homogenously distributed mRNAs. **B** Posterior enrichment achieved by degradation in the somatic cells. **C** P-granule associated RNAs. **D** Anteriorly or posteriorly enriched mRNAs. References: (Seydoux and Fire, 1994)(**A**, **B** and **C**), (Hashimshony et al., 2012) (**D**).

In conclusion, to date, non-uniform distribution of a given mRNA has not been reported in the one-cell stage embryo. To explore if such an mRNA may exist, we investigated the localization of the 11.237 mRNAs available in the publicly available *in situ* hybridization database (Nematode Expression Database (NEXTDB), http://nematode.lab.nig.ac.jp). In this database, the ESTs are listed on all chromosomes and by clicking on the EST one can retrieve the *in situ* hybridization image of early embryos and adult worms. This analysis confirmed that almost all transcripts displayed homogenous localization, indicating that the *C. elegans* one-cell stage embryo markedly differs form other systems, like the *Drosophila* embryo (Lecuyer et al., 2007).

However, Sachin Kotak uncovered a very striking localization pattern for the *lin-5* mRNA. Moreover, I found that the mRNA of the uncharacterized gene W02F12.3 (dubbed *era-1*) is also non-uniformly distributed in the one-cell stage embryo. Exploring the mechanism and function of these two mRNA localization patterns constitutes the major topics of this thesis.

Furthermore, I also continued a project that was initiated by a former PhD student, Kalyani Thyagarajan, to investigate the role of clathrin heavy chain in pulling force generation in one cell stage embryos.

2. AIMS OF THE STUDY

- Characterization of the mechanisms and function of *lin-5* mRNA localization
- Characterization of the mechanisms driving *era-1* mRNA distribution
- Characterization of the effect of the clathrin cheavy chain on force generation

3. CHARACTERIZATION OF THE MECHANISMS AND FUNCTION OF *LIN-5* MRNA LOCALIZATION

3A. RESULTS

lin-5 mRNA is enriched around centrosomes in early *C. elegans* embryos

We explored whether the mRNAs encoding cortical force generator components may display an unusual localization by browsing the publicly available Nematode Expression Database. This analysis revealed that *lin-5* mRNA, as opposed to the mRNA of other members of the force generator complex, appears to exhibit a non-uniform localization in early embryos.

We decided to further investigate *lin-5* mRNA localization. As a first step, we set up the *in situ* hybridization method used for *C. elegans* embryos. Conducting conventional, digoxigenin- and alkaline-phosphatase (DIG-AP) based *in situ* hybridization experiments, we found that *lin-5* mRNA is enriched around centrosomes throughout the first cell cycle and displays an analogous localization in later stages of embryogenesis (Figure 15A-D). We noted that this enrichment becomes more pronounced during the first cell cycle as centrosomes mature.

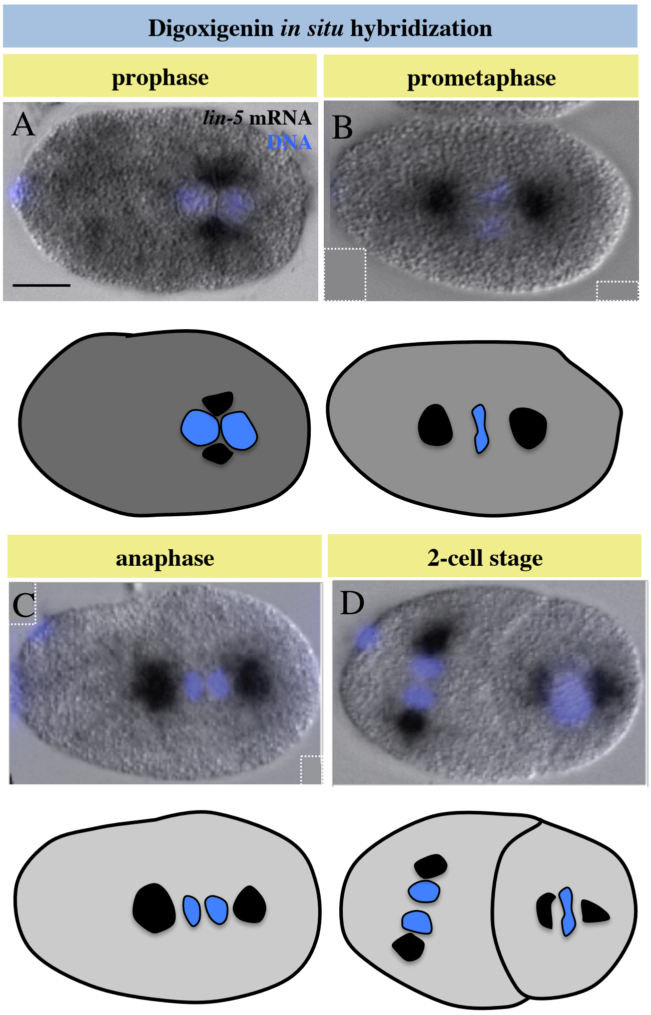

Figure 15. *lin-5* mRNA is enriched around centrosomes in early *C. elegans* embryos
A-D Digoxygenin-AP *in situ* hybridization against *lin-5* mRNA in one-cell embryos at prophase (**A**), prometaphase (**B**), anaphase (**C**), as well as at the end of the two-cell stage (**D**). Schematics below show the distribution of the mRNA in different stages. Moreover, unless stated otherwise, all *in situ* hybridization experiments are conducted with digoxigenin, with mRNA shown in black and DNA in blue. Here and in other cases, n>50 embryos were analyzed and representative images are shown. In panel **B** and **C**, a black region from the original image resulting from image rotation was filled with grey dashed shapes.

We also implemented the single molecule FISH method (Raj et al., 2008) that confirmed enrichment of *lin-5* mRNA around centrosomes (Figure 16E-H). This method allows for more precise quantification of mRNA localization that we will take advantage of later on (see page 70-71).

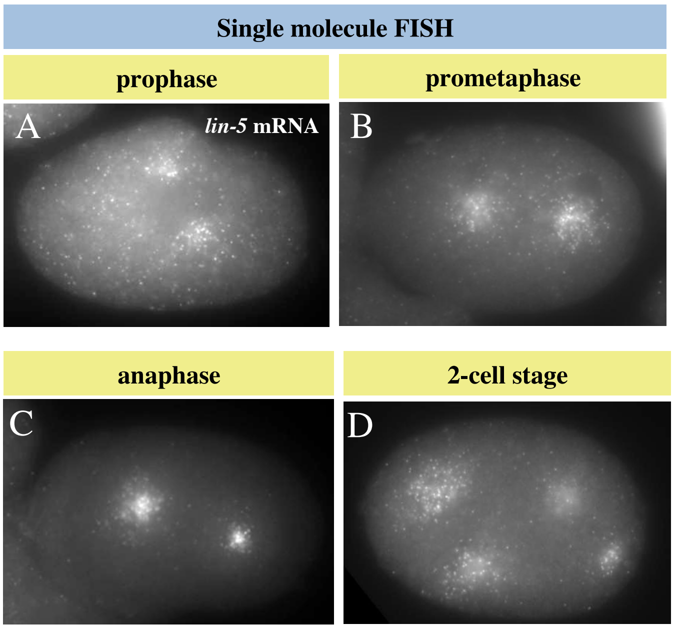
Single molecule FISH
prophase
prometaphase
A
lin-5 mRNA
B
anaphase
2-cell stage
C
D

Figure 16. Single molecule FISH confirms centrosomal enrichment of *lin-5* mRNA
A-D Single molecule FISH against *lin-5* mRNA at the same stages as in Figure 15A-D. *lin-5* mRNA is visualized with wide-field microscopy and shown in white. Small foci in the cytoplasm should correspond to single mRNA molecules.

The signal detected by the DIG-AP *in situ* hybridization is specific to *lin-5* mRNA since it is not observed in *lin-5*(*RNAi*) embryos (Figure 17C and D). By contrast to *lin-5* mRNA, *in situ* hybridization revealed a uniform cytoplasmic distribution for *goa-1* mRNA (Figure 17E and F). Moreover, when browsing the Nematode Expression Database, we did not observe similar localization for any of the other 11,237 mRNAs, indicating that such centrosomal localization is very rare, or even unique.

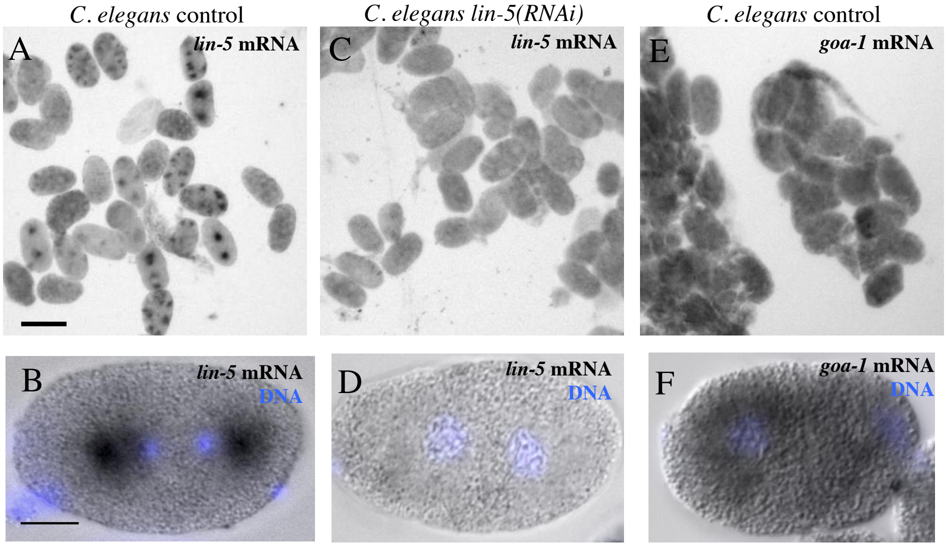
C. elegans control
C. elegans lin-5(RNAi)
C. elegans control
A
lin-5 mRNA
C
lin-5 mRNA
E
goa-1 mRNA
B
lin-5 mRNA
DNA
D
lin-5 mRNA
DNA
F
goa-1 mRNA
DNA

Figure 17. *lin-5 in situ* hybridization signal is specific to *lin-5* mRNA and centrosomal enrichment is not observed for *goa-1* mRNA
A, B Localization of *lin-5* mRNA in wild type *C. elegans* embryos viewed at low (**A**) and high (**B**) magnification. The scale bar corresponds to 50 µm in the low and 10 µm in the high magnification views. **C, D** Localization of *lin-5* mRNA in *lin-5(RNAi) C. elegans* embryos

viewed at low (**C**) and high (**D**) magnification. **E, F** Localization of *goa-1* mRNA in wild type *C. elegans* embryos viewed at low (**E**) and high (**F**) magnification.

As an initial step to evaluate the potential relevance of *lin-5* mRNA localization, we addressed whether it is similarly enriched in the sister species *C. briggsae*, which is though to have diverged from *C. elegans* ~100 million years ago (Hillier et al., 2007). As shown in Figure 18A and B, we found this to be the case, supporting the notion that such localization may be functionally relevant.

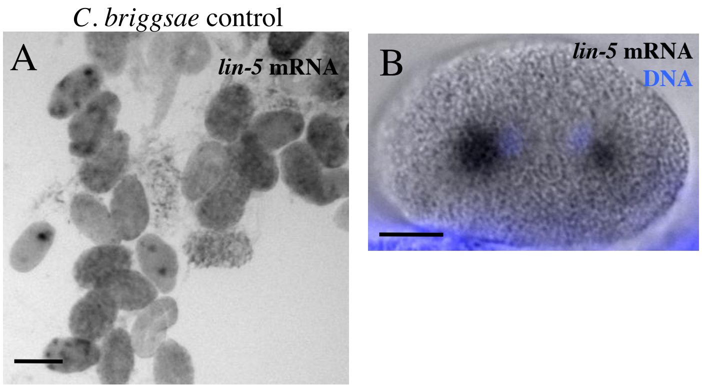

Figure 18. *Caenorhabditis briggsae lin-5* mRNA is likewise enriched at centrosomes
A, B Localization of *lin-5* mRNA in *C. briggsae* viewed at low (**A**) and high magnification (**B**). The scale bar corresponds to 50 µm in the low and 10 µm in the high magnification view.

Microtubules and dynein are necessary for *lin-5* mRNA enrichment around centrosomes

We set out to dissect the mechanisms underlying *lin-5* mRNA enrichment around centrosomes. To test if centrosomes are sufficient, we analyzed *zyg-12*(*RNAi*) embryos, in which centrosomes detach from pronuclei and nuclei. As shown in Figure 19A, we found that *lin-5* mRNA follows centrosome position in such embryos, demonstrating that centrosomes are sufficient to dictate localization. Moreover, we asked if centrosomes are necessary for *lin-5* mRNA localization by examining *spd-5*(*RNAi*) embryos, in which centrosome assembly is impaired (Hamill et al., 2002). We found that *lin-5* mRNA still exhibits focused enrichment around pronuclei and chromatin in these embryos (Figure 19B). Therefore, centrosomes are not essential for *lin-5* mRNA localization. Since microtubules are still nucleated to some extent around pronuclei and chromatin in the absence of SPD-5 function (Hamill et al., 2002), we reasoned that *lin-5* mRNA enrichment in *spd-5*(*RNAi*) embryos may be due to the presence of microtubules. To test this hypothesis, we interfered with microtubules by using RNAi against the gene *tbb-1* (Sonnichsen et al., 2005), and found that *lin-5* mRNA distribution is uniform in this case (Figure 19C). Through which mechanism could microtubules be needed for *lin-5* mRNA localization around centrosomes? The minus-end directed microtubule-dependent motor dynein seemed like a plausible candidate. Accordingly, we found that *lin-5* mRNA is distributed uniformly in the cytoplasm in embryos depleted of the dynein heavy chain DHC-1 (Figure 19D). Overall, we conclude that dynein-dependent transport of *lin-5* mRNA towards the minus-end of microtubules ensures *lin-5* mRNA enrichment around centrosomes.

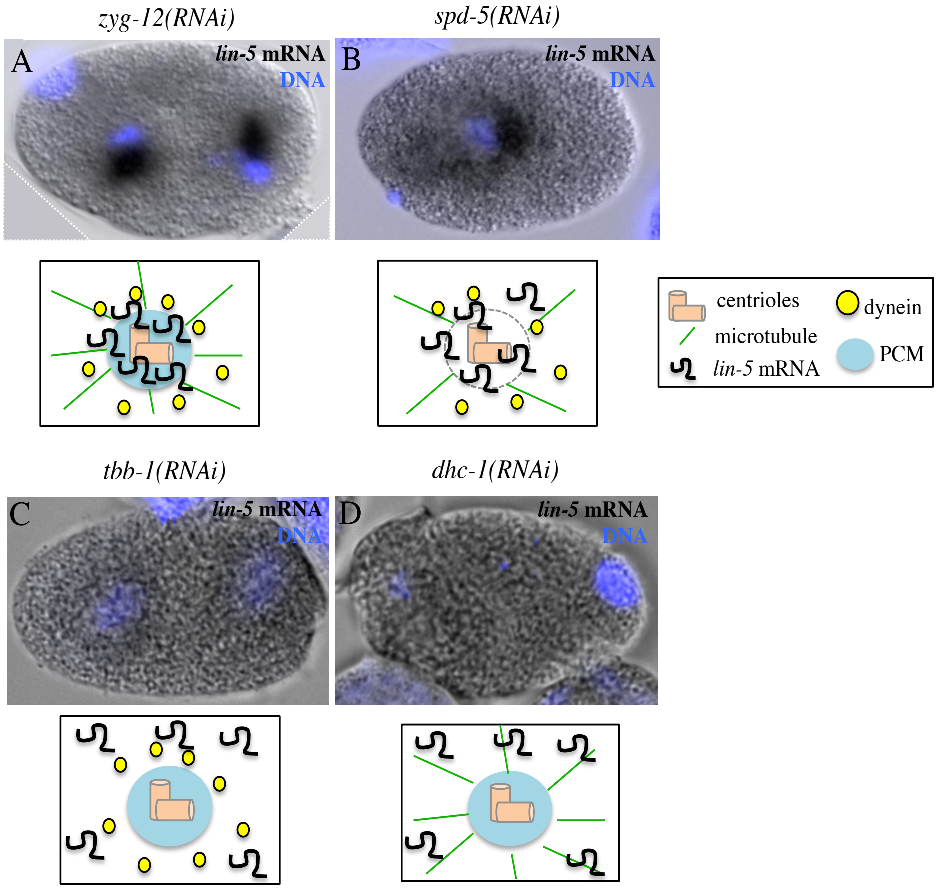
zyg-12(RNAi)
spd-5(RNAi)
A
lin-5 mRNA
DNA
B
lin-5 mRNA
DNA
centrioles
dynein
microtubule
PCM
lin-5 mRNA
tbb-1(RNAi)
dhc-1(RNAi)
C
lin-5 mRNA
DNA
D
lin-5 mRNA
DNA

Figure 19. Microtubules and dynein drive *lin-5* mRNA localization
A-D *lin-5* mRNA localization in one-cell mitotic embryos depleted by RNAi of ZYG-12 (**A**), SPD-5 (**B**), TBB-1 (**C**) or DHC-1 (**D**). Cartoons below the embryos represent the status of centrosomes, microtubules, dynein and *lin-5* mRNA in each condition. PCM: pericentriolar material.

The 3’ UTR is dispensable for *lin-5* mRNA localization

We next sought to identify the *cis*-acting elements of the *lin-5* mRNA that direct its centrosomal enrichment. Since in many mRNAs the 3’ untranslated region (3’ UTR) is responsible for subcellular localization (reviewed in Andreassi and Riccio, 2009), we tested the role of the *lin-5* 3’ UTR in mRNA centrosomal enrichment. To this end, we utilized a LIN-5-GFP strain in which the *pie-1* promoter drives transcription of a chimeric mRNA comprising the protein coding region of the *lin-5* cDNA fused to *gfp* and to heterologous 5’ and 3‘ UTRs from the *pie-1* gene (Figure 20C). Performing *in situ* hybridization against *gfp* mRNA, we found that *lin-5-gfp* mRNA is enriched around centrosomes in a manner analogous to endogenous *lin-5* (compare Figure 20B with 20D). We also found that *lin-5-gfp* mRNA is enriched at centrosomes even in a condition in which the endogenous mRNA is mislocalized (Figure 20E, see later section for clarification of the root of the mislocalization caused by the *ev571* mutation). This rules out the possibility that the transgene is localized simply because it hitchhikes on the endogenous mRNA.

Based on these experiments, we conclude that the *lin-5* 5’ UTR and 3’ UTR are dispensable, whereas the *lin-5* coding region is sufficient, for enrichment of *lin-5* mRNA around centrosomes.

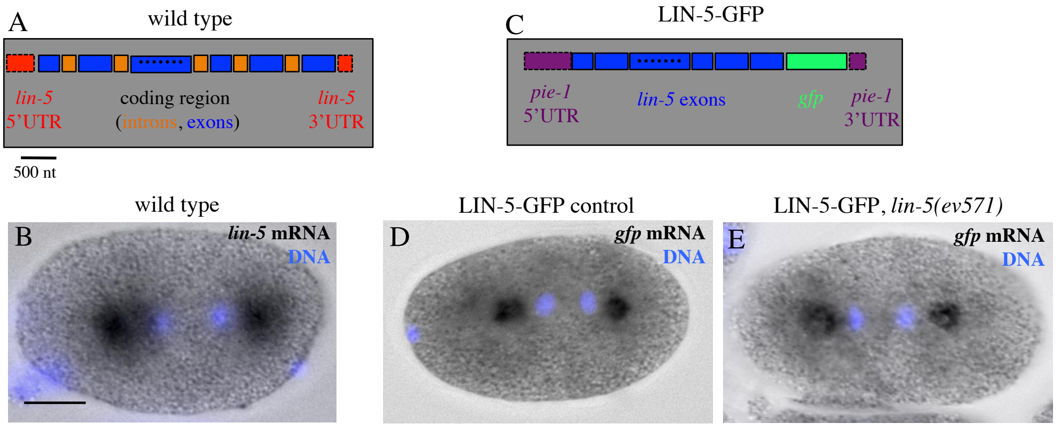
A
wild type
lin-5 5’UTR
coding region (introns, exons)
lin-5 3’UTR
500 nt
C
LIN-5-GFP
pie-1 5’UTR
lin-5 exons
gfp
pie-1 3’UTR
wild type
B
lin-5 mRNA
DNA
LIN-5-GFP control
D
gfp mRNA
DNA
LIN-5-GFP, lin-5(ev571)
E
gfp mRNA
DNA

Figure 20. The 3’ UTR is dispensable, while the coding region is sufficient for *lin-5* mRNA localization
A Cartoon representing the linear structure of *lin-5* mRNA. Exon 3 is marked with black dots, see explanation later for this. **B** Endogenous *lin-5* mRNA localization. **C** Cartoon representing the linear structure of *lin-5-gfp* mRNA. **D** *lin-5-gfp* mRNA visualized with *gfp* probe. **E** *lin-5-gfp* mRNA visualized with *gfp* probe in the *lin-5(ev571)* mutant background.

The coding region is necessary for *lin-5* mRNA localization

Next, we sought to identify the mRNA localization sequence within the coding region. To narrow down the position of such a signal, we took advantage of a functional *lin-5* transgene cloned in a *pie-1* promoter/*pie-1* 3' UTR cassette that was recoded in the first 376 nucleotide (*lin-5*[rec376], Figure 21A; Galli et al., 2011). This construct is RNAi resistant against dsRNAs targeting the first 376 nucleotides, allowing one to perform RNAi to deplete endogenous *lin-5*. We hypothesized that, provided the localization sequence is within this first 376 nucleotide of the endogenous mRNA, recoding should interfere with centrosomal localization of the transgene. Performing *in situ* hybridization in the absence of endogenous *lin-5*, we observed centrosomal enrichment of this transcript (Figure 21B). This indicates that the localization signal is not located in the first 376 nucleotides, and further demonstrates that the 3' UTR is dispensable for mRNA localization, even in the absence of the endogenous mRNA. Moreover, these data prove that the nucleotides between the positions 376 and 2466 are sufficient for localization.

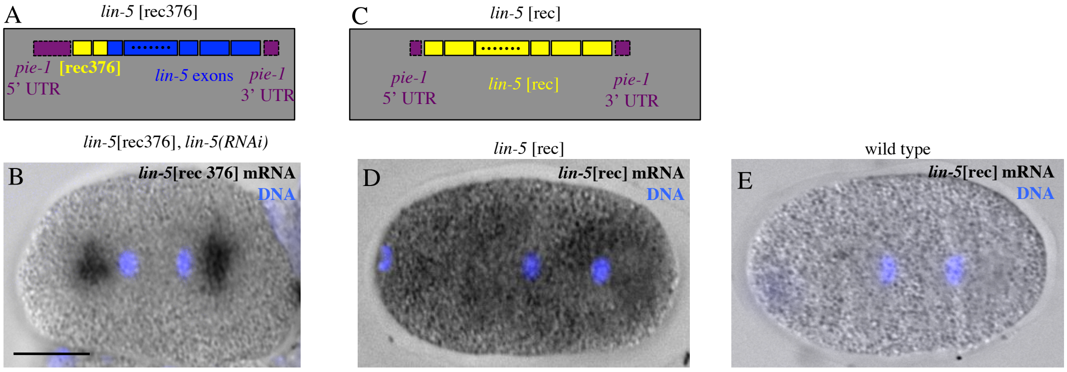

Figure 21. The coding region is necessary for *lin-5* mRNA localization
A Schematic of the strain *lin-5*[rec376]. **B** Localization of the *lin-5*[rec376] mRNA upon endogenous *lin-5* depletion. **C** Schematic of entirely recoded *lin-5* construct (*lin-5*[rec]). **D** *lin-5*[rec] mRNA visualized with probe recognizing the recoded sequence. **E** In situ hybridization with probe against *lin-5*[rec] wild type embryos.

To test whether the entire *lin-5* coding region is necessary for mRNA enrichment, we designed a *lin-5* coding sequence that retains the normal amino acid sequence but contains altered nucleotides along the entire coding region. We inserted this recoded sequence (hereafter referred to as *lin-5*[rec]) in a *pie-1* promoter/*pie-1* 5' UTR/*pie-1* 3'UTR cassette (Figure 21C) and generated a transgenic line with this construct. The expression level of the transgene was only ~13% that of endogenous *lin-5* (Figure 22A), presumably owing to silencing of the transgenic constructs. Nevertheless, we were able to perform *in situ* hybridization against the *lin-5*[rec] transcript and found that *lin-5*[rec] is distributed uniformly in the cytoplasm (Figure 21C). Due to the low expression level of this transcript, we could not test the function of mislocalized *lin-5* mRNA. Generation of new lines that might allow for such analysis is in progress.

Based on the above-mentioned results, we conclude that the *lin-5* coding region is sufficient and also necessary for proper mRNA location.

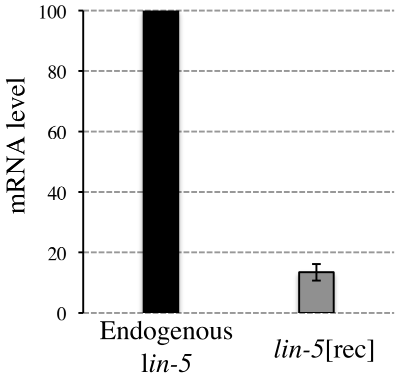

Figure 22. Levels of *lin-5*[rec] mRNA
qPCR analysis of *lin-5*[rec] mRNA. Levels of *lin-5*[rec] is expressed relative to endogenous *lin-5*. n=3 experiments.

A 9-nucleotide insertion in the coding region interferes with *lin-5* mRNA localization

We then wondered if extant *lin-5* mutant alleles could help narrow down the sequence directing mRNA localization. The *lin-5(ev571)* temperature sensitive mutant allele harbors a 9-nucleotide insertion in the coding region that is thought to disrupt function by impairing its coil-coiled domain, giving rise to dead progeny at the restrictive temperature (Figure 25D, Lorson et al., 2000). Although it is reported that LIN-5 protein localization is unaffected in these embryos, careful investigation of immunofluorescence images revealed a slight, but significant drop of centrosomal LIN-5 level (Figure 23A-C). On the other hand, overall cortical levels are not affected in these embryos.

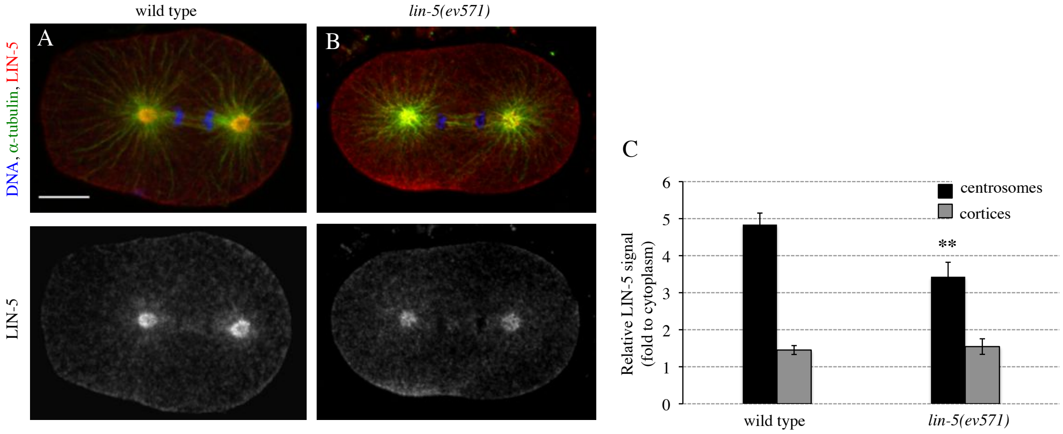

Figure 23. Centrosomal LIN-5 protein levels are reduced in *lin-5(ev571)* embryos
A-B LIN-5 protein localization at anaphase in wild type and in *lin-5(ev571)* embryos at the restrictive temperature. The upper images show the merge of DNA (blue), α-tubulin (green) and LIN-5 (red), the lower image displays LIN-5. **C** Quantification of centrosomal and cortical (both anterior and posterior) signal both relative to cytoplasmic values in wild type and *lin-5(ev571)* embryos. n=18 wild type and n=14 *lin-5(ev571)* embryos.

Intriguingly, we found that *lin-5* mRNA is mislocalized in *lin-5(ev571)* embryos at the restrictive temperature (Figure 25F). This result suggests either that LIN-5 protein function and proper centrosomal LIN-5 levels are needed for correct localization of *lin-5* mRNA or that the 9-nucleotide insertion disrupts the mRNA localization signal. As a step towards distinguishing between these possibilities, we analyzed *aspm-1(RNAi)* embryos, in which LIN-5 protein is absent from centrosomes (van der Voet et al., 2009). We confirmed the absence of spindle positioning phenotype of *aspm-1(RNAi)* embryos, indicating that the centrosomal pool of LIN-5 protein is not crucial for spindle positioning. More importantly, we found that *lin-5* mRNA distribution is normal in embryos depleted of ASPM-1 (Figure 24), demonstrating that centrosomal LIN-5 protein is dispensable for *lin-5* mRNA centrosomal enrichment.

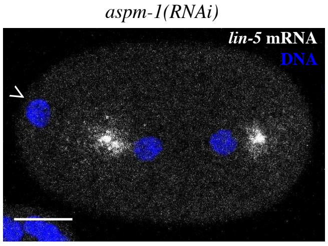

Figure 24. Centrosomal LIN-5 protein is dispensable for *lin-5* mRNA localization
A *lin-5* mRNA localization in *aspm-1(RNAi)* embryos. Arrowhead points to evidence of meiotic defects.

Compatible with LIN-5 protein not being required elsewhere in the cell either, we found furthermore that *lin-5* mRNA is also mislocalized in *lin-5(ev571)* embryos at the permissive temperature (data not shown). Next, we took advantage of a *lin-5(ev571)* revertant line, *lin-5(ev571he63)*, which harbors a single nucleotide missense mutation 16 nucleotides upstream of the *ev571* insertion site (Figure 25G; Fisk Green et al., 2004). This revertant exhibits a near-complete rescue of embryonic lethality at the restrictive temperature (Fisk Green et al., 2004), indicating that LIN-5 protein is functional, presumably through restoration of the coil-coiled domain (Fisk Green et al., 2004). Importantly, we found that *lin-5* mRNA nevertheless remains distributed uniformly in *lin-5(ev571he63)* embryos (Figure 25I). This reinforces the notion that *lin-5* mRNA can be mislocalized despite LIN-5 protein being functional and that the *ev571* insertion impairs the localization signal. Overall, these results raise the possibility that the localization signal *per se* is disrupted by the *ev571* insertion.

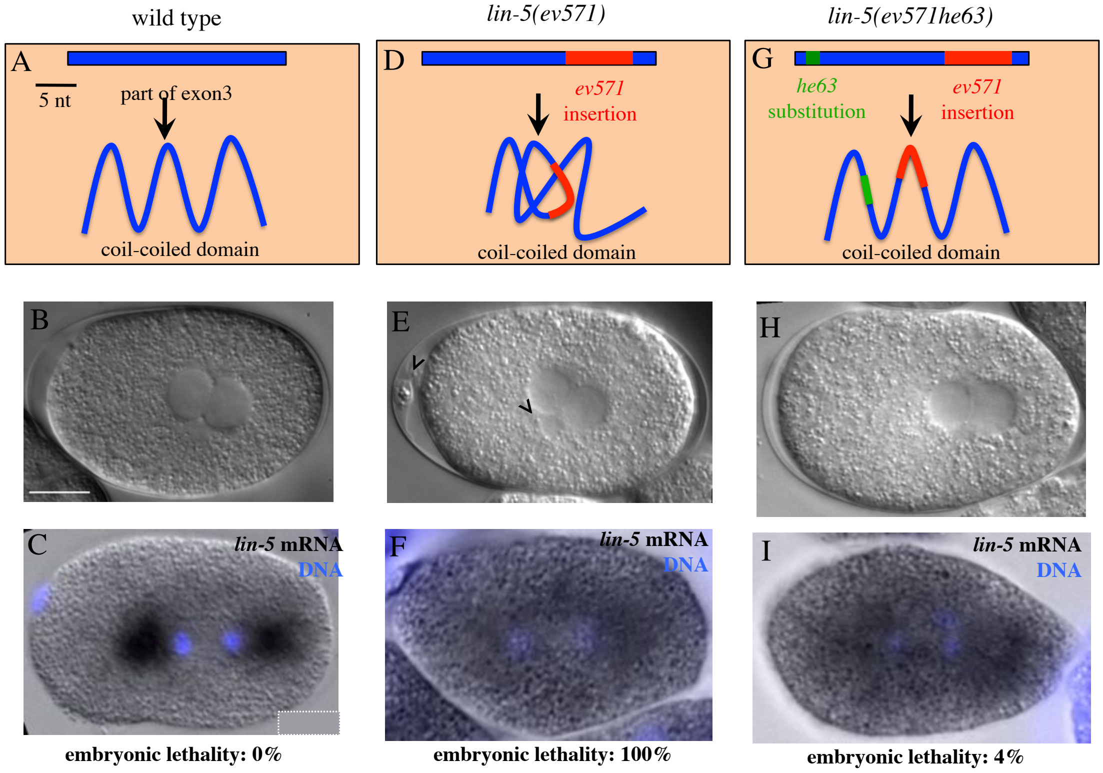
wild type
lin-5(ev571)
lin-5(ev571he63)
A
5 nt
part of exon3
coil-coiled domain
D
ev571
insertion
coil-coiled domain
G
he63
substitution
ev571
insertion
coil-coiled domain
B
E
H
C
lin-5 mRNA
DNA
F
lin-5 mRNA
DNA
I
lin-5 mRNA
DNA
embryonic lethality: 0%
embryonic lethality: 100%
embryonic lethality: 4%

Figure 25. A 9-nucleotide insertion in the coding region interferes with *lin-5* mRNA localization
A Schematics of wild type *lin-5* exon 3 and the predicted structure of the coil-coiled domain translated from this region. The same holds for **D** and **G**. **B** Wild type embryo at the stage of centration/rotation showing no meiotic defect. **C** Endogenous *lin-5* mRNA localization. Embryonic viability at 25°C is given below the images in **C**, **F** and **I**. **D** Schematics of exon 3 in *lin-5(ev571)*. The red region represents the 9-nucleotide/3-amino acids insertion. **E** *lin-5(ev571)* embryo at restrictive temperature at the stage of centration/rotation displaying meiotic defects (arrowheads). Note that no meiotic defect is observed at the permissive temperature. **F** *lin-5* mRNA distribution in *lin-5(ev571)* mutant embryo at the restrictive temperature. **G** Schematics of exon 3 in *lin-5(ev571he63)*. The green region shows the single nucleotide reverting substitution. **F** *lin-5(ev571he63)* embryo at the stage of centration/rotation showing no meiotic defect. **I** *lin-5* mRNA distribution in the *lin-5(ev571he63)* revertant.

We found wild type levels of total *lin-5* mRNA and total LIN-5 protein in *lin-5(ev571)* and in *lin-5(ev571he63)* embryos (Figure 26A and B), indicating that mRNA mislocalization does not influence mRNA- and protein stability.

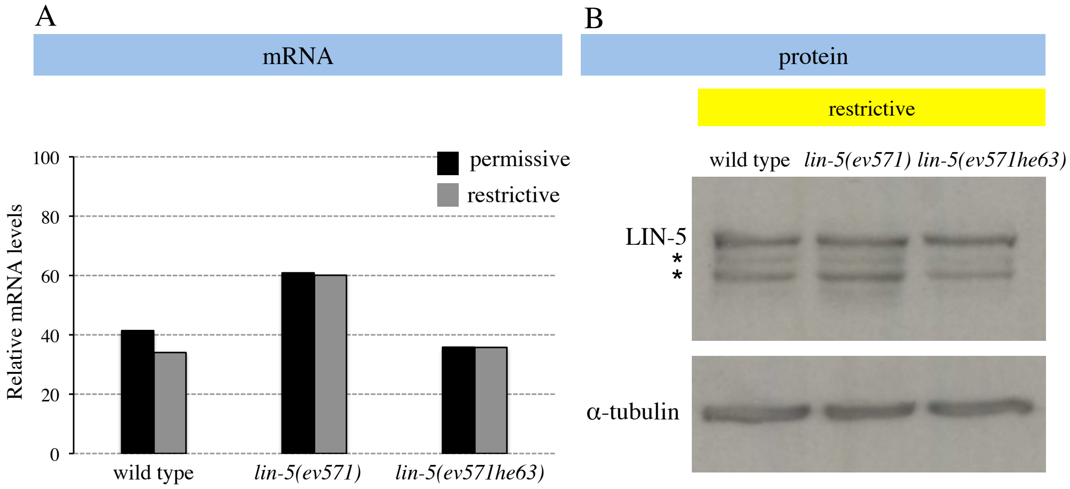

Figure 26. Embryos with mislocalized *lin-5* mRNA exhibit wild-type level of *lin-5* mRNA and LIN-5 protein
A qPCR analysis of *lin-5* mRNA in wild type, *lin-5(ev571)* and in *lin-5(ev571he63)* embryos at permissive (black) and restrictive (grey) temperatures. Values are expressed relative to *act-1* mRNA. n=1 experiment. **B** Western blot analysis of LIN-5 protein from embryonic lysates in wild type, *lin-5(ev571)* and in *lin-5(ev571he63)* embryos at the restrictive temperature. Asterisks mark bands that are sometimes detected by LIN-5 antibodies (Nguyen-Ngoc et al., 2008). α-tubulin was used as a loading control. n=2 experiments.

Prompted by these findings, we sought to identify conserved mRNA motifs in the vicinity of the region disrupted by the *ev571* insertion in four related nematode species (*C. elegans*, *C. briggsae*, *C. remanei and C. brenneri*). Suggestively, we found a 15-nucleotide stretch spanning the *ev571* insertion site that is highly conserved among these species (Figure 27A). This observation might indicate that this 15-nucleotide stretch is somehow important for *lin-5* mRNA localization around centrosomes. We sought to test if the region around the *ev571* insertion site forms any stem loop structure, indicative for RNA-protein interaction. We utilized three RNA structure prediction softwares, Mfold, RNAstructure and RNAfold, and found that a 75-nt region around the *ev571* site forms a secondary structure (Figure 27B-D). However, these secondary structures do not show any obvious similarities when comparing these species, perhaps because the 75-nt long region is not long enough to reveal structural similarities. On the other hand, this might indicate that the nucleotide sequence, rather than the secondary structure is important for mRNA localization. Further experiments, including ones in which the nucleotides in that region would be recoded, will be needed to address the function of this 15-nt stretch.

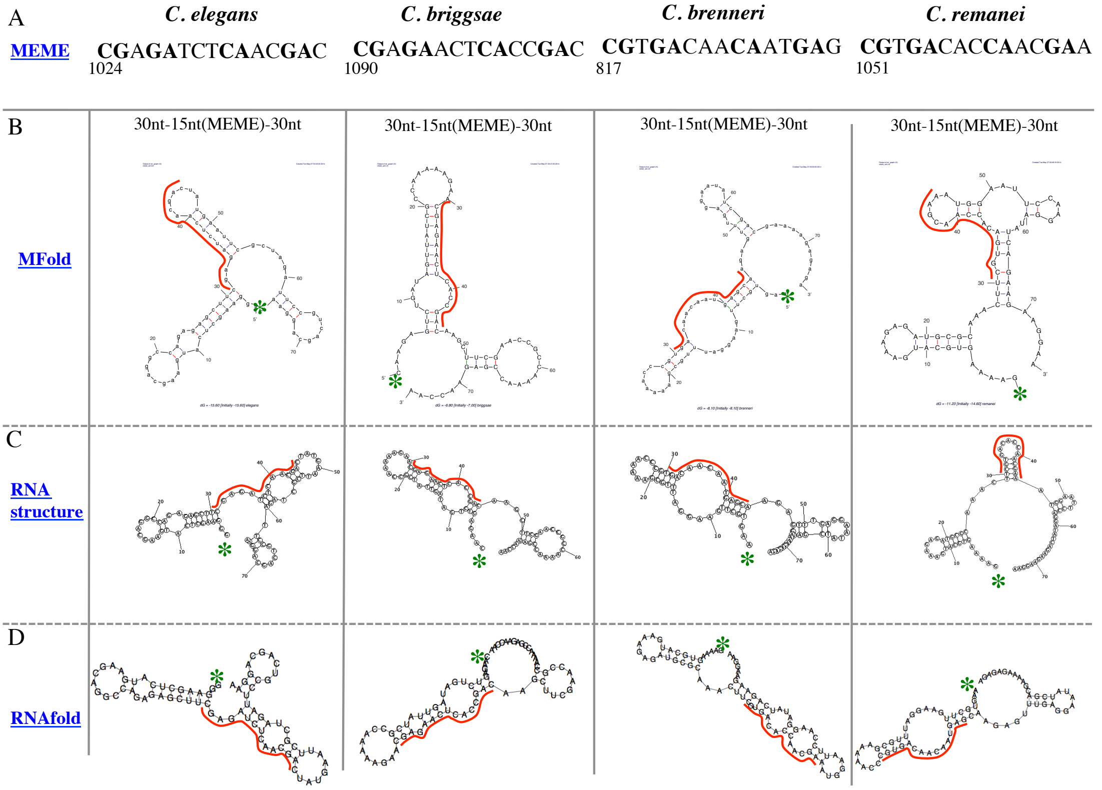
A
C. elegans
C. briggsae
C. brenneri
C. remanei
MEME
CGAGATCTCAACGAC
1024
CGAGAACTCACCGAC
1090
CGTGACAACAATGAG
817
CGTGACACCAACGAA
1051
B
30nt-15nt(MEME)-30nt
30nt-15nt(MEME)-30nt
30nt-15nt(MEME)-30nt
30nt-15nt(MEME)-30nt
MFold
C
RNA structure
D
RNAfold

Figure 27. An evolutionary conserved 15-nt region in the vicinity of the *ev571* site forms secondary structures

A An evolutionary conserved 15-nucleotide stretch around the *ev571* insertion site in *C. elegans, C. briggsae, C. remanei* and *C. brenneri* found by the MEME algorithm (Bailey et al., 2009). The starting position of this stretch in the cDNA sequence of each species is indicated below the first nucleotide. Bold letters show conserved region, normal ones variable ones. **B-D** RNA structure prediction of a 75-nt long region around the *ev571* site (30 nucleotides 5’ and 3’ from the 15-nt conserved region) with the softwares Mfold (B), RNAstructure (C) and RNAfold (D). Red line indicates the position of the 15-nt stretch; green star marks the starting point of the 75-nt region.

lin-5 mRNA mislocalization correlates with decreased posterior pulling forces and with misdistribution of the force generator complex

To test the relevance of *lin-5* mRNA localization, we took advantage of *lin-5(ev571)* embryos at the permissive temperature and *lin-5(ev571he63)* revertant embryos at the restrictive temperature. In both cases, *lin-5* mRNA is mislocalized despite what appears to be functional LIN-5 protein. Importantly, although *lin-5(ev571he63)* mutants exhibit only ~4% embryonic lethality (Fisk Green et al., 2004), analysis by time-lapse DIC microscopy enabled us to uncover fully penetrant spindle positioning defects in one-cell embryos. In particular, the robust oscillations of the posterior spindle pole during anaphase characteristic of the wild-type (Figure 28A) are not observed in *lin-5(ev571he63)* embryos (Figure 28D). To estimate the extent of pulling forces acting on spindle poles, we performed spindle severing experiments on these embryos. In line with the presence of decreased posterior spindle oscillations, we revealed a significant decrease in net pulling forces on the posterior side (Figure 28E). These experiments further support the notion that LIN-5 protein function is restored in these revertants, since anterior peak velocities are indistinguishable from the wild type. Importantly, posterior spindle pole oscillations are also diminished in *lin-5(ev571)* embryos at the permissive temperature (Figure 28B), further demonstrating that mislocalized *lin-5* mRNA correlates with a diminished pulling forces acting on the posterior side. Importantly, we cannot exclude that the protein is not fully functional in these backgrounds. Meiotic defects that are prevalent in embryos where LIN-5 function is perturbed are not observed in *lin-5(ev571)* embryos at the permissive temperature or in *lin-5(ev571he63)* embryos at the restrictive temperature (Figure 25B, E and H), suggesting that, as far as meiosis in concerned, LIN-5 protein regained function in the revertant strain. Note, however that partial reduction of GPR-1 leads to a dramatic drop in the amplitude of posterior spindle pole oscillation (Pecreaux et al., 2006). Therefore, we cannot rule out the possibility that different thresholds of functional LIN-5 protein operate for proper spindle pole oscillation and pulling forces, and the phenotypes observed are the consequence of not fully functional LIN-5 protein.

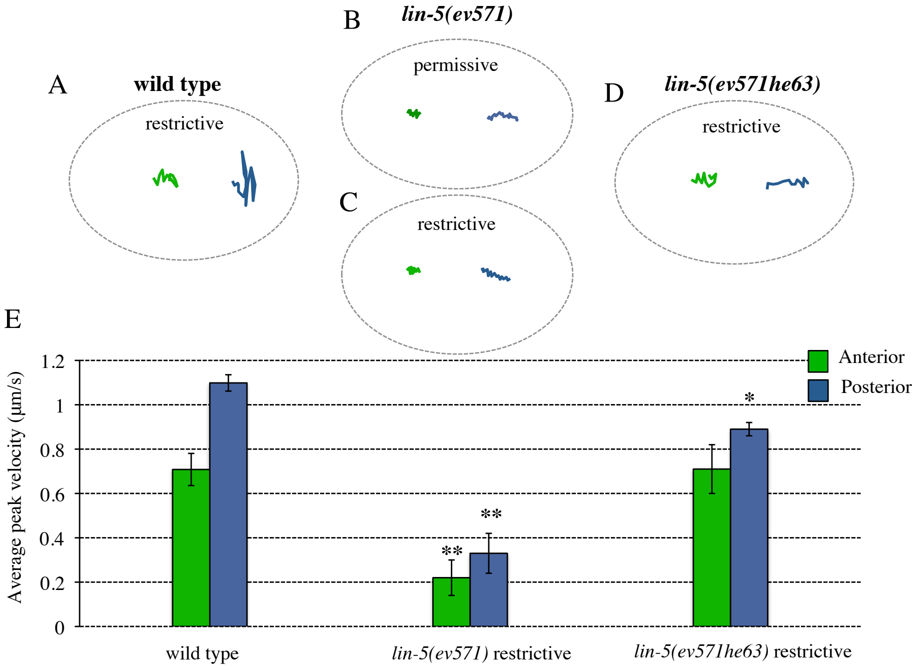

Figure 28. Mislocalization of *lin-5* mRNA results in decreased posterior pulling forces
A-D Representative anterior (green) and posterior (blue) spindle pole oscillations in wild type (**A**), *lin-5(ev571)* at permissive (**B**) and restrictive temperature (**C**) or *lin-5(ev571he63)* (**D**). Tracking of spindle poles was performed from the onset of posterior spindle displacement until cytokinesis onset. **E** Spindle severing experiments revealing net pulling forces acting on spindle poles at anaphase. Number of embryos analyzed: wild type (n=7), *lin-5(ev571)* (n=5) and *lin-5(ev571he63)* (n=8).

Having this possibly caveat in mind, we decided to investigate *lin-5(ev571he63)* embryos. As an other means to investigate the consequence of the decrease in pulling forces on the posterior side, we challenged *lin-5(ev571he63)* embryos with *goa-1(RNAi*), in which spindle positioning is slightly impaired. We found that *goa-1(RNAi*) results in ~25% embryonic lethality in the wild type, but in ~80% embryonic lethality in the *lin-5*(*ev571,he63*) background (Figure 29), suggesting that pulling forces are impaired in the revertant.

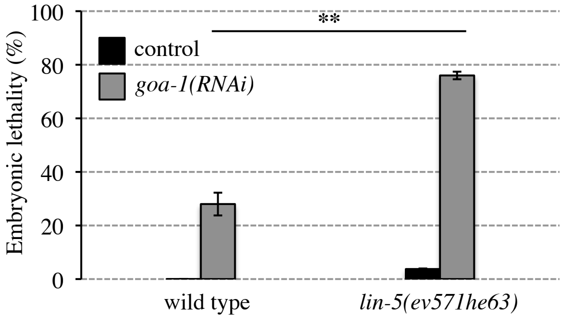

Figure 29. Mislocalization of *lin-5* mRNA sensitizes the embryos to slight malfunction of the force generator complex
Embryonic lethality in wild type and *lin-5(ev571he63)* embryos upon *goa-1(RNAi)*. n>100 embryos were analyzed in each case.

To investigate the cause of decreased posterior pulling forces in *lin-5(ev571he63)*, we performed immunofluorescence analysis to reveal the distribution of cortical force generator components in *lin-5(ev571)* embryos at the permissive temperature and in *lin-5*(*ev571he63*) embryos at the restrictive temperature. As GPR-1/2 exhibits the most obvious asymmetry between the anterior and posterior cortices in the wild-type, we focused our analysis on this component. We found that whereas GPR-1/2 is slightly enriched on the posterior cortex during mitosis in the wild-type (Figure 30A, quantified in D), this slight asymmetry is absent at the restrictive temperature in *lin-5(ev571)* and *lin-5*(*ev571he63*) embryos (Figure 30B and C, quantified in D). These findings establish that there is less GPR-1/2 at the posterior cortex in these conditions than there is in the wild-type, which likely explains the observed decrease in net forces pulling on the posterior side.

Taken together, these results indicate that *lin-5* mRNA enrichment around centrosomes is important for proper generation of pulling forces acting on the posterior spindle pole in one-cell *C. elegans* embryos.

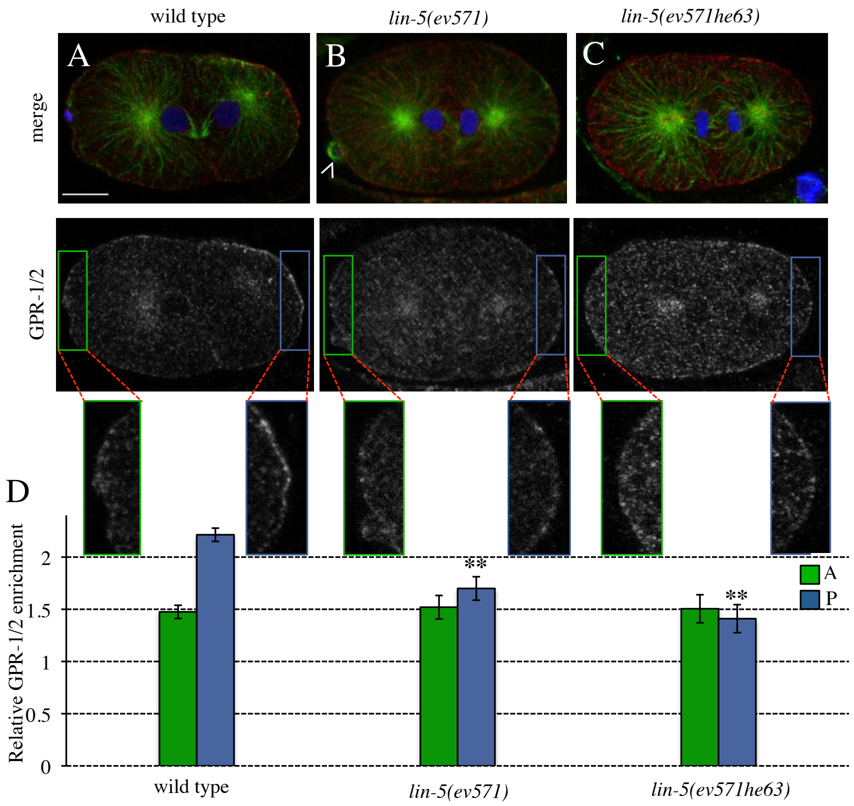

Figure 30. Mislocalization of *lin-5* mRNA leads to misdistribution of the force generator complex

A-C GPR-1/2 immunostaining of wild type (**A**), *lin-5(ev571)* (**B**) and *lin-5(ev571he63)* (**C**) anaphase embryos at restrictive temperature. The upper images show the merge of DNA (blue), α-tubulin (green) and GPR-1/2 (red), the lower images the GPR-1/2 signal alone. The arrowhead in B points to meiotic defects. **D** Quantification of cortical GPR-1/2 enrichment relative to the cytoplasm in embryos of indicated genotypes. Insets display magnified region of anterior (green) and posterior (blue) cortex. Number of embryos analyzed: wild type (n=9), *lin-5(ev571)* (n=10) and *lin-5(ev571he63)* (n=9).

lin-5 mRNA centrosomal enrichment is asymmetric in anaphase

How could centrosomal localization of *lin-5* mRNA promote the asymmetric distribution of cortical force generators? To begin addressing this question, we quantified *lin-5* mRNA enrichment around the two centrosomes through the first cell cycle using single molecule FISH (Figure 31). Interestingly, this analysis revealed that *lin-5* mRNA enrichment at the anterior centrosome increases as the cell progresses from prometaphase to anaphase, while the posterior signal is unchanged. Such unequal enrichment leads to asymmetric enrichment at anaphase between the two centrosomes, with significantly less *lin-5* mRNA present around the posterior centrosome compared to the anterior one (Figure 31).

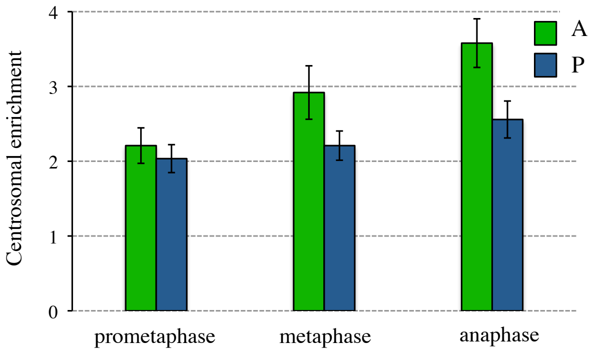

Figure 31. *lin-5* mRNA enrichment increases at the anterior spindle pole during the first cell cycle.
Centrosomal enrichment relative to cytoplasmic signal were quantified in prometaphase, metaphase and anaphase embryos. n= 13, 8 and 14, respectively.

We next tested if such centrosomal asymmetry in anaphase depends on A-P polarity cues by examining *lin-5* mRNA localization in embryos lacking the function of the anterior PAR protein PAR-3 or the posterior PAR protein PAR-2. Importantly, we found that *par-3(it74)* embryos or *par-2*(*RNAi*) embryos exhibit no difference in the extent of *lin-5* mRNA enrichment around the two centrosomes (Figure 32B-C, and

G-H). We conclude that A-P polarity cues regulate the asymmetric enrichment of *lin-5* mRNA around centrosomes in anaphase.

The above experiments revealed that *lin-5* mRNA enrichment at centrosomes is symmetric when pulling forces acting on spindle poles are either low or high on both sides. To address if unequal forces are indeed important for the asymmetric enrichment of *lin-5* mRNA around the two centrosomes, beyond conditions in which A-P polarity is perturbed, we examined embryos with normal A-P polarity but altered pulling forces. We found that embryos in which forces are higher on both sides due to expression of YFP-GPR-1 exhibit more similar *lin-5* mRNA enrichment around both anterior and posterior spindle poles (Figure 32D and I). Similarly, upon depletion of GPR-1/2 when pulling forces are equally weak on both sides, the extent of *lin-5* mRNA enrichment at the two spindle poles is equal (Figure 32E and J). Overall, these findings establish that unequal net pulling forces contribute to asymmetric *lin-5* mRNA enrichment at centrosomes, suggesting a positive feedback mechanism whereby increased pulling forces on the posterior side contribute to lowering the amount of *lin-5* mRNA around the posterior spindle pole (see Discussion).

Although we have not performed quantitative single molecule FISH in *C. briggsae*, the difference of *lin-5* mRNA signal between the two spindle poles at anaphase is seemingly also present in this species (see Figure 18B), suggesting that this feature is evolutionary conserved and thus of biological relevance.

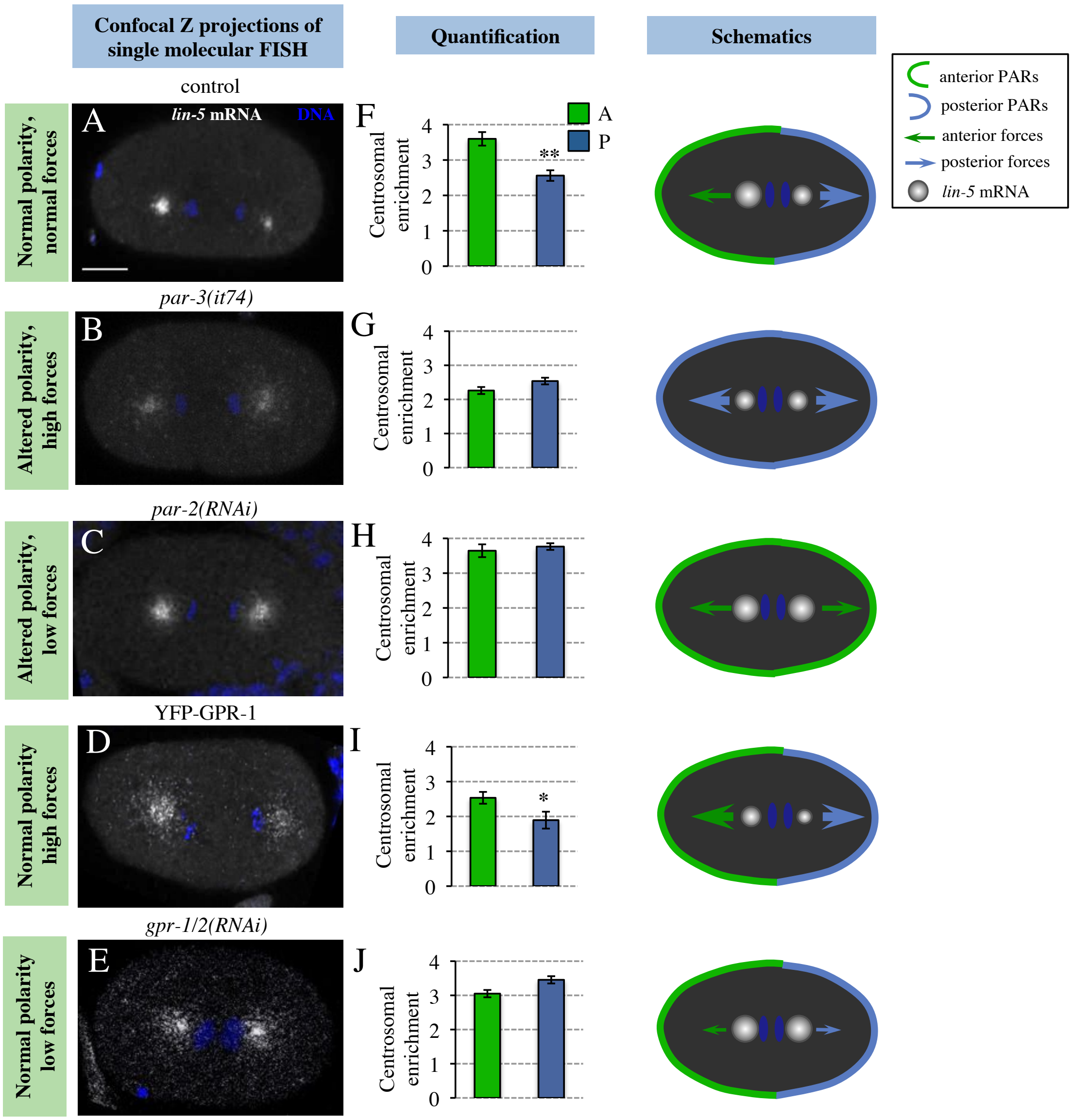

Figure 32. Asymmetric enrichment of *lin-5* mRNA at anaphase is polarity- and force-dependent
A-E Z projection of confocal sections of *lin-5* mRNA single molecular FISH probes in wild type (**A**), *par-3(it74)* (**B**), *par-2(RNAi)* (**C**), YFP-GPR-1 (**D**) or *gpr-1/2(RNAi)* (**E**) anaphase embryos. Cartoons on the right represent the status of polarity (green: anterior, blue: posterior), of forces acting on the two spindle poles (green and blue arrows, respectively) and of *lin-5* mRNA centrosomal enrichment in each condition. **F-J** Quantification of *lin-5* mRNA centrosomal enrichment (relative to cytoplasm) in the conditions described in A-E. Numbers of embryos analyzed: wild-type (n=16), *par-3(it74)* (n=9), *par-2(RNAi)* (n=8), YFP-GPR-1 (n=10), *gpr-1/2(RNAi)* (n=8).

de novo lin-5 translation/folding occurs preferentially in the cytoplasm during mitosis

To explore the potential importance of having less *lin-5* mRNA around the posterior centrosome, we addressed if *lin-5* mRNA is translated during mitosis using embryos expressing LIN-5-GFP. Cortical LIN-5-GFP is not detectable in one-cell embryos of this strain, and we focused our analysis on the centrosomal and cyoplasmic signals (Figure 34A-E). To address whether *lin-5* mRNA is translated during mitosis, we developed an assay that we dubbed Fluorescence Recovery After complete Photobleaching (FRAcP). The goal of this assay is to completely bleach the LIN-5-GFP signal in the embryo and record fluorescence intensity thereafter to investigate the extent of *de novo* protein synthesis and protein folding (Figure 33A). If no fluorescence recovery is observed, the conclusion would be that no protein is translated/folded *de novo* (Figure 33B, upper most scenario). By contrast, if fluorescence signal recovery is observed, this could reflect *de novo* protein synthesis or the folding of already translated LIN-5-GFP.

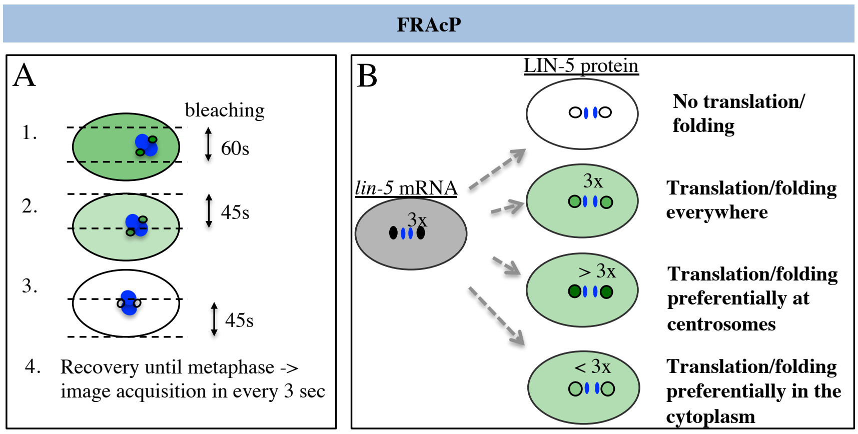
FRAcP
A
bleaching
1.
60s
2.
45s
3.
45s
4. Recovery until metaphase -> image acquisition in every 3 sec
B
LIN-5 protein
No translation/ folding
lin-5 mRNA
3x
3x
Translation/folding everywhere
> 3x
Translation/folding preferentially at centrosomes
< 3x
Translation/folding preferentially in the cytoplasm

Figure 33. Principle of the FRAcP experiment and its possible interpretations
A Schematic illustration of the Fluorescent Recovery after Complete Photobleaching (FRAcP) experiment. **B** Possible outcomes of FRAcP experiments with corresponding conclusions.

As shown in Figure 34F-K, FRAcP experiments revealed that LIN-5-GFP fluorescence does recover after complete bleach to ~17% at centrosomes and to ~22% in the cytoplasm of the initial intensities measured before the bleach. Therefore, LIN-5-GFP undergoes folding and/or translation during mitosis in one-cell *C. elegans* embryos. We attempted to block translation by treating the embryos with the translational inhibitor cycloheximide (CHX). However, we found no major phenotypic effect, such as cell cycle arrest, suggesting that the concentration of CHX used in these experiments (10mg/ml) is not high enough or that the drug cannot act within the time frame of the experiment. Thus, not having discriminated between the two processes, we will refer to the observed recovery as translation/folding.

We reasoned that FRAcP might also reveal whether *lin-5* mRNA translation/folding takes place preferentially at centrosomes or in the cytoplasm (Figure 33B). Given that *lin-5* mRNA exhibits a ~3 fold enrichment at centrosomes compared to the cytoplasm, a similar 3:1 centrosomal versus cytoplasmic ratio is expected for LIN-5-GFP signal recovery if translation/folding takes place with similar efficiency regardless of subcellular localization. By contrast, a ratio higher than 3:1 would suggest preferential translation/folding of the centrosomal pool. Conversely, a ratio smaller than 3:1 would suggest preferential translation/folding of the cytoplasmic pool. As shown in Figure 34L, we found that GFP recovery is observed initially in the cytoplasm and that the centrosomal versus cytoplasmic ratio of the fluorescence intensities is ~1. Therefore, *lin-5* mRNA is translated/folded preferentially in the cytoplasm.

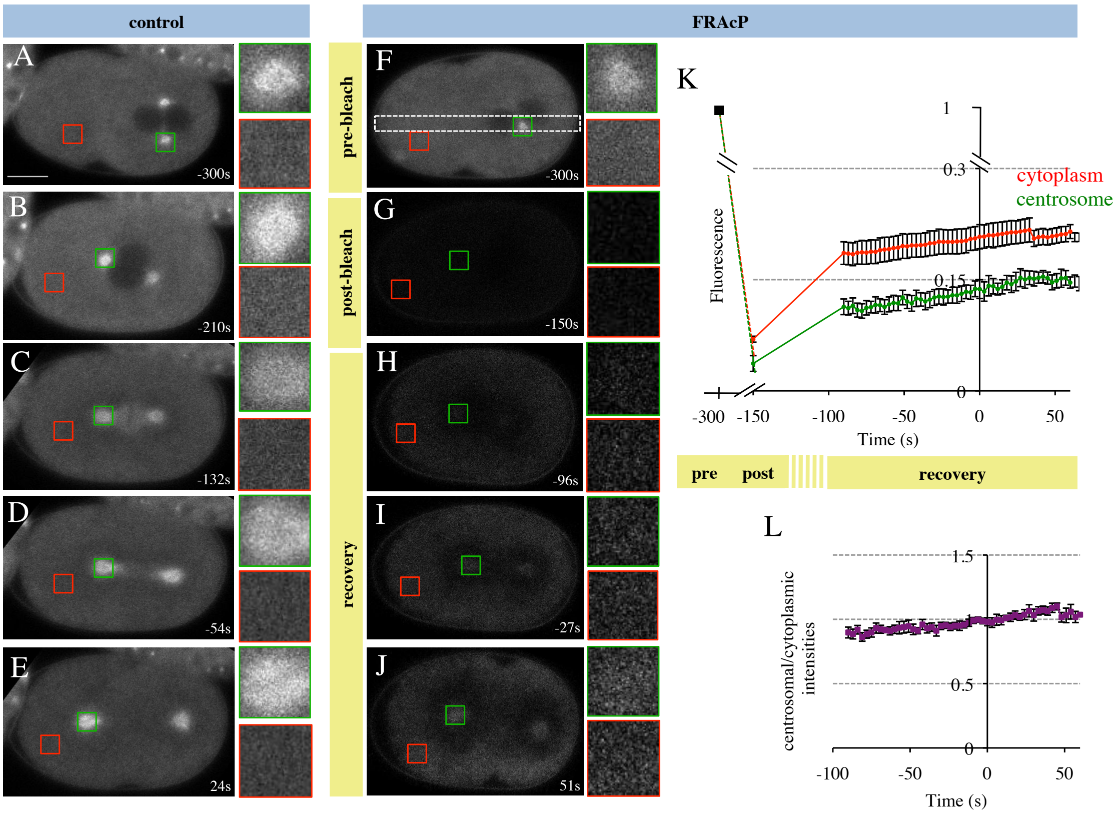
control
FRAcP
A
-300s
B
-210s
C
-132s
D
-54s
E
24s
pre-bleach
post-bleach
recovery
F
-300s
G
-150s
H
-96s
I
-27s
J
51s
K
1
0.3
0.15
0
cytoplasm
centrosome
Fluorescence
-300
-150
-100
-50
0
50
Time (s)
pre
post
recovery
L
1.5
0.5
0
centrosomal/cytoplasmic intensities
-100
-50
0
50
Time (s)

Figure 34. LIN-5 is *de novo* translated/folded during mitosis
A-E Images from a time-lapse recording of one-cell embryo expressing LIN-5-GFP. Insets show magnified region of the cytoplasm (red) and the centrosome (green) at prophase (**A**), prometaphase (**B**), metaphase (**C**), anaphase (**D**) and telophase (**E**). t=0 corresponds to cytokinesis onset. **F-O** Complete FRAP (cFRAP) in LIN-5-GFP embryo; insets are as in A-E. **F** Pre-bleach fluorescence intensities. **G** Post-bleach fluorescence intensities. **H-J** Fluorescence recovery at metaphase (**H**), anaphase (**I**) and telophase (**J**). **K** Cytoplasmic (red) and centrosomal (green) signal recovery relative to pre-bleach values (black square) plotted as a function of time. Intensities in the cytoplasm and at centrosomes are shown relative to pre-

bleach signals. n=8 embryos. **L** Centrosomal/cytoplasmic signal intensities during mitosis. n=8.

Next, in order to address if LIN-5-GFP molecules shuttle between the cytoplasm and centrosomes, we performed two types of Fluorescence Loss In Photobleaching (FLIP) experiments (Figure 35A). We either bleached extensively the anterior centrosome and measured fluorescence intensities in the neighboring cytoplasm (referred to as ‘centro-bleach’) or bleached a cytoplasmic region and then quantified fluorescence intensities of the centrosome (‘cyto-bleach’). We found decreased intensities of the unbleached region in both cases (Figure 35B), showing that LIN-5-GFP molecules are transported bi-directionally during mitosis. Quantifying the extent of fluorescence decrease in the unbleached regions revealed that the centrosomal pool decreases to a greater extent upon cyto-bleach than does the cytoplasmic pool upon centro-bleach (38% vs. 19%, Figure 35C). This is not the consequence of unequal bleach, because the two post-bleach values were comparable. Given that the LIN-5-GFP signal and thus supposedly the number of molecules are ~2-fold higher at centrosomes at the time of the bleach as compared to the cytoplasm, we likely bleach 2 times more molecules during the centro-bleach than during the cyto-bleach. Based on this, we speculate that the bias in the direction of the transport is underestimated by this method and is higher in reality. These results, together with the FRAcP data, suggest that LIN-5-GFP molecules synthetized/folded *de novo* in the cytoplasm move to the centrosome, explaining how LIN-5 protein can accumulate at that location despite preferential translation in the cytoplasm.

Taken together, these experiments suggest that *lin-5* mRNA is translated/folded preferentially in the cytoplasm during mitosis.

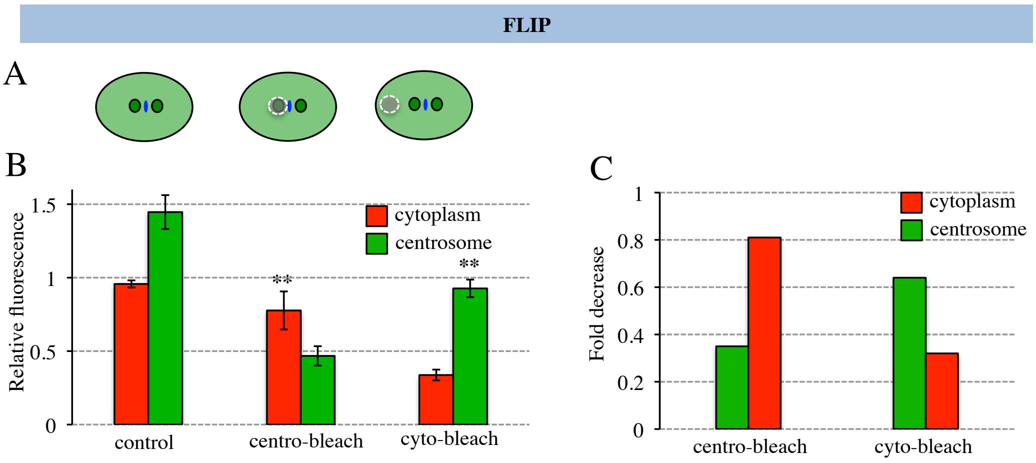

Figure 35. Bi-directional transport of LIN-5-GFP is favored from cytoplasm to centrosome than from centrosome to cytoplasm during mitosis
A Schematics explaining two versions of Fluorescence loss after photobleaching (FLIP) experiments performed in LIN-5-GFP embryos. Either the centrosome was bleached and the intensities in the cytoplasm were measured (centro-bleach), or the cytoplasm was bleached and the centrosomal intensity was registered (cyto-bleach). **B** Relative signal intensities measured for untreated, centro-bleach and cyto-bleach conditions. Fluorescence intensities at centrosomes (green) and in the cytoplasm (red) were measured at telophase and plotted relative to the metaphase values. n=6 embryos. **C** Fold decrease of centrosomes (green) and cytoplasm (red) after centro- or cyto-bleach.

Morpholino-mediated inhibition of *lin-5* mRNA translation leads to decreased posterior pulling forces

We sought to test the importance of *de novo* synthesized LIN-5 protein by inhibiting *lin-5* mRNA translation using morpholinos (MO). MOs efficiently block protein synthesis by binding to the translational initiation site of mRNAs and have been widely used in model systems such as *Xenopus* or zebrafish as well as in other nematode species (Louvet-Vallee et al., 2003). However, to our knowledge, MOs have never been utilized in *C. elegans*. To evaluate the potency of MOs in *C. elegans*, we injected *lin-5* MOs in the gonad and found that the majority of the resulting embryos exhibit a strong *lin-5* phenotype, included pronounced meiotic defects (Figure 36D). For the exact quantification of this phenotype, see the Materials and Methods section on page 136.

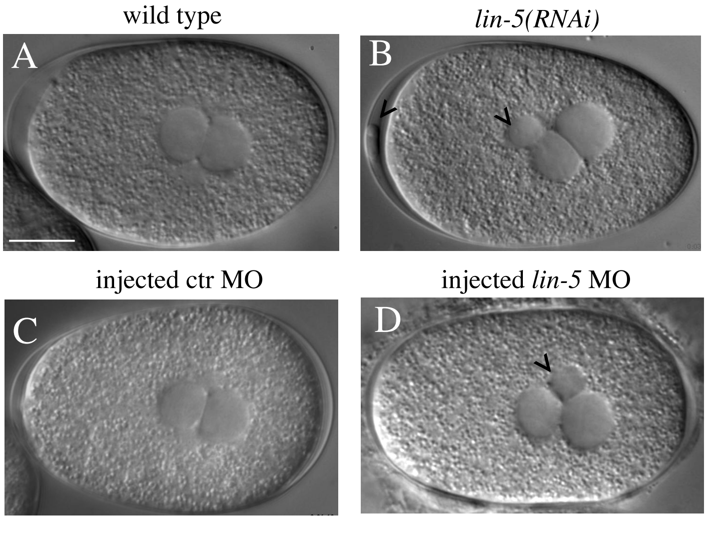

Figure 36. *lin-5* morpholinos are capable of inhibiting *lin-5* translation in the gonad
A-D: One-cell embryos during centration/rotation: wild type (**A**), *lin-5(RNAi)* (**B**), control MO injected (**C**) and *lin-5* MO injected (**D**). Arrowheads indicate the presence of aberrant polar bodies and multiple female pronuclei, which are both hallmarks of meiotic defects.

Next, to block *lin-5* translation specifically in the first cell cycle, we reasoned that MOs coated with lipofectamine (LF) could enter the embryo after piercing the eggshell with a laser beam, as done previously for drug treatments (Figure 37A). After piercing the eggshell, we investigated the impact of interfering with *lin-5* translation during mitosis on anaphase pulling forces. Strikingly, we found that whereas embryos treated with control MOs exhibit normal oscillations (Figure 35B), impairing *lin-5* translation results in decreased oscillations of the posterior spindle pole (Figure 37C). Moreover, spindle severing experiments uncovered a significant decrease in pulling forces specifically on the posterior spindle pole (Figure 37D). These findings demonstrate that *lin-5* mRNA translation during mitosis contributes to generating proper pulling forces.

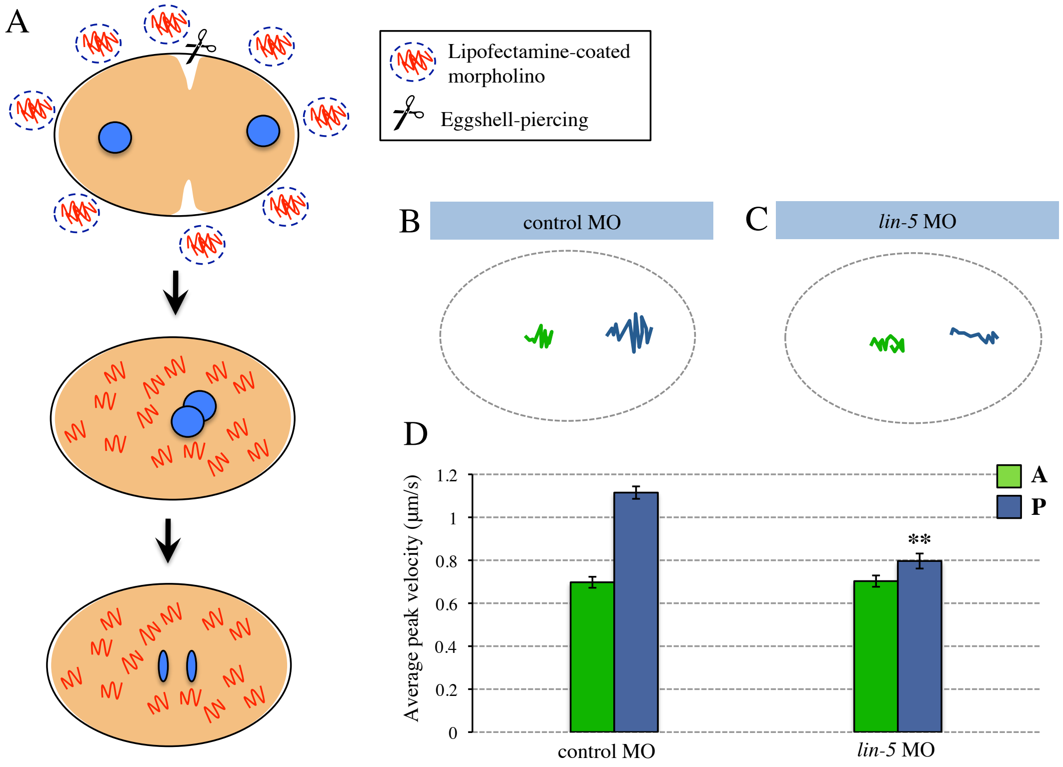

Figure 37. Impairing translation of *lin-5* mRNA during mitosis results in decreased posterior pulling forces

A Schematic representation of morpholino experiment. Wild type embryos were used for DIC and for spindle severing experiments. The eggshell was pierced with a UV-laser at the pseudocleavage stage to let the lipofectamine-coated morpholino molecules enter the cell. **B-C** Spindle pole oscillations of representative wild type embryo treated with control (**B**) or *lin-5* (**C**) MOs. Anterior (green) and posterior (blue) spindle pole were tracked. Tracking of spindle poles was performed from the onset of posterior spindle displacement until cytokinesis onset. **D** Spindle severing experiments performed in embryos treated with control or *lin-5* MOs. Number of embryos analyzed: control MO (n=14), *lin-5* MO (n=15) from 3 experiments.

3B. DISCUSSION

We uncovered here that *lin-5* mRNA is enriched around centrosomes during early *C. elegans* development. We demonstrated that this enrichment is less pronounced around the posterior spindle pole than around the anterior spindle pole in anaphase one-cell embryos. We also established that embryos in which *lin-5* mRNA is distributed in a uniform manner exhibit reduced pulling forces on the posterior spindle pole. Combined with the fact that translation/folding of LIN-5-GFP occurs more readily in the cytoplasm than at centrosomes, these findings lead us to propose a working model that is summarized in Figure 38. In this model, following the capture of the mRNA at the anterior centrosome in anaphase, more *lin-5* mRNA is available for translation in the posterior cytoplasm. As a result, slightly more LIN-5 protein is available on the posterior side, which contributes to generating a larger net pulling force on the posterior spindle pole. Even though the trigger for the capture of *lin-5* mRNA from at the posterior centrosome remains to be identified, we postulate that more *lin-5* mRNA in the cytoplasm can lead to increased LIN-5 production and increased pulling forces on the posterior side, thus creating a positive feedback loop. That this is the case is underscored by the finding that modulating pulling forces by altering GPR-1/2 levels impacts on *lin-5* mRNA localization. Importantly in addition, we found that seemingly different levels of *lin-5* mRNA on the two centrosomes are also present in *C. briggsae* embryos during mitosis, demonstrating that asymmetric *lin-5* mRNA localization at anaphase is evolutionary conserved.

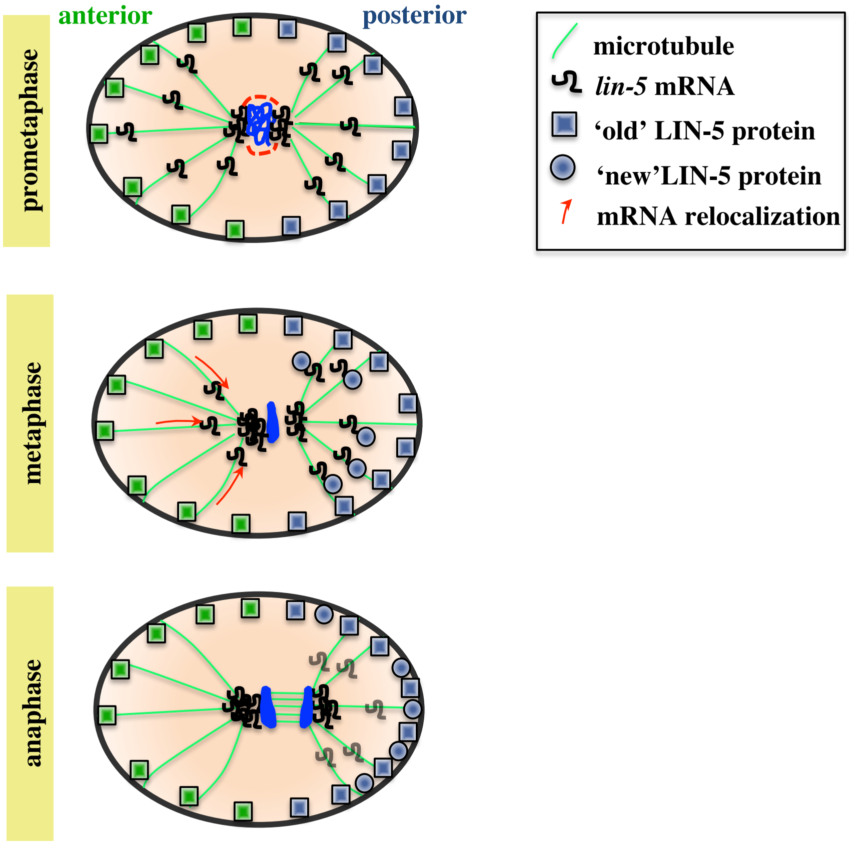
anterior
posterior
prometaphase
metaphase
anaphase
microtubule
lin-5 mRNA
'old' LIN-5 protein
'new'LIN-5 protein
mRNA relocalization

Figure 38. Model explaining the function of *lin-5* mRNA localization in asymmetric pulling force generation.
See text for details.

mRNA enrichment around centrosomes: beyond *lin*-5

There is ample precedent in other systems for mRNAs being enriched around centrosomes. For instance, many mRNAs, including ones encoding putative developmental transcription factors, are enriched around centrosomes in embryonic blastomeres of the spiralian lophotrochozoan gastropod *Crepidula fornicata* (Henry et al., 2010). Similarly, mRNAs are enriched at centrosomes in the mollusk *Spisula solidisima* (Alliegro and Alliegro, 2008; Alliegro et al., 2006). Likewise, numerous transcripts localize to the Centrosome Attracting Body (CAB), an organelle associated with one of the two centrosomes in ascidian embryos (reviewed in Prodon et al., 2007). As a result, these mRNAs are inherited by only one of the two daughter cells following mitosis. Similarly, centrosomal mRNA enrichment ensures asymmetric segregation of transcripts crucial for developmental patterning and in cell fate specification in the mollusk *Illyana obsolete* (Chan and Lambert, 2011; Kingsley et al., 2007; Lambert and Nagy, 2002; Rabinowitz et al., 2008; Rabinowitz and Lambert, 2010; Swartz et al., 2008). The asymmetric inheritance is achieved by the transport of these mRNAs in a microtubule-dependent manner from the centrosome to the cortex where they are anchored by the actin cytoskeleton (Lambert and Nagy, 2002). Our findings in *C. elegans* indicate by contrast that the overall amount of *lin-5* mRNA is similar in the two daughters of the one-cell embryo. Accordingly, *lin-5* is not in the list of mRNAs differentially expressed between isolated AB and P_1 blastomeres (Hashimshony et al., 2012).

Is the enrichment around centrosomes conserved amongst mRNAs encoding LIN-5-related molecules across evolution? We showed that such localization is also observed in *C. briggsae*, indicating conservation for at least ~100 million years. We note, however, that the mRNA encoding the LIN-5 related protein NuMA is not amongst the microtubule-associated transcripts that have been identified in *Xenopus* egg extracts, indicating that centrosomal enrichment might not extend to vertebrates (Blower et al., 2007). The situation may differ in *Drosophila*, where examination of a publicly available *in situ* hybridization resource reveals that the mRNA encoding the LIN-5-related protein Mud exhibits an intriguing perinuclear focal localization compatible with centrosomal enrichment (see Figure 39 and http://fly-fish.ccbr.utoronto.ca/insitu_image_storage/img_dir_43/insitu43389.jpeg; DNA in red, *mud* mRNA in green (Lecuyer et al., 2007). Therefore, it may be that the enrichment around centrosomes uncovered in this study will prove significant in other systems.

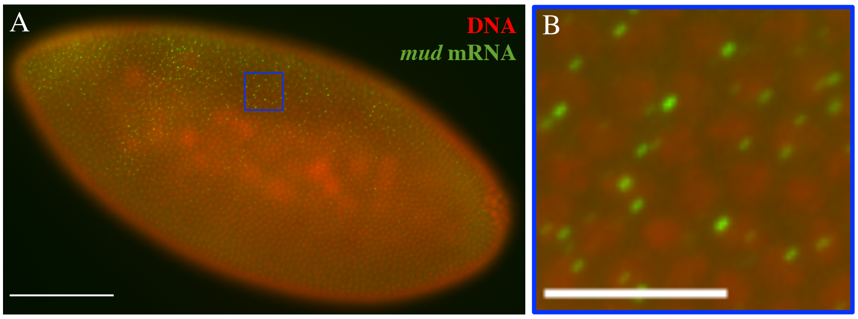

Figure 39. *mud* mRNA appears to form perinuclear punctae resembling centrosomes in *Drosophila* embryos.
Low (A) and high magnification (B) of an mRNA probed for *mud* mRNA (green) and stained for DNA (red). Scale bars are 100 and 20 microns. Image source: Lecuyer et al., 2007.

Localization as a means to control translation of *lin-5* mRNA

Translational repression is a widespread mechanism regulating localized mRNAs, which can act at different steps of the translational process. Thus, the Fragile X Mental retardation protein (FMRP) RNA binding protein recruits the eIF4E binding protein CYFIP1 to target mRNAs as they are transported from neuronal cell bodies to dendrites, thereby interfering with translation initiation (Napoli et al., 2008). Furthermore, as mentioned in the Introduction, complex mechanisms ensure translational regulation of the *ash1* mRNA in budding yeast or of *oskar*, *bicoid*, *nanos* and *gurken* mRNAs in the *Drosophila* oocyte (see Introduction on pages 42-44). Translational repression can occur via inhibition of the 40S and the 60S ribosomal subunit assembly (in the case of *ash1* mRNA) or by interfering with the elongation factor 4E (for *oskar* and *nanos* mRNAs). It will be interesting to investigate at which step *lin-5* mRNA translation is repressed at centrosomes.

In other systems, mislocalization of mRNAs can result in premature and thus excess translation, as for *ash1* in budding yeast (Gu et al., 2004; Paquin et al., 2007) or *oskar* in *Drosophila* (Kim-Ha et al., 1995; Nakamura et al., 2004). By contrast, our data indicate that mis-localization of *lin-5* mRNA to the cytoplasm is not sufficient for excess translation. This suggests that, regardless of the mechanism, another regulatory step, perhaps coupled to cell cycle progression, must take place to render *lin-5* mRNA ready to be translated/folded in the cytoplasm. Interestingly, the phosphorylation status and thereby the membrane-binding capability of the LIN-5 homologue NuMA is regulated at the metaphase to anaphase transition by CDK1 in human cells (Kotak et al., 2013). It is intriguing to speculate that *lin-5* mRNA translation is under the control of similar mechanisms.

We revealed that GPR-1/2 asymmetry in anaphase is lost when *lin-5* mRNA is mislocalized, and we speculate that GPR-1/2 imunostaining is a reliable proxy for probing the overall distribution of force generator complexes. As far as LIN-5 is concerned, we found that overall cortical levels of LIN-5 are unchanged in *lin-5(ev571)* embryos (Figure 23), indicating that LIN-5 protein localization is seemingly independent of *lin-5* mRNA localization. How about the asymmetry in LIN-5 cortical enrichment? LIN-5 asymmetry between the anterior and posterior cortex at anaphase is marginal, as only half of the embryos show more posterior enrichment at the cortex compared to the anterior one (see Introduction on page 25; Park and Rose, 2008). Therefore, addressing this important question is experimentally difficult.

lin-5 mRNA localization, preferential translation and asymmetric pulling forces

Although this study represents the first report regarding the importance of translational regulation in one-cell *C. elegans* embryos, translational regulation has been established in other instances during early *C. elegans* development (see Introduction on pages 48-51). In all of these cases, orchestrated action of translational repressors and activators lead to localized protein translation. By analogy, at the subcellular level, perhaps preferential translation of *lin-5* mRNA in the cytoplasm is due to the presence of a translational repressor at centrosomes or of a translational activator away from them.

Is it possible that translational repressors, which may act specifically on *lin-5* mRNA or on other mRNAs as well, are enriched around centrosomes in *C. elegans* embryos? The existence of such factors is plausible, especially given that in human tissue culture cells GW/P bodies marking microRNA-mediated translational repression events (Jakymiw et al., 2005; Liu et al., 2005a; Liu et al., 2005b) are enriched around centrosomes (Aizer et al., 2008; Moser et al., 2011). In fact, there is precedent for differential translation of mRNAs enriched around centrosomes, except that protein synthesis occurs preferentially at centrosomes in those cases, in contrast to the situation with *lin-5* mRNA. Thus, *Xenopus* Cyclin B1 and Xbub mRNAs are enriched at centrosomes, where they are translated preferentially (Groisman et al., 2000). Similarly, also in *Xenopus*, local translation on the mitotic spindle was postulated for mRNAs encoding components regulating chromosome segregation (Eliscovich et al., 2008).

Which proteins could regulate the translation of *lin-5* mRNA? Two RNA-binding proteins acting in the zygote, SPN-2 and SPN-4, are potential candidates. Loss of SPN-2 causes a spindle alignment phenotype that is rescued by the depletion of the katanin protein, MEI-1 (Li et al., 2009). However, whether pulling forces acting on posterior pole is also rescued by reducing MEI-1 levels was not investigated, and could be potentially interesting from the point of view of *lin-5* mRNA translation and LIN-5/GPR-1/2 distribution. Interestingly, loss of SPN-4 function results in the mitotic spindle in P_1 being misoriented although the exact mechanism remains elusive (Gomes et al., 2001). Furthermore, a genome wide RNAi screen revealed that *spn-4* depletion leads to decreased posterior spindle pole oscillation in 8/10 embryos (Sonnichsen et al., 2005). It is interesting to speculate that SPN-4 positively regulates *lin-5* mRNA translation thereby affecting spindle oscillation and spindle positioning. Recently, it was shown that in human cells, Casein Kinase Iε and δ isoforms are involved in the maturation of the 40S ribosomal subunit and that inhibition of the ε isoform interferes with mRNA translation by compromising eIF4E (Shin et al., 2014; Zemp et al., 2014). It is possible that CSNK-1 likewise effects general translation and thereby maybe LIN-5 protein distribution in *C. elegans* one-cell stage embryos.

We found that dynein and microtubules dictate centrosomal *lin-5* mRNA localization. Dynein-dependent transport localizes numerous mRNAs in other systems where adaptor proteins link the mRNAs with the dynein complex (see Introduction on page 42 and 45). It is tempting to speculate that such adaptor proteins also take part in localizing *lin-5* mRNA to the centrosome in *C. elegans*, and that their relocalization to the cytoplasm may be the initial trigger leading to the relocalization of *lin-5* mRNA away from the posterior pole during anaphase.

Regardless of the mechanism at play in *C. elegans* one-cell embryos, our finding that *lin-5* mRNA is translated/folded preferentially in the cytoplasm, coupled with the fact that there is less *lin-5* mRNA around the posterior centrosome compared to the anterior one during anaphase, prompted us to test the importance of *lin-5* protein synthesis during mitosis. To this end, we developed a time-resolved MO-based method to prevent *lin-5* mRNA translation specifically in one-cell embryos. Although MOs have been widely used in model systems such as *Xenopus* or zebrafish to interrogate gene function, they have not been used in *C. elegans* prior to this work, nor have they been employed to interfere in a time-resolved manner with protein synthesis. These experiments enabled us to demonstrate that translation of *lin-5* mRNA during mitosis is critical for achieving strong net pulling forces on the posterior spindle pole, while being dispensable for those acting on the anterior side. There is precedent for such rapid translational action in the case of retinal axonal growth cones in *Xenopus*. The transport and translation of β-actin mRNA is triggered by an external gradient of the chemotropic Netrin-1 that leads to polarized β-actin translation within 5 minutes. As a result, the axon turns toward the source of the gradient (Leung et al., 2006; Yao et al., 2006).

In conclusion, these findings lead us to propose that the remarkable localization of *lin-5* mRNA around centrosomes might be important for ensuring a robust asymmetry in pulling forces during the first division of *C. elegans* embryos by inhibiting *lin-5* mRNA translation on the anterior side (Figure 38).

4. CHARACTERIZATION OF THE MECHANISMS DRIVING *ERA-1* MRNA DISTRIBUTION

4A RESULTS

The mRNA of the W02F12.3 gene is enriched on the anterior side of P_0 and is inherited by the anterior lineage

Prompted by the intriguing localization of *lin-5* mRNA, we decided to browse through the entire *in situ* hybridization database with the aim of identifying other interesting localization patterns. Surprisingly, we found only a few non-homogenous distributions amongst all ~11.237 ESTs analyzed. Among these, the transcript of an uncharacterized gene, W02F12.3, showed the most striking localization pattern: the mRNA displayed a very clear bias towards the anterior side of the zygote and this anterior distribution was seemingly maintained in later embryonic stages as well. We dubbed this gene *era-1* (e̲mbryonic mR̲NA a̲nterior) and decided to investigate it further.

We confirmed the asymmetric distribution of *era-1* mRNA by digoxygenin-alkaline phosphatase based *in situ* hybridization (Figure 40A-D). We found that the asymmetric enrichment of *era-1* mRNA becomes apparent at the stage of pronuclear meeting and persists thereafter in the zygote. Moreover, *era-1* mRNA is significantly enriched in the anterior blastomere AB compared to the posterior blastomere P_1 in two cell-stage embryos (Figure 41E), a difference that is also apparent when comparing the AB daughters ABa and ABp with the P_1 daughters EMS and P_2 (Figure 40D). We detected no signal in *era-1(RNAi)* embryos, indicating probe specificity (Figure 41B and 41E).

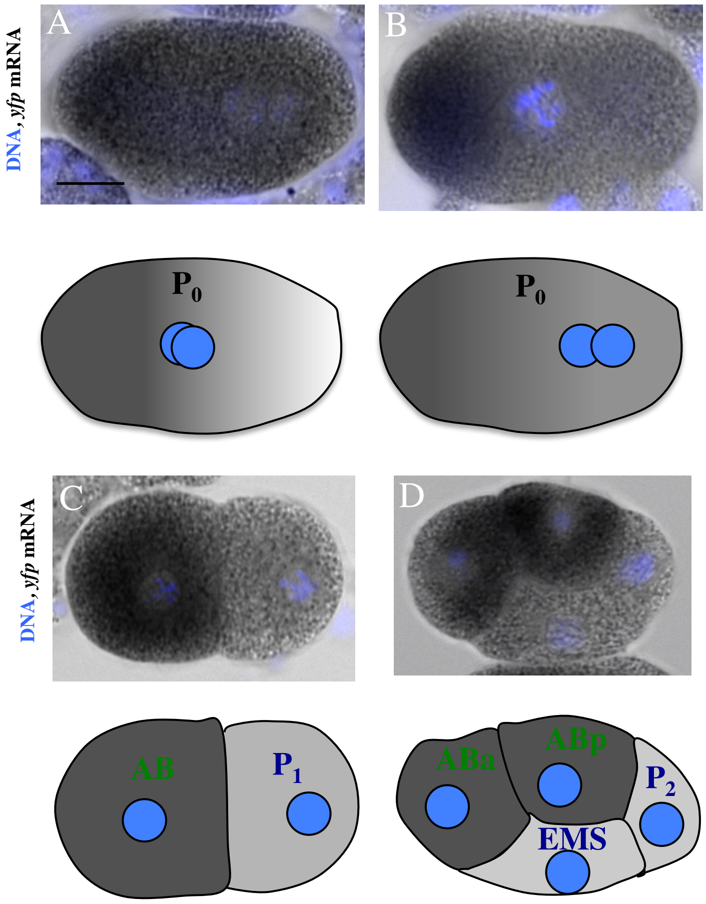

Figure 40. *era-1* mRNA is enriched in the anterior side of the zygote and in anterior blastomeres
A-D *era-1* mRNA localization in P_0 prophase (A), P_0 prometaphase (B), 2-cell stage (C) and 4-cell stage embryos. Here and in the following figures, the mRNA signal appears dark grey; the DNA is shown in blue. The schematics below the embryos illustrate where the mRNA is distributed. Scale bar here and in the following figures correspond to 10 microns.

era-1 mRNA localization is driven by MEX-5 and its 3'UTR

We sought to address what regulates the remarkable localization of the *era-1* mRNA. First we asked if the anterior enrichment is polarity-dependent. To address this question, we analyzed *era-1* mRNA distribution in *par-3(it71)* mutant embryos and found uniform transcript localization in this case (Figure 41C, 41E). We conclude that polarity mediates the asymmetric localization of *era-1* mRNA.

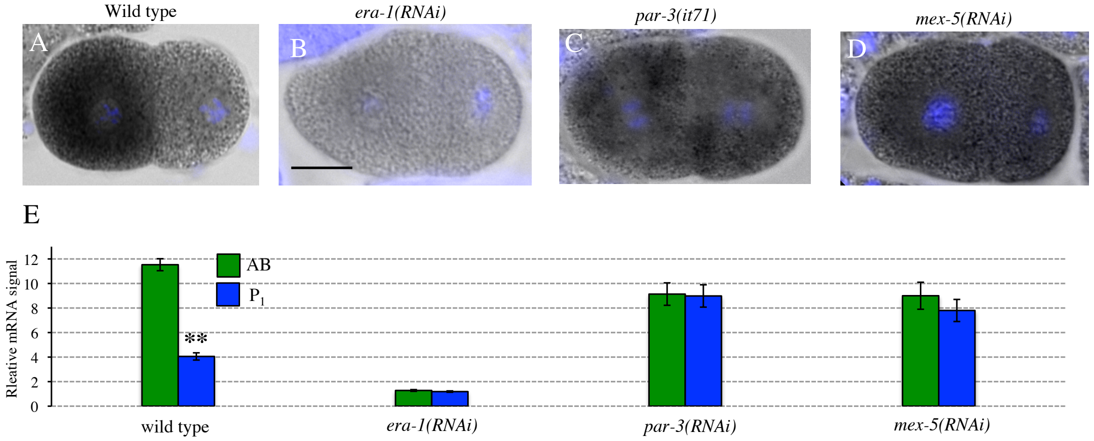

Figure 41. Asymmetric *era-1* mRNA distribution is regulated by polarity and MEX-5. **A-D** *era-1* mRNA localization in wild type (A), *era-1(RNAi)* (B), *par-3(RNAi)* (C) and *mex-5(RNAi)* (D) embryos. **E** Quantification of relative mRNA enrichment in AB and in P_1 blastomeres of control, *era-1(RNAi)*, *par-3(RNAi)* and *mex-5(RNAi)* embryos. Here and elsewhere, the average values are indicated with the error bars representing the standard error of the mean. Statistical analysis was performed using unpaired Student's t-test. *: p<0.05, **: p<0.001. Statistical analysis was used to compare values in AB and in P_1. Number of embryos used for quantification: control (n=9), *era-1(RNAi)* (n=12), *par-3(it71)* (n=10), *mex-5(RNAi)* (n=7).

In addition to polarity, we revealed that *era-1* mRNA asymmetry is disrupted in embryos depleted of the anteriorly localized RNA-binding protein MEX-5 (Schubert et al., 2000, Figure 41D, quantified in 41E). Even though we found that polarity establishment is slightly impaired in embryos *mex-5(RNAi)* embryos (Figure 42), we hypothesize that MEX-5 does not regulate *era-1* mRNA localization through such a slight malfunction of polarity but in a more direct manner (see below).

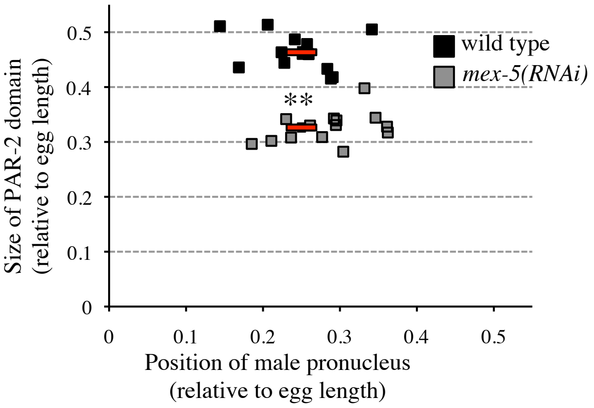

Figure 42. *mex-5(RNAi)* leads to a slight delay in polarity establishment
Size of endogenous PAR-2 domain evaluated by immunofluorescence in embryos at the stage of centration/rotation with or without *mex-5* depletion. n= 13 (control), n=16 (*mex-5(RNAi)*).

To identify the *cis*-acting element driving the localization of *era-1* mRNA, we fused the sequence coding for the yellow fluorescent protein (YFP) to the *era-1* genomic sequence (exons, introns and 3'UTR) in an expression vector driven by the *pie-1* promoter and the *pie-1* 5'UTR (yielding the *yfp-era-1*[e3'] construct, Figure 43A). We generated a transgenic line expressing this construct and performed *in situ* hybridization against *yfp* mRNA. We found that the *yfp-era-1*[e3'] mRNA is enriched in the anterior of the zygote and is present in anterior blastomeres thereafter (Figure 43B, quantified in 43G). This enrichment is less pronounced than that of the endogenous *era-1* mRNA (compare Figure 41A and 43B), suggesting that the *era-1* 5'UTR also contributes to mRNA distribution or that the presence of the *yfp* sequence interferes slightly with the localization signal.

Sequences in the 3'UTR are responsible for the localization of a variety of mRNAs (Merritt et al., 2008). To test the contribution of the *era-1* 3'UTR in mRNA localization, we generated a chimeric transgenic line expressing *yfp* fused directly to the *era-1* 3'UTR (yielding the *yfp*[e3'], construct, Figure 43C). As shown in Figure 43D, our analysis uncovered a significant anterior bias of *yfp*[e3'], mRNA, although the extent of enrichment in AB versus P_1 is much less pronounced than with the endogenous transcript or with *yfp-era-1*[e3'] mRNA (compare Figure 43D with 41A and 43B). We conclude that the *era-1* 3'UTR, while not being sufficient for, contributes to the anterior localization of the mRNA.

To test if the *era-1* 3'UTR is necessary for anterior mRNA localization, we modified the *yfp-era-1*[e3'] construct by replacing the *era-1* 3'UTR with the *pie-1* 3'UTR (yielding the *yfp-era-1*[p3'] construct, Figure 43E), and generated a corresponding transgenic line. Strikingly, we found that the *yfp-era-1[*p3'] mRNA localizes in a homogenous manner, with no difference between the anterior and posterior blastomeres (Figure 43F, quantified in 43G). Therefore, the 3'UTR of *era-1* is necessary for anterior mRNA localization.

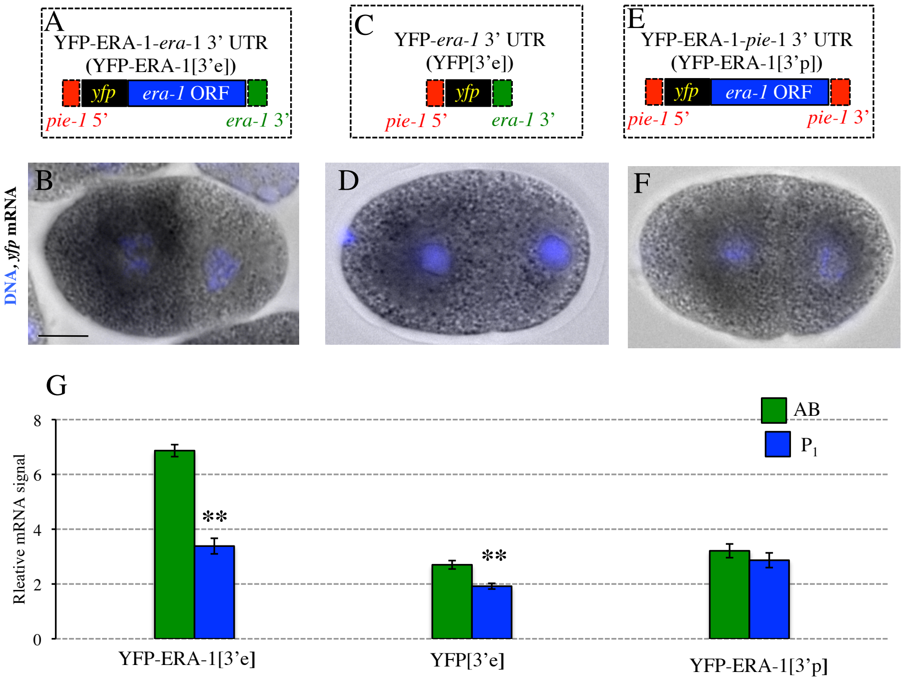

Figure 43. *yfp*-tagged *era-1* mRNA distribution is similar to endogenous mRNA localization and is regulated in a 3'UTR-dependent manner
A Schematic representation of the YFP-ERA-1-*era-1* 3'UTR (YFP-ERA-1[e3']) construct. *yfp* (yellow) is cloned 5'to the *era-1* genomic DNA (blue) carrying the *era-1* 3'UTR (green). **B** Localization of *yfp-era[e3']* mRNA in two-cell stage embryos. **C** Schematic representation of the YFP-*era-1* 3'UTR (YFP[e3']) construct. *yfp* (yellow) is cloned 5' to *era-1* 3'UTR (green). **D** Localization of *yfp[e3']* mRNA in two-cell stage embryos. **E** Schematic representation of the YFP-ERA-1-*pie*-1 3'UTR (YFP-ERA-1[p3']) construct. *yfp* (yellow) is cloned 5' to the *era-1* genomic DNA coding sequence (blue) and the *era-1* 3'UTR was replaced by the *pie-1* 3'UTR (red). **F** Localization of *yfp-era-1[p3']* mRNA in two-cell stage embryos. **G** Quantification of mRNA enrichment in YFP-ERA-1[e3'] (n=9), YFP[e3'] (n=8) and YFP-ERA-1[p3'] (n=10) embryos. Statistical analysis was used to compare values in AB and in P_1.

YFP-ERA-1 protein is enriched in anterior blastomeres and is negatively regulated by the *era-1* 3'UTR

To address whether the anterior enrichment of *era-1* mRNA is accompanied by a likewise distribution of protein, we analyzed live embryos derived from the three transgenic strains described above using dual differential interference contrast (DIC) and fluorescent time-lapse microscopy. This revealed that YFP-ERA-1[e3'] protein can be detected starting from the ~10 cell stage and is present solely in descendants of the anterior blastomere AB (Figure 44).

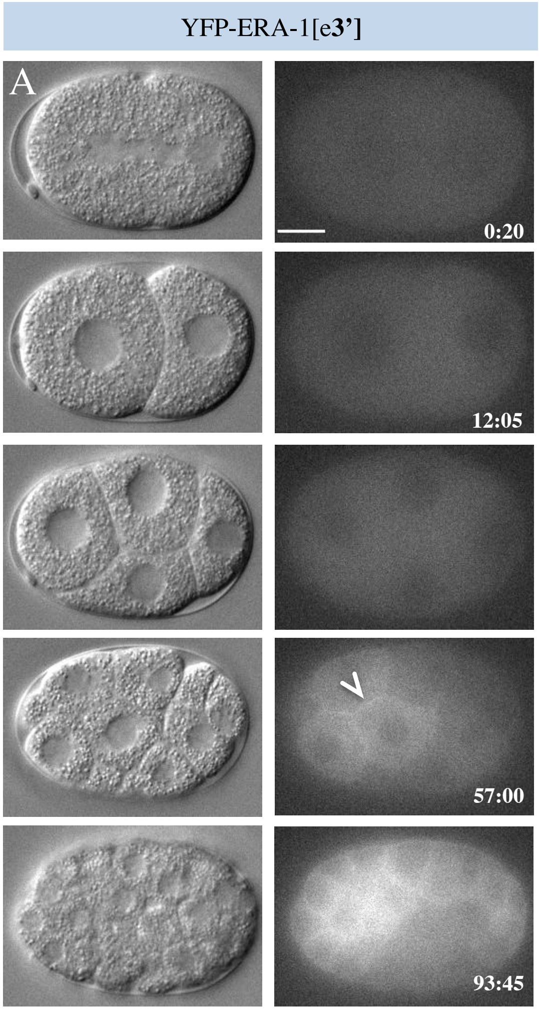

Figure 44. YFP-ERA-1 distribution during embryogenesis
Snapshots of an embryo expressing YFP-ERA-1[e3’] imaged with dual DIC and fluorescence time-lapse microscopy. DIC image is on the left; YFP signal is on the right. Here and in Figures 47 and 48, t=0 corresponds to cytokinesis onset of P_0. Arrowhead points to YFP signal detected at cell-cell boundaries.

We also performed immunofluorescence analysis using antibodies against YFP, which offers a more sensitive means of detecting proteins than live imaging. We thus found that YFP-ERA-1[e3’] is distributed homogenously in the zygote and becomes enriched thereafter in the AB cell (Figure 45A and B), an anterior bias that is even more pronounced in 4-cell stage embryos (Figure 46A). Intriguingly, we noted also that YFP-ERA-1[e3’] protein is slightly enriched on the plasma membrane, something that is most apparent at the boundary between anterior blastomeres such as ABa and ABp (Figure 46A).

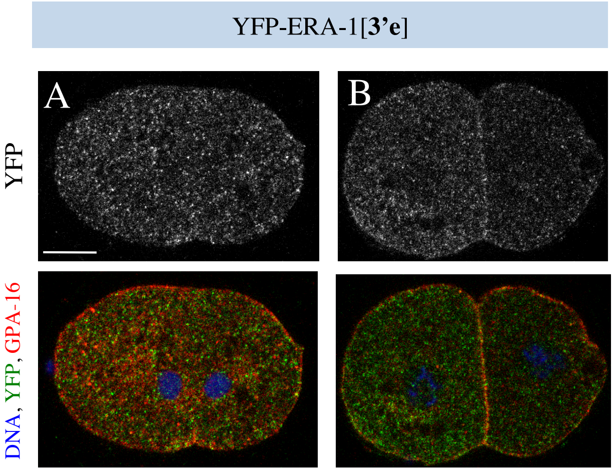

Figure 45. YFP-ERA-1 distribution in one- and 2-cell stage embryos
A-B YFP-ERA-1[e3'] stained with Hoechst (blue), anti-GFP antibodies (green) and anti GPA-16 antibodies (red) at telophase of the first cell division (A) and in the 2-cell stage (B) The upper images show the merge, the lower ones the YFP signal alone.

To estimate the relative cell membrane enrichment of the protein in the 4-cell stage, we performed quantification using the GPA-16 staining as a cell membrane marker. This analysis revealed that YFP-ERA-1[e3'] is enriched in the plasma membranes of the anterior cells, whereas this is not the case between the posterior cells (Figure 46F). To address if the anterior enrichment of YFP-ERA-1[e3'] protein is dependent on A-P polarity, we analyzed embryos depleted of PAR-3. As anticipated from the uniform distribution of the *era-1* mRNA in such embryos (see Figure 41C), we found that YFP-ERA-1[e3'] protein is now present at comparable levels in all blastomeres (Figure 46C, 46F).

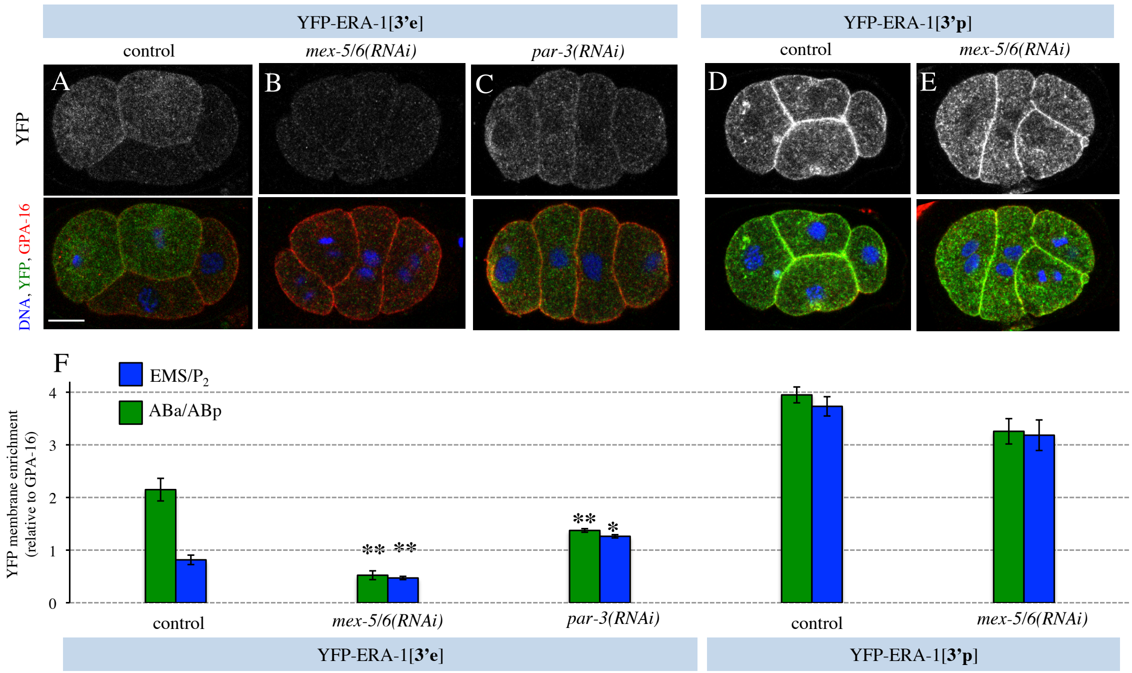
YFP-ERA-1[3'e]
YFP-ERA-1[3'p]
control
mex-5/6(RNAi)
par-3(RNAi)
control
mex-5/6(RNAi)
A
B
C
D
E
YFP
DNA, YFP, GPA-16
F
EMS/P2
ABa/ABp
YFP membrane enrichment (relative to GPA-16)
4
3
2
1
0
** **
** *
control
mex-5/6(RNAi)
par-3(RNAi)
control
mex-5/6(RNAi)
YFP-ERA-1[3'e]
YFP-ERA-1[3'p]

Figure 46. YFP-ERA-1 distribution in 4-cell stage embryos in MEX-5/6-dependent. **A-C** 4-cell stage embryos expressing YFP-ERA-1[e3'] in control (A), *mex-5/6(RNAi)* (B) and in *par-3(RNAi)* (C) conditions stained with Hoechst (blue), anti-GFP antibodies (green) and anti GPA-16 antibodies (red). The upper images show the merge, the lower ones the YFP signal alone. The signal intensities at the cell-cell boundaries of ABa/ABp and at EMS/P_2 were measured and quantified in F. Quantification of signal intensities is shown in panel F. **D-E** 4-cell stage embryos expressing YFP-ERA-1[p3'] in control (D) and in *mex-5/6(RNAi)* (E) conditions. The quantification of signal intensities is shown in panel F. Note that the brightness and contrast properties of the images are equivalent, resulting in seemingly overexposed YFP signal in these panels. **F** Quantification of relative cell membrane enrichment. Number of embryos used for quantification: YFP-ERA-1[e3'] control (n=10), YFP-ERA-1[e3'] *mex-5/6(RNAi)* (n=10), YFP-ERA-1[e3'] *par-3(RNAi)* (n=9), YFP-ERA-1[p3'] control (n=10), YFP-ERA-1[p3'] *mex-5(RNAi)* (n=10) and YE$_{p3'}$ *mex-5/6(RNAi)* (n=8). Statistical analysis show comparison of untreated and RNAi conditions.

Furthermore, as anticipated from the likewise distribution of the corresponding mRNA, we found that YFP[e3'] protein is present solely in anterior blastomeres, albeit at lower levels than for YFP-ERA-1[e3'] (Figure 47A), indicating that the *era-1* 3'UTR can drive anterior protein distribution. Moreover, we found that YFP-ERA-1[p3'] protein exhibits a homogenous distribution throughout the embryo and that it is present at higher levels than YFP-ERA-1[e3'] protein (Figure 47B). Taken together, these observations indicate that the *era-1* 3'UTR is needed to prevent translation of the *era-1* mRNA.

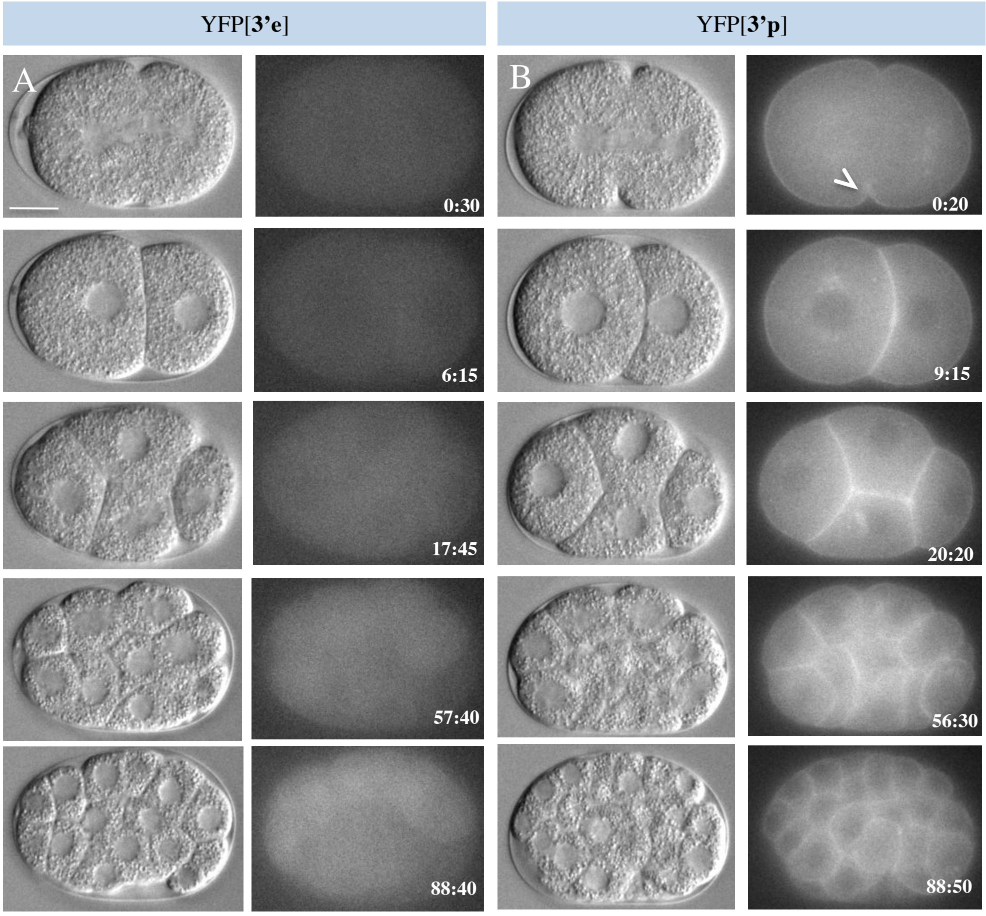

Figure 47. YFP[e3'] and YFP-ERA-1[p3'] distribution during embryogenesis
A Snapshots of an embryo expressing YFP[e3'] imaged with dual DIC and fluorescence time-lapse microscopy. **B** Snapshots of an embryo expressing YFP-ERA-1[p3'] with dual DIC and fluorescence time-lapse microscopy. Note that the brightness and contrast were lowered in panel B in order to avoid blasting of the signal, indicating that the expression level of this strain is higher than two others.

MEX-5/6 positively regulates *era-1* translation via the *era-1* 3'UTR

What *trans*-acting factor(s), if any, could be responsible for mediating the anterior translation of ERA-1 protein? The partially redundant mRNA binding zinc-finger proteins MEX-5 and MEX-6 appeared as plausible candidates since they are themselves enriched on the anterior of the zygote (Schubert et al., 2000). To address if MEX-5/6 affects the translation of ERA-1, we analyzed embryos expressing YFP-ERA-1[e3'] depleted of MEX-5/6. We found that in *mex-5/6(RNAi)* embryos, YFP-ERA-1[e3'] protein is greatly reduced in embryonic blastomeres (Figure 48A).

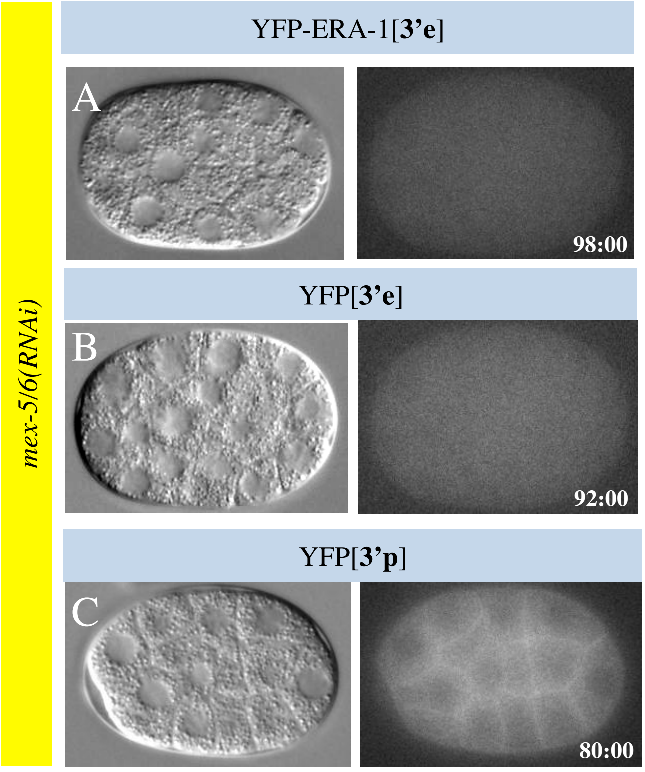

Figure 48. MEX-5/6 regulates YFP-ERA-1 translation via the *era-1* 3'UTR
A-C YFP signal by TimeLapse fluorescent microscope of ~30 cell stage *mex-5/6(RNAi)* YFP-ERA-1[e3'] (A), YFP[e3'] (B) and YFP-ERA-1[p3'] (C) embryos. Compare images to Figures 44 and 47.

This reduction at the protein level can not be explained by destabilized mRNAs, as RT-qPCR analysis revealed no difference in *era-1* mRNA levels between control and *mex-5/6(RNAi)* embryos (Figure 49), raising the possibility of translational regulation. Similarly to YFP-ERA-1[e3'], the levels of YFP[e3'] are also diminished in *mex-5/6(RNAi)* (Figure 48B). These observations suggest that MEX-5/6 are needed to activate the translation of *era-1* mRNA through the *era-1* 3'UTR. Importantly, MEX-5/6-directed translational regulation seems to involve the *era-1* 3'UTR, as levels of YFP-ERA-1[p3'], protein in *mex-5/6(RNAi)* embryos appear to be unaffected (Figure 48C).

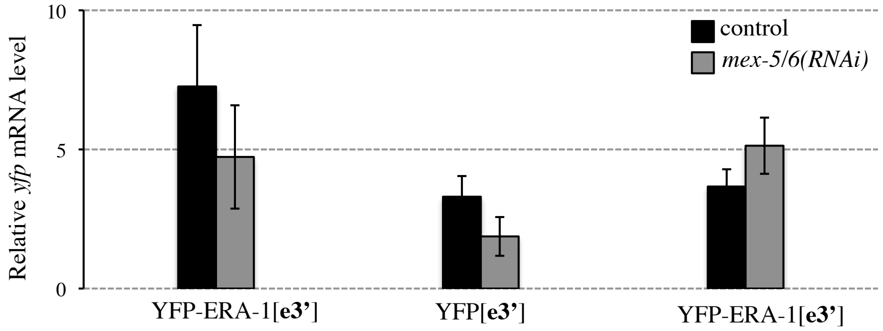

Figure 49. MEX-5/6 depletion does not influence mRNA levels of ERA-1 transgenes. Relative mRNA levels measured by RT-qPCR in YFP-ERA-1[e3'], YFP[e3'] and YFP-ERA-1[p3'] embryos with or without *mex-5/6* depletion. Values are shown relative to *act-1* mRNA. The experiment was performed 3 times.

Quantification of cell membrane enrichment in 4-cell stage embryos further demonstrated that interfering with MEX-5/6 leads to a drop of YFP-ERA-1[e3'], but not of YFP-ERA-1[p3'] protein levels (Figure 46B and E, quantified in 4F). Importantly, the decreased YFP-ERA-1[e3'] levels are not due to the misdistribution of *era-1* mRNA in *mex-5(RNAi)* embryos, since the fluorescent signal in *par-3(RNAi)* embryos are higher than the ones observed in *mex-5/6(RNAi)* (Figure 46F). MEX-6 depletion alone does not alter the cell membrane signal of YFP-ERA-1[e3'] (Figure 50). Similarly, in the absence of an other anteriorly localized translational regulator MEX-3, YFP-ERA-1[e3'] levels are unaffected (Figure 50).

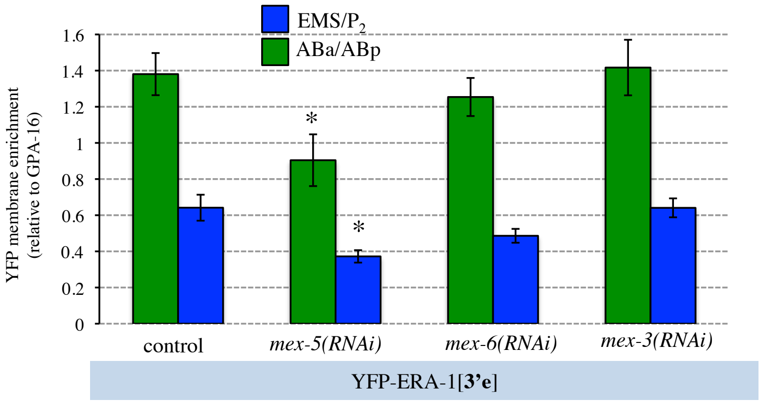

Figure 50. MEX-6 and MEX-3 depletion do not lead to decreased YFP-ERA-1[e3'] signal
Quantification of relative membrane enrichment in 4-cell stage YFP-ERA-1[e3'] embryos upon single *mex-5*, *mex-6* and *mex-3* depletion. Embryos used for quantification: n=11 (control), n=7 (*mex-5(RNAi)*), n=7 (*mex-6(RNAi)*), n=7 (*mex-3(RNAi)*).

Is it possible that *era-1* mRNA is a direct MEX-5/6 target? MEX-5 binds to RNA motifs that contain six or more uridines within a 9-13 nucleotide window. Suggestively, we found several such motifs in the *era-1* 3'UTR of *C. elegans* and of the sister species, *C. briggsae* (Figure 51). Of note, these AU-rich sequences are very abundant in 3'UTR's of *C. elegans* genes (Pagano et al., 2007), therefore the involvement of these motifs should be proven experimentally to establish a link between the *era-1* 3'UTR and MEX-5.

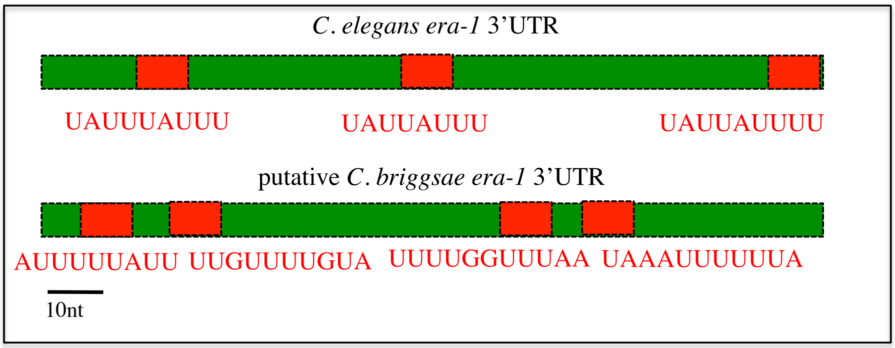

Figure 51. Putative MEX-5-binding sites in the 3'UTR of *C. elegans* and *C. birggsae era-1*

Putative MEX-5 binding sites (red boxes) along the *era-1* 3'UTR (green) in *C. briggsae* and *C. elegans*. The sequence of the regions is shown below in red.

Bioinformatic analysis of *era-1*

In the hope of gaining insight into the function of ERA-1, we sought to perform a small bioinformatic exploration, in collaboration with the Biostatistics and Bioinformatics Core Facility at EPFL.

First, we sought to identify domains and motifs in ERA-1 using the NCBI and ScanProsite webservers. We found a putative transcriptional regulator ICP4 domain in the ERA-1 sequence, but given that our YFP-fusions do not show nuclear localization, ERA-1 does not appear to be a transcriptional factor, at least not in early embryos. Of course, it is possible that endogenous ERA-1 distribution differs from that of the YFP-fusion proteins. Moreover, the ScanProsit server identified several motifs in the amino acid sequence (Figure 52A), although all are annotated as motifs with 'high probability occurrence', meaning that these motifs are found in numerous amino acid sequences. Among these, the putative phosphorylation sites of protein kinase C and Casein kinase II could be of potential interest, as PKC-3 is part of the anterior PAR complex and since CSNK-1 is involved in generation of pulling forces in the zygote (Panbianco et al., 2008). Moreover, the presence of predicted myristoylation sites is indicative of the potential for autonomous membrane binding. Of note, these predicted motifs are not located in the N-terminus of ERA-1, thus their relevance is questionable.

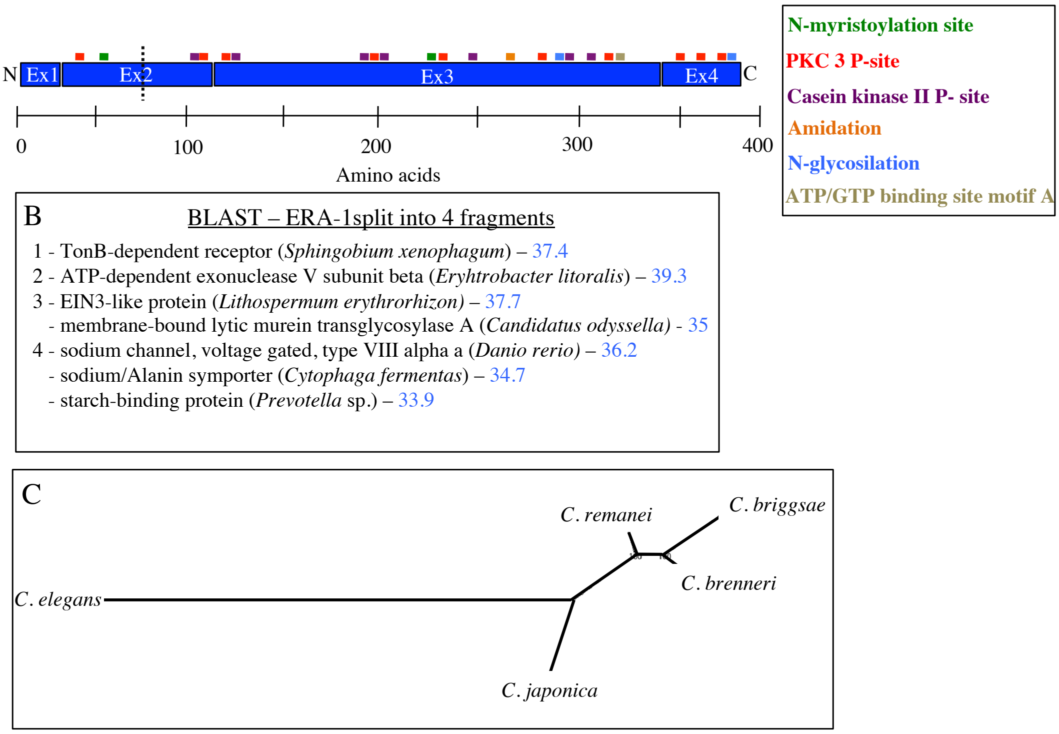

BLAST – ERA-1split into 4 fragments

1 - TonB-dependent receptor (*Sphingobium xenophagum*) – 37.4
2 - ATP-dependent exonuclease V subunit beta (*Eryhtrobacter litoralis*) – 39.3
3 - EIN3-like protein (*Lithospermum erythrorhizon)* – 37.7
 - membrane-bound lytic murein transglycosylase A (*Candidatus odyssella)* - 35
4 - sodium channel, voltage gated, type VIII alpha a (*Danio rerio)* – 36.2
 - sodium/Alanin symporter (*Cytophaga fermentas*) – 34.7
 - starch-binding protein (*Prevotella* sp.) – 33.9

Figure 52. Potential motifs in ERA-1, potential related proteins identified by BLAST analysis and phylogenetic tree

A Motifs identified with the ScanProsit software in the ERA-1 protein sequence. The four ERA-1 exons are in blue, the ruler indicates the length in amino acid. Dashed black line shows the truncated protein in the *era-1(tm5854)* line (see later section). **B** Blast performed in the NCBI website based on the ERA-1 sequence chopped into four fragments. The description of the proteins and the species where they act are indicated next to the fragment number. The score displayed by the algorithm of a given hit is indicated in blue. We excluded hypothetical proteins from the hits. **C** Phylogenetic tree based on ERA-1 amino acid sequence in *C. elegans*, *C. japonica*, *C. brenneri*, *C. briggsae* and *C. remanei*. The analysis was done with the RXML blackbox (http://embnet.vital-it.ch/raxml-bb/) based on sequence alignment performed with the MAFFT server (http://mafft.cbrc.jp/alignment/server/).

We were interested in identifying potential paralogs of ERA-1 in *C. elegans* and homologues in other systems. However, we failed to find paralogs in *C. elegans* by blasting the sequence against the genome using the BLASTn algorithm. To find potential homologues, we chopped the ERA-1 amino acid sequence into four ~100 amino acid-long fragments and performed BLASTp search (Figure 52B). We identified proteins that bear similarity scores ranging from 33 to 39 as compared to the score of ~97 for the ERA-1 sequence itself. These proteins are shown in Figure 52B and C. Out of these, given the membrane localization of ERA-1, proteins with membrane-association are potentially interesting, like a sodium-channel protein in Zebrafish, a Ton-B dependent receptor in the proteobacterium *Sphingobium xenophagum* or a membrane-bound lytic murein transglycosylase in the bacterium *Candidatus odyssella*. However, whether ERA-1 shares functional similarities with these proteins remains to be investigated.

To investigate the evolutionary conservation of ERA-1, we decided to build a phylogenetic tree derived from related nematode species based on ERA-1 protein sequence (Figure 52C). Interestingly we found that *C. elegans* ERA-1 has greatly diverged from the other nematodes. This suggests that ERA-1 might become redundant with other protein(s) in *C. elegans* during evolution. Based on this, it is possible that investigating the function of ERA-1 in related species could lead to exciting discoveries (see in the light of the next chapter).

Attempts to analyze the phenotypic consequences of *era-1* depletion

We found that RNAi-mediated depletion of *era-1* by feeding, soaking or injection does not lead to embryonic lethality or to any obvious defect in the adult worm. This is likely not the consequence of inefficient RNAi, as *era-1* mRNA is decreased to ~8% of the wild type levels following RNAi by feeding (Figure 53A). We also took advantage of a deletion allele of *era-1*, *era-1(tm5854),* that harbors a 500-bp deletion from exon 2 to exon 3 and results in a premature STOP codon in exon 3 (Figure 53B). We verified the deletion by genomic PCR and found by RT-PCR that exon 1 is expressed at a lower level in *era-1(tm5854)* as compared to wild type (Figure 53C and D). Based on this, we handle *era-1(tm5854)* as a potential hypomorphic allele, although it is most likely a null. Careful examination of these embryos and worms did not reveal any defects at any stage at any temperature.

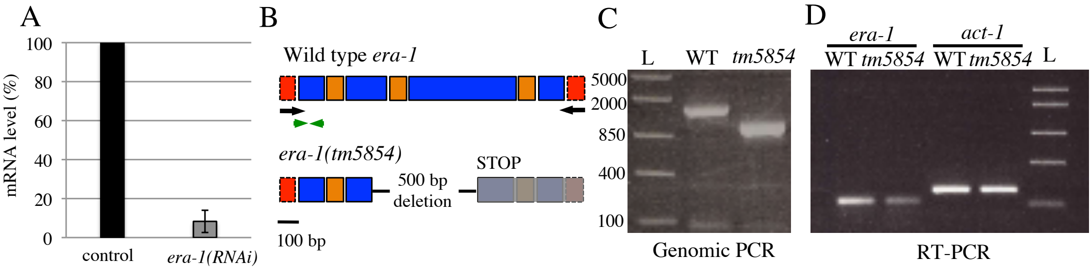

Figure 53. RNAi-mediated depletion of *era-1* and the *era-1(tm5854)* allele
A RT-qPCR analysis of *era-1* mRNA isolated from control and *era-1(RNAi)* embryos. *act-1* was used as control, N=2 experiments. **B** Molecular nature of the *era-1(tm5854)* allele. The 500 bp deletion between exons 2 and 3 gives rise to a premature STOP codon. **C** Genomic PCR confirming the 500 bp deletion using primer pairs indicated with black arrows in panel **B**. Here and in panel **D**, 'L' marks the DNA ladder lane; numbers indicate nucleotides sizes. **D** Semi-quantitative RT-PCR analysis of *era-1* mRNA in wild type and *era-1(tm5854)* embryos using primer pairs amplifying a region in exon 1 (green arrowheads in panel **B**).

We also analyzed a strain carrying a 700 bp deletion starting from the 5'UTR of the *era-1* gene, *era-1(tm6426)* (Figure 54A), which we consider a complete null. This strain is embryonic viable and displays no apparent phenotypes in adult stages. Based on this, we conclude that *era-1* is not an essential gene. Interestingly, however, we found that *era-1(tm6426)* embryos are sensitive to partial loss of the polarity proteins, PAR-3 or PAR-2 (Figure 54B). A possible interpretation of this finding is that ERA-1 acts redundantly with partner protein(s) during development, but the exact process in which ERA-1 might function remains elusive.

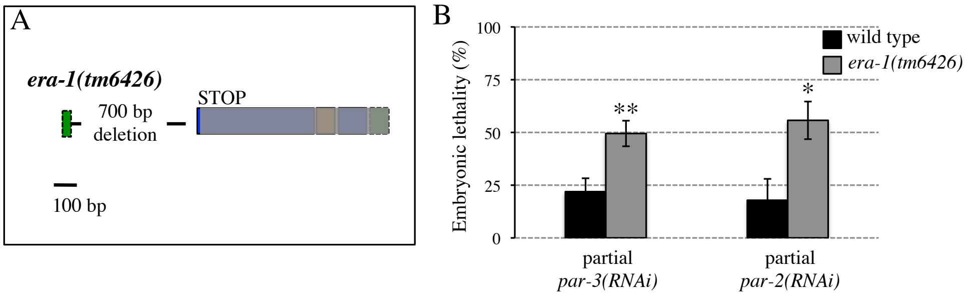

Figure 54. *era-1(tm6426)* is sensitive to slight perturbation of polarity
A Schematics of endogenous *era-1* gene and of the *era-1(tm6426)* allele. **B** Embryonic lethality following partial depletion of *par-3* and *par-2* in wild type and in *era-1(tm6426)* worms. >800 embryos were scored in total of the 8 independent *par-3(RNAi)* experiments and >200 embryos were scored in total of the 3 independent *par-2(RNAi)* experiments.

Since we thought that the lack of phenotype could result from *era-1* functioning redundantly with another gene, we decided to take a candidate approach to identify such a potential partner protein. Single cell sequencing methods uncovered several mRNAs that are enriched in AB as compared to P_1 (Table 1; Hashimshony et al., 2012). Besides this list, we were aware of other anteriorly-enriched mRNAs identified in the Lieb lab (Jason Lieb, personal communication). We reasoned that *era-1* might function together with mRNAs that have analogous localization. Therefore, we depleted each of these genes by feeding RNAi in the wild type and the *era-1(tm5854)* background to reveal a potential genetic enhancement. First, we analyzed the genes that, similarly to *era-1*, do not cause embryonic lethality. Although we did not test the efficiency of RNAi for each gene, we did not find any trace of synthetic lethality. In the case of genes causing embryonic lethality on their own, we performed partial RNA experiments that similarly lead to no enhancement with *era-1(tm5854)*. Our mini-screen thus failed to find conditions where the loss of *era-1* leads to developmental defects.

AB-enriched Class IV mRNAs			
gene name	**NEXTDB**	**PhenoBank**	**enhancement on *era-1(tm5854)***
E02H4.6	ND	WT	no
F32D1.6	ND	WT	no
mig-5	saturated signal	WT	no
T21B10.4	ND	WT	no
Y59A8B.12	ND	WT	no
ZK1127.6	symmetric	WT	no
mex-3	asymmetric	100% Emb	no
par-3	ND	100% Emb	no
hmp-2	symmetric	100% Emb	no
Y73F8A.24	no signal	70-90% Emb	no
sca-1	symmetric	Ste	no
erm-1	symmetric	weak Dumpy	ND
hsp-4	symmetric	Ste	ND

Table 1. mRNAs displaying relative enrichment in AB versus P_1
These genes were identified by single cell mRNA sequencing method (Hashimshony et al., 2012). The second column indicates if the transcript exhibits asymmetry in early embryos based on the *in situ* image in the publicly available NEXTDB. PhenoBank shows the phenotype upon depletion of the gene by RNAi, the last column display the lack of synthetic lethality/enhancement when treating *era-1(tm5854)* embryos with RNAi.

Phenotypic consequences of ERA-1 mislocalization

The overall conclusion from the above-mentioned experiments is that *era-1* depletion alone leads to no observable consequences. We sought to test if this was also the case in embryos in which ERA-1 is mislocalized. We did not detect embryonic lethality in the YFP-ERA-1[p3’] strain. Thus, in the presence of functional endogenous protein, the mislocalization of ERA-1 does not result in developmental problems. Note that we do not have means to test if the YFP fusion of ERA-1 is functional, as we do not have a clear phenotypic readout that we could use to address this question. It is thus possible that the apparent absence of phenotype stems from the fact that YFP-ERA-1 is not functional. We next crossed the YFP-ERA-1[p3’] strain into the *era-1(tm5854)* and into the *era-1(tm6426)* mutants to be in a condition where the sole source of ERA-1 in the embryos is the mislocalized YFP fusion. The resulting strain was embryonic viable and displayed no apparent adult phenotype. Thus, we conclude that ERA-1 mislocalization under laboratory conditions is tolerable for embryonic development of *C. elegans*.

4B. DISCUSSION

era-1 mRNA and ERA-1 protein distribution

In this part of the thesis work, we provided evidence that the mRNA of the uncharacterized gene W02F12.3, hereby named *era-1,* is enriched in the anterior part of the *C. elegans* zygote and is inherited in anterior blastomeres. We found that analogous to the mRNA, YFP-ERA-1 protein is enriched in the anterior blastomeres where it localizes to the plasma membrane. We found that the asymmetric enrichment of *era-1* mRNA is mediated by polarity and is dependent on its 3'UTR.

Interestingly, neither *era-1*, nor another asymmetrically enriched mRNA, *mek-1,* are among the genes identified by single cell mRNA sequencing of blastomeres of being asymmetrically enriched in AB versus P_1 (Hashimshony et al., 2012). Conversely, 6 out of 13 transcripts identified in this study clearly show no asymmetric localization based on *in situ* images in the Nematode Expression Database (Table 1). This discrepancy demonstrates that the mRNA sequencing and large-scale *in situ* hybridization methods probably fail to reveal all mRNAs with asymmetric distribution. More reliable techniques and analyses, similar to those have been implemented in the case of *Drosophila* embryos (Lecuyer et al., 2007) would be needed to get clearer picture about asymmetrically enriched mRNAs in *C. elegans* embryos.

Regulation by MEX-5

We found that embryos depleted of MEX-5 show aberrant *era-1* mRNA localization and absence of ERA-1 protein. This translational regulation exerted by MEX-5, and potentially also its impact on mRNA localization, is mediated through the *era-1* 3'UTR. Thereby, we propose a model where MEX-5 plays a dual role in *era-1* mRNA regulation (Figure 55). First, by binding to the *era-1* 3'UTR, MEX-5 contributes to the transport of *era-1* mRNA to the anterior side of the cell during the polarization phase. Second, MEX-5 promotes translational activation of *era-1* mRNA in the AB cell in the 2-cell stage. On top of this MEX-5-mediated translational activation, it is plausible that translational repression ensures low ERA-1 levels before the 2-cell stage acting via the 3' UTR, as our construct harboring the *pie-1* 3'UTR shows high ERA-1 protein levels already in P_0

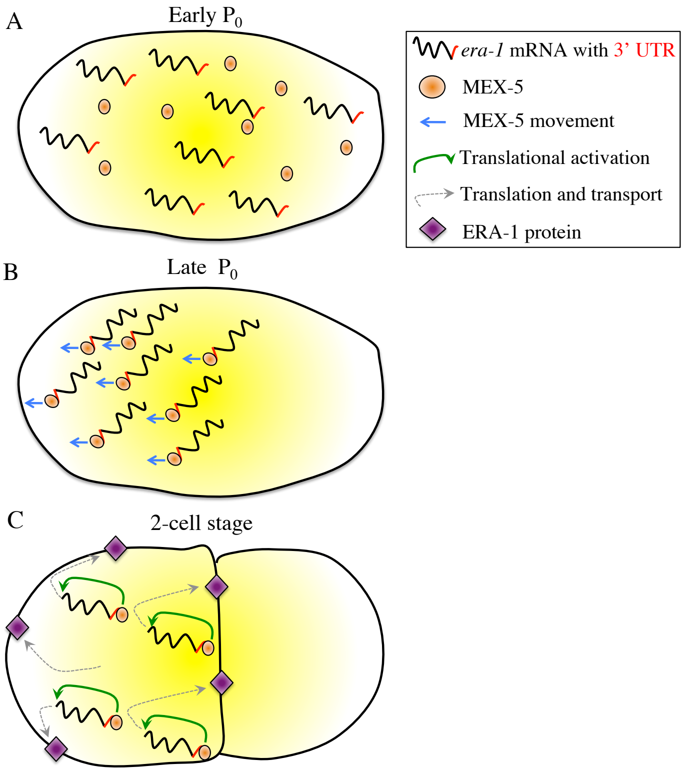

Figure 55. Model of *era-1* mRNA localization and translation regulation
A *era-1* mRNA (black curve) and MEX-5 (orange circle) are uniformly distributed in early P_0. **B** *era-1* mRNA is asymmetrically enriched by MEX-5 mediated anterior movement through the *era-1* 3'UTR in late P_0. **C** MEX-5 activates *era-1* translation, newly translated ERA-1 protein (purple diamond) is transported to the plasma membrane.

MEX-5 acts redundantly in several aspects with another CCCH zinc-finger protein, MEX-6 (Schubert et al., 2000). Slight polarity defects, for instance, have been observed in embryos depleted of both MEX-5 and MEX-6, while such an effect has not been reported for single depletion. It would be interesting to address if *era-1* mRNA regulation is restricted to MEX-5 or if MEX-6 is likewise involved.

Is such regulation exerted by MEX-5 specific to *era-1* mRNA? Although MEX-5 has been shown to regulate mRNA localization and translation, this is the first case where MEX-5 is implicated in both mRNA localization and translational activation. Thus, as opposed to the wild type situation where *pos-1* mRNA is enriched in P_1 as compared to AB, in single *mex-5* mutant embryos, the asymmetry at the mRNA level is no longer observed. Interestingly, however, POS-1 protein is still enriched in the posterior cell (Tenlen et al., 2006). This is no longer the case in double *mex-5/6* mutant embryos, where POS-1 protein distribution is uniform (Schubert 2000), serving as another example of redundancy between MEX-5 and MEX-6. Furthermore, GLP-1 protein normally decorating the anterior plasma membranes is diminished in *mex-5/6* double mutant embryos (Schubert et al., 2000), indicating a role for MEX-5/6 in translational activation of *glp-1* mRNA. Of note, the mRNA levels of *glp-1* were not investigated in this case, thus we can not rule out the possibility that the loss of GLP-1 protein enrichment is the consequence of decreased mRNA levels.

era-1 mRNA distribution by other mechanisms

Based on the fact that the asymmetric localization of GFP-MEX-5 in the one cell stage embryo is not as sharp as that of *era-1* mRNA (Cuenca et al., 2003) it is plausible that other factors are involved in setting up asymmetric *era-1* mRNA distribution. What could be nature of these other factors? The endosomal network, the endoplasmic reticulum and the acto-myosin network all have been implicated in contributing to mRNA localization in other instances and, suggestively, they are all enriched in the anterior side of P_0 (Andrews and Ahringer, 2007; Aronov et al., 2007; Balklava et al., 2007; Estrada et al., 2003; Irion and St Johnston, 2007; Munro et al., 2004; Poteryaev et al., 2005; Schmid et al., 2006; Velarde et al., 2007; Zhao et al., 2001). It is plausible that these components contribute to *era-1* mRNA localization. Testing the involvement of these components could be possible by utilizing fast-acting temperature-sensitive mutants of *nmy-2* or of the dynamin gene *dyn-1*. Moreover, during centration/rotation, when *era-1* mRNA loading in the anterior is being established, there is a relative enrichment of microtubule plus ends at the anterior side of the cell. Given this, it is plausible that *era-1* mRNA is transported with the help of kinesins, as in the case of *osk* and Vg1 mRNAs (Betley et al., 2004; Brendza et al., 2000; Yoon and Mowry, 2004). This hypothesis can be tested by RNAi-mediated depletion of the plus-end directed kinesin genes present in *C. elegans* (reviewed in Siddiqui, 2002).

Potential function of ERA-1

The exact function of ERA-1 remains elusive. We found that slight perturbation of polarity leads to synthetic lethality in *era-1(tm6426)* embryos. This suggests that ERA-1 functions redundantly with other protein(s) whose distribution is under the control of polarity. What could be the nature of such proteins? The Notch pathway is crucial for defining the fate of ABp by signaling stemming from P_2 (see Introduction on page 50). Given that YFP-ERA-1 localization exactly maches that of the Notch receptor, GLP-1, it is possible that ERA-1 influences Notch signaling.

We found that both YFP-ERA-1 fusion proteins are enriched at the cell membranes. What could be the function of ERA-1 in the cell membrane? Our BLAST analysis found several membrane-associated proteins that share similarity with ERA-1, one of them being a voltage-gated sodium channel (VGSC) protein from Zebrafish. Although VGSCs mostly function in excitable cells, there is ample evidence of their importance in nonexcitable cells regulating diverse processes, such as phagocytosis, cell motility and metastasis (reviewed in Black and Waxman, 2013), raising the possibility that VGSCs could also play a role in cells where ERA-1 is present.

5. CHARACTERIZATION OF THE EFFECT OF THE CLATHRIN HEAVY CHAIN ON FORCE GENERATION

5A. RESULTS

The clathrin heavy chain CHC-1 negatively regulates pulling forces in *C. elegans* embryos

In the course of an RNAi-based functional genomic screen (Gönczy et al., 2000), it was found that depletion of the clathrin heavy chain CHC-1 results in several phenotypes visible by DIC in one-cell embryos, which we set out to further investigate. As in other systems, clathrin plays a role in receptor-mediated endocytosis in *C. elegans* and is thus required for proper yolk intake in the oocyte (Figure 56A and B; Grant and Hirsh, 1999). We found in addition that *chc-1(RNAi*) one-cell embryos exhibit stereotyped MTOC positioning defects that are detailed below.

During centration/rotation, instead of the smooth movement of centrosomes and associated pronuclei towards the anterior that are characteristic of the wild-type, excess back and forth movements are observed in *chc-1*(*RNAi)* embryos (Figure 56A-D). To quantify this phenotype, we determined the velocity of the movements of centrosomes as well as their angular displacement during centration/rotation (see Figure 56E for a schematic of the quantification methods). We found that both metrics are significantly higher in *chc-1(RNAi)* embryos than in the wild type (Figure 56F and G).

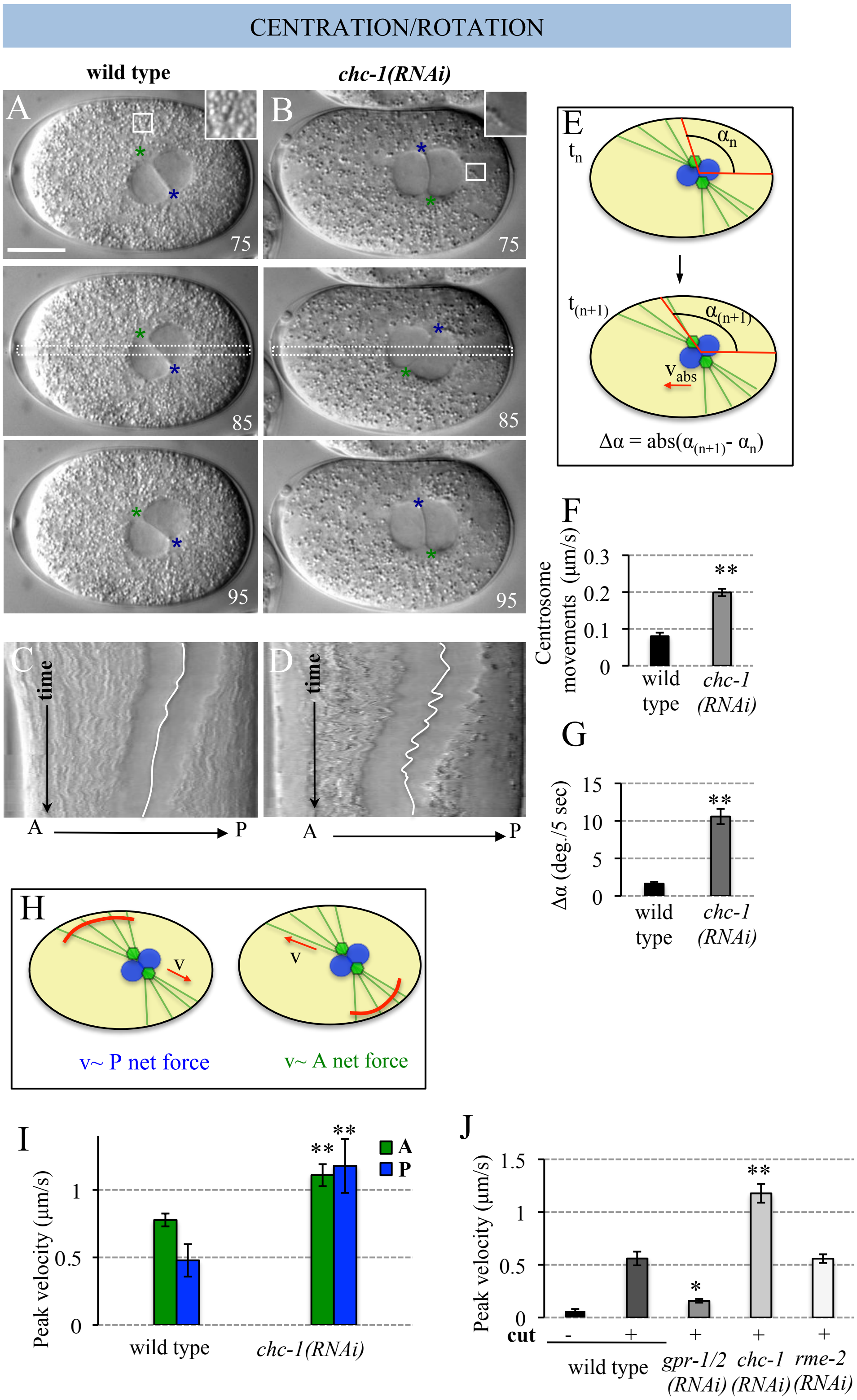

Figure 56. Clathrin negatively regulates net pulling forces acting on centrosomes during centration/rotation

A, B Centrosome position in wild type (**A**) and *chc-1(RNAi)* (**B**) embryos monitored by time-lapse DIC microscopy. Centrosomes are marked with green and blue asterisks. Insets illustrate the depletion of yolk granules in *chc-1(RNAi)* embryos. Here and in other figures, time is indicated in seconds, with t=0 corresponding to pronuclear meeting unless stated otherwise, and scale bars represent 10 microns. **C, D** Kymographs of the areas marked by dashed white rectangles in A and B. White line delineates the position of the nuclear envelopes of the joined pronuclei. The embryos were imaged with a frame rate of 0.5 s to acquire a kymograph with high resolution. Here and in the following cases, we used the first 150 seconds from pronuclear meeting onwards to compose the kymographs. **E** Schematic illustration of the quantification methods of centrosome movements during centration and of their angular displacement. **F**, **G** Average centrosome movements (**F**) and average angular displacement (**G**) in wild type and *chc-1(RNAi)* embryos. n=10 embryos from 3 experiments in every case. **H** Schematic illustrating the experiment aimed at assessing net pulling forces acting on the anterior or posterior centrosome during centration/rotation. Microtubules were severed with the laser microbeam close to the cell cortex, as indicated by the red line, and the resulting displacement of the pronuclei in the opposite direction determined. The extent of this displacement reflects the extent of net pulling forces acting on the posterior (upper panel) or anterior (lower panel) centrosome. **I** Average peak velocities of centrosomes following laser severing of microtubules during centration rotation. Posterior cuts (red) and anterior cuts (blue) were performed to evaluate forces acting in both directions. **J** Average posterior-directed peak velocities of centrosomes following laser severing of anteriorly directed astral microtubules in embryos of the indicated conditions.

As mentioned before, the net pulling force acting on spindle poles during anaphase can be estimated using laser microbeam-mediated severing of astral microtubules (Grill et al., 2001). We designed an analogous assay during centration/rotation, performing severing of astral microtubules emanating from the anterior or the posterior centrosome. The extent of anteriorly directed net pulling forces was inferred from the velocity of anteriorly directed movements following posterior severing, and that of posteriorly directed net pulling forces from the velocity of posteriorly directed movements following anterior severing (see Figure 56H for a schematic of these experiments). The resulting analysis revealed that net forces are larger on the anterior than on the posterior at this stage (Figure 56I), in line with analogous experiments in which centrosomes were targeted with a laser microbeam (Labbe et al., 2004). Moreover, we found that peak velocities following an anterior cut are lower in *gpr-1/2(RNAi)* embryos than in the wild-type (Figure 56J), as anticipated from the ternary complex playing a role in centration/rotation (Park and Rose, 2008). Most importantly, these experiments revealed also that net pulling forces are substantially higher both on the anterior and posterior centrosomes in *chc-1(RNAi)* compared to the wild-type (Figure 56I). This increase is not due merely to the depletion of yolk granules, since peak velocities after an anterior cut are indistinguishable from the wild-type in *rme-2(RNAi)* embryos (Figure 56J), in which yolk granules are also sparse due to defective endocytosis (Grant and Hirsh, 1999).

We also observed that even though centrosomes in *chc-1*(*RNAi*) embryos occupy a normal position by the end of centration, they are displaced prematurely towards the posterior by the time of nuclear envelope breakdown (NEBD), suggestive of higher posterior pulling forces (Figure 57A). Nevertheless, the spindle is oriented along the AP axis in *chc-1*(*RNAi*) embryos as it is in the wild-type (Figure 57B and C).

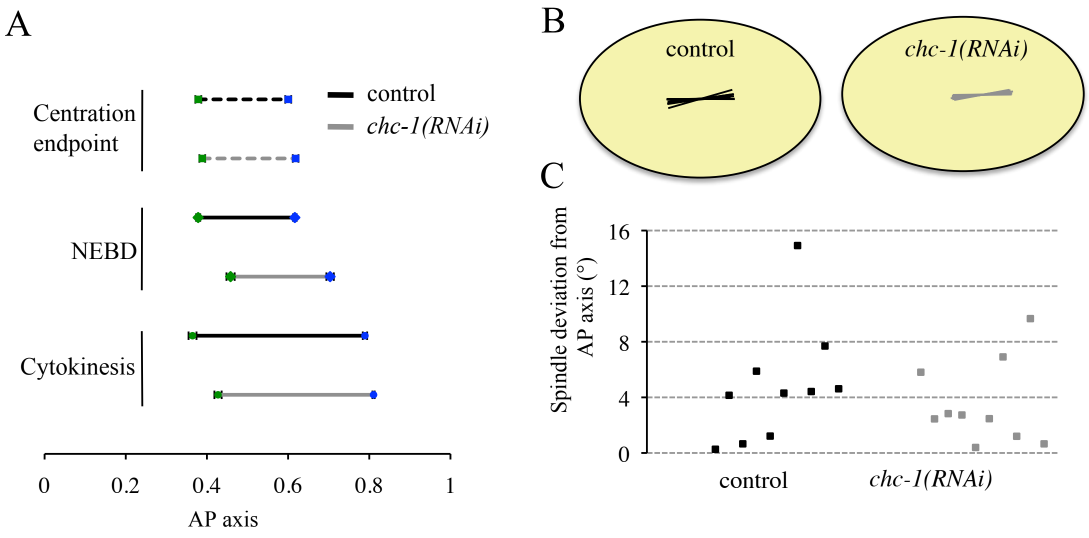

Figure 57. Clathrin depletion leads to premature posterior spindle displacement
A Quantification of the position of centrosomes at the end of centration, nuclear envelope breakdown (NEBD) or the onset of cytokinesis in wild type (black lines) and *chc-1(RNAi)* embryos (grey lines). The position of the anterior (green) and the posterior (blue) MTOCs was projected onto the AP-axis of the embryo. Filled lines indicate the spindle, the dashed line the shortest path between the two centrosomes. n=10 embryos each from 3 experiments. **B, C** Spindle position (**B**) and quantification of its alignment with the AP axis (**C**) at metaphase in 10 control (black) and 10 *chc-1(RNAi)* (grey) embryos.

An MTOC positioning phenotype was also observed thereafter in *chc-1*(*RNAi*) embryos. Thus, we found that the anterior spindle pole of *chc-1*(*RNAi*) embryos exhibits excess oscillations during anaphase (Figure 58A-D), suggestive of increased net forces pulling on the anterior spindle pole. To test whether this is the case, we performed spindle-severing experiments during anaphase and found that the average peak velocity of the liberated anterior spindle pole is higher indeed in *chc-1(RNAi)* embryos than in the wild-type (Figure 58E). Despite such alterations in net pulling forces, the final position of the anaphase spindle and thus the placement of the cleavage furrow are essentially unchanged in *chc-1(RNAi)* embryos, presumably because of the above mentioned premature posterior displacement of centrosomes at the time of NEBD (Figure 58A).

Overall, we conclude that the clathrin heavy chain negatively regulates pulling forces on the anterior side during centration/rotation and anaphase in *C. elegans* embryos.

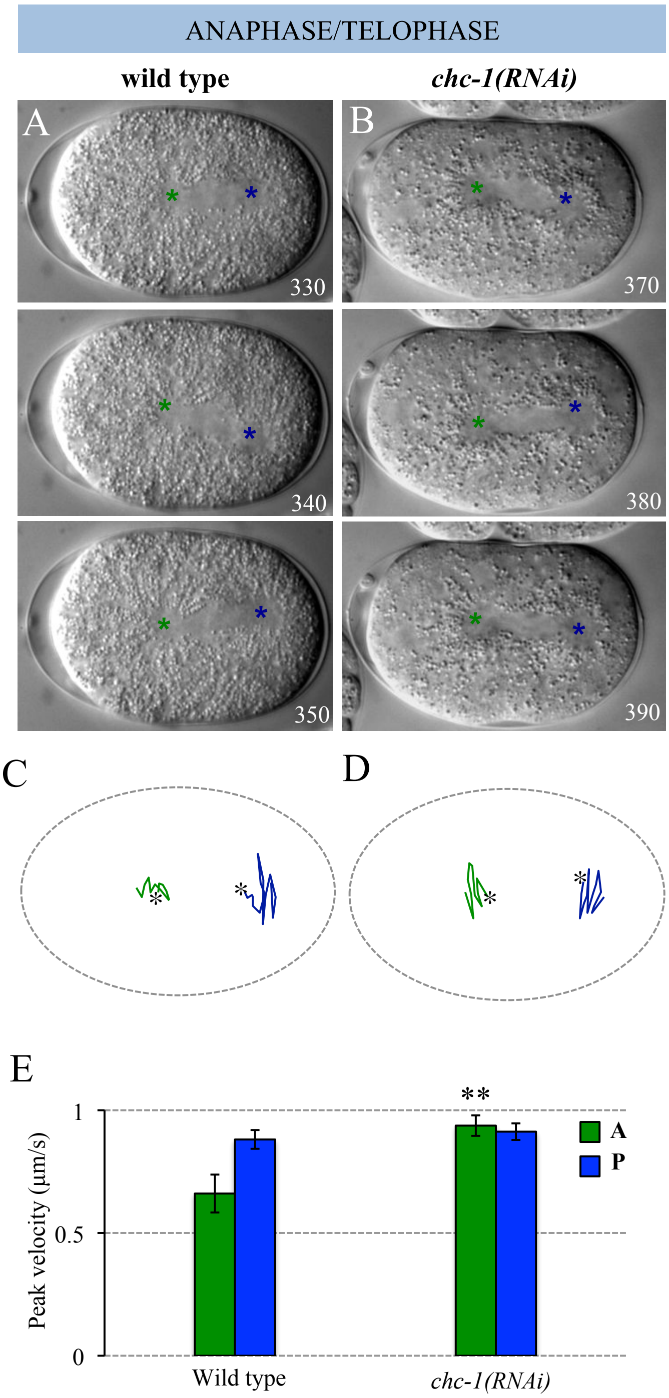

Figure 58. Clathrin negatively regulates net pulling forces acting on centrosomes during anaphase **A, B** Position of the anaphase spindle in wild type (**A**) and *chc-1(RNAi)* (**B**) embryos. Spindle poles are marked with green (anterior) and blue (posterior) asterisks. **C, D** Anterior (green) and posterior (blue) spindle pole positions during anaphase in embryos shown in A and B. Spindle poles were tracked for one minute before cytokinesis onset at a frame rate of 5 s. Dashed grey oval lines represent the embryo, black asterisks mark the initial position of the spindle poles. **E** Average peak velocities of anterior (green) and posterior (blue) spindle poles after spindle severing in wild type and *chc-1(RNAi)* embryos. n=10 embryos each from 3 experiments.

CAR-1 depletion also leads to MTOC positioning defects and results in lower CHC-1 levels

We were intrigued by the fact that embryos depleted of the cytokinesis/apoptosis/RNA-binding protein CAR-1 exhibit MTOC positioning phenotypes that appeared reminiscent of those in *chc-1*(*RNAi*) embryos (Squirrell et al., 2006). CAR-1 is a multifunctional RNA binding protein that plays a role in germline apoptosis (Boag et al., 2005), in regulating P-granule-related mRNAs (Noble et al., 2008) and in cytokinesis (Audhya et al., 2005). Intriguingly, overexpression of the CAR-1 homologue Scd6p/Lsm13p in budding yeast suppresses clathrin deficiency (Nelson and Lemmon, 1993). Although several aspects of CAR-1 function have been characterized previously in *C. elegans*, we focused on the fact that CAR-1 depletion leads to excess back and forth movements of centrosomes during centration/rotation, resulting in increased centrosome movements and angular displacement during centration/rotation compared to the wild type (Figure 59).

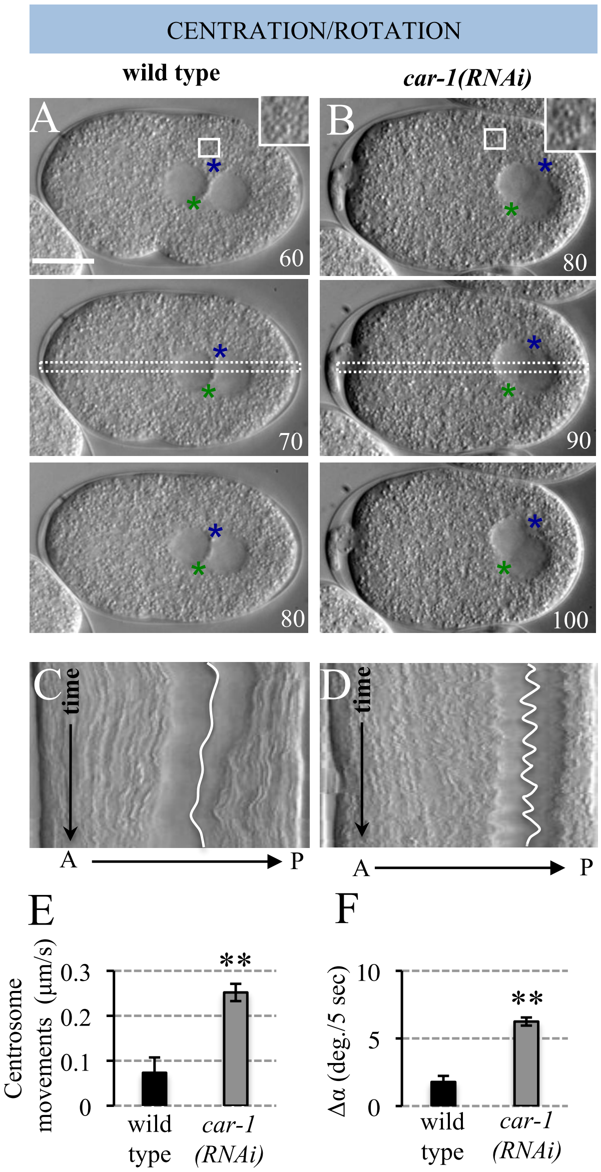
CENTRATION/ROTATION
wild type
car-1(RNAi)
A
B
60
80
70
90
80
100
C
D
time
time
A
P
A
P
E
F
Centrosome movements (μm/s)
0.3
0.2
0.1
0
**
wild type
car-1 (RNAi)
Δα (deg./5 sec)
10
5
0
**
wild type
car-1 (RNAi)

Figure 59. CAR-1 negatively regulates centrosome/spindle positioning during centration/rotation

A, B Centrosome position in wild type (**A**) and *car-1(RNAi)* (**B**) embryos monitored by time-lapse DIC microscopy. Centrosomes are marked with green and blue asterisks. Insets show that yolk granules are present normally in *car-1(RNAi)* embryos. Note that cell cycle progression is delayed in *car-1(RNAi)* embryos. **C, D** See legend of Fig. 58C, D. Because of the delay in cell cycle progression, only the first 3 minutes of centration/rotation are shown in *car-1(RNAi)* embryos, although excess movements are present throughout centration/rotation. **E, F** Average centrosomal movements (**E**) and average angular displacement (**F**) in wild type and *car-1(RNAi)* embryos. n=10 embryos from 3 experiments in every case.

Moreover, we found that the anterior spindle pole undergoes excess oscillations during mitosis in *car-1(RNAi)* embryos (Figure 60). Overall these phenotypic manifestations are similar to the ones in *chc-1*(*RNAi*) embryos.

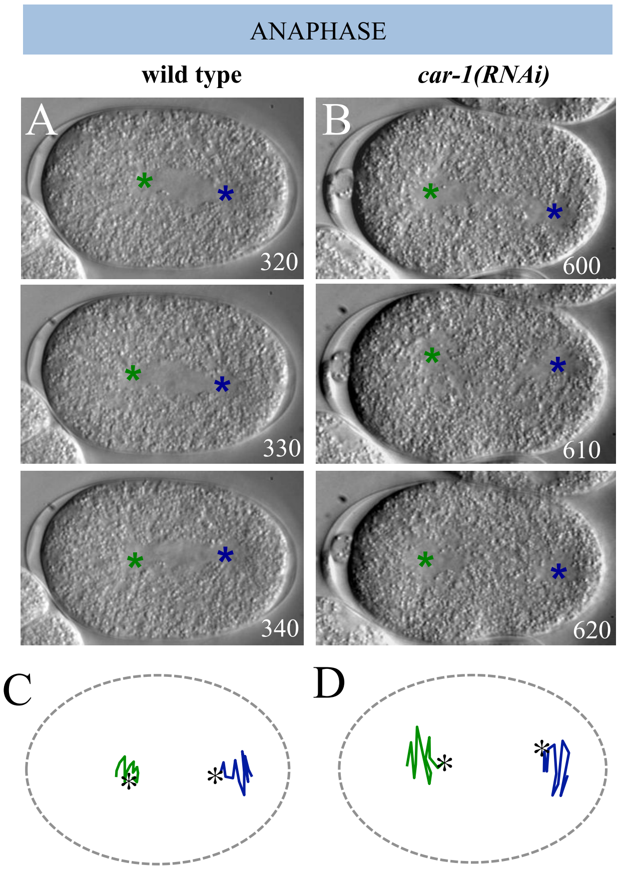

Figure 60. CAR-1 negatively regulates centrosome/spindle positioning during anaphase
A, B Position of the anaphase spindle in wild type (**A**) and *car-1(RNAi)* (**B**) embryos. Centrosomes are marked with green (anterior) and blue (posterior) asterisks. **C, D** Anterior (green) and posterior (blue) spindle pole positions during anaphase in the embryos shown in G and H. Spindle poles were tracked for one minute before cytokinesis onset at a frame rate of 5 seconds. Dashed grey oval lines represent the embryo, black asterisks mark the initial position of the spindle poles.

Therefore, we examined the distribution of clathrin in *car-1(RNAi)* embryos. In wild-type one-cell embryos, GFP-CHC-1 is present primarily in the cytoplasm, is enriched on the spindle and is also detectable in the vicinity of the cortex (Figure 61A). Strikingly, we found that the overall levels of GFP-CHC-1 are markedly reduced in *car-1(RNAi)* embryos (Figure 61B and C). How CHC-1 levels depend on CAR-1 function remains to be investigated but, regardless of the mechanism, this requirement is not bidirectional, since CAR-1 levels and distribution appear unaffected in *chc-1(RNAi)* embryos (Figure 61D and E). Moreover, we observed that yolk granules are not altered in *car-1(RNAi)* embryos (Figure 59B), further demonstrating that the *chc-1*(*RNAi*) MTOC positioning phenotype is not due to depletion of yolk granules.

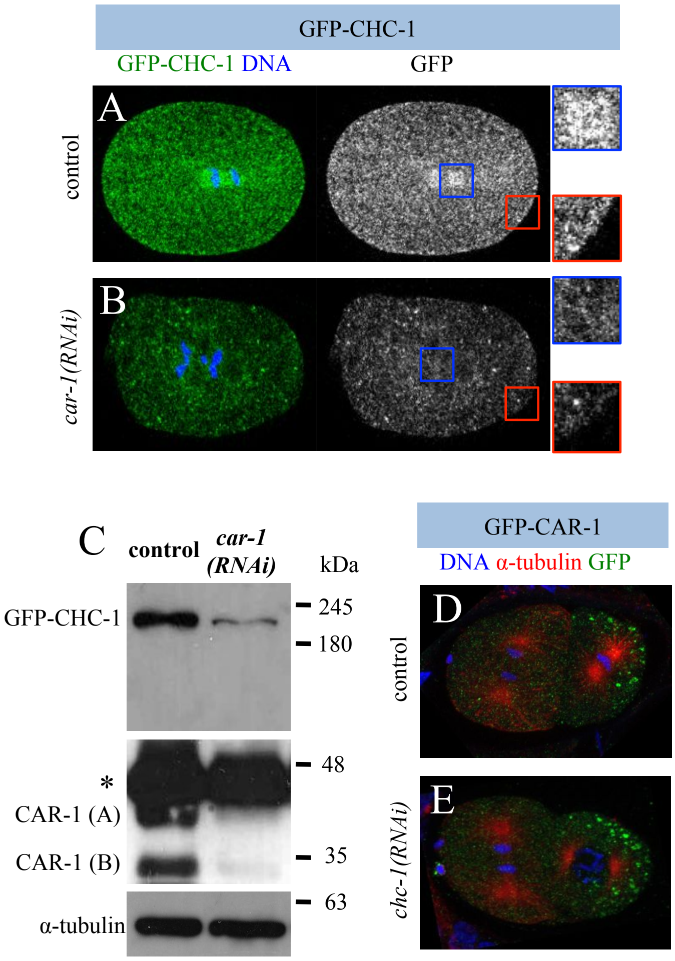

Figure 61. CAR-1 depletion leads to decreased CHC-1 levels in embryos

A, B Immunofluorescence analysis of control (**A**) and *car-1(RNAi)* (**B**) embryos expressing GFP-CHC-1, stained with antibodies against GFP (green on the left, grey on the right); DNA is seen in blue. Insets display magnified region of the spindle (blue box) and cortex (red box). **C** Western blot analysis of lysates from control and *car-1(RNAi)* embryos expressing GFP-CHC-1, using antibodies against GFP, α -tubulin or CAR-1, as indicated. The CAR-1 antibody specifically recognizes two species (Audhya et al., 2005); asterisk denotes a non-specific band. **D, E** Immunofluorescence analysis of GFP-CAR-1 in control (**D**) and *chc-1(RNAi)* (**E**) embryos. Panels on the left show the merge of DNA (blue), α-tubulin (red) and GFP (green), right panels show GFP alone (grey).

Overall, we conclude that CAR-1 is needed for appropriate CHC-1 levels in the early embryo. The above results indicate that the CAR-1 phenotype can be explained by the impact on CHC-1, and we thus investigated the *chc-1*(*RNAi*) phenotype in more detail to uncover how clathrin negatively regulates pulling forces.

Higher forces in *chc-1(RNAi)* do not arise from increased levels of cortical force generators

We set out to determine the root of the higher net pulling force phenotype upon CHC-1 depletion. We tested whether polarity is affected, but found that the distribution of P-granules is not changed in *chc-1(RNAi)* embryos (Figure 62A and B). Given the role of clathrin in organizing spindle pole structure in human cells (Foraker et al., 2012), we also investigated whether MTOC structure is altered in *chc-1(RNAi)* embryos. However, staining with antibodies against the MTOC component TAC-1 (Bellanger and Gönczy, 2003; Le Bot et al., 2003; Srayko et al., 2003) did not reveal a difference with the wild-type during either centration/rotation or mitosis (Figure 62C-F).

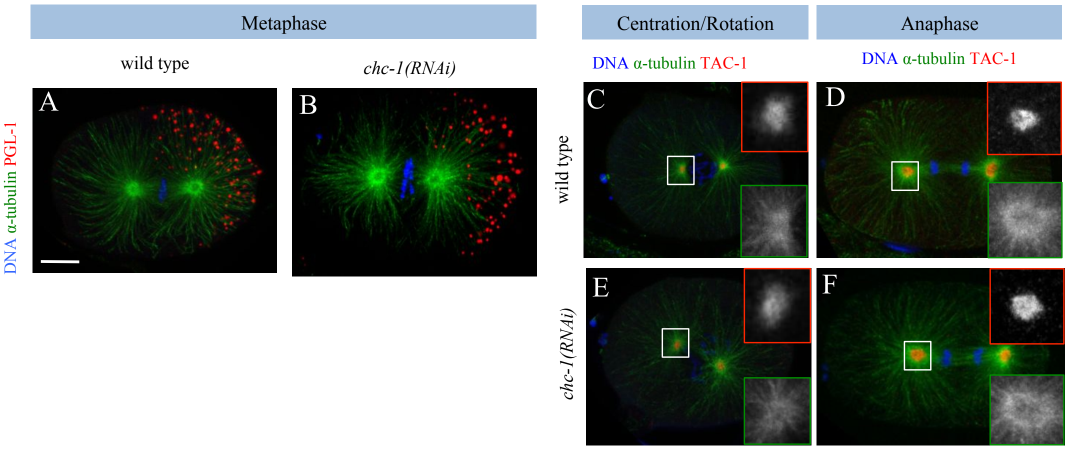

Figure 62. Polarity and centrosomes are not affected in *chc-1(RNAi)* embryos
A, B Immunofluorescence analysis with PGL-1 antibodies to mark P granules in wild type (**A**) and *chc-1(RNAi)* (**B**) anaphase embryos. Z-projection merge images of DNA (blue), α-tubulin (green) and PGL-1 (red). **C-F** Immunostaining of DNA (blue), α-tubulin (green) and TAC-1 (red) in wild-type (**C, D**) and *chc-1(RNAi)* (**E, F**) embryos during centration/rotation and during anaphase. The insets show magnified region of TAC-1 (upper insets) and α-tubulin (lower insets) single channels.

The *chc-1*(*RNAi*) phenotype bears similarity with that of embryos depleted of Gβγ, in which cortical levels of ternary complex components and of dynein are increased because more Gα is available for interaction with GPR-1/2 (Afshar et al., 2004; Tsou et al., 2003). Therefore, we set out to test whether decreased cortical GPB-1 may be what causes the MTOC phenotype in *chc-1*(*RNAi*) embryos. We did find that cortical GPB-1 is diminished in *chc-1(RNAi)* embryos both during centration/rotation and mitosis (Figure 56A-B and G-H). Instead, GPB-1 accumulates in intracellular punctae that are positive for the late endosomal protein, RAB-7 (Figure 63N), indicating that clathrin is required for GPB-1 trafficking. However, unexpectedly considering the observed diminution of cortical GPB-1, we found that cortical levels of LIN-5 and of the dynein heavy chain DHC-1 are not increased in *chc-1(RNAi)* embryos (Figure 63C-F and I-M). This observation suggests that clathrin also promotes the presence of the ternary complex and of dynein at the cell cortex. Overall, the above analysis fails to explain why there is an increase in net pulling forces upon CHC-1 depletion.

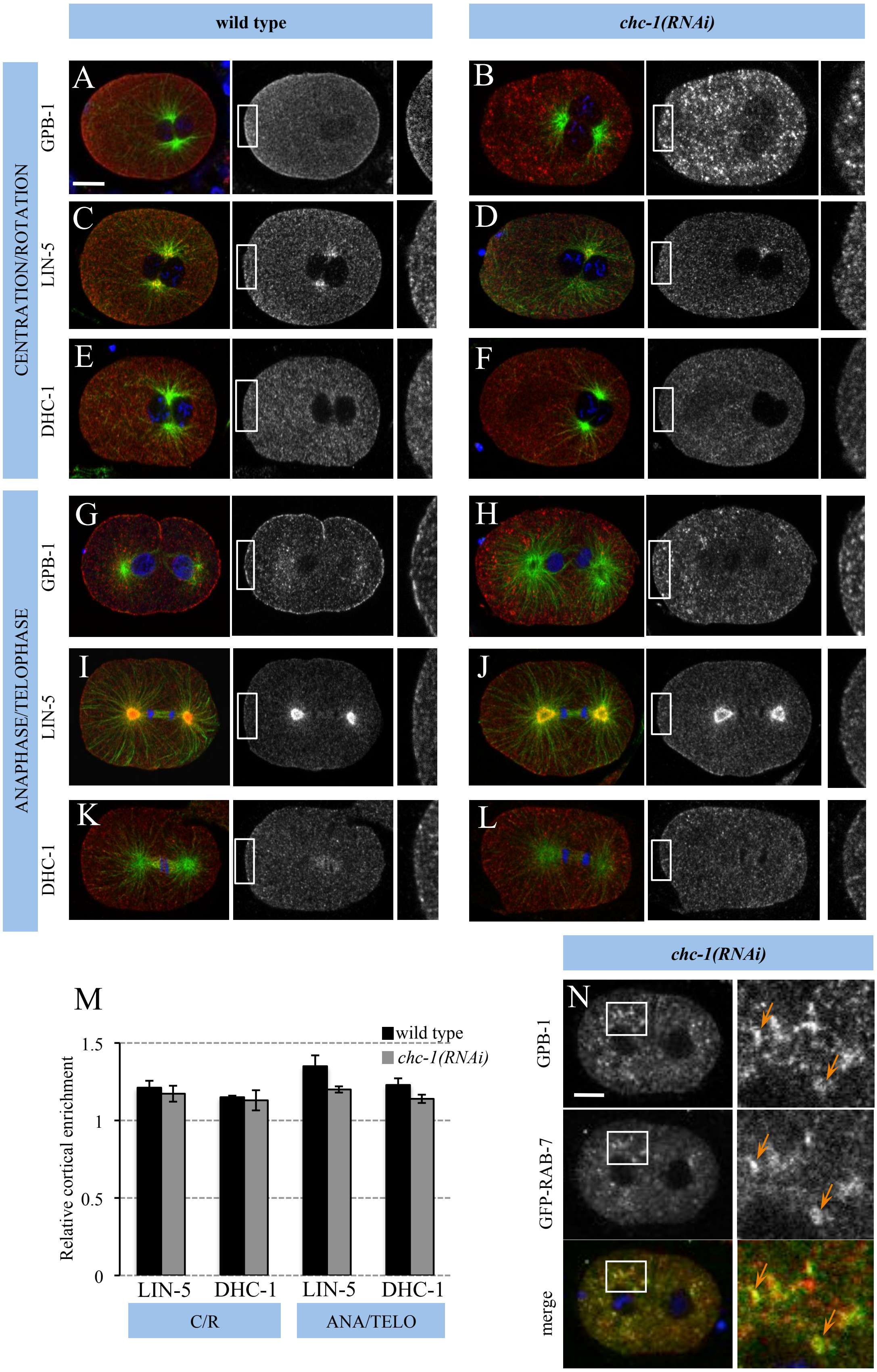
wild type
chc-1(RNAi)
CENTRATION/ROTATION
ANAPHASE/TELOPHASE
GPB-1
LIN-5
DHC-1
GPB-1
LIN-5
DHC-1
A
B
C
D
E
F
G
H
I
J
K
L
M
Relative cortical enrichment
1.5
1
0.5
0
wild type
chc-1(RNAi)
LIN-5
DHC-1
LIN-5
DHC-1
C/R
ANA/TELO
chc-1(RNAi)
N
GPB-1
GFP-RAB-7
merge

Figure 63. The levels of cortical force generators are not increased upon *chc-1(RNAi)*, **A**-**L** Immunofluorescence analysis during centration/rotation (**A**-**F**) and anaphase/telophase (**G**-**L**) monitoring the distribution of GPB-1 (**A**, **B** and **G**, **H**), LIN-5 (**C, D** and **I, J**) or DHC-1 (**E, F** and **K**, **L**) in wild type and *chc-1(RNAi)* embryos, as indicated. The images on the left are merges of the above respective signals (red, also shown alone on the right) with the α-tubulin signal (green); DNA is shown in blue. Insets display magnified region of the anterior cell cortex. Note intracellular accumulation of GPB-1 upon CHC-1 depletion. **M** Quantification of relative cortical LIN-5 and DHC-1 enrichment during centration/rotation and anaphase/telophase in wild type (black) and *chc-1(RNAi)* embryos (grey). Intensities at the cortex and in the underlying cytoplasm were determined and expressed as a ratio. 10 embryos were analyzed for each condition. **N** Immunofluorescence analysis of GPB-1 localization in embryos expressing GFP-RAB-7 upon CHC-1 depletion. Lowest panel shows the merge of GFP (green) and GPB-1 (red) signals; DNA is stained in blue. Insets display magnified region of cytoplasm.

Given that depletion of CHC-1 gives rise to a particularly striking phenotype during centration/rotation, we focused further analysis on this stage and asked whether the excess back and forth movements observed in *chc-1*(*RNAi*) embryos requires the function of cortical force generators. To this end, we depleted simultaneously CHC-1 and individual components of the ternary complex. As shown in Figure 64, we found that impairing the function of GOA-1, GPA-16, GPR-1/2 or LIN-5 suppresses excess centrosome movements during centration/rotation in *chc-1*(*RNAi*) embryos. We conclude that although cortical levels of force generator components are not augmented in *chc-1(RNAi)* embryos, the increase in net pulling forces is somehow dependent on cortical force generators.

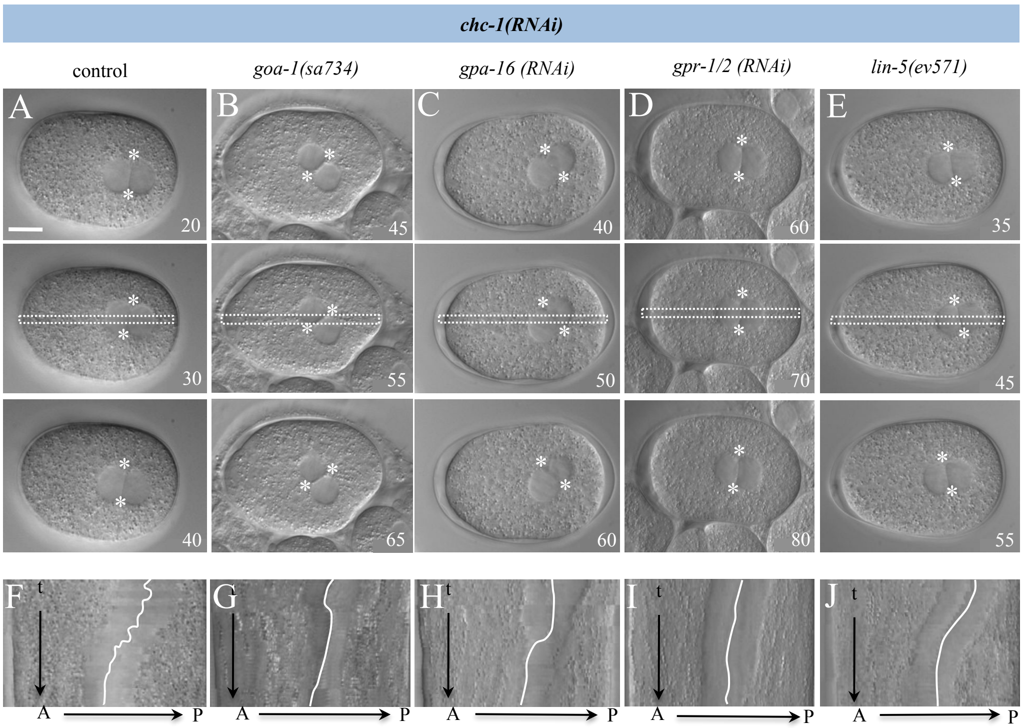

Figure 64. Depletion of force generator components rescues excess forces in *chc-1(RNAi)*
A-E Centration/rotation in embryos co-depleted of clathrin and of the indicated component. *chc-1(RNAi)* was performed on *goa-1(sa734)* (**B**) or *lin-5(ev571)* (**E**) mutant animals, or applied together with *gpa-16*(*RNAi*) (**C**) or *gpr-1*/*2*(*RNAi*) (**D**). **F-J** Kymographs of the area marked by dashed white rectangles in A-E, with time represented vertically. White line delineates the position of the nuclear envelopes of the joined pronuclei.

Clathrin is needed for proper organization and tension of the cortical acto-myosin network

Since clathrin is known to organize the actin network in other systems (Calabia-Linares et al., 2011; Humphries et al., 2012), we explored whether CHC-1 depletion affects the acto-myosin network in early *C. elegans* embryos. To this end, we performed spinning disk microscopy imaging of the cortical acto-myosin network in live embryos expressing GFP::MOE to visualize filamentous (F) actin. As reported previously (Velarde et al., 2007) and shown in Figure 65A, we observed small F-actin foci at the time of pronuclear meeting in the anterior of control embryos. Strikingly, we found that CHC-1 depletion results in larger cortical F-actin foci (Figure 65B, quantified in C). We similarly imaged embryos expressing GFP-NMY-2 to visualize non-muscle myosin. We found that instead of the large foci normally present in the anterior of control embryos (Figure 65D, Munro et al., 2004), *chc-1(RNAi)* embryos harbor smaller foci (Figure 65E, quantified in F). Overall, we conclude that the acto-myosin network, whilst not absent, is perturbed upon CHC-1 depletion.

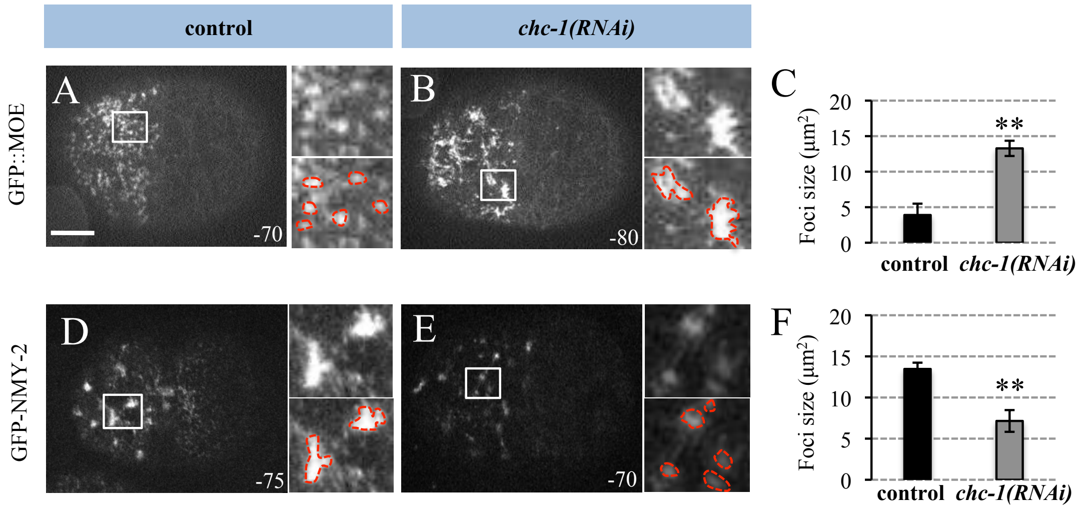
control
chc-1(RNAi)
GFP::MOE
A
-70
B
-80
C
Foci size (µm²)
20
15
10
5
0
**
control
chc-1(RNAi)
GFP-NMY-2
D
-75
E
-70
F
Foci size (µm²)
20
15
10
5
0
**
control
chc-1(RNAi)

Figure 65. Clathrin is needed for proper organization of the acto-myosin network in early *C. elegans* embryos
A, B Cortical imaging of control (**A**) and *chc-1*(*RNAi*) (**B**) embryos expressing the actin-binding fusion protein GFP::MOE visualized with spinning disk microscopy at the onset of pronuclear migration. Insets show magnified cortical regions; some actin foci are delineated in red. **C,** Quantification of GFP::MOE foci size in control and *chc-1*(*RNAi*) embryos; n=8 embryos each from 3 experiments, 8-10 foci per embryo. **D**, **E** Cortical imaging of control (**D**) and *chc-1*(*RNAi*) (**E**) embryos expressing GFP-NMY-2 imaged as above. Insets show magnified region of the cortex; GFP-NMY-2 foci are delineated in red. Note that GFP-NMY-2 intensities are lower in *chc-1*(*RNAi*) embryos. **F** Quantification of GFP-NMY-2 foci size in control and *chc-1*(*RNAi*) embryos. Note also that apart from the difference in size, there is an apparent drop in intensity of the foci in *chc-1(RNAi);* n=8 embryos each from 3 experiments, 8-10 foci per embryo.

Next, we tested whether such altered organization of the cortical acto-myosin network is accompanied by diminished cortical tension. To this end, we performed cortical laser ablation (COLA) experiments at pronuclear formation (Mayer et al., 2010). In this assay, cortical tension is deduced from measuring the outward velocities of GFP-NMY-2 foci following a laser cut along the longitudinal axis of the embryo (Figure 66).

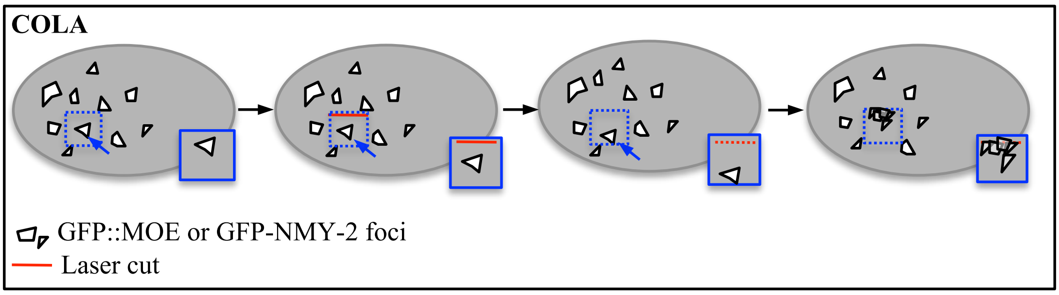
COLA
GFP::MOE or GFP-NMY-2 foci
Laser cut

Figure 66. Principle of Cortical Laser Ablation (COLA). Following a longitudinal laser cut in the acto-myosin cell cortex (red line), the movement of GFP::MOE or GFP-NMY-2 foci (white structures) is monitored. Blue arrows point to one specific focus, whose motion (blue dashed rectangle) is magnified in the insets; red line marks the position of the cut. The resulting outward velocity is an indirect measure of cortical tension (Mayer et al., 2010).

As can be seen in Figure 60, these experiments demonstrated that *chc-1(RNAi)* embryos exhibit significantly lower outward velocities compared to the wild-type at pronuclear formation. We next tested whether such a decrease persists into prophase when the most dramatic phenotypic manifestations take place in *chc-1(RNAi)* embryos. Because cortical levels of NMY-2-GFP are low at this stage, we performed COLA experiment using embryos expressing GFP::MOE, which give rise to a stronger fluorescence signal at this time. Importantly, these experiments established that there is a likewise significant decrease in cortical tension during centration/rotation compared to the wild-type (Figure 68).

These experiments taken together indicate that clathrin is needed for proper organization and cortical tension of the acto-myosin network in one-cell *C. elegans* embryos.

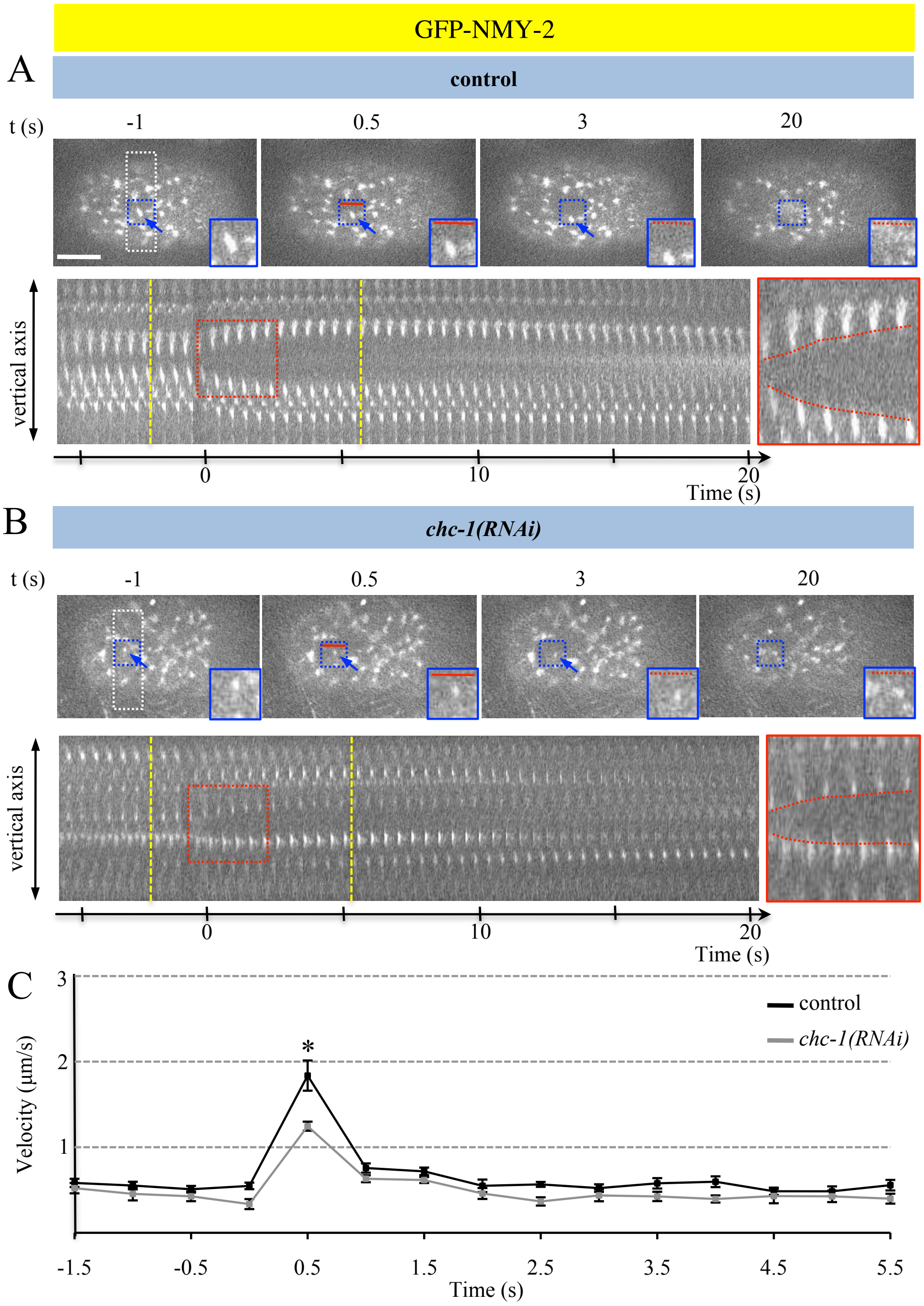

Figure 67. Clathrin depletion leads to lower cortical tension at pronuclear formation
A, B COLA in control (**A**) and *chc-1(RNAi)* (**B**) embryos expressing GFP-NMY-2. Four images from a movie monitoring the cell cortex using spinning disc microscopy are shown, with t=0 corresponding to the time of cut. Blue arrows mark a specific GFP-NMY-2 focus, red line indicates the cut. The cortex is monitored until complete recovery of GFP-NMY-2 foci; the inset in the last frame shows the sealed cortex with the tracked focus coalesced. Below are the kymographs constructed from the area marked by the white rectangle, with the area contoured with the red dashed box magnified on the right to better appreciate the outwards motion (dashed red lines within the box indicate the front of the outward movement). **C** Quantification of initial outward velocities from 1.5 seconds before to 5.5 seconds after the cut (time interval indicated with dashed yellow lines on the kymographs); n=8 embryos each from 3 experiments were analyzed.

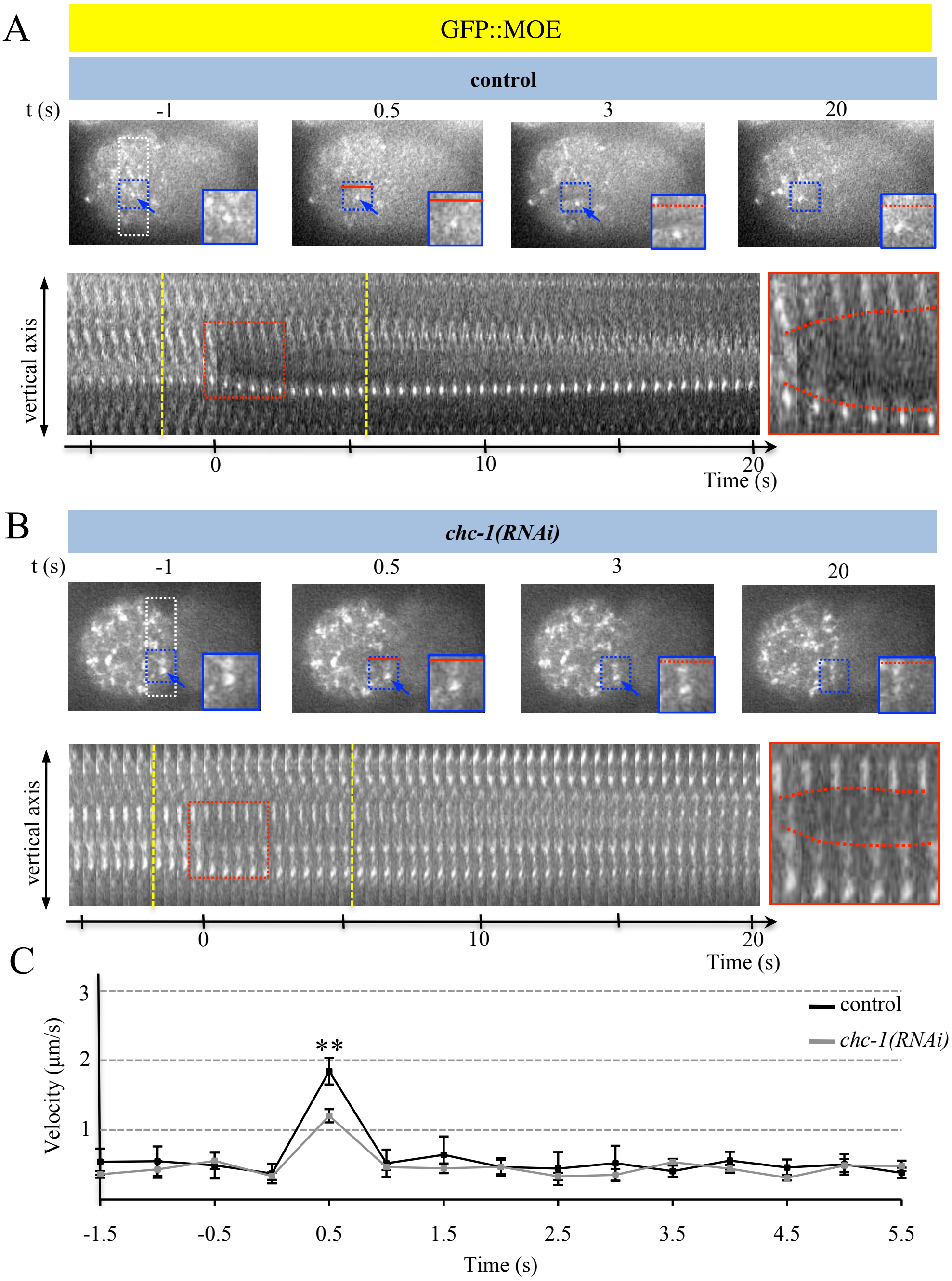
A
GFP::MOE
control
t (s)
-1
0.5
3
20
vertical axis
0
10
20
Time (s)
B
chc-1(RNAi)
t (s)
-1
0.5
3
20
vertical axis
0
10
20
Time (s)
C
Velocity (µm/s)
3
2
1
**
control
chc-1(RNAi)
-1.5
-0.5
0.5
1.5
2.5
3.5
4.5
5.5
Time (s)

Figure 68. Clathrin depletion leads to lower cortical tension at centration/rotation
A, B COLA in control (**A**) and *chc-1(RNAi)* (**B**) embryos expressing GFP::MOE. Four images from a movie monitoring the cell cortex using spinning disc microscopy are shown, with t=0 corresponding to the time of cut. Blue arrows mark a specific GFP::MOE focus, the red line indicates the cut. The cortex is monitored until the complete recovery of GFP::MOE, the inset in the last frame shows the sealed cortex with the tracked focus coalesced. Below are the kymographs constructed from the area marked by the white rectangle, with the area contoured with the red dashed box magnified on the right to better appreciate the outwards motion (dashed red lines within the box indicate the front of the outward movement).
C Quantification of initial outward velocities from 1.5 seconds before to 5.5 seconds after the cut (time interval indicated with dashed yellow lines on the kymographs); n=9 embryos each from 3 experiments were analyzed.

Alterations in the acto-myosin network likely cause the centrosome positioning phenotype of *chc-1(RNAi)* embryos

We reasoned that if the increase in net pulling forces upon CHC-1 depletion is a consequence of defective acto-myosin organization, then stabilizing the actin cytoskeleton should rescue the centrosome positioning phenotype of *chc-1(RNAi)* embryos. Jasplakinolide is a macrocyclic peptide that promotes F-actin formation by stimulating filament nucleation (Bubb et al., 1994). We subjected embryos to Jasplakinolide during centration/rotation by piercing holes on the eggshell using the laser microbeam, thus ensuring temporal control to drug exposure and avoiding potential complications due to earlier requirements of the acto-myosin network in A-P polarity (Hill and Strome, 1988). Strikingly, we found that whereas the drug does not alter centrosome movements in the wild-type (Figure 69A-F, quantified in I), Jasplakinolide alleviates excess movements of *chc-1(RNAi)* embryos (Figure 69 C-H, quantified in I). We observed an analogous rescue during anaphase (Figure 69J and K). We conclude that alterations in the acto-myosin network are likely responsible for the MTOC positioning phenotype of embryos depleted of clathrin.

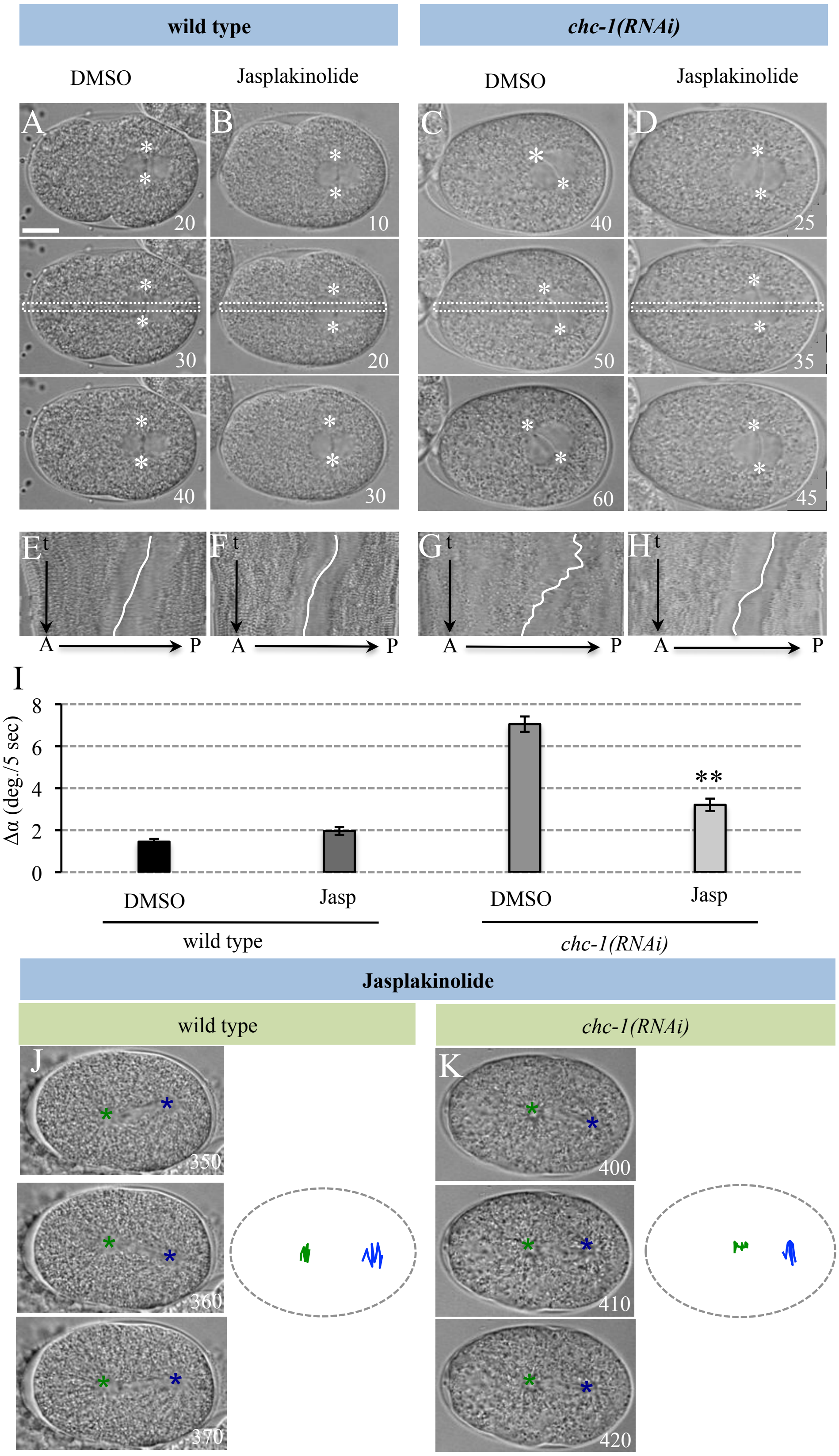
wild type
chc-1(RNAi)
DMSO
Jasplakinolide
DMSO
Jasplakinolide
A
B
C
D
20
10
40
25
30
20
50
35
40
30
60
45
E
F
G
H
t
A
P
I
Δα (deg./5 sec)
8
6
4
2
0
**
DMSO
Jasp
DMSO
Jasp
wild type
chc-1(RNAi)
Jasplakinolide
wild type
chc-1(RNAi)
J
K
350
360
370
400
410
420

Figure 69. Stabilizing the acto-myosin network alleviates the *chc-1(RNAi)* phenotypes at centration/rotation and at anaphase

A-D Centration/rotation in control (**A**, **B**) and *chc-1(RNAi)* (**C**, **D**) embryos treated with 0.5% DMSO (**A**, **C**) or 70μM Jasplakinolide in 0.5% DMSO (**B**, **D**) and monitored by time-lapse microscopy. Centrosomes are marked with white asterisks. Note that the image quality is less good on this microscope equipped with the laser microbeam needed to pierce the eggshell; the same holds for the next two figures. **E-H** Kymographs corresponding to the white rectangle depicted in **A-D**. **I** Angular displacement of centrosomes in all experimental conditions; n=10 embryos each from 3 experiments in each case. Note that treating *chc-1(RNAi)* embryos with DMSO alone leads to a slight drop in the angular displacement compared to untreated *chc-1(RNAi)* embryos (see Figure 49). Note also that Jasplakinolide led to defective cytokinesis of *chc-1(RNAi)*, but not control, embryos (data not shown), suggesting that CHC-1 depletion sensitizes embryos to acto-myosin perturbations. **J-K** Anaphase spindle pole oscillations following Jasplakinolide treatment in wild type (**J**) and in *chc-1(RNAi)* (**K**) embryos. n=6; representative embryos are shown.

The above findings raise the possibility that small alterations in the acto-myosin network in otherwise wild-type embryos might result in centrosome positioning phenotypes reminiscent of those observed in *chc-1(RNAi)* embryos. We tested this prediction in two ways. First, we subjected embryos to increasing concentrations of the F-actin destabilizing drug Latrunculin A (LatA) during centration/rotation. Whereas treating embryos with high concentration of LatA (240μM) completely depolymerizes actin as judged by GFP::MOE cortical imaging (compare Figure 70A with C) lower levels of the drug (20μM) lead to an accumulation of GFP::MOE foci analogous to that observed in *chc-1(RNAi)* embryos (Figure 70B, quantified in D).

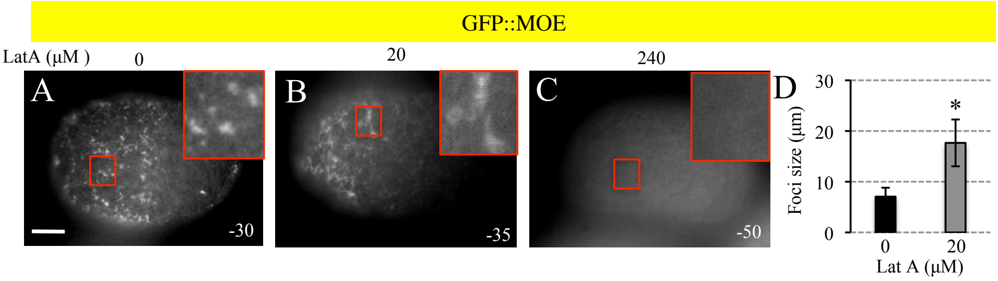

Figure 70. Slight destabliziation of the actin network results in the formation of GFP::MOE foci analogous to that observed in *chc-1(RNAi)*
A-C Cortical snapshot of embryos expressing GFP::MOE at centration/rotation treated with 0.5% DMSO (**A**), 20μM (**B**) and 240μM (**C**) LatrunculinA. Quantification is shown in **D**. 10 embryos each were quantified from 2 independent experiments.

Moreover, we found that embryos exposed to low (10 μM) or high (240 μM) concentrations of LatA are indistinguishable from control embryos with respect to centrosome positioning (Figure 71A and C). In sharp contrast, embryos subjected to intermediate concentrations (20 μM and 50 μM) of the drug exhibit excess back and forth movements of centrosomes and excess angular displacement (Figure 71 B, quantified in G).

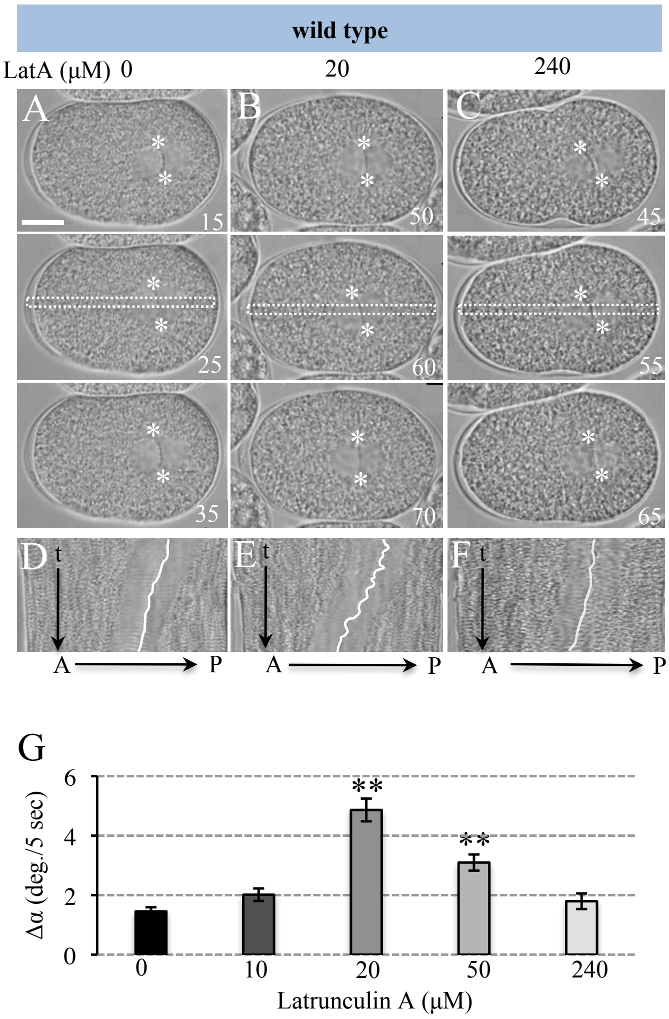

Figure 71. Partial disruption of the actin network resembles the *chc-1*(*RNAi*) phenotype
A-C Centration/rotation in embryos treated with 0 (**A**), 20 (**B**) or 240 (**C**) μM latrunculin A and monitored by time-lapse microscopy. Centrosomes are marked with white asterisks.
D-F Kymographs corresponding to the white rectangle depicted in **A-C.** **G** Angular displacement of centrosomes in all experimental conditions; n=10 embryos each from 3 experiments were analyzed. The corresponding DMSO controls did not affect angular displacement.

As a second means to impart small alterations to the acto-myosin network, we utilized embryos homozygous for the fast inactivating temperature-sensitive allele *nmy-2(ne3409)*, which is indistinguishable from the wild-type at the permissive temperature of 16°C and from *nmy-2*(*RNAi*) at the restrictive temperature of 25°C (Liu et al., 2010). We reasoned that we might observe a centrosome positioning phenotype at intermediate temperatures. As shown in Figure 72B we indeed found excess centrosome movements during centration/rotation at 20 °C, with a corresponding increased angular displacement (Figure 74G). Overall, we conclude that slight impairment of the acto-myosin network leads to a centrosome positioning phenotype analogous to that observed after depleting clathrin.

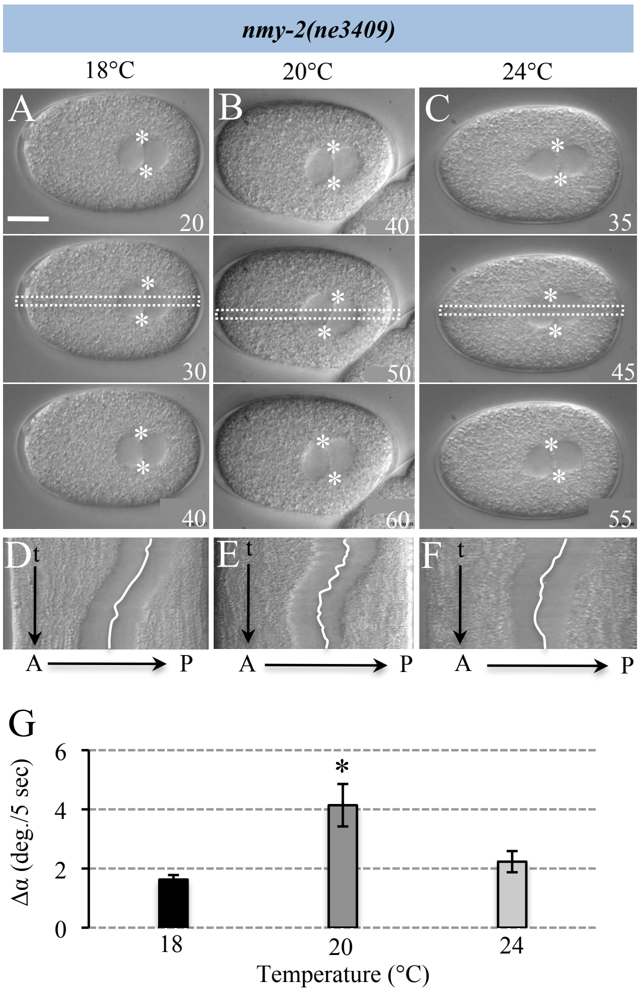
nmy-2(ne3409)
18°C
20°C
24°C
A
20
30
40
B
40
50
60
C
35
45
55
D
t
A
P
E
t
A
P
F
t
A
P
G
Δα (deg./5 sec)
0
2
4
6
*
18
20
24
Temperature (°C)

Figure 72. Partial disruption of myosin function resembles the *chc-1*(*RNAi*) phenotype
A-F Centration/rotation in *nmy-2(ne3409)* temperature sensitive embryos imaged with time-lapse DIC microscopy at 18°C (**A**), 20°C (**B**) or 24°C (**C**). **D-F** Kymographs corresponding to the white rectangle depicted in **A-C. G** Angular displacement of centrosomes in all experimental conditions; n=10 embryos each from 3 experiments were analyzed. Note that embryos imaged at 20 and 21°C, as well as 24 and 25°C, were pooled for the analysis. Wild type embryos at 25°C do not differ from ones at lower temperature in terms of angular displacement (not shown).

5B. DISCUSSION

In this study, we uncovered that clathrin negatively regulates pulling forces acting on centrosomes and spindle poles in one-cell *C. elegans* embryos. Furthermore, we demonstrated that clathrin maintains proper tension of the acto-myosin cortex, which likely explains how clathrin participates in the control of centrosome positioning.

Clathrin, as a regulator of the acto-myosin network

There are other conditions besides *chc-1*(*RNAi*) in which centrosomes undergo excess back and forth movements during centration/rotation, as well as excess spindle oscillations during anaphase, including upon depletion of GPB-1 or CSNK-1 (Tsou et al., 2003; Afshar et al., 2004; Panbianco et al., 2008). In both cases, the increase in net pulling forces is accompanied by elevated levels of cortical force generators. By contrast, we found that this is not the case in *chc-1*(*RNAi*) embryos and thus inferred that clathrin must modulate force generation by another means. We discovered that this involves the acto-myosin network. We found that the organization and tension of the actin-myosin cortex are impaired upon clathrin depletion in *C. elegans* embryos. This appears to be causative of the *chc-1*(*RNAi*) MTOC positioning phenotype since stabilizing the actin cytoskeleton alleviates these phenotypic manifestations. The contribution of clathrin for an intact acto-myosin network has been reported in other systems. Thus, clathrin located on endosomes plays a role in organizing the actin network at the immunological synapse in T-cells (Calabia-Linares et al., 2011). Moreover, clathrin is needed for actin polymerization promoted by vaccinia viral infection (Humphries et al., 2012). Our findings contribute to this body of work and underscore the influence of clathrin on acto-myosin function in a range of biological settings. The interaction between clathrin and actin in other systems occurs via the clathrin light chain and the huntingtin interacting protein 1 related (*hipr-1* in *C. elegans*) (Boettner et al., 2011; Poupon et al., 2008; Wilbur et al., 2008). However, we found that neither the depletion of the clathrin light chain *clic-1* nor of *hipr-1* leads to MTOC positioning defects in *C. elegans* (data not shown). This raises the possibility that there may be a novel mechanism through which the clathrin heavy chain interacts with actin in the worm.

Is clathrin-dependent modulation of the acto-myosin network distinct from its well-known role in endocytosis? A definite answer to this important question is difficult to obtain. First, endocytosis in general affects the actin cytoskeleton and reciprocally, making it challenging to analyze the two processes separately (reviewed in Galletta and Cooper, 2009). Second, inhibiting endocytosis in one-cell *C. elegans* embryos using a dynamin mutant results in lower levels of cortical GPB-1, thus likely influencing force generation via increased cortical dynein (Thyagarajan et al., 2011). This could explain the clathrin-like centration/rotation phenotype observed upon depletion of the early endosomal protein RAB-5 (Hyenne et al., 2012). Note also that RAB-5 localization is slightly affected in *chc-1(RNAi)* embryos (Audhya et al., 2007), but whether CHC-1 may be altered upon RAB-5 depletion is not known. Despite these limitations, our results lead us to favor the view that the impact of clathrin on MTOC is uncoupled from its role in endocytosis. Indeed, we found that *rme-2*(*RNAi*) embryos, in which endocytosis is altered (Grant and Hirsh, 1999), do not exhibit an MTOC positioning phenotype. Conversely, *car-1*(*RNAi)* embryos, in which endocytosis is not altered, but in which CHC-1 levels are compromised, exhibit an MTOC positioning phenotype analogous to that of *chc-1*(*RNAi)* embryos.

Slight perturbation in the actin network and force generation

An involvement of the acto-myosin network during centration/rotation has been proposed previously (Goulding et al., 2007). Based on the movements of cortical foci of NMY-2-GFP, it was hypothesized that acto-myosin-derived forces can be directed towards either the anterior or the posterior of the embryo, and that LET-99 favors anterior-directed movements and thus centration (Goulding et al., 2007). Although there might be a slight mislocalization of LET-99 in *chc-1(RNAi)* embryos, perhaps as a result of perturbations in the acto-myosin cytoskeleton (data not shown), the centration/rotation phenotype of *chc-1(RNAi)* embryos is not suppressed by removing LET-99 (data not shown), indicating that LET-99 mislocalization cannot be causative in this case.

How, then, can perturbations in the acto-myosin network lead to the generation of higher net pulling forces acting on centrosomes and spindle poles of one-cell *C. elegans* embryos? We found that the angular displacement of centrosomes during centration/rotation differs from the wild type only when the acto-myosin network is disturbed slightly, but not when it is compromised more severely. These observations are consistent with predictions from 3D simulations of anaphase spindle positioning, whereby medium levels of cortical rigidity were predicted to result in increased oscillations compared to either lower or higher cortical rigidity (Kozlowski et al., 2007). Inspired by this work, in collaboration with a physicist in the lab, Alessandro de Simone, we set out to model centrosome movements during prophase as a function of cortical rigidity. We were able to simulate the experimental data, whereby medium cortical rigidity results in maximal centrosome oscillations. The rationale behind such a force curve is that a cortex with medium rigidity, as in *chc-1*(*RNAi*) embryos, can stretch more upon being pulled whilst maintaining the interaction between the force generator and the depolymerizing microtubule, leading to higher total work (Figure 73). We note that large membrane invaginations are indeed observed in embryos that have likely impaired cortical rigidity as a result from partial depletion of NMY-2, although overall spindle positioning appears unaffected in such embryos as in *chc-1*(*RNAi*) embryos (Redemann et al., 2010).

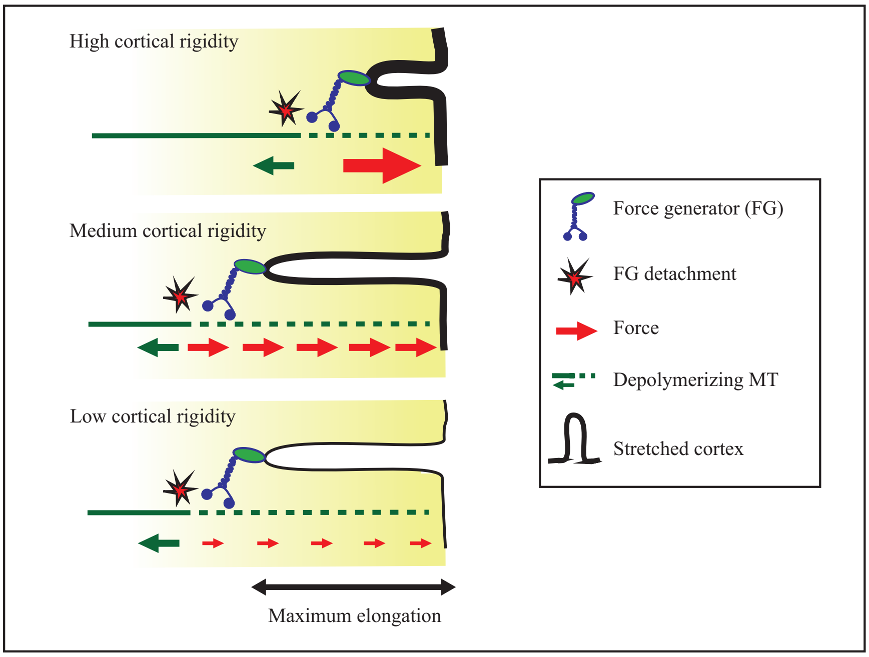

Figure 73. Model describing the relationship between force generation and cortical tension
Model of cortical force generation. The depolymerizing microtubule bound to a cortical force generator stretches the cortex and thus experiences a pulling reaction force. For high cortical rigidity, a strong elastic force is applied, but the force generator detaches rapidly. For medium cortical rigidity, the stretch reaches the maximum elongation before the force generator detaches, resulting in high total forces (i.e. work). For low cortical rigidity, the stretch also reaches the maximum elongation, but the cortex is too loose to apply a large force.

Does the model we propose here for centration/rotation apply during anaphase? Intriguingly, treating mitotic embryos with the actin-depolymerizing agent Latrunculin A leads to an increase of net forces pulling on the anterior spindle pole (Afshar et al., 2010; Berends et al., 2013). However, this is the case either with high (Afshar et al., 2010; Berends et al., 2013) or intermediate (data not shown) levels of Latrunculin A. Although it may be that the effective drug concentration inside the embryo is lower during mitosis, thus resulting in medium cortical rigidity even with high levels of the drug, more work will be needed to elucidate whether the mechanisms at play during centration/rotation apply during anaphase.

A requirement for balanced levels of cortical tension may extend to human cells, in which perturbation of the acto-myosin network also affects spindle positioning on a uniform fibronectin substrate (Toyoshima and Nishida, 2007). It would be interesting to test whether the depletion of clathrin likewise affects spindle positioning in that system. We note that the cortical acto-myosin network also plays a critical role during asymmetric division of Q neuroblast in *C. elegans*, where asymmetric contractile forces are key for generating daughter cells of different sizes (Ou et al., 2010). Our findings indicate that modulation of cortical tension can be harnessed to ensure proper centrosome positioning in different biological systems.

The clathrin project was conducted as a collaboration between several people in the lab. The anterior cytoplasmic cuts (Figure 56J), the anaphase spindle severing experiments (Figure 58E), the GPB-1 immunostaining (Figure 73A, B, G and H) and the experiments testing the dependency of the *chc-1(RNAi)* phenotype on the force generator complex (Figure 64) were performed by Kalyani Thyagarajan a previous PhD student in the lab, the modeling part (Figure 66) was done by Alessandro de Simone and Sylvain Träger contributed in the CAR-1 part.

This work has been published in *Development*:

Spiró, Z., Thyagarajan, K., De Simone, A., Trager, S., Afshar, K. and Gönczy, P. (2014) 'Clathrin regulates centrosome positioning by promoting acto-myosin cortical tension in C. elegans embryos', *Development* 141(13): 2712-23.

6. MATERIALS AND METHODS

Worm strains and RNAi

Wild type N2 (*C. elegans*), wild type AF16 (*C. briggsae*), *lin-5(ev571he63)* (Fisk Green et al., 2004), *par-3(it71)* (Kemphues et al., 1988), *era-1(tm5854) and era-1(tm6426)* strains were maintained at 20-24°C. Transgenic worms expressing GFP-LIN-5 (gift from Myeko D. Mana and Fabio Piano), *lin-5* mRNA with recoded nucleotides 1-376 (Galli et al., 2011), YFP-GPR-1 (Redemann et al., 2011), YFP-ERA-1-*era-1* 3' UTR, YFP-ERA-1-*pie-1* 3'UTR, GFP-RAB-7 (gift from Barth Grant), GFP-NMY-2 (Munro et al., 2004), GFP::MOE (Velarde et al., 2007), GFP-CHC-1 (Greener et al., 2001) were maintained at 24°C. *lin-5(ev571)* (Lorson et al., 2000) was kept at 16°C and shifted to 24°C for 24 hours before the experiments unless otherwise stated. The *nmy-2(ne3409)* temperature sensitive strain (Liu et al., 2010) was kept at 16°C, dissected in M9 stored at 16°C and shifted to the indicated temperatures at the time of pronuclear meeting. Transgenic lines were generated by ballistic bombardment in the *unc-119(ed3)* strain (Praitis et al., 2001).

Bacterial feeding strains for *spd-5, aspm-1*, *zyg-12*, *tbb-1, mex-5, rme-2, car-1, par-3, era-1* were from the Vidal library (Rual et al., 2004), that for *par-2* from the Ahringer library (Fraser et al., 2000). Clones for *dhc-1*(*RNAi*) (Cockell et al., 2004), *gpa-16, goa-1* and *gpr-1/2(RNAi)* (Colombo et al., 2003) were described before. The RNAi feeding strain targeting the first 376 nucleotides of *lin-5* was a gift from Sander van den Heuvel. RNAi was performed by feeding L3-L4 animals at 24°C for 20-24 hours for all the genes except for *gpr-1/2* where the incubation was performed at 20°C for 48 hours.

Recoding of the entire *lin-5* coding region was performed by manually changing each codon, considering the codon usage properties of *C. elegans*. Of note, in some cases, the most optimal codon had to be downgraded in order to introduce the most changes possible. As a result, the codon adaptation index of *lin-5*[rec] was comparable to that of *lin-5*.

Microscopy, spindle severing, drug treatment and image analysis

Embryos were observed by time-lapse DIC microscopy as described (Gönczy et al., 1999). Spindle pole oscillation was tracked by a MatLab code written by Aitana Neves De Silva. Centrosome movements during centration were determined by automatically tracking the position of the associated pronuclei using a MatLab script computing the average absolute movement of centrosomes every 5 seconds for 10 frames following pronuclear meeting. The average angular displacement during centration/rotation was calculated using ImageJ, with the X and Y coordinates of the two centrosomes computed every 5 seconds for 10 frames after pronuclear meeting. The temperature control device used for imaging *nmy-2(ne3409)* embryos was described previously (Nguyen-Ngoc et al., 2007).

Spindle severing experiments were performed essentially as described (Afshar et al., 2004) using a Leica LMD microscope equipped with a pulsed N2 laser (λ=337nm). Astral microtubules were severed during centration/rotation either anterior or posterior from the centrosome/pronuclear complex, whereas the spindle was severed at the onset of anaphase. Tracking of the MTOCs and calculation of peak velocities was performed as described (Grill et al., 2001) using the MatLab code mentioned above.

For drug treatment, the Leica LMD microscope was used to pierce a hole in the eggshell of pseudocleavage stage embryos bathed in Jasplakinolide (Lifetechnologies) or Latrunculin A (MerckMillipore), both resuspended in 0.5% DMSO. Embryos were then imaged every 5 seconds until the end of the first cell cycle.

Imaging of NMY-2-GFP and GFP::MOE was performed using an inverted Zeiss Axiovert 200 microscope with a 60x 1.4 NA lens, acquiring cortical images with a *COOLSNAP HQ B/W* camera every 500 ms using 250 ms excitation with a 488nm Solid State Laser. Transmission light was used every minute to unambiguously identify the embryo stage. We used ImageJ to manually mark cortical foci and determine their size, applying an empirical threshold to distinguish between two foci; 8-10 foci were analyzed per embryo.

For Cortical Laser Ablation experiments (COLA) (Mayer et al., 2010), we used an inverted Zeiss Axiovert 200 microscope equipped with a 355nm pulsed UV laser for ablation. Images were acquired with a frame rate of 500 ms using 250 ms excitation time with a 488nm Argon laser. The ~10 μm ablation was performed on the anterior cortex along the longitudinal axis either at pronuclear formation (GFP-NMY-2 embryos) or at the onset of centration/rotation (GFP::MOE embryos). Only those embryos in which the cut sealed and that divided normally were analyzed. We used ImageJ to manually track the foci over 15 frames (3 prior to the cut and 11 afterwards) and calculate their velocity (tracking 5-10 foci or 2-3 foci per embryo for GFP-NMY-2 and GFP::MOE, respectively). The mean velocity per embryo was averaged and plotted over time. Statistical analysis was performed on the velocities measured 500 ms after the cut. The values reported here for control embryos during pronuclear migration are larger than in the literature (Mayer et al., 2010), most likely because in the previous work imaging began only 5 seconds after the cut, as compared to 500 ms here.

Dual time-lapse DIC and fluorescence imaging was performed on a Zeiss Axioplan 2 as described (Bellanger and Gonczy 2003). The motorized filter wheel, two external shutters, and the 1,392 x 1,040 pixels 12-bit Photometrics CoolSNAP ES2 were controlled by μManager. Images were acquired with an exposure time of 10-100ms for the DIC and 300 ms for the fluorescence channel using the Zeiss Filter Set 10 (GFP). The embryos were allowed to develop under the coverslip without imaging and snapshots taken at the indicating times.

Digoxigenin *in situ* hybridization and single molecular FISH

Digoxigenin-labeled single stranded DNA probes were prepared using the PCR DIG Probe Synthesis Kit (Roche) following the manufacturer’s instructions. Briefly, the plasmid carrying the gene of interest served as template in a PCR-based reaction and a reverse primer binding to the 3’UTR was added together with the DIG-11-dUTP containing dNTP mix. The resulting PCR product was ethanol-precipitated and resuspended in hybridization buffer (50% deionized formamide, 5x SSC, 100 µg/ml sonicated salmon testis DNA, 100 µg/ml yeast tRNA, 100 µg/ml heparin, 0.1% Tween-20) at a concentration of 50 ng/µl, boiled at 95°C for 75 minutes to reduce its size (Seydoux and Fire, 1995) and stored at -20°C.

The *in situ* hybridization protocol we developed is a combination of two previously available procedures (Motohashi et al., 2006; Seydoux and Fire, 1995).

Gravid hermaphrodites were bleached and the resulting embryos placed on a poly-L-lysin coated slide in a total volume of 7µl. Then a coverslip was gently deposited on the embryos, and the freeze-crack method was used to remove their eggshell. The slides were then submerged into 150 ml -20°C methanol and thereafter into sequential mixtures of methanol and Hepes-PBS-formaldehyde solutions at 4°C (1x PBS, 75mM Hepes pH=6.9, 0.03% EGTA, 1.5 mM $MgSO_4$, 1.6% formaldehyde; ratios of water:methanol:Hepes-PBS-formaldehyde being first 50:15:35, then 50:25:25 and finally 50:35:15), for 2 minutes each, before fixation in 3.6% formaldehyde in Hepes-PBS-formaldehyde for 20 minutes at 4°C. Proteinase K (5.6 µg/ml) digestion was then performed for 10 minutes at 24°C and then stopped by submerging the slides into 2 g/l glycine dissolved in PBS for 2 min followed by 2 washes in PBS-Tween (0.1%) (PBS-T) for 2 minutes each. The slides were then re-fixed in Hepes-PBS-formaldehyde for 50 minutes at room temperature, washed twice with PBS-T for 5 minutes each, treated with 2 mg/ml glycine for 5 minutes and washed again once with PBS-T. Slides were then submerged into Formamide-SSC solution (50% formamide-5xSSC-100 µg/ml heparin, 0.1% Tween-20), mixed with PBS-T in a 1:1 ratio for 10 minutes and thereafter in Formamide-SSC for an other 10 minutes. Pre-hybridization was carried out in 50 µl hybridization buffer (50% deionized formamide 50%, 5xSSC (pH=7), 100 µg/ml sonicated salmon testis DNA, 100 µg/ml yeast tRNA, 100 µg/ml, heparin 0.1% Tween 20) for 1 hour at 48°C, after which the probe was applied at a concentration of 40 ng/µl in 50 µl overnight, again at 48°C. To prevent evaporation, parafilm squares glued with rubber cement were mounted on the slides. The probe was washed off twice with Formamide-SSC:PBS-T (1:1) for 10 minutes and then 4 times using 0.1% Chaps in 0.8x PBS at 48°C for 20 minutes each, after which a blocking step was included using 0.1%BSA - 0.1%Triton-X PBS for 1.5 hours at room temperature. The alkaline-phosphatase (AP)-conjugated anti-DIG antibody (Roche) was diluted in 1:2000 in 1x PBS and incubated at 4°C overnight. The slides were washed 5 times with 0.1%BSA - 0.1%Triton-X in PBS and twice with staining buffer (100 mM Tris-HCl pH=9.5), 100mM NaCl, 5mM $MgCl_2$, 1mM Levamisol, 0.1% Tween-20); the signal was developed using a mixture of 333 µg/ml NBT (Roche) and 70 µg/ml BCIP (AppliChem) for 20-60 minutes at room temperature. The slides were then washed, stained with 1mg/ml Hoechst 33258 (Sigma), mounted and stored at 4°C. All *in situ* hybridization experiments were performed at least twice and representative embryos are shown in the figure panels. Moreover, control embryos were included on one side of the slide in each instance.

The fluorescent probes for single molecule FISH were designed and synthesized by Biosearch Technologies. The technique was executed mostly as advised on the vendor's website (http://www.biosearchtech.com/assets/bti_custom_stellaris_celegans_protocol.pdf) with one exception: embryos were treated as for the conventional *in situ* method (i.e. using bleaching and freeze-cracking). The diluted probes (40 nM for *lin-5* and 250 nM for *gfp*) were incubated overnight (at 30°C for *lin-5* and at 37°C for *gfp*). 1mg/ml Hoechst 33258 (Sigma) was used to counterstain the DNA. To visualize single molecules, we used the wide-field setup of a Zeiss LSM700 microscope. To quantify the enrichment around centrosomes, optical slices in Z were captured with the LSM700 confocal microscope and Z-projections performed. Thereafter, using ImageJ, a circle within the centrosome was drawn and the average pixel intensity measured in that region of interest. The average pixel intensities were also measured in the cytoplasm and the two values expressed as a ratio. The background intensity was negligible.

Quantification of relative *era-1* mRNA enrichment was performed by measuring 1.) mean intensities in the cytoplasm of AB and P_1, 2.) of the background, and 3.) in later stage embryos where the hybridization did not give any signal, but considerable amount of intensity arises from the yolk granules ('empty' embryos). Then the multiplicative inverse of the values was taken and after subtraction of the background, the values were expressed as ratio to the intensities of the 'empty' embryos.

RT-qPCR

To measure mRNA levels by qRT-PCR, embryos were bleached and total mRNA isolated using the trizol-chloroform extraction method (Portman, 2006). 250 µg of total RNA was then reverse transcribed using poly-dT primers. Specific primer pairs were used to amplify the cDNA with the Power SYBR Green PCR mix (Applied Biosystems). The PCR reaction was performed in the 7900HT Fast Real-Time PCR System machine (Applied Biosystems) with the SDS2.4 software using 60°C for annealing and 72°C for elongation. The $\Delta\Delta C_T$ method was used to quantify mRNA levels relative to the reference gene, *act-1*. The primer sequences were as follow:

act-1 F - AGTCCGCCGGAATCCACGAG

act-1 R - CTTGATCTTCATGGTTGATG

lin-5 F - TTCCTCGCCGATAATGGACC

lin-5 R - TTCCTCGCCGATAATGGACC

lin-5[rec] F - CCGCGAAAGCATCTGTAGCC

lin-5[rec] R – AATGGCTGTTTAAATTCGCCG

yfp F - GGGAACTACAAGACACGTGC

yfp R - GTGTCCAAGAATGTTTCC

Antibodies, western blotting and indirect immunofluorescence

SDS-PAGE and western blot analyses were performed according to standard protocols. Antibodies against GFP (Roche, mouse, 1/500), CAR-1 (gift from Karen Oegama and Jon Audhya (Audhya et al., 2005) rabbit, 1/1000), LIN-5 (1/1000, Nguyen-Ngoc, 2008) and α-tubulin (DM1A, Sigma, mouse, 1/2000) were used as primary antibodies. HRP-conjugated goat anti-rabbit and anti-mouse secondary antibodies (Promega) were used at 1/5000 and the signal detected using standard chemiluminescence (Roche).

For immunostaining, embryos were fixed in methanol at -20°C for one hour (except for 15 minutes in the case of GPR-1/2) followed by overnight incubation at 4°C with primary antibodies. Primary mouse antibodies against α-tubulin (1/300; DM1A, Sigma), GFP (1/100; MAB3580, Millipore) were used together with rabbit antibodies against GPA-16 (1/200, Afhsar et al., 2004), GPB-1 (1/200; Thyagarajan et al., 2011), GPR-1/2 (1/100, Afshar et al., 2010) LIN-5 (1/300; Nguyen-Ngoc et al., 2007), DHC-1 (1/100; Kotak et al., 2012), PGL-1 (1/300, Kawasaki et al., 1998) or TAC-1 (1/500, Bellanger and Gonczy, 2003). Secondary antibodies were Alexa488-conjugated goat anti-mouse (1/500; Molecular Probes) and Cy3-conjugated goat anti-rabbit (1/1000; Dianova). Slides were counterstained with 1mg/ml Hoechst 33258 (Sigma) to visualize DNA. Images were acquired on an LSM700 confocal microscope (Zeiss) and processed in ImageJ and Adobe Photoshop, maintaining relative image intensities within a series.

Fluorescence Recovery After Complete Photobleaching (FRAcP) and Fluorescence Loss in Photobleaching (FLIP)

Embryos expressing GFP-LIN-5 were analyzed using a Zeiss LSM700 confocal microscope. For FRAcP, we started photobleaching at the time of pronuclear migration, using the 40X objective and activating the 488 nm laser at 100% laser power with an open pinhole. Bleaching was carried out for 60 sec in the middle plane of the embryo, followed by 45 seconds each in the upper and lower halves of the embryo. This resulted in embryos at the stage of nuclear envelope breakdown with a ~95% reduction in fluorescence throughout the whole cell. After 1 minute of recovery without recording, the embryos were imaged with the 40X objective every 3 seconds with an open pinhole until mitosis was completed. Fluorescence intensities were determined using ImageJ by measuring average intensities in every frame (3 seconds) by drawing a circle around the anterior centrosome and a polygon in the anterior cytoplasm, between the cortex and the black region just outside the centrosome.

FLIP experiments were performed with the same microscope using the same laser settings. Photobleaching was conducted in a 7x7 μm^2 region of the anterior cytoplasm for one minute starting at the onset of posterior spindle displacement. The anterior cytoplasm and centrosome were analyzed in this experiment to avoid the posterior centrosome reaching the bleached region during anaphase spindle elongation. Fluorescence intensities of the cytoplasm and of the centrosome were measured before and after the bleach (i.e. at metaphase and late anaphase/telophase) and expressed as a ratio. Unbleached embryos served as control.

Morpholino treatment

The following morpholino oligonucleotides (MO, Gene Tools) were used:
Control MO - CCTCTTACCTCAGTTACAATTTATA
lin-5 MO – ACAACTGATGTGCTCACGCTCATTC

The morpholinos were dissolved in water and diluted in M9 just prior to the experiment at a working concentration of 100µM. Gonad injection was performed with a Zeiss Axiovert S100 microscope equipped with an Eppendorf Transjector 5246 and the embryos analyzed after an incubation time of 7-9 hours. We found a clear meiotic phenotype in 13/24 early embryos (1-8 cell stage) upon injection of freshly dissolved MOs from two different batches obtained from the vendor. We speculate that the reason for such incomplete penetrance may be due to the injection not always being successful and/or the incubation period after injection being insufficient. We noted also that the efficiency of the MOs decreased after the stock solution was stored at room temperature for 45 days, with only 1/10 embryos exhibiting meiotic defects following injection in that case. The results of these experiments are summarized in Table 1.

Morpholino stock	**A**	**B**	**B'**	**C**
Strong meiotic defect after injection	ND	5(10)	1 (10)	8(14)
Decreased posterior spindle pole oscillation in P_0 after eggshell piercing	5(5)	ND	3(15)	ND
Decreased posterior pulling forces in P_0 after eggshell piercing	yes (10)	ND	ND	yes (5)

Table 1. Efficiency of different MO stocks tested by injection and eggshell piercing.
A, B and C indicate three separately synthesized MO stocks. The experiments in the case of stocks A, B and C were performed within two weeks of dissolving the MO, B' is stock B stored for 45 days at room temperature.

To subject one-cell embryos to MOs, the MOs were mixed with 2% P_0 Lipofectamine 2000 (LF, Life Technologies) and the reaction mix incubated at room temperature for 20 minutes to allow liposomes to form. The embryos were placed in M9 containing the LF-MO mix and the eggshell was pierced at pseudocleavage with the pulsed laser of the LMD microscope.

Statistical analysis

All statistical analysis was performed using unpaired Student's t-test in Excel. An F-test was run on the samples beforehand to decide if Type2 (in case F test < 0.05) or Type3 (in case F test > 0.05) unpaired t-test should be applied. *: $p<0.05$, **: $p<0.01$.

The error bars in the graphs show the standard error of the mean.

7. ACKNOWLEDGMENTS

First of all, I would like to express how thankful I am to my supervisor, Pierre. He has been giving me huge amount of support during these years, both professionally and personally. I am truly happy that I got the opportunity to work with him and to learn from him. He doubted when I was too positive and encouraged when I become too negative, thereby creating permanent motivation in me. He is an outstanding group leader and a very reasonable boss (how come he was fine with my obsessed globetrotter phenotype during these 4 years!?). My future bosses will be in a hard situation: the threshold Pierre set up is very high. Köszönöm, Pierre!

Pierre's spirit spreads in his lab and gets incorporated in the lab members. The Gönczy lab is an excellent place to work in, where people are helpful, they think with you, they give you advice and they really care about you. This is very apparent during the super interactive lab meetings – one receives great ideas for half a year that are, if things go well, are tested for the next lab meeting. Here I am thanking all of them with whom I had the chance to work. Aitana, thanks for the MatLab codes and for the great concert in Cully! Alessandro, great collaboration in the clathrin project, and tons of fun CPs, obviously. Alex, you always get the point and have awesome ideas and thanks for the comments on my carving skiing style! Benita, I will never forget: 'everyone is crazy in a way in this lab', it was very reassuring! Christian, frocius-amico-amore, you would deserve a whole chapter here; it's really nice I can be among those 10000 people you know! Coralie, I don't know if I am now more grateful for the injections or for the delicious cakes you prepared; but it doesn't matter, thanks a lot for both! Daiju, I really liked your biochemical ideas, it's a pity I couldn't explore them all! Debora, your Nespresso capsules saved me very often…! Fernando, you were right – at some point one gets calmed down; but I did what you asked me to do in the Satellite 4 years ago! Isabelle, we had nice time in the wineyards in Ollon, now I regret I didn't join you guys more often! Kalyani, your never-fading smile and joyful mood gave me lots of energy! And obviously, thanks for the collaboration in the clathrin story! Katy, you gave me tons of nice ideas and thanks for showing me the non-obvious parts of the LMD system. Lukas, good luck with your money making, and don't forget to call me if you are looking for someone to give a share! Melina, I was happy to work with you and to show you some techniques – good luck

with your PhD! Meritxell, I really enjoyed the Xmas party in 2012 with the hot ABBA girl, and the ‘how to put on a baby sling’ session. Nicola, your minivan was so great that brought us to Verbier, I hope to do some stuff together again! Paul, good luck for the new adventures (I am not talking about science now…). Sachin, thanks for spotting the *lin-5* mRNA localization and for being hungry any time for scientific discussions. I learned a lot from you! Simon, even though I had to do the laundry very often, we had some great parties together. All the best with the kiwis! Veronika, I am amazed that you can bike so much after work... Slavic spirit, no question! Virginie, thanks for being a great neighbour and for the useful comments on the papers. Zhou, thanks for all the weird chinese sweets and I am hoping that you will find fun in your new life. Yemima, many thanks for opening the doors for me leading to the exciting realm of *C. elegans* embryology.

Furthermore, I am very thankful to the BiOP team for huge amount of help in various microscopy-related questions, I am especially grateful to Olivier. Nicole and Tatiana did great jobs in stearing me through the administrative mazes (that are, now I realize, nothing compared to the ones in Singapore…). Special thanks goes for my committee members, who agreed on allocating time for reading this thesis work and provided me useful comments on the projects: Anne Ephrussi, Joachim Lingner, Daniel Constam and Helge Grosshans.

I am extremely grateful for the support I received from my family. My mom always was/is/will be a strong pillar in my life, her presence, understanding, caring, curiosity, love helped me during these years. Unfortunately, my grandma, to whom this thesis work is dedicated can not be here with us any more. I will never forget the moment when I was explaining her the processes of asymmetric cell division in *C. elegans* for a couple of hours drawing on sheets of papers. I am also thankful for the support and realistic criticism from my dad and for the enthusiasm of my sister. My sibling-cousins, Ádám, Eszter, Farkas and László and my uncle and aunt, Misi and Kinga, also contributed to create a stable basis of my life. I am immensely grateful for my girlfriend, Kalina, whose amazing personality and beautiful smile motivated and armored me a lot. I can thank a lot to my friends too. They might not even think, but they gave me a such personal energy that was necessary for completing my PhD. I am thankful to those who I had met before my arrival to Lausanne (impressive that almost all came to visit me): Hoki, Urbi, Era, Flóra, Peták, Dalma, Jals, Csöri, Norbi,

Halmos, Julian, Djoni, Matyi, Évi, Lőrinc, Kirschi, Áron, Szacsi, Tomi, Niki, Feri, Luca, Oszi, Marci, Gergő, Judit, Dani, Máté, Kinguc. And to those, who I met here: Vigorino, Lisalina, Tanjita, Livio, Rosy, Ilu, Fabri, Marco, Edu, Makuka úr, Szabesz, Gézu, Laci, Juan. Besides, numerous people had great influence on my life during these years, and I am grateful for all them for having made my life in Lausanne truly memorable.

8. REFERENCES

- Aceto, D., Beers, M., and Kemphues, K.J. (2006). Interaction of PAR-6 with CDC-42 is required for maintenance but not establishment of PAR asymmetry in C. elegans. Dev Biol *299*, 386-397.
- Afshar, K., Werner, M.E., Tse, Y.C., Glotzer, M., and Gönczy, P. (2010). Regulation of cortical contractility and spindle positioning by the protein phosphatase 6 PPH-6 in one-cell stage C. elegans embryos. Development *137*, 237-247.
- Afshar, K., Willard, F.S., Colombo, K., Johnston, C.A., McCudden, C.R., Siderovski, D.P., and Gönczy, P. (2004). RIC-8 is required for GPR-1/2-dependent Galpha function during asymmetric division of C. elegans embryos. Cell *119*, 219-230.
- Afshar, K., Willard, F.S., Colombo, K., Siderovski, D.P., and Gonczy, P. (2005). Cortical localization of the Galpha protein GPA-16 requires RIC-8 function during C. elegans asymmetric cell division. Development *132*, 4449-4459.
- Aist, J.R., and Berns, M.W. (1981). Mechanics of chromosome separation during mitosis in Fusarium (Fungi imperfecti): new evidence from ultrastructural and laser microbeam experiments. J Cell Biol *91*, 446-458.
- Aist, J.R., Liang, H., and Berns, M.W. (1993). Astral and spindle forces in PtK2 cells during anaphase B: a laser microbeam study. J Cell Sci *104 (Pt 4)*, 1207-1216.
- Aizer, A., Brody, Y., Ler, L.W., Sonenberg, N., Singer, R.H., and Shav-Tal, Y. (2008). The dynamics of mammalian P body transport, assembly, and disassembly in vivo. Mol Biol Cell *19*, 4154-4166.
- Albertson, D.G. (1984). Formation of the first cleavage spindle in nematode embryos. Dev Biol *101*, 61-72.
- Alberts, B., Johnson, A., Lewis, J., Raff, M., Roberts, K. and Walter, P. (2002). Molecular Biology of the Cell. 4th Edition. New York, Garland Science.
- Allard, J., and Mogilner, A. (2013). Traveling waves in actin dynamics and cell motility. Curr Opin Cell Biol *25*, 107-115.
- Alliegro, M.C., and Alliegro, M.A. (2008). Centrosomal RNA correlates with intron-poor nuclear genes in Spisula oocytes. Proc Natl Acad Sci U S A *105*, 6993-6997.
- Alliegro, M.C., Alliegro, M.A., and Palazzo, R.E. (2006). Centrosome-associated RNA in surf clam oocytes. Proc Natl Acad Sci U S A *103*, 9034-9038.
- Amiri, A., Keiper, B.D., Kawasaki, I., Fan, Y., Kohara, Y., Rhoads, R.E., and Strome, S. (2001). An isoform of eIF4E is a component of germ granules and is required for spermatogenesis in C. elegans. Development *128*, 3899-3912.
- Andreassi, C., and Riccio, A. (2009). To localize or not to localize: mRNA fate is in 3'UTR ends. Trends Cell Biol *19*, 465-474.
- Andrews, R., and Ahringer, J. (2007). Asymmetry of early endosome distribution in C. elegans embryos. PLoS One *2*, e493.
- Aronov, S., Gelin-Licht, R., Zipor, G., Haim, L., Safran, E., and Gerst, J.E. (2007). mRNAs encoding polarity and exocytosis factors are cotransported with the cortical endoplasmic reticulum to the incipient bud in Saccharomyces cerevisiae. Mol Cell Biol *27*, 3441-3455.
- Audhya, A., Hyndman, F., McLeod, I.X., Maddox, A.S., Yates, J.R., 3rd, Desai, A., and Oegema, K. (2005). A complex containing the Sm protein CAR-1 and the RNA helicase CGH-1 is required for embryonic cytokinesis in Caenorhabditis elegans. J Cell Biol *171*, 267-279.
- Bailey, T.L., Boden, M., Buske, F.A., Frith, M., Grant, C.E., Clementi, L., Ren, J., Li, W.W., and Noble, W.S. (2009). MEME SUITE: tools for motif discovery and searching. Nucleic Acids Res *37*, W202-208.
- Balklava, Z., Pant, S., Fares, H., and Grant, B.D. (2007). Genome-wide analysis identifies a general requirement for polarity proteins in endocytic traffic. Nat Cell Biol *9*, 1066-1073.
- Barros, C.S., Phelps, C.B., and Brand, A.H. (2003). Drosophila nonmuscle myosin II promotes the asymmetric segregation of cell fate determinants by cortical exclusion rather than active transport. Dev Cell *5*, 829-840.
- Bastock, R., and St Johnston, D. (2008). Drosophila oogenesis. Curr Biol *18*, R1082-1087.
- Becalska, A.N., and Gavis, E.R. (2009). Lighting up mRNA localization in Drosophila oogenesis. Development *136*, 2493-2503.
- Becalska, A.N., Kim, Y.R., Belletier, N.G., Lerit, D.A., Sinsimer, K.S., and Gavis, E.R. (2011). Aubergine is a component of a nanos mRNA localization complex. Dev Biol *349*, 46-52.
- Beers, M., and Kemphues, K. (2006). Depletion of the co-chaperone CDC-37 reveals two modes of PAR-6 cortical association in C. elegans embryos. Development *133*, 3745-3754.

- Bellanger, J.M., and Gonczy, P. (2003). TAC-1 and ZYG-9 form a complex that promotes microtubule assembly in C. elegans embryos. Curr Biol *13*, 1488-1498.
- Bello, B., Reichert, H., and Hirth, F. (2006). The brain tumor gene negatively regulates neural progenitor cell proliferation in the larval central brain of Drosophila. Development *133*, 2639-2648.
- Berends, C.W., Munoz, J., Portegijs, V., Schmidt, R., Grigoriev, I., Boxem, M., Akhmanova, A., Heck, A.J., and van den Heuvel, S. (2013). F-actin asymmetry and the endoplasmic reticulum-associated TCC-1 protein contribute to stereotypic spindle movements in the Caenorhabditis elegans embryo. Mol Biol Cell *24*, 2201-2215.
- Bergsten, S.E., and Gavis, E.R. (1999). Role for mRNA localization in translational activation but not spatial restriction of nanos RNA. Development *126*, 659-669.
- Berleth, T., Burri, M., Thoma, G., Bopp, D., Richstein, S., Frigerio, G., Noll, M., and Nusslein-Volhard, C. (1988). The role of localization of bicoid RNA in organizing the anterior pattern of the Drosophila embryo. Embo J *7*, 1749-1756.
- Berns, M.W., Aist, J., Edwards, J., Strahs, K., Girton, J., McNeill, P., Rattner, J.B., Kitzes, M., Hammer-Wilson, M., Liaw, L.H.*, et al.* (1981). Laser microsurgery in cell and developmental biology. Science *213*, 505-513.
- Besse, F., and Ephrussi, A. (2008). Translational control of localized mRNAs: restricting protein synthesis in space and time. Nat Rev Mol Cell Biol *9*, 971-980.
- Besse, F., Lopez de Quinto, S., Marchand, V., Trucco, A., and Ephrussi, A. (2009). Drosophila PTB promotes formation of high-order RNP particles and represses oskar translation. Genes Dev *23*, 195-207.
- Betley, J.N., Heinrich, B., Vernos, I., Sardet, C., Prodon, F., and Deshler, J.O. (2004). Kinesin II mediates Vg1 mRNA transport in Xenopus oocytes. Curr Biol *14*, 219-224.
- Betschinger, J., Eisenhaber, F., and Knoblich, J.A. (2005). Phosphorylation-induced autoinhibition regulates the cytoskeletal protein Lethal (2) giant larvae. Curr Biol *15*, 276-282.
- Betschinger, J., Mechtler, K., and Knoblich, J.A. (2006). Asymmetric segregation of the tumor suppressor brat regulates self-renewal in Drosophila neural stem cells. Cell *124*, 1241-1253.
- Bienkowska, D., and Cowan, C.R. (2012). Centrosomes can initiate a polarity axis from any position within one-cell C. elegans embryos. Curr Biol *22*, 583-589.
- Black, J.A., and Waxman, S.G. (2013). Noncanonical roles of voltage-gated sodium channels. Neuron *80*, 280-291.
- Blanchoin, L., Boujemaa-Paterski, R., Sykes, C., and Plastino, J. (2014). Actin dynamics, architecture, and mechanics in cell motility. Physiol Rev *94*, 235-263.
- Blower, M.D., Feric, E., Weis, K., and Heald, R. (2007). Genome-wide analysis demonstrates conserved localization of messenger RNAs to mitotic microtubules. J Cell Biol *179*, 1365-1373.
- Boag, P.R., Nakamura, A., and Blackwell, T.K. (2005). A conserved RNA-protein complex component involved in physiological germline apoptosis regulation in C. elegans. Development *132*, 4975-4986.
- Boettner, D.R., Friesen, H., Andrews, B., and Lemmon, S.K. (2011). Clathrin light chain directs endocytosis by influencing the binding of the yeast Hip1R homologue, Sla2, to F-actin. Mol Biol Cell *22*, 3699-3714.
- Bohl, F., Kruse, C., Frank, A., Ferring, D., and Jansen, R.P. (2000). She2p, a novel RNA-binding protein tethers ASH1 mRNA to the Myo4p myosin motor via She3p. Embo J *19*, 5514-5524.
- Bond, J., Roberts, E., Mochida, G.H., Hampshire, D.J., Scott, S., Askham, J.M., Springell, K., Mahadevan, M., Crow, Y.J., Markham, A.F.*, et al.* (2002). ASPM is a major determinant of cerebral cortical size. Nat Genet *32*, 316-320.
- Bonifacino, J.S., and Rojas, R. (2006). Retrograde transport from endosomes to the trans-Golgi network. Nat Rev Mol Cell Biol *7*, 568-579.
- Bossing, T., Udolph, G., Doe, C.Q., and Technau, G.M. (1996). The embryonic central nervous system lineages of Drosophila melanogaster. I. Neuroblast lineages derived from the ventral half of the neuroectoderm. Dev Biol *179*, 41-64.
- Bowerman, B., Tax, F.E., Thomas, J.H., and Priess, J.R. (1992). Cell interactions involved in development of the bilaterally symmetrical intestinal valve cells during embryogenesis in Caenorhabditis elegans. Development *116*, 1113-1122.
- Bowman, S.K., Neumuller, R.A., Novatchkova, M., Du, Q., and Knoblich, J.A. (2006). The Drosophila NuMA Homolog Mud regulates spindle orientation in asymmetric cell division. Dev Cell *10*, 731-742.
- Boyd, L., Guo, S., Levitan, D., Stinchcomb, D.T., and Kemphues, K.J. (1996). PAR-2 is asymmetrically distributed and promotes association of P granules and PAR-1 with the cortex in C. elegans embryos. Development *122*, 3075-3084.

- Braat, A.K., Yan, N., Arn, E., Harrison, D., and Macdonald, P.M. (2004). Localization-dependent oskar protein accumulation; control after the initiation of translation. Dev Cell *7*, 125-131.
- Brendza, R.P., Serbus, L.R., Duffy, J.B., and Saxton, W.M. (2000). A function for kinesin I in the posterior transport of oskar mRNA and Staufen protein. Science *289*, 2120-2122.
- Broadus, J., Fuerstenberg, S., and Doe, C.Q. (1998). Staufen-dependent localization of prospero mRNA contributes to neuroblast daughter-cell fate. Nature *391*, 792-795.
- Brodsky, F.M., Chen, C.Y., Knuehl, C., Towler, M.C., and Wakeham, D.E. (2001). Biological basket weaving: formation and function of clathrin-coated vesicles. Annu Rev Cell Dev Biol *17*, 517-568.
- Bubb, M.R., Senderowicz, A.M., Sausville, E.A., Duncan, K.L., and Korn, E.D. (1994). Jasplakinolide, a cytotoxic natural product, induces actin polymerization and competitively inhibits the binding of phalloidin to F-actin. J Biol Chem *269*, 14869-14871.
- Bultje, R.S., Castaneda-Castellanos, D.R., Jan, L.Y., Jan, Y.N., Kriegstein, A.R., and Shi, S.H. (2009). Mammalian Par3 regulates progenitor cell asymmetric division via notch signaling in the developing neocortex. Neuron *63*, 189-202.
- Cabernard, C., and Doe, C.Q. (2009). Apical/basal spindle orientation is required for neuroblast homeostasis and neuronal differentiation in Drosophila. Dev Cell *17*, 134-141.
- Calabia-Linares, C., Robles-Valero, J., de la Fuente, H., Perez-Martinez, M., Martin-Cofreces, N., Alfonso-Perez, M., Gutierrez-Vazquez, C., Mittelbrunn, M., Ibiza, S., Urbano-Olmos, F.R.*, et al.* (2011). Endosomal clathrin drives actin accumulation at the immunological synapse. J Cell Sci *124*, 820-830.
- Campos-Ortega, J.A. (1993). Mechanisms of early neurogenesis in Drosophila melanogaster. J Neurobiol *24*, 1305-1327.
- Cha, B.J., Koppetsch, B.S., and Theurkauf, W.E. (2001). In vivo analysis of Drosophila bicoid mRNA localization reveals a novel microtubule-dependent axis specification pathway. Cell *106*, 35-46.
- Chan, X.Y., and Lambert, J.D. (2011). Patterning a spiralian embryo: a segregated RNA for a Tis11 ortholog is required in the 3a and 3b cells of the Ilyanassa embryo. Dev Biol *349*, 102-112.
- Chartrand, P., Meng, X.H., Singer, R.H., and Long, R.M. (1999). Structural elements required for the localization of ASH1 mRNA and of a green fluorescent protein reporter particle in vivo. Curr Biol *9*, 333-336.
- Cheeks, R.J., Canman, J.C., Gabriel, W.N., Meyer, N., Strome, S., and Goldstein, B. (2004). C. elegans PAR proteins function by mobilizing and stabilizing asymmetrically localized protein complexes. Curr Biol *14*, 851-862.
- Chenn, A., and McConnell, S.K. (1995). Cleavage orientation and the asymmetric inheritance of Notch1 immunoreactivity in mammalian neurogenesis. Cell *82*, 631-641.
- Cho, P.F., Poulin, F., Cho-Park, Y.A., Cho-Park, I.B., Chicoine, J.D., Lasko, P., and Sonenberg, N. (2005). A new paradigm for translational control: inhibition via 5'-3' mRNA tethering by Bicoid and the eIF4E cognate 4EHP. Cell *121*, 411-423.
- Choksi, S.P., Southall, T.D., Bossing, T., Edoff, K., de Wit, E., Fischer, B.E., van Steensel, B., Micklem, G., and Brand, A.H. (2006). Prospero acts as a binary switch between self-renewal and differentiation in Drosophila neural stem cells. Dev Cell *11*, 775-789.
- Clark, A., Meignin, C., and Davis, I. (2007). A Dynein-dependent shortcut rapidly delivers axis determination transcripts into the Drosophila oocyte. Development *134*, 1955-1965.
- Clark-Maguire, S., and Mains, P.E. (1994a). Localization of the mei-1 gene product of Caenorhaditis elegans, a meiotic-specific spindle component. J Cell Biol *126*, 199-209.
- Clark-Maguire, S., and Mains, P.E. (1994b). mei-1, a gene required for meiotic spindle formation in Caenorhabditis elegans, is a member of a family of ATPases. Genetics *136*, 533-546.
- Cockell, M.M., Baumer, K., and Gönczy, P. (2004). lis-1 is required for dynein-dependent cell division processes in C. elegans embryos. J Cell Sci *117*, 4571-4582.
- Colombo, K., Grill, S.W., Kimple, R.J., Willard, F.S., Siderovski, D.P., and Gönczy, P. (2003). Translation of polarity cues into asymmetric spindle positioning in Caenorhabditis elegans embryos. Science *300*, 1957-1961.
- Cook, H.A., Koppetsch, B.S., Wu, J., and Theurkauf, W.E. (2004). The Drosophila SDE3 homolog armitage is required for oskar mRNA silencing and embryonic axis specification. Cell *116*, 817-829.
- Couwenbergs, C., Labbe, J.C., Goulding, M., Marty, T., Bowerman, B., and Gotta, M. (2007). Heterotrimeric G protein signaling functions with dynein to promote spindle positioning in C. elegans. J Cell Biol *179*, 15-22.

- Cowan, C.R., and Hyman, A.A. (2004a). Asymmetric cell division in C. elegans: cortical polarity and spindle positioning. Annu Rev Cell Dev Biol *20*, 427-453.
- Cowan, C.R., and Hyman, A.A. (2004b). Centrosomes direct cell polarity independently of microtubule assembly in C. elegans embryos. Nature *431*, 92-96.
- Cowan, C.R., and Hyman, A.A. (2006). Cyclin E-Cdk2 temporally regulates centrosome assembly and establishment of polarity in Caenorhabditis elegans embryos. Nat Cell Biol *8*, 1441-1447.
- Crucs, S., Chatterjee, S., and Gavis, E.R. (2000). Overlapping but distinct RNA elements control repression and activation of nanos translation. Mol Cell *5*, 457-467.
- Cuenca, A.A., Schetter, A., Aceto, D., Kemphues, K., and Seydoux, G. (2003). Polarization of the C. elegans zygote proceeds via distinct establishment and maintenance phases. Development *130*, 1255-1265.
- Dale, L., Matthews, G., and Colman, A. (1993). Secretion and mesoderm-inducing activity of the TGF-beta-related domain of Xenopus Vg1. Embo J *12*, 4471-4480.
- Daniels, B.R., Dobrowsky, T.M., Perkins, E.M., Sun, S.X., and Wirtz, D. (2010). MEX-5 enrichment in the C. elegans early embryo mediated by differential diffusion. Development *137*, 2579-2585.
- Delanoue, R., Herpers, B., Soetaert, J., Davis, I., and Rabouille, C. (2007). Drosophila Squid/hnRNP helps Dynein switch from a gurken mRNA transport motor to an ultrastructural static anchor in sponge bodies. Dev Cell *13*, 523-538.
- Deng, Y., Singer, R.H., and Gu, W. (2008). Translation of ASH1 mRNA is repressed by Puf6p-Fun12p/eIF5B interaction and released by CK2 phosphorylation. Genes Dev *22*, 1037-1050.
- DeRenzo, C., Reese, K.J., and Seydoux, G. (2003). Exclusion of germ plasm proteins from somatic lineages by cullin-dependent degradation. Nature *424*, 685-689.
- Deshler, J.O., Highett, M.I., and Schnapp, B.J. (1997). Localization of Xenopus Vg1 mRNA by Vera protein and the endoplasmic reticulum. Science *276*, 1128-1131.
- Doe, C.Q., Chu-LaGraff, Q., Wright, D.M., and Scott, M.P. (1991). The prospero gene specifies cell fates in the Drosophila central nervous system. Cell *65*, 451-464.
- Doherty, G.J., and McMahon, H.T. (2009). Mechanisms of endocytosis. Annu Rev Biochem *78*, 857-902.
- Driever, W., and Nusslein-Volhard, C. (1988). The bicoid protein determines position in the Drosophila embryo in a concentration-dependent manner. Cell *54*, 95-104.
- Du, Q., and Macara, I.G. (2004). Mammalian Pins is a conformational switch that links NuMA to heterotrimeric G proteins. Cell *119*, 503-516.
- Dubnau, J., and Struhl, G. (1996). RNA recognition and translational regulation by a homeodomain protein. Nature *379*, 694-699.
- Dumont, J.N. (1972). Oogenesis in Xenopus laevis (Daudin). I. Stages of oocyte development in laboratory maintained animals. J Morphol *136*, 153-179.
- Edgar, L.G., Carr, S., Wang, H., and Wood, W.B. (2001). Zygotic expression of the caudal homolog pal-1 is required for posterior patterning in Caenorhabditis elegans embryogenesis. Dev Biol *229*, 71-88.
- Eliscovich, C., Peset, I., Vernos, I., and Mendez, R. (2008). Spindle-localized CPE-mediated translation controls meiotic chromosome segregation. Nat Cell Biol *10*, 858-865.
- Ephrussi, A., Dickinson, L.K., and Lehmann, R. (1991). Oskar organizes the germ plasm and directs localization of the posterior determinant nanos. Cell *66*, 37-50.
- Ephrussi, A., and Lehmann, R. (1992). Induction of germ cell formation by oskar. Nature *358*, 387-392.
- Erben, V., Waldhuber, M., Langer, D., Fetka, I., Jansen, R.P., and Petritsch, C. (2008). Asymmetric localization of the adaptor protein Miranda in neuroblasts is achieved by diffusion and sequential interaction of Myosin II and VI. J Cell Sci *121*, 1403-1414.
- Estrada, P., Kim, J., Coleman, J., Walker, L., Dunn, B., Takizawa, P., Novick, P., and Ferro-Novick, S. (2003). Myo4p and She3p are required for cortical ER inheritance in Saccharomyces cerevisiae. J Cell Biol *163*, 1255-1266.
- Etemad-Moghadam, B., Guo, S., and Kemphues, K.J. (1995). Asymmetrically distributed PAR-3 protein contributes to cell polarity and spindle alignment in early C. elegans embryos. Cell *83*, 743-752.
- Evans, T.C., Crittenden, S.L., Kodoyianni, V., and Kimble, J. (1994). Translational control of maternal glp-1 mRNA establishes an asymmetry in the C. elegans embryo. Cell *77*, 183-194.
- Evans, T.C., and Hunter, C.P. (2005). Translational control of maternal RNAs. WormBook, 1-11.
- Feng, Y., and Walsh, C.A. (2004). Mitotic spindle regulation by Nde1 controls cerebral cortical size. Neuron *44*, 279-293.

- Ferrandon, D., Elphick, L., Nusslein-Volhard, C., and St Johnston, D. (1994). Staufen protein associates with the 3'UTR of bicoid mRNA to form particles that move in a microtubule-dependent manner. Cell *79*, 1221-1232.
- Fisk Green, R., Lorson, M., Walhout, A.J., Vidal, M., and van den Heuvel, S. (2004). Identification of critical domains and putative partners for the Caenorhabditis elegans spindle component LIN-5. Mol Genet Genomics *271*, 532-544.
- Foraker, A.B., Camus, S.M., Evans, T.M., Majeed, S.R., Chen, C.Y., Taner, S.B., Correa, I.R., Jr., Doxsey, S.J., and Brodsky, F.M. (2012). Clathrin promotes centrosome integrity in early mitosis through stabilization of centrosomal ch-TOG. J Cell Biol *198*, 591-605.
- Forrest, K.M., Clark, I.E., Jain, R.A., and Gavis, E.R. (2004). Temporal complexity within a translational control element in the nanos mRNA. Development *131*, 5849-5857.
- Forristall, C., Pondel, M., Chen, L., and King, M.L. (1995). Patterns of localization and cytoskeletal association of two vegetally localized RNAs, Vg1 and Xcat-2. Development *121*, 201-208.
- Fraser, A.G., Kamath, R.S., Zipperlen, P., Martinez-Campos, M., Sohrmann, M., and Ahringer, J. (2000). Functional genomic analysis of C. elegans chromosome I by systematic RNA interference. Nature *408*, 325-330.
- Frohnhofer, H.G., Lehmann, R., and Nusslein-Volhard, C. (1986). Manipulating the anteroposterior pattern of the Drosophila embryo. J Embryol Exp Morphol *97 Suppl*, 169-179.
- Fuchs, E., and Raghavan, S. (2002). Getting under the skin of epidermal morphogenesis. Nat Rev Genet *3*, 199-209.
- Fuerstenberg, S., Peng, C.Y., Alvarez-Ortiz, P., Hor, T., and Doe, C.Q. (1998). Identification of Miranda protein domains regulating asymmetric cortical localization, cargo binding, and cortical release. Mol Cell Neurosci *12*, 325-339.
- Fuse, N., Hisata, K., Katzen, A.L., and Matsuzaki, F. (2003). Heterotrimeric G proteins regulate daughter cell size asymmetry in Drosophila neuroblast divisions. Curr Biol *13*, 947-954.
- Galletta, B.J., and Cooper, J.A. (2009). Actin and endocytosis: mechanisms and phylogeny. Curr Opin Cell Biol *21*, 20-27.
- Galli, M., Munoz, J., Portegijs, V., Boxem, M., Grill, S.W., Heck, A.J., and van den Heuvel, S. (2011). aPKC phosphorylates NuMA-related LIN-5 to position the mitotic spindle during asymmetric division. Nat Cell Biol *13*, 1132-1138.
- Gallo, C.M., Wang, J.T., Motegi, F., and Seydoux, G. (2010). Cytoplasmic partitioning of P granule components is not required to specify the germline in C. elegans. Science *330*, 1685-1689.
- Gamberi, C., Peterson, D.S., He, L., and Gottlieb, E. (2002). An anterior function for the Drosophila posterior determinant Pumilio. Development *129*, 2699-2710.
- Gavis, E.R., and Lehmann, R. (1992). Localization of nanos RNA controls embryonic polarity. Cell *71*, 301-313.
- Glick, B.S., and Nakano, A. (2009). Membrane traffic within the Golgi apparatus. Annu Rev Cell Dev Biol *25*, 113-132.
- Gomes, J.E., Encalada, S.E., Swan, K.A., Shelton, C.A., Carter, J.C., and Bowerman, B. (2001). The maternal gene spn-4 encodes a predicted RRM protein required for mitotic spindle orientation and cell fate patterning in early C. elegans embryos. Development *128*, 4301-4314.
- Gönczy, P. (2008). Mechanisms of asymmetric cell division: flies and worms pave the way. Nat Rev Mol Cell Biol *9*, 355-366.
- Gonczy, P., Bellanger, J.M., Kirkham, M., Pozniakowski, A., Baumer, K., Phillips, J.B., and Hyman, A.A. (2001). zyg-8, a gene required for spindle positioning in C. elegans, encodes a doublecortin-related kinase that promotes microtubule assembly. Dev Cell *1*, 363-375.
- Gönczy, P., Echeverri, C., Oegema, K., Coulson, A., Jones, S.J., Copley, R.R., Duperon, J., Oegema, J., Brehm, M., Cassin, E., *et al.* (2000). Functional genomic analysis of cell division in C. elegans using RNAi of genes on chromosome III. Nature *408*, 331-336.
- Gönczy, P., and Rose, L.S. (2005). Asymmetric cell division and axis formation in the embryo. WormBook, 1-20.
- Gonczy, P., Schnabel, H., Kaletta, T., Amores, A.D., Hyman, T., and Schnabel, R. (1999). Dissection of cell division processes in the one cell stage Caenorhabditis elegans embryo by mutational analysis. J Cell Biol *144*, 927-946.
- Gönczy, P., Schnabel, H., Kaletta, T., Amores, A.D., Hyman, T., and Schnabel, R. (1999). Dissection of cell division processes in the one cell stage Caenorhabditis elegans embryo by mutational analysis. J Cell Biol *144*, 927-946.
- Gonzalez, I., Buonomo, S.B., Nasmyth, K., and von Ahsen, U. (1999). ASH1 mRNA localization in yeast involves multiple secondary structural elements and Ash1 protein translation. Curr Biol *9*, 337-340.

- Gotta, M., Abraham, M.C., and Ahringer, J. (2001). CDC-42 controls early cell polarity and spindle orientation in C. elegans. Curr Biol *11*, 482-488.
- Gotta, M., and Ahringer, J. (2001). Distinct roles for Galpha and Gbetagamma in regulating spindle position and orientation in Caenorhabditis elegans embryos. Nat Cell Biol *3*, 297-300.
- Gotta, M., Dong, Y., Peterson, Y.K., Lanier, S.M., and Ahringer, J. (2003). Asymmetrically distributed C. elegans homologs of AGS3/PINS control spindle position in the early embryo. Curr Biol *13*, 1029-1037.
- Goulding, M.B., Canman, J.C., Senning, E.N., Marcus, A.H., and Bowerman, B. (2007). Control of nuclear centration in the C. elegans zygote by receptor-independent Galpha signaling and myosin II. J Cell Biol *178*, 1177-1191.
- Grant, B., and Hirsh, D. (1999). Receptor-mediated endocytosis in the Caenorhabditis elegans oocyte. Mol Biol Cell *10*, 4311-4326.
- Grant, B.D., and Donaldson, J.G. (2009). Pathways and mechanisms of endocytic recycling. Nat Rev Mol Cell Biol *10*, 597-608.
- Greener, T., Grant, B., Zhang, Y., Wu, X., Greene, L.E., Hirsh, D., and Eisenberg, E. (2001). Caenorhabditis elegans auxilin: a J-domain protein essential for clathrin-mediated endocytosis in vivo. Nat Cell Biol *3*, 215-219.
- Griffin, E.E., Odde, D.J., and Seydoux, G. (2011). Regulation of the MEX-5 gradient by a spatially segregated kinase/phosphatase cycle. Cell *146*, 955-968.
- Grill, S.W., Gönczy, P., Stelzer, E.H., and Hyman, A.A. (2001). Polarity controls forces governing asymmetric spindle positioning in the Caenorhabditis elegans embryo. Nature *409*, 630-633.
- Grill, S.W., Howard, J., Schaffer, E., Stelzer, E.H., and Hyman, A.A. (2003). The distribution of active force generators controls mitotic spindle position. Science *301*, 518-521.
- Groisman, I., Huang, Y.S., Mendez, R., Cao, Q., Theurkauf, W., and Richter, J.D. (2000). CPEB, maskin, and cyclin B1 mRNA at the mitotic apparatus: implications for local translational control of cell division. Cell *103*, 435-447.
- Gu, W., Deng, Y., Zenklusen, D., and Singer, R.H. (2004). A new yeast PUF family protein, Puf6p, represses ASH1 mRNA translation and is required for its localization. Genes Dev *18*, 1452-1465.
- Guo, S., and Kemphues, K.J. (1995). par-1, a gene required for establishing polarity in C. elegans embryos, encodes a putative Ser/Thr kinase that is asymmetrically distributed. Cell *81*, 611-620.
- Guo, S., and Kemphues, K.J. (1996). A non-muscle myosin required for embryonic polarity in Caenorhabditis elegans. Nature *382*, 455-458.
- Hachet, O., and Ephrussi, A. (2001). Drosophila Y14 shuttles to the posterior of the oocyte and is required for oskar mRNA transport. Curr Biol *11*, 1666-1674.
- Hachet, O., and Ephrussi, A. (2004). Splicing of oskar RNA in the nucleus is coupled to its cytoplasmic localization. Nature *428*, 959-963.
- Hamill, D.R., Severson, A.F., Carter, J.C., and Bowerman, B. (2002). Centrosome maturation and mitotic spindle assembly in C. elegans require SPD-5, a protein with multiple coiled-coil domains. Dev Cell *3*, 673-684.
- Hao, Y., Boyd, L., and Seydoux, G. (2006). Stabilization of cell polarity by the C. elegans RING protein PAR-2. Dev Cell *10*, 199-208.
- Hashimshony, T., Wagner, F., Sher, N., and Yanai, I. (2012). CEL-Seq: single-cell RNA-Seq by multiplexed linear amplification. Cell Rep *2*, 666-673.
- Haydar, T.F., Ang, E., Jr., and Rakic, P. (2003). Mitotic spindle rotation and mode of cell division in the developing telencephalon. Proc Natl Acad Sci U S A *100*, 2890-2895.
- Heasman, J., Quarmby, J., and Wylie, C.C. (1984). The mitochondrial cloud of Xenopus oocytes: the source of germinal granule material. Dev Biol *105*, 458-469.
- Henry, J.J., Perry, K.J., Fukui, L., and Alvi, N. (2010). Differential localization of mRNAs during early development in the mollusc, Crepidula fornicata. Integr Comp Biol *50*, 720-733.
- Hernandez, G., Altmann, M., Sierra, J.M., Urlaub, H., Diez del Corral, R., Schwartz, P., and Rivera-Pomar, R. (2005). Functional analysis of seven genes encoding eight translation initiation factor 4E (eIF4E) isoforms in Drosophila. Mech Dev *122*, 529-543.
- Hess, H.A., Roper, J.C., Grill, S.W., and Koelle, M.R. (2004). RGS-7 completes a receptor-independent heterotrimeric G protein cycle to asymmetrically regulate mitotic spindle positioning in C. elegans. Cell *119*, 209-218.
- Hill, D.P., and Strome, S. (1988). An analysis of the role of microfilaments in the establishment and maintenance of asymmetry in Caenorhabditis elegans zygotes. Dev Biol *125*, 75-84.
- Hillier, L.W., Miller, R.D., Baird, S.E., Chinwalla, A., Fulton, L.A., Koboldt, D.C., and Waterston, R.H. (2007). Comparison of C. elegans and C. briggsae genome sequences reveals extensive conservation of chromosome organization and synteny. PLoS Biol *5*, e167.

- Hirata, J., Nakagoshi, H., Nabeshima, Y., and Matsuzaki, F. (1995). Asymmetric segregation of the homeodomain protein Prospero during Drosophila development. Nature *377*, 627-630.
- Hird, S.N., and White, J.G. (1993). Cortical and cytoplasmic flow polarity in early embryonic cells of Caenorhabditis elegans. J Cell Biol *121*, 1343-1355.
- Homem, C.C., and Knoblich, J.A. (2012). Drosophila neuroblasts: a model for stem cell biology. Development *139*, 4297-4310.
- Horb, M.E., and Thomsen, G.H. (1997). A vegetally localized T-box transcription factor in Xenopus eggs specifies mesoderm and endoderm and is essential for embryonic mesoderm formation. Development *124*, 1689-1698.
- Houston, D.W., Zhang, J., Maines, J.Z., Wasserman, S.A., and King, M.L. (1998). A Xenopus DAZ-like gene encodes an RNA component of germ plasm and is a functional homologue of Drosophila boule. Development *125*, 171-180.
- Hsu, V.W., and Prekeris, R. (2010). Transport at the recycling endosome. Curr Opin Cell Biol *22*, 528-534.
- Huang, N.N., Mootz, D.E., Walhout, A.J., Vidal, M., and Hunter, C.P. (2002). MEX-3 interacting proteins link cell polarity to asymmetric gene expression in Caenorhabditis elegans. Development *129*, 747-759.
- Humphries, A.C., Dodding, M.P., Barry, D.J., Collinson, L.M., Durkin, C.H., and Way, M. (2012). Clathrin potentiates vaccinia-induced actin polymerization to facilitate viral spread. Cell Host Microbe *12*, 346-359.
- Hung, T.J., and Kemphues, K.J. (1999). PAR-6 is a conserved PDZ domain-containing protein that colocalizes with PAR-3 in Caenorhabditis elegans embryos. Development *126*, 127-135.
- Hunter, C.P., and Kenyon, C. (1996). Spatial and temporal controls target pal-1 blastomere-specification activity to a single blastomere lineage in C. elegans embryos. Cell *87*, 217-226.
- Huttner, W.B., and Brand, M. (1997). Asymmetric division and polarity of neuroepithelial cells. Curr Opin Neurobiol *7*, 29-39.
- Hwang, S.Y., and Rose, L.S. (2010). Control of asymmetric cell division in early C. elegans embryogenesis: teaming-up translational repression and protein degradation. BMB Rep *43*, 69-78.
- Hyenne, V., Desrosiers, M., and Labbe, J.C. (2008). C. elegans Brat homologs regulate PAR protein-dependent polarity and asymmetric cell division. Dev Biol *321*, 368-378.
- Hyenne, V., Tremblay-Boudreault, T., Velmurugan, R., Grant, B.D., Loerke, D., and Labbe, J.C. (2012). RAB-5 controls the cortical organization and dynamics of PAR proteins to maintain C. elegans early embryonic polarity. PLoS One *7*, e35286.
- Igreja, C., and Izaurralde, E. (2011). CUP promotes deadenylation and inhibits decapping of mRNA targets. Genes Dev *25*, 1955-1967.
- Ikeshima-Kataoka, H., Skeath, J.B., Nabeshima, Y., Doe, C.Q., and Matsuzaki, F. (1997). Miranda directs Prospero to a daughter cell during Drosophila asymmetric divisions. Nature *390*, 625-629.
- Irie, K., Tadauchi, T., Takizawa, P.A., Vale, R.D., Matsumoto, K., and Herskowitz, I. (2002). The Khd1 protein, which has three KH RNA-binding motifs, is required for proper localization of ASH1 mRNA in yeast. Embo J *21*, 1158-1167.
- Irion, U., and St Johnston, D. (2007). bicoid RNA localization requires specific binding of an endosomal sorting complex. Nature *445*, 554-558.
- Ito, K., and Hotta, Y. (1992). Proliferation pattern of postembryonic neuroblasts in the brain of Drosophila melanogaster. Dev Biol *149*, 134-148.
- Izumi, Y., Ohta, N., Hisata, K., Raabe, T., and Matsuzaki, F. (2006). Drosophila Pins-binding protein Mud regulates spindle-polarity coupling and centrosome organization. Nat Cell Biol *8*, 586-593.
- Jadhav, S., Rana, M., and Subramaniam, K. (2008). Multiple maternal proteins coordinate to restrict the translation of C. elegans nanos-2 to primordial germ cells. Development *135*, 1803-1812.
- Jain, R.A., and Gavis, E.R. (2008). The Drosophila hnRNP M homolog Rumpelstiltskin regulates nanos mRNA localization. Development *135*, 973-982.
- Jakymiw, A., Lian, S., Eystathioy, T., Li, S., Satoh, M., Hamel, J.C., Fritzler, M.J., and Chan, E.K. (2005). Disruption of GW bodies impairs mammalian RNA interference. Nat Cell Biol *7*, 1267-1274.
- Jambor, H., Brunel, C., and Ephrussi, A. (2011). Dimerization of oskar 3' UTRs promotes hitchhiking for RNA localization in the Drosophila oocyte. Rna *17*, 2049-2057.
- Jaramillo, A.M., Weil, T.T., Goodhouse, J., Gavis, E.R., and Schupbach, T. (2008). The dynamics of fluorescently labeled endogenous gurken mRNA in Drosophila. J Cell Sci *121*, 887-894.

- Jenkins, N., Saam, J.R., and Mango, S.E. (2006). CYK-4/GAP provides a localized cue to initiate anteroposterior polarity upon fertilization. Science *313*, 1298-1301.
- Johannes, L., and Popoff, V. (2008). Tracing the retrograde route in protein trafficking. Cell *135*, 1175-1187.
- Johnston, C.A., Afshar, K., Snyder, J.T., Tall, G.G., Gonczy, P., Siderovski, D.P., and Willard, F.S. (2008). Structural determinants underlying the temperature-sensitive nature of a Galpha mutant in asymmetric cell division of Caenorhabditis elegans. J Biol Chem *283*, 21550-21558.
- Johnstone, O., and Lasko, P. (2004). Interaction with eIF5B is essential for Vasa function during development. Development *131*, 4167-4178.
- Kalifa, Y., Huang, T., Rosen, L.N., Chatterjee, S., and Gavis, E.R. (2006). Glorund, a Drosophila hnRNP F/H homolog, is an ovarian repressor of nanos translation. Dev Cell *10*, 291-301.
- Kaltschmidt, J.A., Davidson, C.M., Brown, N.H., and Brand, A.H. (2000). Rotation and asymmetry of the mitotic spindle direct asymmetric cell division in the developing central nervous system. Nat Cell Biol *2*, 7-12.
- Kawasaki, I., Amiri, A., Fan, Y., Meyer, N., Dunkelbarger, S., Motohashi, T., Karashima, T., Bossinger, O., and Strome, S. (2004). The PGL family proteins associate with germ granules and function redundantly in Caenorhabditis elegans germline development. Genetics *167*, 645-661.
- Kawasaki, I., Shim, Y.H., Kirchner, J., Kaminker, J., Wood, W.B., and Strome, S. (1998). PGL-1, a predicted RNA-binding component of germ granules, is essential for fertility in C. elegans. Cell *94*, 635-645.
- Kemphues, K.J., Priess, J.R., Morton, D.G., and Cheng, N.S. (1988). Identification of genes required for cytoplasmic localization in early C. elegans embryos. Cell *52*, 311-320.
- Kim-Ha, J., Kerr, K., and Macdonald, P.M. (1995). Translational regulation of oskar mRNA by bruno, an ovarian RNA-binding protein, is essential. Cell *81*, 403-412.
- Kim-Ha, J., Webster, P.J., Smith, J.L., and Macdonald, P.M. (1993). Multiple RNA regulatory elements mediate distinct steps in localization of oskar mRNA. Development *119*, 169-178.
- Kimura, A., and Onami, S. (2005). Computer simulations and image processing reveal length-dependent pulling force as the primary mechanism for C. elegans male pronuclear migration. Dev Cell *8*, 765-775.
- Kimura, K., and Kimura, A. (2011). Intracellular organelles mediate cytoplasmic pulling force for centrosome centration in the Caenorhabditis elegans early embryo. Proc Natl Acad Sci U S A *108*, 137-142.
- King, R.C. (1970). The meiotic behavior of the Drosophila oocyte. Int Rev Cytol *28*, 125-168.
- Kingsley, E.P., Chan, X.Y., Duan, Y., and Lambert, J.D. (2007). Widespread RNA segregation in a spiralian embryo. Evol Dev *9*, 527-539.
- Kirchhausen, T. (2000). Three ways to make a vesicle. Nat Rev Mol Cell Biol *1*, 187-198.
- Kiyomitsu, T., and Cheeseman, I.M. (2012). Chromosome- and spindle-pole-derived signals generate an intrinsic code for spindle position and orientation. Nat Cell Biol *14*, 311-317.
- Kloc, M., Bilinski, S., Dougherty, M.T., Brey, E.M., and Etkin, L.D. (2004). Formation, architecture and polarity of female germline cyst in Xenopus. Dev Biol *266*, 43-61.
- Kloc, M., Bilinski, S., Pui-Yee Chan, A., and Etkin, L.D. (2000). The targeting of Xcat2 mRNA to the germinal granules depends on a cis-acting germinal granule localization element within the 3'UTR. Dev Biol *217*, 221-229.
- Kloc, M., Dougherty, M.T., Bilinski, S., Chan, A.P., Brey, E., King, M.L., Patrick, C.W., Jr., and Etkin, L.D. (2002). Three-dimensional ultrastructural analysis of RNA distribution within germinal granules of Xenopus. Dev Biol *241*, 79-93.
- Kloc, M., and Etkin, L.D. (1995). Two distinct pathways for the localization of RNAs at the vegetal cortex in Xenopus oocytes. Development *121*, 287-297.
- Kloc, M., and Etkin, L.D. (1998). Apparent continuity between the messenger transport organizer and late RNA localization pathways during oogenesis in Xenopus. Mech Dev *73*, 95-106.
- Kloc, M., Larabell, C., and Etkin, L.D. (1996). Elaboration of the messenger transport organizer pathway for localization of RNA to the vegetal cortex of Xenopus oocytes. Dev Biol *180*, 119-130.
- Knoblich, J.A. (2008). Mechanisms of asymmetric stem cell division. Cell *132*, 583-597.
- Knoblich, J.A., Jan, L.Y., and Jan, Y.N. (1995). Asymmetric segregation of Numb and Prospero during cell division. Nature *377*, 624-627.
- Knoblich, J.A., Jan, L.Y., and Jan, Y.N. (1999). Deletion analysis of the Drosophila Inscuteable protein reveals domains for cortical localization and asymmetric localization. Curr Biol *9*, 155-158.
- Kollman, J. M., Merdes, A., Mourey, L. and Agard, D. A. (2011) 'Microtubule nucleation by gamma-tubulin complexes', *Nature reviews. Molecular cell biology* 12(11): 709-21.
-

- Konno, D., Shioi, G., Shitamukai, A., Mori, A., Kiyonari, H., Miyata, T., and Matsuzaki, F. (2008). Neuroepithelial progenitors undergo LGN-dependent planar divisions to maintain self-renewability during mammalian neurogenesis. Nat Cell Biol *10*, 93-101.
- Kotak, S., Busso, C., and Gonczy, P. (2013). NuMA phosphorylation by CDK1 couples mitotic progression with cortical dynein function. Embo J *32*, 2517-2529.
- Kotak, S., Busso, C., and Gönczy, P. (2012). Cortical dynein is critical for proper spindle positioning in human cells. J Cell Biol *199*, 97-110.
- Kotak, S., and Gönczy, P. (2013). Mechanisms of spindle positioning: cortical force generators in the limelight. Curr Opin Cell Biol.
- Kozlowski, C., Srayko, M., and Nedelec, F. (2007). Cortical microtubule contacts position the spindle in C. elegans embryos. Cell *129*, 499-510.
- Kraemer, B., Crittenden, S., Gallegos, M., Moulder, G., Barstead, R., Kimble, J., and Wickens, M. (1999). NANOS-3 and FBF proteins physically interact to control the sperm-oocyte switch in Caenorhabditis elegans. Curr Biol *9*, 1009-1018.
- Kraut, R., and Campos-Ortega, J.A. (1996). inscuteable, a neural precursor gene of Drosophila, encodes a candidate for a cytoskeleton adaptor protein. Dev Biol *174*, 65-81.
- Kraut, R., Chia, W., Jan, L.Y., Jan, Y.N., and Knoblich, J.A. (1996). Role of inscuteable in orienting asymmetric cell divisions in Drosophila. Nature *383*, 50-55.
- Krueger, L.E., Wu, J.C., Tsou, M.F., and Rose, L.S. (2010). LET-99 inhibits lateral posterior pulling forces during asymmetric spindle elongation in C. elegans embryos. J Cell Biol *189*, 481-495.
- Kumfer, K.T., Cook, S.J., Squirrell, J.M., Eliceiri, K.W., Peel, N., O'Connell, K.F., and White, J.G. (2010). CGEF-1 and CHIN-1 regulate CDC-42 activity during asymmetric division in the Caenorhabditis elegans embryo. Mol Biol Cell *21*, 266-277.
- Laan, L., Pavin, N., Husson, J., Romet-Lemonne, G., van Duijn, M., Lopez, M.P., Vale, R.D., Julicher, F., Reck-Peterson, S.L., and Dogterom, M. (2012). Cortical dynein controls microtubule dynamics to generate pulling forces that position microtubule asters. Cell *148*, 502-514.
- Labbe, J.C., McCarthy, E.K., and Goldstein, B. (2004). The forces that position a mitotic spindle asymmetrically are tethered until after the time of spindle assembly. J Cell Biol *167*, 245-256.
- Labbe, J.C., Pacquelet, A., Marty, T., and Gotta, M. (2006). A genomewide screen for suppressors of par-2 uncovers potential regulators of PAR protein-dependent cell polarity in Caenorhabditis elegans. Genetics *174*, 285-295.
- Lambert, J.D., and Nagy, L.M. (2002). Asymmetric inheritance of centrosomally localized mRNAs during embryonic cleavages. Nature *420*, 682-686.
- Lan, L., Lin, S., Zhang, S., and Cohen, R.S. (2010). Evidence for a transport-trap mode of Drosophila melanogaster gurken mRNA localization. PLoS One *5*, e15448.
- Lasko, P. (2012). mRNA localization and translational control in Drosophila oogenesis. Cold Spring Harb Perspect Biol *4*.
- Le Bot, N., Tsai, M.C., Andrews, R.K., and Ahringer, J. (2003). TAC-1, a regulator of microtubule length in the C. elegans embryo. Curr Biol *13*, 1499-1505.
- Lechler, T., and Fuchs, E. (2005). Asymmetric cell divisions promote stratification and differentiation of mammalian skin. Nature *437*, 275-280.
- Lecuyer, E., Yoshida, H., Parthasarathy, N., Alm, C., Babak, T., Cerovina, T., Hughes, T.R., Tomancak, P., and Krause, H.M. (2007). Global analysis of mRNA localization reveals a prominent role in organizing cellular architecture and function. Cell *131*, 174-187.
- Lee, C.Y., Andersen, R.O., Cabernard, C., Manning, L., Tran, K.D., Lanskey, M.J., Bashirullah, A., and Doe, C.Q. (2006a). Drosophila Aurora-A kinase inhibits neuroblast self-renewal by regulating aPKC/Numb cortical polarity and spindle orientation. Genes Dev *20*, 3464-3474.
- Lee, C.Y., Wilkinson, B.D., Siegrist, S.E., Wharton, R.P., and Doe, C.Q. (2006b). Brat is a Miranda cargo protein that promotes neuronal differentiation and inhibits neuroblast self-renewal. Dev Cell *10*, 441-449.
- Lehmann, R., and Nusslein-Volhard, C. (1986). Abdominal segmentation, pole cell formation, and embryonic polarity require the localized activity of oskar, a maternal gene in Drosophila. Cell *47*, 141-152.
- Lehmann, R., and Nusslein-Volhard, C. (1991). The maternal gene nanos has a central role in posterior pattern formation of the Drosophila embryo. Development *112*, 679-691.
- Lei, H., Liu, J., Fukushige, T., Fire, A., and Krause, M. (2009). Caudal-like PAL-1 directly activates the bodywall muscle module regulator hlh-1 in C. elegans to initiate the embryonic muscle gene regulatory network. Development *136*, 1241-1249.

- Leslie, R.J., and Pickett-Heaps, J.D. (1983). Ultraviolet microbeam irradiations of mitotic diatoms: investigation of spindle elongation. J Cell Biol *96*, 548-561.
- Leung, K.M., van Horck, F.P., Lin, A.C., Allison, R., Standart, N., and Holt, C.E. (2006). Asymmetrical beta-actin mRNA translation in growth cones mediates attractive turning to netrin-1. Nat Neurosci *9*, 1247-1256.
- Li, H., Guo, F., Rubinstein, B., and Li, R. (2008). Actin-driven chromosomal motility leads to symmetry breaking in mammalian meiotic oocytes. Nat Cell Biol *10*, 1301-1308.
- Li, L., and Vaessin, H. (2000). Pan-neural Prospero terminates cell proliferation during Drosophila neurogenesis. Genes Dev *14*, 147-151.
- Li, P., Yang, X., Wasser, M., Cai, Y., and Chia, W. (1997). Inscuteable and Staufen mediate asymmetric localization and segregation of prospero RNA during Drosophila neuroblast cell divisions. Cell *90*, 437-447.
- Li, W., DeBella, L.R., Guven-Ozkan, T., Lin, R., and Rose, L.S. (2009). An eIF4E-binding protein regulates katanin protein levels in C. elegans embryos. J Cell Biol *187*, 33-42.
- Liu, J., Maduzia, L.L., Shirayama, M., and Mello, C.C. (2010). NMY-2 maintains cellular asymmetry and cell boundaries, and promotes a SRC-dependent asymmetric cell division. Dev Biol *339*, 366-373.
- Liu, J., Rivas, F.V., Wohlschlegel, J., Yates, J.R., 3rd, Parker, R., and Hannon, G.J. (2005a). A role for the P-body component GW182 in microRNA function. Nat Cell Biol *7*, 1261-1266.
- Liu, J., Valencia-Sanchez, M.A., Hannon, G.J., and Parker, R. (2005b). MicroRNA-dependent localization of targeted mRNAs to mammalian P-bodies. Nat Cell Biol *7*, 719-723.
- Long, R.M., Gu, W., Lorimer, E., Singer, R.H., and Chartrand, P. (2000). She2p is a novel RNA-binding protein that recruits the Myo4p-She3p complex to ASH1 mRNA. Embo J *19*, 6592-6601.
- Lorson, M.A., Horvitz, H.R., and van den Heuvel, S. (2000). LIN-5 is a novel component of the spindle apparatus required for chromosome segregation and cleavage plane specification in Caenorhabditis elegans. J Cell Biol *148*, 73-86.
- Louvet-Vallee, S., Kolotuev, I., Podbilewicz, B., and Felix, M.A. (2003). Control of vulval competence and centering in the nematode Oscheius sp. 1 CEW1. Genetics *163*, 133-146.
- Lu, B., Ackerman, L., Jan, L.Y., and Jan, Y.N. (1999). Modes of protein movement that lead to the asymmetric localization of partner of Numb during Drosophila neuroblast division. Mol Cell *4*, 883-891.
- Lu, B., Rothenberg, M., Jan, L.Y., and Jan, Y.N. (1998). Partner of Numb colocalizes with Numb during mitosis and directs Numb asymmetric localization in Drosophila neural and muscle progenitors. Cell *95*, 225-235.
- MacArthur, H., Bubunenko, M., Houston, D.W., and King, M.L. (1999). Xcat2 RNA is a translationally sequestered germ plasm component in Xenopus. Mech Dev *84*, 75-88.
- Manabe, N., Hirai, S., Imai, F., Nakanishi, H., Takai, Y., and Ohno, S. (2002). Association of ASIP/mPAR-3 with adherens junctions of mouse neuroepithelial cells. Dev Dyn *225*, 61-69.
- Marin, V.A., and Evans, T.C. (2003). Translational repression of a C. elegans Notch mRNA by the STAR/KH domain protein GLD-1. Development *130*, 2623-2632.
- Matsuzaki, F., Ohshiro, T., Ikeshima-Kataoka, H., and Izumi, H. (1998). miranda localizes staufen and prospero asymmetrically in mitotic neuroblasts and epithelial cells in early Drosophila embryogenesis. Development *125*, 4089-4098.
- Mayer, M., Depken, M., Bois, J.S., Julicher, F., and Grill, S.W. (2010). Anisotropies in cortical tension reveal the physical basis of polarizing cortical flows. Nature *467*, 617-621.
- Mayor, S., and Pagano, R.E. (2007). Pathways of clathrin-independent endocytosis. Nat Rev Mol Cell Biol *8*, 603-612.
- Mello, C.C., Schubert, C., Draper, B., Zhang, W., Lobel, R., and Priess, J.R. (1996). The PIE-1 protein and germline specification in C. elegans embryos. Nature *382*, 710-712.
- Merdes, A., Ramyar, K., Vechio, J.D., and Cleveland, D.W. (1996). A complex of NuMA and cytoplasmic dynein is essential for mitotic spindle assembly. Cell *87*, 447-458.
- Merritt, C., Rasoloson, D., Ko, D. and Seydoux, G. (2008) '3' UTRs are the primary regulators of gene expression in the C. elegans germline', *Current biology : CB* 18(19): 1476-82.
- Messitt, T.J., Gagnon, J.A., Kreiling, J.A., Pratt, C.A., Yoon, Y.J., and Mowry, K.L. (2008). Multiple kinesin motors coordinate cytoplasmic RNA transport on a subpopulation of microtubules in Xenopus oocytes. Dev Cell *15*, 426-436.
- Mickey, K.M., Mello, C.C., Montgomery, M.K., Fire, A., and Priess, J.R. (1996). An inductive interaction in 4-cell stage C. elegans embryos involves APX-1 expression in the signalling cell. Development *122*, 1791-1798.

- Micklem, D.R., Adams, J., Grunert, S., and St Johnston, D. (2000). Distinct roles of two conserved Staufen domains in oskar mRNA localization and translation. Embo J *19*, 1366-1377.
- Miller, K.G., and Rand, J.B. (2000). A role for RIC-8 (Synembryn) and GOA-1 (G(o)alpha) in regulating a subset of centrosome movements during early embryogenesis in Caenorhabditis elegans. Genetics *156*, 1649-1660.
- Mische, S., Li, M., Serr, M., and Hays, T.S. (2007). Direct observation of regulated ribonucleoprotein transport across the nurse cell/oocyte boundary. Mol Biol Cell *18*, 2254-2263.
- Morton, D.G., Roos, J.M., and Kemphues, K.J. (1992). par-4, a gene required for cytoplasmic localization and determination of specific cell types in Caenorhabditis elegans embryogenesis. Genetics *130*, 771-790.
- Moser, J.J., Fritzler, M.J., and Rattner, J.B. (2011). Repression of GW/P body components and the RNAi microprocessor impacts primary ciliogenesis in human astrocytes. BMC Cell Biol *12*, 37.
- Mosquera, L., Forristall, C., Zhou, Y., and King, M.L. (1993). A mRNA localized to the vegetal cortex of Xenopus oocytes encodes a protein with a nanos-like zinc finger domain. Development *117*, 377-386.
- Motegi, F., and Sugimoto, A. (2006). Sequential functioning of the ECT-2 RhoGEF, RHO-1 and CDC-42 establishes cell polarity in Caenorhabditis elegans embryos. Nat Cell Biol *8*, 978-985.
- Motegi, F., Zonies, S., Hao, Y., Cuenca, A.A., Griffin, E., and Seydoux, G. (2011). Microtubules induce self-organization of polarized PAR domains in Caenorhabditis elegans zygotes. Nat Cell Biol *13*, 1361-1367.
- Motohashi, T., Tabara, H., and Kohara, Y. (2006). Protocols for large scale in situ hybridization on C. elegans larvae. WormBook, 1-8.
- Mowry, K.L., and Cote, C.A. (1999). RNA sorting in Xenopus oocytes and embryos. Faseb J *13*, 435-445.
- Munro, E., Nance, J., and Priess, J.R. (2004). Cortical flows powered by asymmetrical contraction transport PAR proteins to establish and maintain anterior-posterior polarity in the early C. elegans embryo. Dev Cell *7*, 413-424.
- Nakamura, A., Sato, K., and Hanyu-Nakamura, K. (2004). Drosophila cup is an eIF4E binding protein that associates with Bruno and regulates oskar mRNA translation in oogenesis. Dev Cell *6*, 69-78.
- Nakayama, Y., Shivas, J.M., Poole, D.S., Squirrell, J.M., Kulkoski, J.M., Schleede, J.B., and Skop, A.R. (2009). Dynamin participates in the maintenance of anterior polarity in the Caenorhabditis elegans embryo. Dev Cell *16*, 889-900.
- Napoli, I., Mercaldo, V., Boyl, P.P., Eleuteri, B., Zalfa, F., De Rubeis, S., Di Marino, D., Mohr, E., Massimi, M., Falconi, M.*, et al.* (2008). The fragile X syndrome protein represses activity-dependent translation through CYFIP1, a new 4E-BP. Cell *134*, 1042-1054.
- Nelson, K.K., and Lemmon, S.K. (1993). Suppressors of clathrin deficiency: overexpression of ubiquitin rescues lethal strains of clathrin-deficient Saccharomyces cerevisiae. Mol Cell Biol *13*, 521-532.
- Nelson, M.R., Leidal, A.M., and Smibert, C.A. (2004). Drosophila Cup is an eIF4E-binding protein that functions in Smaug-mediated translational repression. Embo J *23*, 150-159.
- Neuman-Silberberg, F.S., and Schupbach, T. (1993). The Drosophila dorsoventral patterning gene gurken produces a dorsally localized RNA and encodes a TGF alpha-like protein. Cell *75*, 165-174.
- Newmark, P.A., and Boswell, R.E. (1994). The mago nashi locus encodes an essential product required for germ plasm assembly in Drosophila. Development *120*, 1303-1313.
- Nguyen-Ngoc, T., Afshar, K., and Gönczy, P. (2007). Coupling of cortical dynein and G alpha proteins mediates spindle positioning in Caenorhabditis elegans. Nat Cell Biol *9*, 1294-1302.
- Nigon, V., Guerrier, P. and Monin, H. (1960). L'architecture polaire de l'oeuf et les movements des constituants cellulaires au cours des premieres étapes du développement chez quelques nématodes. *Bull. Biol. Fr. Belg.* 94, 131-202.
- Noble, S.L., Allen, B.L., Goh, L.K., Nordick, K., and Evans, T.C. (2008). Maternal mRNAs are regulated by diverse P body-related mRNP granules during early Caenorhabditis elegans development. J Cell Biol *182*, 559-572.
- Noctor, S.C., Martinez-Cerdeno, V., Ivic, L., and Kriegstein, A.R. (2004). Cortical neurons arise in symmetric and asymmetric division zones and migrate through specific phases. Nat Neurosci *7*, 136-144.
- O'Connell, K.F., Maxwell, K.N., and White, J.G. (2000). The spd-2 gene is required for polarization of the anteroposterior axis and formation of the sperm asters in the Caenorhabditis elegans zygote. Dev Biol *222*, 55-70.

- Ogura, K., Kishimoto, N., Mitani, S., Gengyo-Ando, K., and Kohara, Y. (2003). Translational control of maternal glp-1 mRNA by POS-1 and its interacting protein SPN-4 in Caenorhabditis elegans. Development *130*, 2495-2503.
- Ohshiro, T., Yagami, T., Zhang, C., and Matsuzaki, F. (2000). Role of cortical tumour-suppressor proteins in asymmetric division of Drosophila neuroblast. Nature *408*, 593-596.
- Pacquelet, A., Zanin, E., Ashiono, C., and Gotta, M. (2008). PAR-6 levels are regulated by NOS-3 in a CUL-2 dependent manner in Caenorhabditiselegans. Dev Biol *319*, 267-272.
- Pagano, J.M., Farley, B.M., Essien, K.I., and Ryder, S.P. (2009). RNA recognition by the embryonic cell fate determinant and germline totipotency factor MEX-3. Proc Natl Acad Sci U S A *106*, 20252-20257.
- Pagano, J.M., Farley, B.M., McCoig, L.M., and Ryder, S.P. (2007). Molecular basis of RNA recognition by the embryonic polarity determinant MEX-5. J Biol Chem *282*, 8883-8894.
- Panbianco, C., Weinkove, D., Zanin, E., Jones, D., Divecha, N., Gotta, M., and Ahringer, J. (2008). A casein kinase 1 and PAR proteins regulate asymmetry of a PIP(2) synthesis enzyme for asymmetric spindle positioning. Dev Cell *15*, 198-208.
- Pane, A., Wehr, K., and Schupbach, T. (2007). zucchini and squash encode two putative nucleases required for rasiRNA production in the Drosophila germline. Dev Cell *12*, 851-862.
- Paquin, N., Menade, M., Poirier, G., Donato, D., Drouet, E., and Chartrand, P. (2007). Local activation of yeast ASH1 mRNA translation through phosphorylation of Khd1p by the casein kinase Yck1p. Mol Cell *26*, 795-809.
- Park, D.H., and Rose, L.S. (2008). Dynamic localization of LIN-5 and GPR-1/2 to cortical force generation domains during spindle positioning. Dev Biol *315*, 42-54.
- Parmentier, M.L., Woods, D., Greig, S., Phan, P.G., Radovic, A., Bryant, P., and O'Kane, C.J. (2000). Rapsynoid/partner of inscuteable controls asymmetric division of larval neuroblasts in Drosophila. J Neurosci *20*, RC84.
- Pecreaux, J., Roper, J.C., Kruse, K., Julicher, F., Hyman, A.A., Grill, S.W., and Howard, J. (2006). Spindle oscillations during asymmetric cell division require a threshold number of active cortical force generators. Curr Biol *16*, 2111-2122.
- Peng, C.Y., Manning, L., Albertson, R., and Doe, C.Q. (2000). The tumour-suppressor genes lgl and dlg regulate basal protein targeting in Drosophila neuroblasts. Nature *408*, 596-600.
- Pepling, M.E., de Cuevas, M., and Spradling, A.C. (1999). Germline cysts: a conserved phase of germ cell development? Trends Cell Biol *9*, 257-262.
- Petersen, P.H., Zou, K., Krauss, S., and Zhong, W. (2004). Continuing role for mouse Numb and Numbl in maintaining progenitor cells during cortical neurogenesis. Nat Neurosci *7*, 803-811.
- Petritsch, C., Tavosanis, G., Turck, C.W., Jan, L.Y., and Jan, Y.N. (2003). The Drosophila myosin VI Jaguar is required for basal protein targeting and correct spindle orientation in mitotic neuroblasts. Dev Cell *4*, 273-281.
- Petronczki, M., and Knoblich, J.A. (2001). DmPAR-6 directs epithelial polarity and asymmetric cell division of neuroblasts in Drosophila. Nat Cell Biol *3*, 43-49.
- Peyre, E., Jaouen, F., Saadaoui, M., Haren, L., Merdes, A., Durbec, P., and Morin, X. (2011). A lateral belt of cortical LGN and NuMA guides mitotic spindle movements and planar division in neuroepithelial cells. J Cell Biol *193*, 141-154.
- Portman, D.S. (2006). Profiling C. elegans gene expression with DNA microarrays. WormBook, 1-11.
- Poteryaev, D., Squirrell, J.M., Campbell, J.M., White, J.G., and Spang, A. (2005). Involvement of the actin cytoskeleton and homotypic membrane fusion in ER dynamics in Caenorhabditis elegans. Mol Biol Cell *16*, 2139-2153.
- Poulson, N.D., and Lechler, T. (2010). Robust control of mitotic spindle orientation in the developing epidermis. J Cell Biol *191*, 915-922.
- Poupon, V., Girard, M., Legendre-Guillemin, V., Thomas, S., Bourbonniere, L., Philie, J., Bright, N.A., and McPherson, P.S. (2008). Clathrin light chains function in mannose phosphate receptor trafficking via regulation of actin assembly. Proc Natl Acad Sci U S A *105*, 168-173.
- Praitis, V., Casey, E., Collar, D., and Austin, J. (2001). Creation of low-copy integrated transgenic lines in Caenorhabditis elegans. Genetics *157*, 1217-1226.
- Priess, J.R. (2005). Notch signaling in the C. elegans embryo. WormBook, 1-16.
- Prodon, F., Yamada, L., Shirae-Kurabayashi, M., Nakamura, Y., and Sasakura, Y. (2007). Postplasmic/PEM RNAs: a class of localized maternal mRNAs with multiple roles in cell polarity and development in ascidian embryos. Dev Dyn *236*, 1698-1715.
- Rabinowitz, J.S., Chan, X.Y., Kingsley, E.P., Duan, Y., and Lambert, J.D. (2008). Nanos is required in somatic blast cell lineages in the posterior of a mollusk embryo. Curr Biol *18*, 331-336.

- Rabinowitz, J.S., and Lambert, J.D. (2010). Spiralian quartet developmental potential is regulated by specific localization elements that mediate asymmetric RNA segregation. Development *137*, 4039-4049.
- Raj, A., van den Bogaard, P., Rifkin, S.A., van Oudenaarden, A., and Tyagi, S. (2008). Imaging individual mRNA molecules using multiple singly labeled probes. Nat Methods *5*, 877-879.
- Rebollo, E., Roldan, M., and Gonzalez, C. (2009). Spindle alignment is achieved without rotation after the first cell cycle in Drosophila embryonic neuroblasts. Development *136*, 3393-3397.
- Redemann, S., Pecreaux, J., Goehring, N.W., Khairy, K., Stelzer, E.H., Hyman, A.A., and Howard, J. (2010). Membrane invaginations reveal cortical sites that pull on mitotic spindles in one-cell C. elegans embryos. PLoS One *5*, e12301.
- Redemann, S., Schloissnig, S., Ernst, S., Pozniakowsky, A., Ayloo, S., Hyman, A.A., and Bringmann, H. (2011). Codon adaptation-based control of protein expression in C. elegans. Nat Methods *8*, 250-252.
- Reese, K.J., Dunn, M.A., Waddle, J.A., and Seydoux, G. (2000). Asymmetric segregation of PIE-1 in C. elegans is mediated by two complementary mechanisms that act through separate PIE-1 protein domains. Mol Cell *6*, 445-455.
- Reinsch, S., and Gonczy, P. (1998). Mechanisms of nuclear positioning. J Cell Sci *111 (Pt 16)*, 2283-2295.
- Rhyu, M.S., Jan, L.Y., and Jan, Y.N. (1994). Asymmetric distribution of numb protein during division of the sensory organ precursor cell confers distinct fates to daughter cells. Cell *76*, 477-491.
- Riechmann, V., and Ephrussi, A. (2004). Par-1 regulates bicoid mRNA localisation by phosphorylating Exuperantia. Development *131*, 5897-5907.
- Rivera-Pomar, R., Niessing, D., Schmidt-Ott, U., Gehring, W.J., and Jackle, H. (1996). RNA binding and translational suppression by bicoid. Nature *379*, 746-749.
- Roberts, A.J., Kon, T., Knight, P.J., Sutoh, K., and Burgess, S.A. (2013). Functions and mechanics of dynein motor proteins. Nat Rev Mol Cell Biol *14*, 713-726.
- Rongo, C., Gavis, E.R., and Lehmann, R. (1995). Localization of oskar RNA regulates oskar translation and requires Oskar protein. Development *121*, 2737-2746.
- Rual, J.F., Ceron, J., Koreth, J., Hao, T., Nicot, A.S., Hirozane-Kishikawa, T., Vandenhaute, J., Orkin, S.H., Hill, D.E., van den Heuvel, S*., et al.* (2004). Toward improving Caenorhabditis elegans phenome mapping with an ORFeome-based RNAi library. Genome Res *14*, 2162-2168.
- Sanada, K., and Tsai, L.H. (2005). G protein betagamma subunits and AGS3 control spindle orientation and asymmetric cell fate of cerebral cortical progenitors. Cell *122*, 119-131.
- Schaefer, M., Petronczki, M., Dorner, D., Forte, M., and Knoblich, J.A. (2001). Heterotrimeric G proteins direct two modes of asymmetric cell division in the Drosophila nervous system. Cell *107*, 183-194.
- Schaefer, M., Shevchenko, A., and Knoblich, J.A. (2000). A protein complex containing Inscuteable and the Galpha-binding protein Pins orients asymmetric cell divisions in Drosophila. Curr Biol *10*, 353-362.
- Schmid, M., Jaedicke, A., Du, T.G., and Jansen, R.P. (2006). Coordination of endoplasmic reticulum and mRNA localization to the yeast bud. Curr Biol *16*, 1538-1543.
- Schnorrer, F., Bohmann, K., and Nusslein-Volhard, C. (2000). The molecular motor dynein is involved in targeting swallow and bicoid RNA to the anterior pole of Drosophila oocytes. Nat Cell Biol *2*, 185-190.
- Schober, M., Schaefer, M., and Knoblich, J.A. (1999). Bazooka recruits Inscuteable to orient asymmetric cell divisions in Drosophila neuroblasts. Nature *402*, 548-551.
- Schonegg, S., and Hyman, A.A. (2006). CDC-42 and RHO-1 coordinate acto-myosin contractility and PAR protein localization during polarity establishment in C. elegans embryos. Development *133*, 3507-3516.
- Schubert, C.M., Lin, R., de Vries, C.J., Plasterk, R.H., and Priess, J.R. (2000). MEX-5 and MEX-6 function to establish soma/germline asymmetry in early C. elegans embryos. Mol Cell *5*, 671-682.
- Schuh, M., and Ellenberg, J. (2008). A new model for asymmetric spindle positioning in mouse oocytes. Curr Biol *18*, 1986-1992.
- Schuldt, A.J., Adams, J.H., Davidson, C.M., Micklem, D.R., Haseloff, J., St Johnston, D., and Brand, A.H. (1998). Miranda mediates asymmetric protein and RNA localization in the developing nervous system. Genes Dev *12*, 1847-1857.
- Semotok, J.L., Cooperstock, R.L., Pinder, B.D., Vari, H.K., Lipshitz, H.D., and Smibert, C.A. (2005). Smaug recruits the CCR4/POP2/NOT deadenylase complex to trigger maternal transcript localization in the early Drosophila embryo. Curr Biol *15*, 284-294.

- Seydoux, G., and Dunn, M.A. (1997). Transcriptionally repressed germ cells lack a subpopulation of phosphorylated RNA polymerase II in early embryos of Caenorhabditis elegans and Drosophila melanogaster. Development *124*, 2191-2201.
- Seydoux, G., and Fire, A. (1994). Soma-germline asymmetry in the distributions of embryonic RNAs in Caenorhabditis elegans. Development *120*, 2823-2834.
- Seydoux, G., and Fire, A. (1995). Whole-mount in situ hybridization for the detection of RNA in Caenorhabditis elegans embryos. Methods Cell Biol *48*, 323-337.
- Seydoux, G., Mello, C.C., Pettitt, J., Wood, W.B., Priess, J.R., and Fire, A. (1996). Repression of gene expression in the embryonic germ lineage of C. elegans. Nature *382*, 713-716.
- Shelton, C.A., Carter, J.C., Ellis, G.C., and Bowerman, B. (1999). The nonmuscle myosin regulatory light chain gene mlc-4 is required for cytokinesis, anterior-posterior polarity, and body morphology during Caenorhabditis elegans embryogenesis. J Cell Biol *146*, 439-451.
- Shen, C.P., Jan, L.Y., and Jan, Y.N. (1997). Miranda is required for the asymmetric localization of Prospero during mitosis in Drosophila. Cell *90*, 449-458.
- Shen, C.P., Knoblich, J.A., Chan, Y.M., Jiang, M.M., Jan, L.Y., and Jan, Y.N. (1998). Miranda as a multidomain adapter linking apically localized Inscuteable and basally localized Staufen and Prospero during asymmetric cell division in Drosophila. Genes Dev *12*, 1837-1846.
- Shepard, K.A., Gerber, A.P., Jambhekar, A., Takizawa, P.A., Brown, P.O., Herschlag, D., DeRisi, J.L., and Vale, R.D. (2003). Widespread cytoplasmic mRNA transport in yeast: identification of 22 bud-localized transcripts using DNA microarray analysis. Proc Natl Acad Sci U S A *100*, 11429-11434.
- Shin, S., Wolgamott, L., Roux, P.P., and Yoon, S.O. (2014). Casein kinase 1epsilon promotes cell proliferation by regulating mRNA translation. Cancer Res *74*, 201-211.
- Shitamukai, A., Konno, D., and Matsuzaki, F. (2011). Oblique radial glial divisions in the developing mouse neocortex induce self-renewing progenitors outside the germinal zone that resemble primate outer subventricular zone progenitors. J Neurosci *31*, 3683-3695.
- Siddiqui, S.S. (2002). Metazoan motor models: kinesin superfamily in C. elegans. Traffic *3*, 20-28.
- Siller, K.H., Cabernard, C., and Doe, C.Q. (2006). The NuMA-related Mud protein binds Pins and regulates spindle orientation in Drosophila neuroblasts. Nat Cell Biol *8*, 594-600.
- Siller, K.H., and Doe, C.Q. (2008). Lis1/dynactin regulates metaphase spindle orientation in Drosophila neuroblasts. Dev Biol *319*, 1-9.
- Siller, K.H., and Doe, C.Q. (2009). Spindle orientation during asymmetric cell division. Nat Cell Biol *11*, 365-374.
- Singh, D., and Pohl, C. (2014). Coupling of rotational cortical flow, asymmetric midbody positioning, and spindle rotation mediates dorsoventral axis formation in C. elegans. Dev Cell *28*, 253-267.
- Smith, C.A., Lau, K.M., Rahmani, Z., Dho, S.E., Brothers, G., She, Y.M., Berry, D.M., Bonneil, E., Thibault, P., Schweisguth, F.*, et al.* (2007). aPKC-mediated phosphorylation regulates asymmetric membrane localization of the cell fate determinant Numb. Embo J *26*, 468-480.
- Snee, M., Benz, D., Jen, J., and Macdonald, P.M. (2008). Two distinct domains of Bruno bind specifically to the oskar mRNA. RNA Biol *5*, 1-9.
- Sonneville, R., and Gonczy, P. (2004). Zyg-11 and cul-2 regulate progression through meiosis II and polarity establishment in C. elegans. Development *131*, 3527-3543.
- Sonnichsen, B., Koski, L.B., Walsh, A., Marschall, P., Neumann, B., Brehm, M., Alleaume, A.M., Artelt, J., Bettencourt, P., Cassin, E.*, et al.* (2005). Full-genome RNAi profiling of early embryogenesis in Caenorhabditis elegans. Nature *434*, 462-469.
- Sousa-Nunes, R., and Somers, W.G. (2013). Mechanisms of asymmetric progenitor divisions in the Drosophila central nervous system. Adv Exp Med Biol *786*, 79-102.
- Southall, T.D., and Brand, A.H. (2009). Neural stem cell transcriptional networks highlight genes essential for nervous system development. Embo J *28*, 3799-3807.
- Spana, E.P., and Doe, C.Q. (1995). The prospero transcription factor is asymmetrically localized to the cell cortex during neuroblast mitosis in Drosophila. Development *121*, 3187-3195.
- Speicher, S., Fischer, A., Knoblich, J., and Carmena, A. (2008). The PDZ protein Canoe regulates the asymmetric division of Drosophila neuroblasts and muscle progenitors. Curr Biol *18*, 831-837.
- Spike, C., Meyer, N., Racen, E., Orsborn, A., Kirchner, J., Kuznicki, K., Yee, C., Bennett, K., and Strome, S. (2008a). Genetic analysis of the Caenorhabditis elegans GLH family of P-granule proteins. Genetics *178*, 1973-1987.
- Spike, C.A., Bader, J., Reinke, V., and Strome, S. (2008b). DEPS-1 promotes P-granule assembly and RNA interference in C. elegans germ cells. Development *135*, 983-993.

- Squirrell, J.M., Eggers, Z.T., Luedke, N., Saari, B., Grimson, A., Lyons, G.E., Anderson, P., and White, J.G. (2006). CAR-1, a protein that localizes with the mRNA decapping component DCAP-1, is required for cytokinesis and ER organization in Caenorhabditis elegans embryos. Mol Biol Cell *17*, 336-344.
- Srayko, M., Buster, D.W., Bazirgan, O.A., McNally, F.J., and Mains, P.E. (2000). MEI-1/MEI-2 katanin-like microtubule severing activity is required for Caenorhabditis elegans meiosis. Genes Dev *14*, 1072-1084.
- Srayko, M., Quintin, S., Schwager, A., and Hyman, A.A. (2003). Caenorhabditis elegans TAC-1 and ZYG-9 form a complex that is essential for long astral and spindle microtubules. Curr Biol *13*, 1506-1511.
- Srinivasan, D.G., Fisk, R.M., Xu, H., and van den Heuvel, S. (2003). A complex of LIN-5 and GPR proteins regulates G protein signaling and spindle function in C elegans. Genes Dev *17*, 1225-1239.
- St Johnston, D., Driever, W., Berleth, T., Richstein, S., and Nusslein-Volhard, C. (1989). Multiple steps in the localization of bicoid RNA to the anterior pole of the Drosophila oocyte. Development *107 Suppl*, 13-19.
- Stennard, F., Carnac, G., and Gurdon, J.B. (1996). The Xenopus T-box gene, Antipodean, encodes a vegetally localised maternal mRNA and can trigger mesoderm formation. Development *122*, 4179-4188.
- Sternberg, P.W. (2005). Vulval development. WormBook, 1-28.
- Stolz, A., and Wolf, D.H. (2010). Endoplasmic reticulum associated protein degradation: a chaperone assisted journey to hell. Biochim Biophys Acta *1803*, 694-705.
- Strand, D., Jakobs, R., Merdes, G., Neumann, B., Kalmes, A., Heid, H.W., Husmann, I., and Mechler, B.M. (1994). The Drosophila lethal(2)giant larvae tumor suppressor protein forms homo-oligomers and is associated with nonmuscle myosin II heavy chain. J Cell Biol *127*, 1361-1373.
- Strome, S., and Wood, W.B. (1983). Generation of asymmetry and segregation of germ-line granules in early C. elegans embryos. Cell *35*, 15-25.
- Styhler, S., Nakamura, A., Swan, A., Suter, B., and Lasko, P. (1998). vasa is required for GURKEN accumulation in the oocyte, and is involved in oocyte differentiation and germline cyst development. Development *125*, 1569-1578.
- Subramaniam, K., and Seydoux, G. (1999). nos-1 and nos-2, two genes related to Drosophila nanos, regulate primordial germ cell development and survival in Caenorhabditis elegans. Development *126*, 4861-4871.
- Sulston, J.E., Schierenberg, E., White, J.G., and Thomson, J.N. (1983). The embryonic cell lineage of the nematode Caenorhabditis elegans. Dev Biol *100*, 64-119.
- Swartz, S.Z., Chan, X.Y., and Lambert, J.D. (2008). Localization of Vasa mRNA during early cleavage of the snail Ilyanassa. Dev Genes Evol *218*, 107-113.
- Tabara, H., Hill, R.J., Mello, C.C., Priess, J.R., and Kohara, Y. (1999). pos-1 encodes a cytoplasmic zinc-finger protein essential for germline specification in C. elegans. Development *126*, 1-11.
- Tabuse, Y., Izumi, Y., Piano, F., Kemphues, K.J., Miwa, J., and Ohno, S. (1998). Atypical protein kinase C cooperates with PAR-3 to establish embryonic polarity in Caenorhabditis elegans. Development *125*, 3607-3614.
- Takizawa, P.A., Sil, A., Swedlow, J.R., Herskowitz, I., and Vale, R.D. (1997). Actin-dependent localization of an RNA encoding a cell-fate determinant in yeast. Nature *389*, 90-93.
- Tanaka, T., and Nakamura, A. (2011). Oskar-induced endocytic activation and actin remodeling for anchorage of the Drosophila germ plasm. Bioarchitecture *1*, 122-126.
- Tenenhaus, C., Subramaniam, K., Dunn, M.A., and Seydoux, G. (2001). PIE-1 is a bifunctional protein that regulates maternal and zygotic gene expression in the embryonic germ line of Caenorhabditis elegans. Genes Dev *15*, 1031-1040.
- Tenlen, J.R., Molk, J.N., London, N., Page, B.D., and Priess, J.R. (2008). MEX-5 asymmetry in one-cell C. elegans embryos requires PAR-4- and PAR-1-dependent phosphorylation. Development *135*, 3665-3675.
- Tenlen, J.R., Schisa, J.A., Diede, S.J., and Page, B.D. (2006). Reduced dosage of pos-1 suppresses Mex mutants and reveals complex interactions among CCCH zinc-finger proteins during Caenorhabditis elegans embryogenesis. Genetics *174*, 1933-1945.
- Thomsen, G.H., and Melton, D.A. (1993). Processed Vg1 protein is an axial mesoderm inducer in Xenopus. Cell *74*, 433-441.
- Thyagarajan, K., Afshar, K., and Gönczy, P. (2011). Polarity mediates asymmetric trafficking of the Gbeta heterotrimeric G-protein subunit GPB-1 in C. elegans embryos. Development *138*, 2773-2782.

- Tomancak, P., Guichet, A., Zavorszky, P., and Ephrussi, A. (1998). Oocyte polarity depends on regulation of gurken by Vasa. Development *125*, 1723-1732.
- Tomari, Y., Du, T., Haley, B., Schwarz, D.S., Bennett, R., Cook, H.A., Koppetsch, B.S., Theurkauf, W.E., and Zamore, P.D. (2004). RISC assembly defects in the Drosophila RNAi mutant armitage. Cell *116*, 831-841.
- Toyoshima, F., and Nishida, E. (2007). Integrin-mediated adhesion orients the spindle parallel to the substratum in an EB1- and myosin X-dependent manner. Embo J *26*, 1487-1498.
- Trcek, T., Chao, J.A., Larson, D.R., Park, H.Y., Zenklusen, D., Shenoy, S.M., and Singer, R.H. (2012). Single-mRNA counting using fluorescent in situ hybridization in budding yeast. Nat Protoc *7*, 408-419.
- Tsai, M.C., and Ahringer, J. (2007). Microtubules are involved in anterior-posterior axis formation in C. elegans embryos. J Cell Biol *179*, 397-402.
- Tsou, M.F., Hayashi, A., DeBella, L.R., McGrath, G., and Rose, L.S. (2002). LET-99 determines spindle position and is asymmetrically enriched in response to PAR polarity cues in C. elegans embryos. Development *129*, 4469-4481.
- Tsou, M.F., Hayashi, A., and Rose, L.S. (2003). LET-99 opposes Galpha/GPR signaling to generate asymmetry for spindle positioning in response to PAR and MES-1/SRC-1 signaling. Development *130*, 5717-5730.
- Uemura, T., Shepherd, S., Ackerman, L., Jan, L.Y., and Jan, Y.N. (1989). numb, a gene required in determination of cell fate during sensory organ formation in Drosophila embryos. Cell *58*, 349-360.
- Updike, D., and Strome, S. (2010). P granule assembly and function in Caenorhabditis elegans germ cells. J Androl *31*, 53-60.
- Van De Bor, V., Hartswood, E., Jones, C., Finnegan, D., and Davis, I. (2005). gurken and the I factor retrotransposon RNAs share common localization signals and machinery. Dev Cell *9*, 51-62.
- van der Voet, M., Berends, C.W., Perreault, A., Nguyen-Ngoc, T., Gonczy, P., Vidal, M., Boxem, M., and van den Heuvel, S. (2009). NuMA-related LIN-5, ASPM-1, calmodulin and dynein promote meiotic spindle rotation independently of cortical LIN-5/GPR/Galpha. Nat Cell Biol *11*, 269-277.
- Vanzo, N., Oprins, A., Xanthakis, D., Ephrussi, A., and Rabouille, C. (2007). Stimulation of endocytosis and actin dynamics by Oskar polarizes the Drosophila oocyte. Dev Cell *12*, 543-555.
- Velarde, N., Gunsalus, K.C., and Piano, F. (2007). Diverse roles of actin in C. elegans early embryogenesis. BMC Dev Biol *7*, 142.
- Wang, C., Dickinson, L.K., and Lehmann, R. (1994). Genetics of nanos localization in Drosophila. Dev Dyn *199*, 103-115.
- Wang, C., and Lehmann, R. (1991). Nanos is the localized posterior determinant in Drosophila. Cell *66*, 637-647.
- Wang, C., Li, S., Januschke, J., Rossi, F., Izumi, Y., Garcia-Alvarez, G., Gwee, S.S., Soon, S.B., Sidhu, H.K., Yu, F., *et al.* (2011). An ana2/ctp/mud complex regulates spindle orientation in Drosophila neuroblasts. Dev Cell *21*, 520-533.
- Wang, H., Ouyang, Y., Somers, W.G., Chia, W., and Lu, B. (2007). Polo inhibits progenitor self-renewal and regulates Numb asymmetry by phosphorylating Pon. Nature *449*, 96-100.
- Wang, H., Somers, G.W., Bashirullah, A., Heberlein, U., Yu, F., and Chia, W. (2006). Aurora-A acts as a tumor suppressor and regulates self-renewal of Drosophila neuroblasts. Genes Dev *20*, 3453-3463.
- Waring, D.A., and Kenyon, C. (1990). Selective silencing of cell communication influences anteroposterior pattern formation in C. elegans. Cell *60*, 123-131.
- Waring, D.A., and Kenyon, C. (1991). Regulation of cellular responsiveness to inductive signals in the developing C. elegans nervous system. Nature *350*, 712-715.
- Wee, B., Johnston, C.A., Prehoda, K.E., and Doe, C.Q. (2011). Canoe binds RanGTP to promote Pins(TPR)/Mud-mediated spindle orientation. J Cell Biol *195*, 369-376.
- Weeks, D.L., and Melton, D.A. (1987). A maternal mRNA localized to the vegetal hemisphere in Xenopus eggs codes for a growth factor related to TGF-beta. Cell *51*, 861-867.
- Weil, T.T., Xanthakis, D., Parton, R., Dobbie, I., Rabouille, C., Gavis, E.R., and Davis, I. (2010). Distinguishing direct from indirect roles for bicoid mRNA localization factors. Development *137*, 169-176.
- Wilbur, J.D., Chen, C.Y., Manalo, V., Hwang, P.K., Fletterick, R.J., and Brodsky, F.M. (2008). Actin binding by Hip1 (huntingtin-interacting protein 1) and Hip1R (Hip1-related protein) is regulated by clathrin light chain. J Biol Chem *283*, 32870-32879.
- Williams, S.E., Beronja, S., Pasolli, H.A., and Fuchs, E. (2011). Asymmetric cell divisions promote Notch-dependent epidermal differentiation. Nature *470*, 353-358.

- Wirtz-Peitz, F., Nishimura, T., and Knoblich, J.A. (2008). Linking cell cycle to asymmetric division: Aurora-A phosphorylates the Par complex to regulate Numb localization. Cell *135*, 161-173.
- Wodarz, A., Ramrath, A., Grimm, A., and Knust, E. (2000). Drosophila atypical protein kinase C associates with Bazooka and controls polarity of epithelia and neuroblasts. J Cell Biol *150*, 1361-1374.
- Wodarz, A., Ramrath, A., Kuchinke, U., and Knust, E. (1999). Bazooka provides an apical cue for Inscuteable localization in Drosophila neuroblasts. Nature *402*, 544-547.
- Woodard, G.E., Huang, N.N., Cho, H., Miki, T., Tall, G.G., and Kehrl, J.H. (2010). Ric-8A and Gi alpha recruit LGN, NuMA, and dynein to the cell cortex to help orient the mitotic spindle. Mol Cell Biol *30*, 3519-3530.
- Yao, J., Sasaki, Y., Wen, Z., Bassell, G.J., and Zheng, J.Q. (2006). An essential role for beta-actin mRNA localization and translation in Ca2+-dependent growth cone guidance. Nat Neurosci *9*, 1265-1273.
- Yisraeli, J.K., Sokol, S., and Melton, D.A. (1990). A two-step model for the localization of maternal mRNA in Xenopus oocytes: involvement of microtubules and microfilaments in the translocation and anchoring of Vg1 mRNA. Development *108*, 289-298.
- Yoon, Y.J., and Mowry, K.L. (2004). Xenopus Staufen is a component of a ribonucleoprotein complex containing Vg1 RNA and kinesin. Development *131*, 3035-3045.
- Yoshiura, S., Ohta, N., and Matsuzaki, F. (2012). Tre1 GPCR signaling orients stem cell divisions in the Drosophila central nervous system. Dev Cell *22*, 79-91.
- Yu, F., Cai, Y., Kaushik, R., Yang, X., and Chia, W. (2003). Distinct roles of Galphai and Gbeta13F subunits of the heterotrimeric G protein complex in the mediation of Drosophila neuroblast asymmetric divisions. J Cell Biol *162*, 623-633.
- Yu, F., Morin, X., Cai, Y., Yang, X., and Chia, W. (2000). Analysis of partner of inscuteable, a novel player of Drosophila asymmetric divisions, reveals two distinct steps in inscuteable apical localization. Cell *100*, 399-409.
- Yu, F., Ong, C.T., Chia, W., and Yang, X. (2002). Membrane targeting and asymmetric localization of Drosophila partner of inscuteable are discrete steps controlled by distinct regions of the protein. Mol Cell Biol *22*, 4230-4240.
- Yu, F., Wang, H., Qian, H., Kaushik, R., Bownes, M., Yang, X., and Chia, W. (2005). Locomotion defects, together with Pins, regulates heterotrimeric G-protein signaling during Drosophila neuroblast asymmetric divisions. Genes Dev *19*, 1341-1353.
- Zaessinger, S., Busseau, I., and Simonelig, M. (2006). Oskar allows nanos mRNA translation in Drosophila embryos by preventing its deadenylation by Smaug/CCR4. Development *133*, 4573-4583.
- Zemp, I., Wandrey, F., Rao, S., Ashiono, C., Wyler, E., Montellese, C., and Kutay, U. (2014). CK1delta and CK1epsilon are components of human 40S subunit precursors required for cytoplasmic 40S maturation. J Cell Sci *127*, 1242-1253.
- Zhang, H., Squirrell, J.M., and White, J.G. (2008). RAB-11 permissively regulates spindle alignment by modulating metaphase microtubule dynamics in Caenorhabditis elegans early embryos. Mol Biol Cell *19*, 2553-2565.
- Zhang, J., and King, M.L. (1996). Xenopus VegT RNA is localized to the vegetal cortex during oogenesis and encodes a novel T-box transcription factor involved in mesodermal patterning. Development *122*, 4119-4129.
- Zhao, W.M., Jiang, C., Kroll, T.T., and Huber, P.W. (2001). A proline-rich protein binds to the localization element of Xenopus Vg1 mRNA and to ligands involved in actin polymerization. Embo J *20*, 2315-2325.
- Zheng, Z., Zhu, H., Wan, Q., Liu, J., Xiao, Z., Siderovski, D.P., and Du, Q. (2010). LGN regulates mitotic spindle orientation during epithelial morphogenesis. J Cell Biol *189*, 275-288.
- Zhong, W., Feder, J.N., Jiang, M.M., Jan, L.Y., and Jan, Y.N. (1996). Asymmetric localization of a mammalian numb homolog during mouse cortical neurogenesis. Neuron *17*, 43-53.
- Zigman, M., Cayouette, M., Charalambous, C., Schleiffer, A., Hoeller, O., Dunican, D., McCudden, C.R., Firnberg, N., Barres, B.A., Siderovski, D.P., *et al.* (2005). Mammalian inscuteable regulates spindle orientation and cell fate in the developing retina. Neuron *48*, 539-545.
- Zilian, O., Saner, C., Hagedorn, L., Lee, H.Y., Sauberli, E., Suter, U., Sommer, L., and Aguet, M. (2001). Multiple roles of mouse Numb in tuning developmental cell fates. Curr Biol *11*, 494-501.
- Zimdahl, B., Ito, T., Blevins, A., Bajaj, J., Konuma, T., Weeks, J., Koechlein, C.S., Kwon, H.Y., Arami, O., Rizzieri, D., *et al.* (2014). Lis1 regulates asymmetric division in hematopoietic stem cells and in leukemia. Nat Genet *46*, 245-252.

- Zimyanin, V.L., Belaya, K., Pecreaux, J., Gilchrist, M.J., Clark, A., Davis, I., and St Johnston, D. (2008). In vivo imaging of oskar mRNA transport reveals the mechanism of posterior localization. Cell *134*, 843-853.
- Zonies, S., Motegi, F., Hao, Y., and Seydoux, G. (2010). Symmetry breaking and polarization of the C. elegans zygote by the polarity protein PAR-2. Development *137*, 1669-1677.

9. CURRICULUM VITAE

Personal Information

Date and place of birth: 1987, Budapest

Homepages:

http://www.linkedin.com/pub/zoltan-spiro/31/a5b/515

https://www.researchgate.net/profile/Zoltan_Spiro/

Education

- 2010 - Graduate studies at École Polytechnique Fédéral de Lausanne (**EPFL**)
- 2005 - 2010: Bachelor and Master studies at the Faculty of Biology, Eötvös Loránd University (**ELTE**), Budapest - specialized in Molecular Biology and Biochemistry

Research activity

- 2010 – onwards: graduate work at EPFL in the Institute of Cancer Research in the Gönczy lab (gonczy-lab.epfl.ch)
- 2007-2010: laboratory work and Master project at Semmelweis University, Department of Medical Chemistry in the Soti lab (stressgroup.semmelweis-univ.hu)
- 2006-2007: undergraduate projects in the field of network biology (linkgroup.hu)

Publications – in preparation as of September, 2014

Spiró, Z. and Gönczy, P: Asymmetric localization and MEX-5/6-dependent translational regulation of the novel mRNA *era-1* in *C. elegans* embryos
Spiró, Z. and Gönczy, P: Centrosomal localization of *lin-5* mRNA contributes to asymmetric pulling forces during spindle positioning in *C. elegans* embryos

Publications – published as of September, 2014

Spiró, Z., Thyagarajan, K., De Simone, A., Trager, S., Afshar, K. and Gönczy, P. (2014) 'Clathrin regulates centrosome positioning by promoting acto-myosin cortical tension in C. elegans embryos', *Development* 141(13): 2712-23.
Spiró, Z., Arslan, M. A., Somogyvari, M., Nguyen, M. T., Smolders, A., Dancso, B., Nemeth, N., Elek, Z., Braeckman, B. P., Csermely, P. et al. (2012) 'RNA interference

links oxidative stress to the inhibition of heat stress adaptation', *Antioxidants & redox signaling* 17(6): 890-901.

Korcsmaros, T., Farkas, I. J., Szalay, M. S., Rovo, P., Fazekas, D., **Spiró, Z**., Bode, C., Lenti, K., Vellai, T. and Csermely, P. (2010) 'Uniformly curated signaling pathways reveal tissue-specific cross-talks and support drug target discovery', *Bioinformatics* 26(16): 2042-50.

Dancso, B., **Spiró, Z**., Arslan, M. A., Nguyen, M. T., Papp, D., Csermely, P. and Soti, C. (2010) 'The heat shock connection of metabolic stress and dietary restriction', *Current pharmaceutical biotechnology* 11(2): 139-45.

Kiss, H. J., Mihalik, A., Nanasi, T., Ory, B., **Spiró, Z**., Soti, C. and Csermely, P. (2009) 'Ageing as a price of cooperation and complexity: self-organization of complex systems causes the gradual deterioration of constituent networks', *BioEssays : news and reviews in molecular, cellular and developmental biology* 31(6): 651-64.

Spiró, Z., Kovacs, I. A. and Csermely, P. (2008) 'Drug-therapy networks and the prediction of novel drug targets', *Journal of biology* 7(6): 20.

Conferences

- 2011 September: Protein Synthesis and Translational Control, EMBL, Heidelberg
- 2012 September: The complex life of mRNA, EMBL, Heidelberg – poster presentation
- 2013 June: International Worm Meeting, UCLA, Los Angeles – poster presentation
- 2014 March: Basel Worm Meeting, FMI, Basel – oral presentation

Scholarships

- Scholar of the Hungarian Republic fellowship in 2008-2009 and in 2009-2010
- Scholar of Science fellowship of ELTE in 2008-2009 and in 2009-2010

Science communication and social activities

- Co-founder of the BioScience Network Lausanne (BSNL) (www.bsnl.ch)
- Member of the organizing committee for EPFL-UNIL PhD retreats and SV Happy Hours
- Leader of Biology Students' Association at Faculty of Biology at ELTE (2007-2010)

Language skills

Hungarian (native), English (C1), German (A2), French (A2), Russian (A1)